REPORT D_CUMENTATION PAGE

Form Approved
OMB No. 0704-0188

1. AGENCY USE ONLY (Leave blank)	2. REPORT DATE	3. REPORT TYPE AND DATES COVERED
	01/30/95	FINAL 2/25/91-11/30/94

4. TITLE AND SUBTITLE

PROCESS DEFECTS IN COMPOSITES

5. FUNDING NUMBERS

DAAL03-91-G-0030

6. AUTHOR(S)

Dusan Krajcinovic and Marc Mignolet

7. PERFORMING ORGANIZATION NAME(S) AND ADDRESS(ES)

Arizona State University
Tempe, AZ 85287

8. PERFORMING ORGANIZATION REPORT NUMBER

9. SPONSORING/MONITORING AGENCY NAME(S) AND ADDRESS(ES)

U. S. Army Research Office
P. O. Box 12211
Research Triangle Park, NC 27709-2211

10. SPONSORING/MONITORING AGENCY REPORT NUMBER

11. SUPPLEMENTARY NOTES

The view, opinions and/or findings contained in this report are those of the author(s) and should not be construed as an official Department of the Army position, policy, or decision, unless so designated by other documentation.

12a. DISTRIBUTION/AVAILABILITY STATEMENT

Approved for public release; distribution unlimited.

12b. DISTRIBUTION CODE

13. ABSTRACT *(Maximum 200 words)*

The principal objective of the present research was to study the causes of the damage and structural disorder in polymers and fiber reinforced polymers attributed to the curing process. It was first demonstrated that the rate at which the molecular chains rupture and damage evolves is at its maximum immediately after the sol to gel transition, i.e. just after gel molecule is formed. This observation implies that the duration of the stage during which the autoclave temperature is lowered can be shortened if so desired but also that a rational model must span at least two scales (micro and macro) and must couple the heat transfer, collision theory (rate of chemical reactions of association and dissociation) and balance of mechanical momentum. Moreover, the material parameters change with time as a result of the evolving order, increased connectivity (progressive crosslinking of molecular links) and attendant viscosity. None of these effects can be described by the traditional tools of the continuum mechanics. A second aspect of the present investigation focused on the clustering of fibers that arises during the curing process. It was shown that this phenomenon is initiated during the transition of the melted matrix from an approximately Newtonian fluid to a non-Newtonian one and that its growth rate increases sharply with the fiber concentration at that time. Thus, to minimize the formation of clusters of fiber, the curing process should minimize both the transition time but also the corresponding fiber concentration. Estimates of the cluster growth rates were provided to provide a quantitative assessment of the fiber clustering potential.

14. SUBJECT TERMS

Composite Materials, Damage Mechanics, Structural Disorder, Chemo-Mechanics, Fiber Clustering

15. NUMBER OF PAGES

4

16. PRICE CODE

17. SECURITY CLASSIFICATION OF REPORT	18. SECURITY CLASSIFICATION OF THIS PAGE	19. SECURITY CLASSIFICATION OF ABSTRACT	20. LIMITATION OF ABSTRACT
UNCLASSIFIED	UNCLASSIFIED	UNCLASSIFIED	UL

PROCESS DEFECTS IN COMPOSITES

FINAL REPORT

Dusan Krajcinovic and Marc Mignolet,

1.25.1994

U.S. ARMY RESEARCH OFFICE

GRANT NUMBER DAAL03-91-G-0030

ARIZONA STATE UNIVERSITY

STATEMENT OF THE STUDIED PROBLEM

Principal objective of the research supported by this ARO grant was to study the causes of the damage and structural disorder in polymers and fiber reinforced polymers attributed to the curing process. This research was motivated by the loss of stiffness and strength associated with this damage. In certain cases the loss of strength attributed to these microcracks and fiber clustering places unacceptable limitations on the use of polymers and fiber reinforced polymer composite in engineering and military applications.

The basic philosophy of the approach used in this research is that the study of the considered phenomena must include two following facts: (a) that the microstructure of the polymer during the cure is strongly disordered, (b) that the damage evolution is activated both by thermal and stress field and (c) that the fiber clustering process may be stable or unstable. In view of the first two statements it is immediately obvious that the traditional, continuum or mean-field micromechanical models will not provide a rational basis for the consideration of processes which are non-deterministic, local and dependent on the extreme statistics of the microcrack distribution in the evolving gel. It is, therefore, concluded that the governing equations must reflect: (a) the randomness of the process and (b) the disordered lattice of the gelling polymer matrix.

The long term objective of this work, which should be reached in the future, is to formulate an analytical model which would enable optimization of the curing process (temperature, pressure and time to which a resin is subjected in the autoclave). This optimization process should allow for the determination of the temperature-time regime during the cure which should minimize the incurred damage and fiber clustering.

SUMMARY OF THE MOST IMPORTANT RESULTS

(1) Chemo-Mechanics of Process Induced Mechanics

The most important conclusion of the research performed and completed during the sponsored period is that the rate at which the molecular chains rupture and damage evolves is at its maximum immediately after the sol to gel transition, i.e. just after gel molecule is formed. In the considered case most of the damage was accumulated during the period between 2 and 4 hours during which the autoclave temperature was held constant. This observation has significant and potentially far reaching consequences.

From the point of view of the cure optimization process this observation means that the thermal shrinkage has little effect on the damage. Therefore, the duration of the stage during which the autoclave temperature is lowered can be shortened if so desired. Further, simulations are needed to provide the effect which different temperatures and hold times have on the cure related damage.

From the analytical point of view this observation means that a rational analytical model cannot be developed using the methods based on the average stresses, strains and damage and the effective (or volume averaged) material properties. The microcrack nucleation and growth

depends almost entirely on the stress concentrations within a strongly disordered gel molecule. Immediately following the sol to gel transition the average stresses in the matrix are very small. However, the stress concentrations are huge since the lattice formed by crosslinked nodules of the evolving gel molecule is strongly disordered. As a result the balance between the forces on individual links and their strength is least favorable in the aftermath of gelation. As soon as the microstructural order is established this balance becomes more favorable even though the average stress may become larger.

From analytical point of view the work performed during this project clearly indicates that a rational model must span at least two scales (micro and macro) and must couple the heat transfer, collision theory (rate of chemical reactions of association and dissociation) and balance of mechanical momentum. Moreover, the material parameters change with time as a result of the evolving order, increased connectivity (progressive crosslinking of molecular links) and attendant viscosity. None of these effects can be described by the traditional tools of the continuum mechanics.

(2) Clustering of Fibers During the Curing Process

The analysis of the fiber clustering problem has focused on, and provided answers to, the following two important questions:

(i) at what point during the curing process does fiber clustering occur ?

and

(ii) what is the rate at which this process develops and what are the parameters that control it ?

Regarding the first question, it was demonstrated that the clustering of fibers occurs early during the curing process when the matrix is a very viscous liquid that starts exhibiting non-Newtonian features. In the later phase of the curing, i.e. when the matrix displays strong non-Newtonian properties, it was shown that relative motions of the fibers are unlikely to occur so that the fibers will remain in the configuration that they possessed at the time of the Newtonian to non-Newtonian transition.

Concerning the second issue, which was approached by analyzing the stability of a Stokes flow through an array of fibers, it was shown that fiber clustering is always initiated but that its rate of growth is very strongly affected by the fiber concentration at the time of the transition. Specifically, a dramatic increase in the growth rate with the ratio of the distance between fiber centers to the fiber radius has been observed. The fiber geometry, i.e. staggered or unstaggered configurations, has been shown to have only a very weak effect on the growth rate, slightly larger for staggered arrays of fibers than for unstaggered ones. Finally, estimates of the growth rates were presented for a variety of conditions.

From the point of view of the optimization of the curing process, the above findings indicate that the clustering of the fibers can be minimized by shortening the time of the transition of the matrix from an at least approximately Newtonian behavior to a non-Newtonian one, and by minimizing the fiber concentration at that transition. The estimates of the growth rate which have been reported can be used to determine appropriate values of the transition time and fiber concentration.

When present, clusters of fibers clearly lead to a spatial nonuniformity of the mechanical properties of a composite material. This observation has motivated the final part of this research effort, i.e. the assessment of the effects of spatial random variations in the strength of the fibers on the global properties of a composite. Under a local load sharing rule, a set of three first order differential equations was derived that govern not only the stress-strain relationship of the composite beyond the elastic regime but also the distribution of the force carried by the fibers and thus permits the prediction of the mechanical behavior of a composite specimen from the spatial description of its mechanical properties.

LIST OF PUBLICATIONS

(A) Publications:

1. K. Mallick and D. Krajcinovic, "Cure Induced Inelastic Deformation in Thermosetting Polymers", in: Recent Advances in Damage Mechanics and Plasticity, J.W. Ju, Ed., AMD-Vol. 132, MD-Vol. 30, pp. 159-172, 1992.
2. M. Mignolet, "Fiber Clustering During the Curing of Composite Materials", in: Recent Advances in Damage Mechanics and Plasticity, J.W. Ju, Ed., AMD-Vol. 132, MD-Vol. 30, pp. 173-185, 1992.
3. K. Mallick and D. Krajcinovic, "Curing Induced Microcracks in Polymer Matrices", in: Damage Mechanics of Composites, D.H. Allen and D.C. Lagoudas, Eds., AMD-Vol. 150 and AD-Vol. 32, pp. 141-154, 1992.
4. M. Mignolet, "Fiber Clustering: A Comparison of Two Resin Flow Models", J. of Composite Materials, Vol. 28, No. 15, pp. 1467-1479, 1994.
5. D. Krajcinovic and K. Mallick, "Creep Rupture of Polymers", in Damage Mechanics of Polymers, D.H. Allen and J.W. Ju, Eds, AMD-Vol. 185, pp. 167-178, 1994.
6. D. Krajcinovic, "Damage Incurred During the Polymerization of Thermosets", in: Size -Scale Effect in the Failure Mechanisms of Materials and Structures, Proc. of IUTAM Symposium, A. Carpinteri, Ed., in print.
7. D. Krajcinovic and K. Mallick, "Micromechanics of the Process Induced Damage Evolution in Thermosets", J. of Mechanics and Physics of Solids, in print.
8. V.A. Lubarda, "An Analysis of Large-Strain Damage Elastoplasticity", Int. J. Solids and Structures, Vol. 31, pp. 2951-2964, 1994 (partial credit to ARO).
9. D. Krajcinovic and S. Mastilovic, "Damage Evolution and Failure Modes", in: Proc. of the Int. Conf. on Computational Engineering Science, to appear.
10. M. Mignolet and K. Mallick, "Random Inelastic Behavior of Composite Materials with Local Load Sharing", Probabilistic Engineering Mechanics, submitted for publication.
11. M. Mignolet, "Fiber Clustering in Composite Materials: A Flow Induced Instability", J. of Fluids and Structures, submitted for publication.

(B) Doctoral Thesis:

1. K. Mallick, Process Defects in Polymers, Mechanical and Aerospace Engineering, Arizona State University, Tempe, AZ. Thesis successfully defended in December of 1993.

LIST OF PARTICIPATING SCIENTIFIC PERSONNEL

Following personnel contributed to the published research sponsored by this grant:

Dusan Krajcinovic, Ph.D., Professor and Principal Investigator, Arizona State University
Marc Mignolet, Ph.D., Associate Professor and Co-Principal Investigator, Arizona State University
Vlado A. Lubarda, Ph.D., Visiting Associate Professor, Arizona State University (1 month).
Kaushik Mallick, Ph.D., formerly graduate student now employed by "All Plastics & Fiberglass", Mobile, AL.
Sreten Mastilovic, graduate student, Arizona State University.

All individuals were employed by the Arizona State University during the period of their involvement with this research.

AMD-Vol. 132/MD-Vol.30, Recent Advances in
Damage Mechanics and Plasticity
ASME 1992

CURE INDUCED INELASTIC DEFORMATION IN THERMOSETTING POLYMERS

Kaushik Mallick and Dusan Krajcinovic
Department of Mechanical and Aerospace Engineering
Arizona State University
Tempe, Arizona

ABSTRACT

The paper focuses on the establishment of a micromechanically based analytical model for the determination of the cure induced average temperature, stress and strain fields in a resin slab. Based on the new aggregation-percolation type of models the proposed algorithm seems to be well suited for the requisite analyses. A geometrically simple problem was selected to illustrate main aspects of the problem and the proposed analytical model.

INTRODUCTION

Mechanical response of polymer matrix composites, and ultimately their strength, is strongly affected by the residual stress and submicro- and micro-defects induced during the curing process. The magnitude of residual stresses and the size of micro-defects depend on the chemical process, thermal gradients and pressure developed within the cured specimen and the duration of the process. Consequently, optimization of the curing process, i.e. minimization of the performance limiting birth defects, is undeniably an important task with far reaching consequences. However, the inherent complexity of the phenomenon, coupling exothermic chemical reactions, heat transfer and attendant emergence of the stress and strain fields defies easy solutions. Additional complexity is introduced by the disordered and evolving (time dependent) microstructure of the polymeric matrix. Consequently, it is unlikely that a rational analytical model for the description of the underlying physico-chemical phenomena can be sought within the framework of the conventional continuum theories.

Polymerization, or more specifically sol-to-gel transition is a process recognized as a critical phenomenon or phase transition. Continuous and gradual formation of bonds, generated during binary collisions of n-mers on the

microscale, results in a singular behavior on the macroscale. In other words, sol becomes gel during the irreversible connectivity transition of the material. Singular behavior of some transport macro-properties further complicates the process and its description.

Some aspects of this physico-chemical process in a strongly disordered medium were studied in the past in isolation using conventional methods. For example, the problem of heat conduction in a body undergoing solidification (Stefan problem) and the associated development of residual stresses has been an area attracting some interest in the past (Weiner and Boley, 1963, Li and Barber, 1989, Guz', et al., 1988). The development of thermal stresses in chemically hardening elastic media has been analyzed by Levitsky and Shaffer (1974). Related problems were also studied within the framework of viscoelasticity by Muki and Sternberg (1961), Lee and Rogers (1963) and Weitsman (1979). Several investigations were focused on the development of residual stresses in thermosetting composite laminates (Hahn and Pagano, 1976) , Bogetti and Gillespie, 1989) or void formation (Halpin, et al., 1984) during the curing process. All of the above models were strictly phenomenological. The relation between the actual chemical processes (often lumped into a vaguely defined degree of cure) and the changing transport properties is at least tenuous and limited to a fitted set of data. In all cases the material was assumed to be homogeneous and the moving surface sharply dividing the sol from the gel (Guz', et al., 1988) geometrically perfect. These deterministic, continuum models may, indeed, suffice for prediction of mean (average) fields. However, the conventional continuum models are inherently unable to predict the fluctuations of temperature, stress and strain fields responsible for damage (and "birth defects") and the attendant spatial-temporal disorder characterizing the phase transition.

The objective of this paper is to recapitulate some of the newer advances in the description of the polymerization process and suggest a rational micromechanically based model for the prediction of the viscoelastic phenomena on the macroscale.

GELATION OF THERMOSETTING POLYMERS

The process of polymerization or gelation is characterized by a sudden, abrupt and dramatic change of the system on the macroscale at a particular value of a continuously varying micro-parameter (number of cross-linking bonds formed between monomers). Pioneering studies of polymerization of branching molecules by Flory (1941,1953) and Stockmayer (1943) later became known as bond percolation on a Bethe lattice. However, the Bethe lattice cannot model the spatial distribution of clusters and the ensuing spatial disorder. More recently the critical phenomena of sol-gel transition has been studied extensively within the framework of the percolation theory by deGennes (1976), Stauffer (1982) and Hermann, et al., (1983). In these studies, monomers are placed in a cubic lattice (instead of an infinitely large Bethe tree) and bonds are allowed to form randomly between them. In the course of this process, formed are macromolecules of different sizes like dimers, trimers, n-mers etc. At some

critical point of the reaction (commonly referred to as the percolation threshold) an infinite cluster appears spanning the entire specimen. This infinitely large macromolecule is known as 'gel', while the collection of finite clusters coexisting with the gel is referred to as 'sol'. The process of gelation is, therefore, the transition of phase from a state without a gel to a state with a large gel network (backbone) spanning the entire specimen. A number of physical properties of the system exhibit singular behavior at the percolation threshold. Even newer studies (Martin, et al., 1989, Martin and Adolf, 1991) focus on certain inconsistencies of the earlier percolation models ignoring aggregation by assuming that the lattice nodes are occupied by monomers.

In dilute solutions monomers are very mobile. As they diffuse through the solution they collide, bond to each other and aggregate into clusters of fractal geometry. In the process of *aggregation* n-mer clusters form long, entangled chains. Essential feature of the chain kinetics is that their macro-behavior is dominated by its large scale properties and that they interact with many neighbors (Doi and Edwards, 1986).

The aggregates (macromolecules or long chains) become immobilized when they fill a certain fraction of the available volume. This irreversible connectivity transition can be conveniently described as a phase transition by a *bond percolation* model. The nodes off the lattice are occupied by the aggregates (rather than monomers). The probability that a bond exists between two neighboring aggregates is denoted by p. At the bond percolation threshold $p = p_c$ a finite cluster emerges and the polymeric liquid crosses into solid (gel). The bond percolation threshold p_c is a universal parameter depending only on the microstructure (lattice geometry), connectivity range and dimensionality. At the percolation threshold, parameters such as cluster radius and viscosity v diverge as a power of the proximity parameter $|p - p_c|$. For example, the scaling law for the bulk viscosity is

$$v \sim (p_c - p)^{-k} \qquad \text{as} \quad p \rightarrow p_c^- \tag{1}$$

where $k = 1.4 \pm 0.2$ (Martin, et al., 1988) for a typical epoxy resin.

Beyond the percolation threshold $p > p_c$ the newly formed gel backbone acquires tensile and shear stiffness and strength. The scaling law for the equilibrium shear stiffness (or somewhat less rigorously macro shear modulus) was found to be

$$G_\infty \sim (p - p_c)^T \qquad \text{as} \quad p \rightarrow p^{c+} \tag{2}$$

where $t = 8/3$ (Adolf and Martin, 1990).

Since the fraction of bonds p is a monotonically increasing function of time, both equilibrium and relaxation modulus change with time as well. Experimental results show that the longest relaxation times for the clusters diverge at the gel point according to the scaling law (Adolf and Martin, 1990) :

$$\tau_z \sim (p - p_c)^{-y} \tag{3}$$

where $y \simeq 4$. All three scaling laws (1) to (3) are universal in a sense that they do not depend on the details of the microstructure, sequence of the bond formation and duration of the process. Finally, these scaling laws are valid only in the vicinity of the percolation threshold. For $p >> p_c$ the gel becomes locally macro-homogeneous allowing application of mean field theories.

From a narrow, parochial view of solid mechanics it might appear that the study of gel (by percolation and mean field models) suffice for the purpose of estimating distribution of micro-defects and residual stresses attributable to the curing process. However, since the nodes of the lattice are occupied by aggregates (rather than monomers) the viscoelasticity of the lattice in an essential manner depends on the aggregation processes. More precisely, the viscoelastic properties of the polymer (and the birth defects) depend on the dynamics of a single cluster including its connectivity, excluded volume and hydrodynamic interactions between constituent monomers, etc. Further support for the combined aggregation-percolation model, advocated in this paper, consists of the measured defect data. In general, the probability of finding defects spanning more than six to seven adjacent nodes is very small. Thus, if the defects are indeed measurable in μm (see Kuksenko and Tamuzs, 1981) the spacing between nodes must be of the order of aggregate rather than monomer size.

VISCOLELASTICITY OF POLYMERS DURING THE CURING PROCESS

The essential attribute of micromechanical models is that they relate the response and transport properties of a solid on the macro-scale to its microstructure. In a process model it is further necessary to relate the change of macro-properties to the evolution of the respective physico-chemical processes on the micro-scale. Thus, the study of viscoelasticity of polymers during the curing process must be related to the dynamics of a single molecular chain and the interactions between adjacent chains.

Dynamics of a polymer chain in dilute suspension is, in dependence of the extent of hydrodynamic interactions, governed either by Rouse or Zimm models (Doi and Edwards, 1986, Martin, et al., 1989, etc.). In a fixed network (cross-linked systems) the dynamics of a polymer chain is typically approximated by the reptation model (deGennes, 1990, Doi and Edwards, 1986, etc.). In all of these cases the relaxation modulus scales in a different manner allowing for relatively precise and convincing experimental determination of the dominant chain dynamics mechanism.

For example, for times larger than that of the Rouse mode, the relaxation modulus of the polymer in the post-gel stage is described by (Martin and Adolf,1990)

$$G_R(t) = AG_\infty(t)\,(1+t/\tau_0)^{-2/3}\exp\{-(t/\tau_z)^{0.4}\} \qquad (4)$$

where A is a constant depending on the instantaneous modulus of the material and τ_0 is a relaxation time in molecular time scale characterizing the Rouse mode of dynamics of a polymer cluster.

The so-called *time-temperature superposition principle* (see, for example, Ferry, 1961) allows for the construction of a master relaxation curve representing hypothetical behavior of a polymer at one temperature over eight decades on the logarithmic time scale from several curves at different (higher) temperatures measured over much shorter time intervals. In other words, using appropriate scaling the duration and the temperature of the test are in a certain, well defined, sense interchangeable insofar as the extent of stress relaxation is concerned. This principle was invariably found to hold for uncross-linked polymers but lacking for the cross-linked polymers. This is a natural consequence of the fact that the relaxation is friction dependent in uncross-linked polymers. In cross-linked (thermoset) polymers the viscous behavior is dominated by the rate of cross-linking rendering the time-temperature superposition principle inadequate.

Considering scaling laws for the relaxation modulus Adolf and Martin (1990) concluded that the scaling law for the relaxation shear modulus G(t) scales equally below and above the percolation threshold. Thus, the master relaxation curve (*time-cure superposition principle*) for the complex shear modulus in the vicinity of the phase transition can be obtained scaling the actual time t by the longest relaxation time τ_z. The inverse of the longest relaxation time $1/\tau_z$ is, physically, a point at which two different limiting behaviors of the complex shear modulus meet. The ensuing time-cure superposition principle is supposed to be valid only for the incipient gel, i.e in the narrow neighborhood of the percolation threshold. However, experimental data indicate (Adolf and Martin, 1990) that this scaling law persists well into what is typically considered the mean field regime.

TRANSIENT CURE INDUCED PROCESSES IN A INFINITE SLAB

Cure Simulation

Consider a slab of thickness $2h_o$ infinitely extended in the direction of x and z axes (Fig.1). The heat diffusion through the thickness of the slab is governed by the classical equation

$$\frac{\partial(\rho S T)}{\partial t} = \frac{\partial}{\partial y}\left[k \frac{\partial T}{\partial y}\right] + \rho H_R \tag{5}$$

The density (ρ), thermal conductivity (k) and specific heat (S) of the material virtually do not change and will, therefore, be assumed to be constant throughout the process. The polymerization process is exothermic and the rate at which the heat is generated is typically assumed to be proportional to the rate of the cross-linking

$$H_R = H_T \frac{\partial p}{\partial t} \tag{6}$$

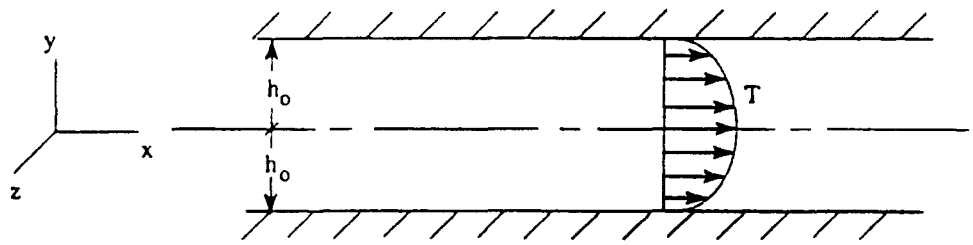

Fig.1 Representation of a infinite slab of resin

In (6) H_T is the total heat generated per unit mass of resin during the curing process. Moreover, a pseudo first order reaction and an Arrhenius relationship is typically used to define the rate at which the bonds are formed as a function of the prevailing temperature T (in degrees of Kelvin)

$$\frac{\partial p}{\partial t} = A_o \exp\left(\frac{E_a}{RT}\right)(1 - p) \tag{7}$$

In (7) A_o is a constant, E_a the activation energy for the reaction and R the universal gas constant.

Taking advantage of the symmetry of the problem, boundary conditions on the temperature field are

$$T\,(y=h_o, t) = T_A(t) \tag{8a}$$

$$\frac{\partial T(y=0, t)}{\partial t} = 0 \tag{8b}$$

where $T_A(t)$ is a prescribed autoclave temperature sketched in Fig.2.

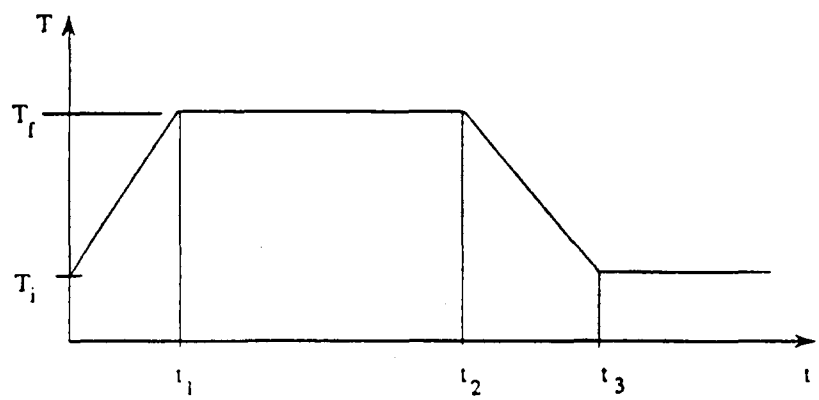

Fig.2 Variation of autoclave temperature with time.

Initially, slab is assumed to be at the room temperature (T_i). Therefore, the initial condition is

$$T(y,0) = T_i \tag{9}$$

The initial boundary value problem, consisting of equations (5) to (7), boundary conditions (8) and initial condition (9), can be solved only numerically to be able to determine the variation of the temperature T and cross-linking p through the thickness of the slab at each instant of time.

Stress and Strain Fields

It has been observed for thermosetting resins that near the gel-point the time-dependent viscoelastic functions form universal curves if the modulus is scaled by the equilibrium modulus and the time by the longest relaxation time τ_z (Adolf and Martin, 1990). The critical regime where this theory of time-cure superposition remains valid has been found to be surprisingly broad. Conservative estimates show that above relationships are valid for most of the post-gel regime.

In order to take advantage of the time-cure superposition principle it is necessary to introduce a reduced time variable defined as

$$\chi(t) = \int_0^t \frac{dt'}{\tau_z} = c \int_0^t (p(t') - p_c)^4 \, dt' \tag{10}$$

where (1/c) is the proportionality constant in the expression (3).

Since the in-plane dimensions of the slab are large compared to its thickness, the stresses, strains and displacements in the regions away from the slab ends are functions of the t and coordinate y, only. If the boundaries are free of stresses and the dead weight negligible the only nonvanishing stresses (equal to each other) are σ_x and σ_z. Using the same argument, the only non-vanishing strain component is found to be ε_y. Following an analysis similar to one suggested in Muki and Sternberg (1961) a constitutive law relating the deviatoric parts of the stress component σ_x and strain rate ε_x can be written in terms of total stress σ_x and total strain rate $\partial\varepsilon_y/\partial t$ as

$$\sigma_x(y,t) = -\int_0^t 2G(y,\chi - \chi') \frac{\partial \varepsilon_y(y,t')}{\partial t'} \, dt' \tag{11}$$

where G is the shear relaxation modulus of the material admitting additive decomposition $G = G_\infty + G_R$. The dependence of G on the degree of cross-linking near the phase transition is defined by the expressions (2) and (4).

Similarly, from the constitutive relations between the hydrostatic components,

$$2\sigma_x(y,t) = \int_0^t 3K(y,\chi-\chi')\frac{\partial}{\partial y}\{\varepsilon_y(y,t) - 3\varepsilon^*(y,t)\}\,dt' \tag{12}$$

where ε^* is the isotropic eigenstrain in the material point due to shrinkage and thermal dilatation

$$\varepsilon^* = \varepsilon_{th} - \varepsilon_{sh} \tag{13}$$

Before the emergence of the infinite cluster the freely moving aggregates shrink without emergence of stresses. Thus, in a mean field approximation it may be assumed that the stress generating shrinkage strain is directly proportional to the degree of cross-linking above the level needed for the formation of the infinite cluster

$$\varepsilon_{sh} = \varepsilon_f (p - p_c) / (1 - p_c) \tag{14}$$

with ε_f being the final magnitude of the shrinkage strain. The thermal strains are defined as

$$\varepsilon_{th} = \alpha (T - T_c) \tag{15}$$

with α being the thermal expansion coefficient for the material, while $T = T_c$ at the percolation threshold.

The rate of change of the eigenstrain is, therefore,

$$\frac{\partial\varepsilon^*(y,t)}{\partial t} = \alpha\frac{\partial T(y,t)}{\partial t} - \frac{\varepsilon_f}{(1-p_c)}\frac{\partial p(y,t)}{\partial t} \tag{16}$$

For the present analysis it will be assumed (as in Lee and Rogers, 1963) that the material is elastic in hydrostatic extension/compression and viscoelastic in shear. This assumption is supported by the observation that the bulk modulus K exists before the phase transition and is, in all probability, not very sensitive to the volume fractions of gel and sol. Thus, in the following expressions, the bulk modulus will be taken as being a time-independent constant.

The final form of the constitutive law can be derived eliminating ε_y from (11) and (12)

$$\sigma_x(y,t) + \frac{4}{3K}\int_0^t \frac{\partial G(y,\chi-\chi')}{\partial\chi'}\sigma(y,t')dt' = -6\int_0^t G(y,\chi-\chi')\frac{\partial\varepsilon^*(y,t')}{\partial t'}dt' \tag{17}$$

As suggested by Lee and Rogers (1963), the nonhomogeneous integral equation (17) can be solved numerically discretizing the time scale into finite time steps t_i , i=0,1,2,.....n, with $t_1=0$ and $t_n = t$. Once the shear modulus of the gelling material and the eigenstrain are determined as a function of the position y and time t, it becomes possible to compute the right hand side of the above equation (denoted below as $F(t_n)$) for each time increment. The left hand side of (17) can be further manipulated into a more convenient form

$$\sigma_x(y,t) = \frac{F(t_n) - \frac{2}{3K}\sum_{i=0}^{n-1}[G(y,\chi_n-\chi_{i+1})p_i - G(y,\chi_n-\chi_{i-1})p_i]}{1 + \frac{2}{3K}[G(y,0)p_n - G(y,\chi_n-\chi_{n-1})p_n]} \qquad (18)$$

where $p_i = p(t_i)$ refers to the extent of the reaction corresponding to the time step t_i and $G(y,t)_{p_i}$ is the modulus evaluated at the same extent of reaction.

Finally, since the change in the thickness dimension due to chemical shrinkage is negligible, the slab thickness ($2h_o$) is assumed, for simplicity, to remain constant throughout the process.

Illustrative Problem

For the purpose of illustration the computations were performed for a polymer slab made of Hercules 3501-6 resin. Following numerical values for the material parameters were selected as representative for the considered boundary value problem (Loos and Springer, 1983, Bogetti and Gillespie, 1989) : conductivity of the resin k = 0.167 W / (m.K), resin density (ρ) = 1.26×10^3 kg/m^3, specific heat of resin (S) = 1.26 KJ/(kg.K), heat of reaction (H_T) = 474 KJ/kg, coefficient of thermal expansion (α) = 7.2×10^{-5} /^{o}C, final shrinkage strain (ε_f) = 2%, shear modulus of the fully cured resin ($G_\infty(p = 1)$) = 1.06×10^3 MPa, bulk modulus (K) = 2.3×10^3 MPa, thickness of the resin bed ($2h_o$) = 1.5 cm, constant for the cure kinetics (A_o) = exp(21), activation energy of the resin (E_a) = 80×10^3 J/mol. The gel point for the resin was identified as the bond percolation threshold on a simple cubic lattice, $p = p_c = 0.25$.

The autoclave temperature was varied as shown in Fig.2 assuming arbitrarily that t_1= 1 hr, t_2 = 3 hrs and t_3 = 5 hrs. The initial temp T_i was 25^o C while the maximum temperature T_f was 177^o C. The constant c in (9) was estimated on the premise that the reduced time variable (χ) coincides with the actual time after which the material is fully cured, i.e. when p=1. The parameter c obtained in this manner was 3.16. In absence of precise experimental data the constant A, characterizing the instantaneous modulus of the material, is assumed to be 1.

RESULTS AND DISCUSSION

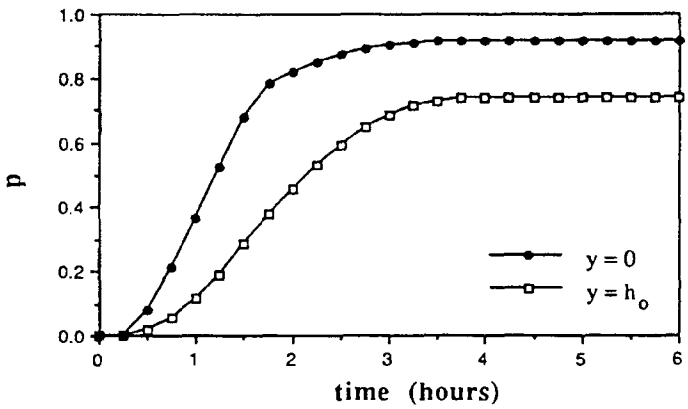

Fig.3 Growth of degree of crosslinking with time

Fig.3 shows the growth of degree of cross-linking with time for points on the surface and in the center of the slab. The rate of gelation is clearly much more rapid near the center due to the higher temperature attained by the interior of the slab in the course of the exothermic reaction. As a result the interior of the slab gets stiffer much faster than the outer layers and consequently locks in higher shrinkage stresses. It can be also observed from Fig.1 that the final degree of gelation in the central region is higher than that of the surface. The strength of the fully cured slab, therefore, varies through the thickness in proportion to the final degree of cross-linking attained.

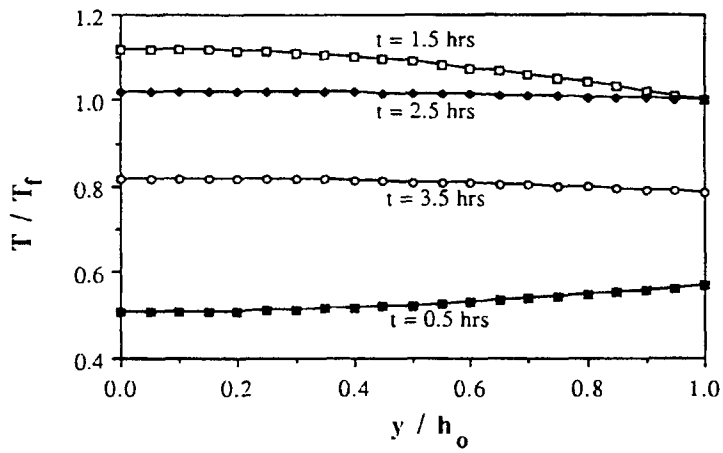

Fig.4 Variation of temperature through slab thickness

The variation of the temperature across the thickness of the slab is depicted in Fig. 4 at four different times. The exothermic reaction due to the cure results

in a significant temperature gradient within the material especially while the material undergoes phase transition from sol to gel. During this time the material is subjected to a shrinkage strain resulting from cross-linking. Fig.5 shows the variation of the degree of cross-linking (p) across the thickness of the slab. The number of cross-links at the center of the slab increases substantially at some critical time when the exothermic reaction taking place near the sol to gel phase transition.

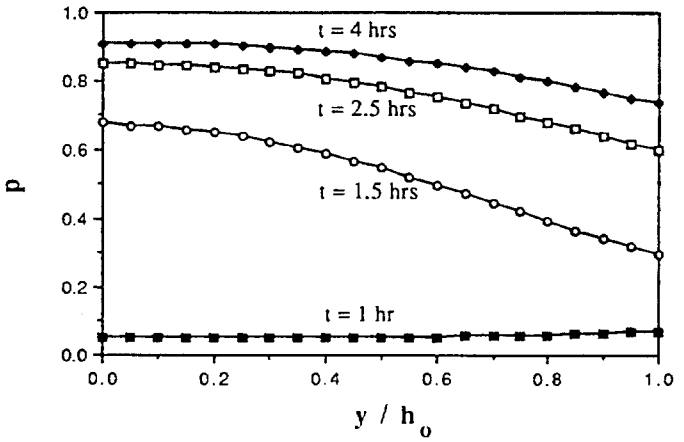

Fig.5 Variation of degree of gelation through the slab thickness

The development of the viscoelastic stresses (σ_x) is quite rapid after the gel-point as shown in Fig.6. After reaching maximum value at t = t_3 (when the autoclave cooling is completed) the stress σ_x decay to an equilibrium value. After sufficient time the stress σ_x stabilises resulting in residual stress.

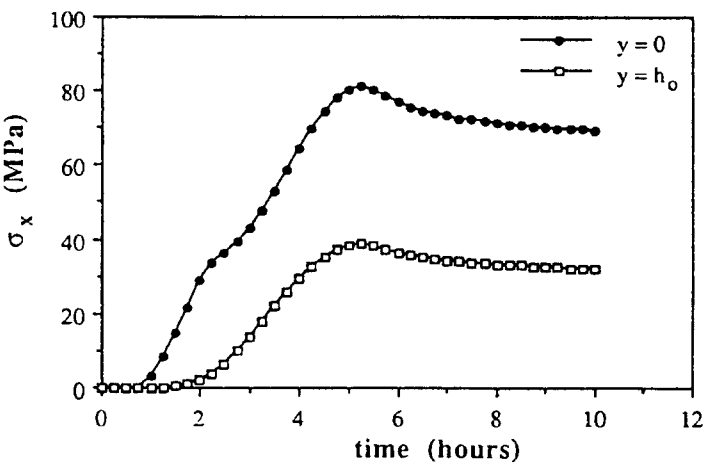

Fig.6 Variation of stresses with time

time resulting in residual stresses. It can be also observed from Fig.6 that the stress at the middle of the slab (y = 0) is significantly higher than that on the boundary (y = h_o). This is a consequence of the exothermic heat generation within the slab and the attendant temperature gradient observed in Fig.4. Fig.7 depicts the variation of σ_x through the thickness of the slab and at different extents of time. Due to the presence of temperature gradient and the gradient in the degree of cross-linking through the thickness of the slab, there is significant gradient in stresses as well. It can be only conjectured at this point that microcracks originate at the center of the slab when the magnitude of the tensile stress exceeds the current strength of the gelling material at that point.

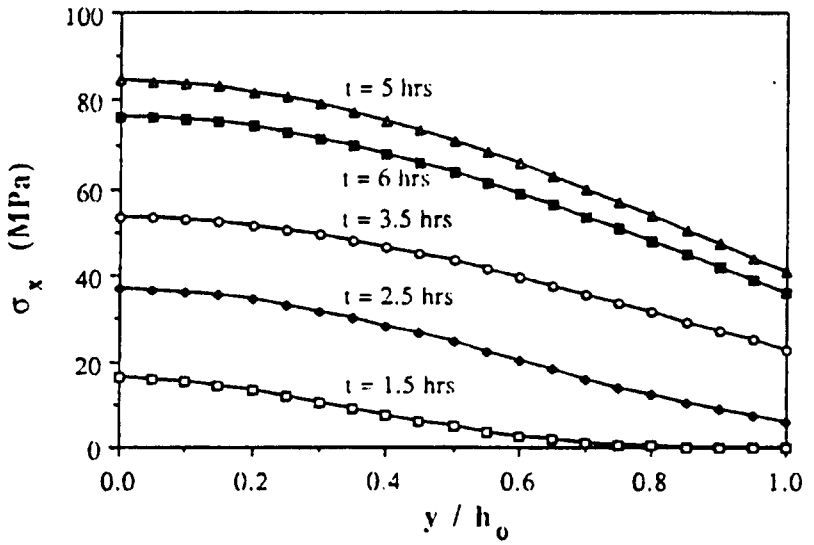

Fig.7 Variation of Stresses through the Slab Thickness

SUMMARY AND CONCLUSIONS

The objective of the present analysis was to incorporate the critical characteristics of a cross-linking thermoset material in the computation of the viscoelastic stresses during its curing process. The objective was reached by formulating an initial boundary value problem for the spatial and temporal curing of a slab of resin exposed to specified autoclave temperatures. The stress-strain law was formulated using time-cure superposition and relaxation integration equations in terms of cure-dependent elastic moduli and shrinkage strains.

Computations indicate that significant tensile stresses are generated shortly after the critical point of sol-gel transition. These stresses result both from the chemical shrinkage as well as thermal shrinkage. The magnitude of stresses in the actual process is observed to be higher than that of the residual stresses.

ACKNOWLEDGEMENT

The research on which this paper is based was made possible by the research grant from the U.S. Army Research Office, Engineering Science Division, Structural Mechanics Branch to the Arizona State University.

REFERENCES

Adolf, D., and Martin, J. E., 1990, "Time-Cure Superposition During Cross-Linking", *Macromolecules*, Vol. 23, pp. 3700-3704.

Bogetti, T. A., and Gillespie, W., Jr., 1989, "Process-Induced Stress and Deformation in Thick-Section Thermosetting Composite Laminates", In *21st International SAMPE Technical Conference*, Atlantic City, N.J.

Coniglio, A., Stanley, H. E., and Klein, W., 1979, "Site-Bond Correlated-Percolation Problem : A Statistical Mechanical Model of Polymer Gelation", *Physical Review Letters*, Vol. 42, pp. 518-522.

deGennes, P. G., 1976, "On a Relation Between Percolation Theory and the Elasticity of Gels", *Journal de Physique Letters*, Vol 37., pp. L1- L2.

deGennes, P. G., 1990, *Introduction to Polymer Dynamics*, Cambridge University Press, New York.

Doi, M. and Edwards, S. F., 1986, *The Theory of Polymer Dynamics*, Oxford Scientific Publication, Clarendon Press, Oxford, UK.

Ferry, J.D., 1961, *Viscolelastic Properties of Polymers*, J. Wiley & Sons, New York, NY.

Flory, P. J., 1941, "Molecular Size Distribution in Three Dimensional Polymers - I & II", *Journal of American Chemical Society*, Vol. 63, pp. 3083-3100.

Flory, P. J., 1953, *Principles of Polymer Chemistry*, Cornell University Press, Ithaca, NY.

Guz', A. N., Tomashevskii, V.T., Shul'ga, N.A. and Iakovlev, V.S., 1988, *Technological Stresses and Deformations in Composite Materials*, Vischa Shkola Publ., Kiev, Ukraine.

Hahn, H.T., and Pagano, N.J., 1976, "Curing Stresses in Composite Laminates", *Journal of Composite Materials*, Vol. 10, pp. 266-277.

Halpin, J. C., Kardos, J. L. and Dudukovic, M. P., 1984, Processing Science: An Approach for Prepreg Composite Systems, in: *Interrelations between Processing Structure and Properties of Polymeric Materials*, J.C. Seferis, P.S. Theocaris, ed., pp.9-22. Elsevier Sci. Publ., Amsterdam.

Herrmann, H. J., Stauffer, D., and Landau, D. P., 1983, "Computer Simulation of a Model for Irreversible Gelation", *Journal of Physics A* , Vol. 16., pp. 1221-1239.

Kuksenko, V. S. and Tamuzs, V. P., 1981, *Fracture Micromechanics of Polymer Materials*, M. Nijhoff Publ., The Hague, Netherlands.

Lee, E. H., and Rogers, T. G., 1963, "Solution of Viscoelastic Stress Analysis Problems Using Measured Creep or Relaxation Functions", *Journal of Applied Mechanics*, Vol. 34, pp. 127-133.

Levitsky, M., and Shaffer, B. W., 1974, "Thermal Stresses in Chemically Hardening Elastic Media with Application to the Molding Process", *Journal of Applied Mechanics*, Vol. 41, pp. 647-651.

Li, N., and Barber, J.H., 1989, "Residual Stresses in Castings with Axisymmetric Solidification", Engineering Science Reprints, 26th Annual Technical Meeting of the Society of Engineering Sciences, An Arbor, MI.

Loos, C. A., and Springer, G. S., 1983, "Curing of Epoxy Matrix Composites", *Journal of Composite Materials*, Vol. 17, pp. 135-169.

Martin, J. E., and Adolf, D., 1990, "Constitutive Equation for Cure-Induced Stresses in a Viscoelastic Material", *Macromolecules*, Vol. 23, pp. 5014-5019.

Martin, J. E., and Adolf, D., 1991, "The Sol-Gel Transition in Chemical Gels", *Annual Reviews of Physical Chemistry*, Vol. 42, pp. 311-339.

Martin, J. E., and Wilcoxon, J. P., 1989, "Spatial Correlations and Growth in Dilute Gels", *Physical Review A*, Vol. 39, pp. 252-258.

Martin, J. E., Douglas, A., and Wilcoxon, J. P., 1989, "Viscoelasticity near the Sol-Gel Transition", *Physical Review A*, Vol. 39, pp. 1325-1332.

Muki, R., and Sternberg, E., 1961, "On Transient Thermal Stresses in Viscoelastic Materials with Temperature-Dependent Properties", *Journal of Applied Mechanics*, Vol. 28, pp. 193-207.

Stauffer, D., Coniglio, A., and Adam, M.,1982, "Gelation and Critical Phenomena", *Advanced Polymer Science*, Vol. 44, pp. 103-158.

Stockmayer, W. H., 1943, "Theory of Molecular Size Distribution and Gel Formation in Branched-Chain Polymers", *The Journal of Chemical Physics*, Vol. 11, pp. 45-55.

Weiner, J. H., and Boley, B. A., 1963, "Elasto-Plastic Thermal Stresses in a Solidifying Body", *Journal of Mechanics and Physics of Solids*, Vol. 11, pp. 145-154.

Weitsman, Y., 1979, "Residual Thermal Stresses Due to Cool-Down of Epoxy-Resin Composites", *Journal of Applied Mechanics*, Vol. 46, pp. 563-567.

AMD-Vol. 132
MD-Vol. 30

RECENT ADVANCES IN DAMAGE MECHANICS AND PLASTICITY

PRESENTED AT
THE ASME SUMMER MECHANICS AND MATERIALS CONFERENCES
TEMPE, ARIZONA
APRIL 28–MAY 1, 1992

SPONSORED BY
THE APPLIED MECHANICS DIVISION AND
THE MATERIALS DIVISION, ASME

EDITED BY
J. W. JU
PRINCETON UNIVERSITY

THE AMERICAN SOCIETY OF MECHANICAL ENGINEERS
345 East 47th Street ■ United Engineering Center ■ New York, N.Y. 10017

AMD-Vol. 132/MD-Vol.30, Recent Advances in
Damage Mechanics and Plasticity
ASME 1991

FIBER CLUSTERING DURING THE CURING OF COMPOSITE MATERIALS

Marc P. Mignolet
Department of Mechanical and Aerospace Engineering
Arizona State University
Tempe, Arizona

ABSTRACT

In an attempt to explain the phenomenon of fiber clustering, the low Reynolds number flow through an array of rigid cylinders is investigated. Both cases of a regular and a slightly perturbed array of cylinders are studied. In particular, the forces exerted on the cylinders by the fluid are derived for both cases and a stability analysis is conducted to predict the motion of the array.

INTRODUCTION

The design of a manufacturing process that lead to composite materials possessing optimal properties represents an important technological challenge. One of the difficulties that are often encountered is the lack of uniformity of the distribution of fibers in the matrix. This generic problem which affects both short and continuous fibers composites originates in particular in the flow of the resin through the arrangement of fibers. Consider for example the process of impregnation of thermoplastic composites which starts with the introduction of a polymeric matrix into a fiber tow. As a result of heating, the matrix softens and starts flowing into the spaces separating the adjacent fiber tows. While flowing through the "channels" formed by the adjacent tows the viscous mass exerts significant pressures and shears on the tows which may cause both their flexure and rigid body displacement. This process may lead to concentration of fibers into small areas, or clusters, and to the formation of matrix-rich domains which are almost devoid of fibers. One of the possible explanation of this phenomenon associates the fiber clustering with an initial irregularity of the array of fibers. The goal of the present investigation is to test the validity of this mechanism. To this end, the motion of a fluid (the resin) through an array of cylinders (the fibers) will be investigated. In particular, the present study will focus on the determination of the change in the forces exerted by the fluid on the cylinders as they move away from their initially regular arrangement. Finally, these results will be used to test the stability of the entire array of fibers.

THE FLOW EQUATIONS

The fluid flow past an array of cylinders has been the subject of a large number of both theoretical and experimental investigations. The two limiting cases of a fully turbulent flow, corresponding to a very large Reynolds number(see Chen et al. (1990), Conca et al. (1990) and references therein), and of a creeping motion, modeling to very low Reynolds number situation (see in particular Tamada and Fujikawa (1957), Miyagi (1958), Hasimoto (1959), Kirsch and Fuchs (1967), Happel and Brenner (1973), White (1974), Drummond and Tahir (1984) and references therein) have been especially emphasized. In the context of the manufacturing of thermo-

plastics it is found that a low mean velocity, U, a high kinematic viscosity, ν, and a small diameter of the fibers, D, lead to a very small Reynolds number

$$Re = \frac{U D}{\nu} \ll 1 \tag{1}$$

The theory of linear creeping flows thus represents an appropriate framework for the present analysis.

The derivation of the flow equations corresponding to the limiting case of a very small Reynolds number is a classical topic of fluid mechanics. Neglecting all inertia terms Stokes first showed that the continuity and momentum equations reduced to

$$div\ \underline{V} = 0 \tag{2}$$

and

$$\mu\ \nabla^2 \underline{V} = \nabla P \tag{3}$$

where $\underline{V}$ and P are the velocity and the pressure fields, respectively. Further, the symbol μ denotes the dynamic viscosity which is defined as

$$\mu = \rho\ \nu \tag{4}$$

where ρ is the mass density of the fluid. Introducing the vorticity vector $\underline{\omega}$ as

$$\underline{\omega} = curl\ \underline{V} \tag{5}$$

it is readily shown that Eq. (2) and (3) can be rewritten in the form

$$\nabla^2 P = 0 \tag{6}$$

and

$$\nabla^2 \underline{\omega} = \underline{0} \tag{7}$$

A series of investigations (see White (1974) and Happel and Brenner 1973, for details) have shown that Eq. (6) and (7) lead, in the case of the three-dimensional flows around immersed bodies to accurate estimates of the flow characteristics, in particular the drag and lift forces in a large domain surrounding the body. In the far field, however, Stokes' equation predicts inertia terms that are not negligible, as was initially assumed in the derivation of Eq. (3). Further, the solution of plane flow problems by relying on Eq. (7) is affected by Stokes' paradox: it is not always possible to find a steady solution in Eq. (6) and (7) that also satisfies the boundary conditions in the surface of the immersed body (no-slip condition) and in the far-field. These weaknesses of Stokes' equation have led Oseen to conserve the inertia term $\rho\ U \frac{\partial \underline{V}}{\partial x}$ in the formulation, leading to the following steady momentum equation

$$\rho\ U \frac{\partial \underline{V}}{\partial x} = -\nabla P + \mu\ \nabla^2 \underline{V} \tag{8}$$

The above relation, at the contrary of Stokes' equation, leads to a uniformly valid approximation of the three dimensional fluid flow around an immersed body. Further, it admits steady two dimensional solutions that satisfy the required boundary conditions on the immersed body and in the far-field. Notwithstanding these advantages, it should be noted that Stokes' and Oseen's equations, Eq. (7) and (8), both represent zeroth order approximations of the Navier-Stokes equations corresponding to a low Reynolds number.

Thus, it cannot in general be inferred that the use of Eq. (8) will lead to estimates of the forces acting on the body that are more accurate than the corresponding approximations derived from Eq. (7). (Happel and Brenner, 1973). In the context of the flow through a perturbed array of fibers, this observation indicates that the simplest of the two momentum equations, that is Eq. (7), be used provided that it yields an acceptable flow field. The lack of a fluid only "far field" and the existence of a Stokes' creeping flow through a regular arrangement of cylinders (see Hasimoto, 1959, Sangani and Acrivos, 1982, Drummond and Tahir, 1984) suggest that Stokes' paradox will not be present. Consequently, Eq. (7) will indeed yield the required low Reynolds number approximation.

ASSUMED SOLUTION

In the case of a three-dimensional flow, the vorticity vector can be written in the form

$$\underline{\omega}^T = \left[0,\ 0,\ \omega_z\right] \tag{9}$$

with

$$\omega_z = \frac{\partial v}{\partial x} - \frac{\partial u}{\partial y} \tag{10}$$

where u and v denote the components of the velocity in the plane of motion,

$$\underline{V} = \left[u, v, 0\right]. \tag{11}$$

Introducing the polar coordinates (r,θ), it can be shown that the solutions of Eq. (7) and (9) admit the representations

$$\omega_z = F_1\theta\ln r + F_2\ln r + F_3\theta + F_4 + \sum_{m=1}^{\infty}\left(B_m r^m e^{im\theta} + C_m r^m e^{-im\theta} + D_m r^{-m} e^{im\theta} + E_m r^{-m} e^{-im\theta}\right) \tag{12}$$

where B_m, C_m, D_m, E_m, $m=1,\ldots$ and F_1, F_2, F_3, F_4 arbitrary constants. The single-valuedness of the vorticity component ω_z under a rotation by an angle 2π around the z-axis requires that the coefficients F_1 and F_3 be identically zero. Further, imposing that ω_z vanish at infinity, $r=\infty$, leads to the condition

$$C_2 = C_4 = 0 \tag{13}$$

and

$$D_m = E_m = 0\,,\ m = 1,\ldots \tag{14}$$

Finally, the real character of the vorticity vector for all values of r and θ requires that the constants B_m and C_m be complex conjugates of each other, or

$$C_m = \bar{B}_m\,,\ m = 1,\ldots \tag{15}$$

Under these conditions, it is found that ω_z can be expressed in the form

$$\omega_z = \sum_{m=1}^{\infty}\left(B_m r^m e^{im\theta} + \bar{B}_m r^m e^{-im\theta}\right) = \sum_{m=1}^{\infty}\left(\frac{B_m}{z^m} + \frac{\bar{B}_m}{\bar{z}^m}\right) \tag{16}$$

where

$$z = x + i\,y = r\,e^{i\theta}. \tag{17}$$

The next step of the analysis consists in the determination of the velocity field $\underline{V}$ that corresponds to the vorticity component ω_z, Eq. (16). This computation is greatly simplified by introducing first the complex velocity W as

$$W = u - i\,v \tag{18}$$

and noting that

$$\frac{\partial W}{\partial \bar{z}} = \frac{1}{2}\left(\frac{\partial}{\partial x} + i\,\frac{\partial}{\partial y}\right)\left(u - i\,v\right) = \frac{1}{2}\left[\left(\frac{\partial u}{\partial x} + \frac{\partial v}{\partial y}\right) - i\left(\frac{\partial v}{\partial x} - \frac{\partial u}{\partial y}\right)\right] = -\frac{i}{2}\,\omega_z \tag{19}$$

where the last equality results from Eq. (2) and (10). Then integrating Eq. (16) with respect to $\bar{z}$ yields

$$W = \frac{1}{2i}\left[\sum_{m=1}^{\infty}\left(\frac{B_m\,\bar{z}}{z^m} - \frac{\bar{B}_m}{(m-1)\,\bar{z}^{m-1}}\right) + B_1\,\frac{\bar{z}}{z} + \bar{B}_1\ln\bar{z}\right] + \sum_{m=1}^{\infty}\frac{A_m}{z^m} + \frac{1}{2i}\,\bar{B}_1\ln z \tag{20}$$

where A_m, $m=1,\ldots$ are arbitrary complex constants. Note that the term $\frac{1}{2i}\bar{B}_1\ln z$ is required to produce single-valued velocity components u and v.

The singularity displayed by the flow field, Eq. (20), at $z=0$ is clearly inadmissible unless that point does not belong to the fluid domain. More precisely, it can be argued that this point must coincide with the center of one of the fibers. Symmetry considerations dictate, however, that no one cylinder have a privileged role in the analysis. Thus, there must be a singularity of the flow field, Eq. (20), at the center of each fiber and (see also Tamada and Fujikawa, 1957, Drummond and Tahir, 1984)

$$W = \sum_{p}\sum_{q} W_{pq} \tag{21a}$$

where

$$W_{pq} = \frac{1}{2i}\left[\sum_{m=2}^{\infty}\left(\frac{B_m^{pq}(\bar{z}-\bar{s}_{pq})}{(z-s_{pq})^m} - \frac{\bar{B}_m^{pq}}{(m-1)(\bar{z}-\bar{s}_{pq})^{m-1}}\right) + B_1^{pq}\frac{(\bar{z}-\bar{s}_{pq})}{(z-s_{pq})} + \bar{B}_1^{pq}\ln\left|\frac{z-s_{pq}}{s_{pq}}\right|^2 + \sum_{m=0}^{\infty}\frac{A_m^{pq}}{(z-s_{pq})^m}\right]. \tag{21b}$$

In the above relation, the double summation over the cylinder indices p and q extends over the entire array and s_{pq} denotes, as in Fig. 1, the complex number associated with the position vector of the fiber in the p^{th} column and the q^{th} row.

The boundary conditions, to be described next, will provide the necessary equations to compute the values of the complex coefficients A_m^{pq} and B_m^{pq} corresponding to each of the fibers (p,q), thus completing the determination of the velocity field in the array. Once this information is available, it is quite simple to determine the pressure field and the forces extended on the cylinders. Specifically, note first from Eq. (3) that

$$\mu\,\nabla^2 W = \mu\left(\nabla^2 u - i\,\nabla^2 v\right) = \mu\left(\frac{\partial P}{\partial x} - i\,\frac{\partial P}{\partial y}\right) = 2\,\frac{\partial P}{\partial \bar{z}}. \tag{22}$$

Then, using the identity

$$\nabla^2 W = 4\,\frac{\partial^2 W}{\partial z\,\partial \bar{z}} \tag{23}$$

and integrating Eq. (22) over z, it is found that

$$P = 2\,\mu\,\frac{\partial W}{\partial \bar{z}} + g(\bar{z}) = -i\,\mu\,\omega_z + g(\bar{z}) \tag{24}$$

where $g(\bar{z})$ denotes a function of $\bar{z}$ such that the corresponding pressure field P is real. Finally, the complex force acting on the fiber pq can be evaluated as (Miyagi, 1958)

$$F^{pq} = F_1^{pq} + i\,F_2^{pq} = \int_{pq}(i\,p + \mu\,\omega)\,dz \tag{25}$$

where the notation $\int_{pq}$ denotes the integral over the contour of the circle pq. Combining Eq. (24) and (25), it is found that

$$F^{pq} = i\int_{pq} g(\bar{z})\,dz + 2\,\mu\int_{pq}\omega\,dz = 4\,i\,\pi\,\mu\,B_1^{pq}. \tag{26}$$

NO-SLIP BOUNDARY CONDITIONS

To give rise to a bonafide velocity distribution, the constants A_m^{pq} and B_m^{pq} must yield vanishing components u and v on the exterior surface of each fiber. Denoting by a the common radius of the fibers, it is then required that

$$W = 0 \quad \text{for } z = s_{rs} + a\,e^{i\theta} \tag{27}$$

at every angle θ and for all cylinder indices p and q. Combining Eq. (21) and (27) and expanding the terms $(s_{rs} - s_{pq} + a\,e^{i\theta})^{-m}$ and $\ln\left|s_{rs} - s_{pq} + a\,e^{i\theta}\right|^2$ in the form

$$(s_{rs} - s_{pq} + a\,e^{i\theta})^{-m} = (s_{rs} - s_{pq})^{-m}\sum_{t=0}^{\infty}\binom{-m}{t}\left[\frac{a}{s_{rs} - s_{pq}}\right]^t e^{it\theta} \qquad \text{for } (r,s)\neq(0,0) \tag{28}$$

and

$$\ln\left|s_{rs} - s_{pq} + a\,e^{i\theta}\right|^2 = \ln\left|s_{rs} - s_{pq}\right|^2 + \sum_{t=1}^{\infty}\frac{(-1)^{t-1}}{t}\left[\frac{a}{s_{rs} - s_{pq}}\right]^t e^{it\theta} + \sum_{t=1}^{\infty}\frac{(-1)^{t-1}}{t}\left[\frac{a}{\bar{s}_{rs} - \bar{s}_{pq}}\right]^t e^{-it\theta} \qquad \text{for } (r,s)\neq(0,0) \tag{29}$$

yields a Fourier-like expansion of W involving the powers of $e^{i\theta}$. Since the functions $e^{it\theta}$ form a basis over the domain $\theta\in[0,2\pi]$, it is necessary, to satisfy Eq. (27), that the coefficient of each power $e^{it\theta}$ in the expansion of W be set to zero. That is,

$$\sum_{\substack{p,q\\(p,q)\neq(0,0)}}\left[\sum_{m=0}^{\infty}\frac{A_m^{pq}}{(z_{ij}-z_{pq})^m}+\frac{1}{2i}B_1^{pq}\left[\frac{\bar z_{ij}-\bar z_{pq}}{z_{ij}-z_{pq}}\right]-\frac{1}{2i}B_1^{pq}\left[\frac{a}{z_{ij}-z_{pq}}\right]^2+\frac{1}{2i}\bar B_1^{pq}\ln\left|\frac{z_{ij}-z_{pq}}{z_{pq}}\right|\right.$$
$$\left.+\sum_{m=2}^{\infty}\frac{B_m^{pq}}{2i}\left[\frac{(\bar z_{ij}-\bar z_{pq})}{(z_{ij}-z_{pq})^m}-\frac{m\,a^2}{(z_{ij}-z_{pq})^{m+1}}\right]-\sum_{m=2}^{\infty}\frac{\bar B_m^{pq}}{2i\,(m-1)\,(\bar z_{ij}-\bar z_{pq})^{m-1}}+A_0''+\frac{\bar B_1''}{i}\ln a=0 \tag{30}$$

$$\sum_{\substack{p,q\\(p,q)\neq(0,0)}}\left[\sum_{m=1}^{\infty}\frac{A_m^{pq}}{(z_{ij}-z_{pq})^{m+t}}a^t\binom{-m}{t}+\frac{1}{2i}B_1^{pq}\left[\frac{(\bar z_{ij}-\bar z_{pq})(-a)^t}{(z_{ij}-z_{pq})^{t+1}}\right.\right.$$
$$\left.+(-1)^{t+1}\left[\frac{a}{z_{ij}-z_{pq}}\right]^{t+2}\right]+\frac{1}{2i}\bar B_1^{pq}\frac{(-1)^{t+1}}{t}\left[\frac{a}{(z_{ij}-z_{pq})}\right]^t$$
$$\left.+\sum_{m=2}^{\infty}\frac{B_m^{pq}}{2i}\left[\frac{(\bar z_{ij}-\bar z_{pq})\,a^t}{(z_{ij}-z_{pq})^{m+t}}\binom{-m}{t}+\frac{a^{t+2}}{(z_{ij}-z_{pq})^{m+t+1}}\binom{-m}{t+1}\right]\right]-\frac{1}{2i}\frac{\bar B_{t+1}''}{t\,a^t}=0 \tag{31}$$

$$\sum_{\substack{p,q\\(p,q)\neq(0,0)}}\left[\frac{B_1^{pq}}{2i}\frac{a}{(z_{ij}-z_{pq})}+\frac{\bar B_1^{pq}}{2i}\frac{a}{(\bar z_{ij}-\bar z_{pq})}+\sum_{m=2}^{\infty}\frac{B_m^{pq}a}{2i\,(z_{ij}-z_{pq})^m}+\sum_{m=2}^{\infty}\frac{\bar B_m^{pq}}{2i}\frac{a}{(\bar z_{ij}-\bar z_{pq})^m}\right]+\frac{A_1''}{a}=0 \tag{32}$$

$$\sum_{\substack{p,q\\(p,q)\neq(0,0)}}\left[-\frac{\bar B_1^{pq}}{2i}\left[\frac{a}{(\bar z_{ij}-\bar z_{pq})}\right]^2-\sum_{m=2}^{\infty}\frac{\bar B_m^{pq}}{2i}\frac{m\,a^2}{(\bar z_{ij}-\bar z_{pq})^{m+1}}\right]+\frac{A_2''}{a^2}+\frac{1}{2i}B_1''=0 \tag{33}$$

$$\sum_{\substack{p,q\\(p,q)\neq(0,0)}}\left[-\frac{\bar B_1^{pq}}{2i}\frac{(-1)^t}{t}\left[\frac{a}{(\bar z_{ij}-\bar z_{pq})}\right]^t-\sum_{m=2}^{\infty}\frac{\bar B_m^{pq}}{2i}\binom{-m+1}{t}\frac{a^t}{(m-1)\,(\bar z_{ij}-\bar z_{pq})^{m+t-1}}\right]$$
$$+\frac{A_t''}{a^t}+\frac{B_{t+1}''}{2i}\frac{1}{a^{t+2}}=0 \tag{34}$$

FLOW PAST A REGULAR ARRAY

It will be seen in the next section that the determination of the flow past a perturbed array of cylinders requires the knowledge of the corresponding solution for a regular arrangement. The latter flow field can be determined either by relying on the power series expressions derived by Drummond and Tahir (1984) or by a direct application of Eq. (31)-(34). In the case of a regular array, it is expected that the cylinders all have an identical effect on the flow, or equivalently, that

$$B_m^{pq}=B_m^0 \quad \text{for } all\ p \text{ and } q \text{ and } m=1,\ldots \tag{35}$$

and

$$A_m^{pq}=A_m^0 \quad \text{for } all\ p \text{ and } q \text{ and } m=1,\ldots \tag{36}$$

for some complex numbers A_m^0 and B_m^0. Then, introducing Eq. (35) and (36) in Eq. (31)-(34) yields the following linear system of equations

$$\sum_{m=1}^{\infty}A_m^0\,a^t\binom{-m}{t}F_{m+t}(0,0)+\frac{B_1^0}{2i}\left[(-a)^t\,G_{t+1}(0,0)+(-1)^{t+1}a^{t+2}F_{t+2}(0,0)\right]+\frac{\bar B_1^0}{2i}\left[\frac{(-1)^{t-1}}{t}a^t\,F_t(0,0)\right]$$
$$+\sum_{m=2}^{\infty}\frac{B_m^0}{2i}\left[\binom{-m}{t}a^t\,G_{m+t}(0,0)+\binom{-m}{t+1}a^{t+2}F_{m+t+1}(0,0)\right]-\frac{1}{t\,a^t}\frac{\bar B_{t+1}^0}{2i}=0 \tag{37}$$

$$\frac{A_1^0}{a} + a\,\frac{B_1^0}{2i}\,F_1(0,0) + a\,\frac{\bar{B}_1^0}{2i}\,\overline{F_1(0,0)} + \sum_{m=2}^{\infty}\frac{B_m^0}{2i}\,a\,F_m(0,0) + \sum_{m=2}^{\infty}\frac{\bar{B}_m^0}{2i}\,a\,\overline{F_m(0,0)} = 0 \tag{38}$$

$$\frac{A_2^0}{a^2} + \frac{B_1^0}{2i} - \frac{\bar{B}_1^0}{2i}\,\frac{a^2}{2}\,\overline{F_2(0,0)} - \sum_{m=2}^{\infty}\frac{\bar{B}_m^0}{2i}\,\frac{m\,a^2}{2}\,\overline{F_{m+1}(0,0)} = 0 \tag{39}$$

and

$$\frac{A_l^0}{a^l} + \frac{1}{a^{l-2}}\,\frac{B_{l-1}^0}{2i} - \frac{\bar{B}_1^0}{2i}\left[\frac{(-a)^l}{l}\,\overline{F_l(0,0)}\right] - \sum_{m=2}^{\infty}\frac{\bar{B}_m^0}{2i}\left[\binom{-m+1}{l}\,\frac{a^l}{(m-1)}\,\overline{F_{m+l-1}(0,0)}\right] = 0. \tag{40}$$

In the above equations, the symbols $F_m(0,0)$ and $G_m(0,0)$ have been used for brevity to designate the following series

$$F_m(0,0) = \sum_{\substack{p\,q\\(p,q)\neq(0,0)}} \frac{1}{s_{pq}^m} \qquad m = 1,\ldots \tag{41}$$

and

$$G_m(0,0) = \sum_{\substack{p\,q\\(p,q)\neq(0,0)}} \frac{\bar{s}_{pq}}{s_{pq}^m} \qquad m = 2,\ldots \tag{42}$$

where the summation over the indices p and q extends over the entire array with the exception of the cylinder 00. It should be noted that the coefficients $F_m(0,0)$ and $G_m(0,0)$ are affected by convergence problems. In particular, $F_2(0,0)$ and $G_3(0,0)$ are indeterminate; their values depend on the order of summation. Drummond and Tahir (1984) have resolved this issue by using symmetries. For the geometries that they considered, (unstaggered array, triangular and square staggered arrays) they have proved that the appropriate values of the coefficients $F_m(0,0)$ and $G_m(0,0)$ are obtained by performing first the summation perpendicular to the mean flow.

The determination of the coefficients A_m^0 and B_m^0 requires a final, scaling condition specifying, for example, the mean fluid velocity across the array (see Drummond and Tahir, 1984, for details).

FLOW PAST A PERTURBED ARRAY

The determination of the fluid flow past an arbitrary irregular array of cylinders can be obtained as in the case of a regular arrangement, by relying on Eq. (30)-(34). Because of the lack of symmetry in the positioning of the fibers, the simplifying assumptions given by Eq. (35) and (36) will however cease to be valid and a severe increase in the level of complexity of the analysis will result. In this respect, note that an investigation of the stability of the array requires only the knowledge of the fluid flow past a slightly perturbed array the cylinders of which are located at the points

$$s'_{pq} = s_{pq} + \delta s_{pq}. \tag{43}$$

In this relation, the symbol s_{pq} denotes the position of the cylinder pq in the regular array while δs_{pq} represents its small mispositioning. Introducing equation (43) in Eq. (30)-(34) and linearizing the resulting relations provides a first order approximation of the forces being exerted on the cylinders as a result of their motions. Retaining only the linear term in δs_{pq}, it is found that the principle of superposition holds; the forces resulting from the mispositioning of two or more cylinders equal the sum of the contributions corresponding to each of the displacements δs_{pq} as if they were acting alone.

This observation implies that the analysis can be conducted by considering that only one cylinder, with indices $p = q = 0$, is not in place, that is

$$\delta s_{pq} = 0 \quad \text{for } (p,q) \neq (0,0) \tag{44}$$

Then, the coefficients A_m^{pq} and B_m^{pq} can be expressed in the form

$$A_m^{pq} = A_m^0 + \delta A_m^{pq} \tag{45}$$

and

$$B_m^{pq} = B_m^0 + \delta B_m^{pq} \tag{46}$$

where δA_m^{pq} and δB_m^{pq} are the small perturbation terms corresponding to the mispositioning δs_{m0}. Further, to account for the finite memory of the fluid, it will be required that

$$\delta A_m^{pq} \to 0 \quad as\ p\ and/or\ q \to \pm\infty \tag{47}$$

and

$$\delta B_m^{pq} \to 0 \quad as\ p\ and/or\ q \to \pm\infty. \tag{48}$$

Letting r and/or s tend toward infinity in Eq. (30), it is readily found that Eq. (47) and (48) imply that

$$\sum_p \sum_q \delta A_m^{pq} = 0 \tag{49}$$

and

$$\sum_p \sum_q \delta B_m^{pq} = 0. \tag{50}$$

Even with the above simplifying assumption, the solution of Eq.(30)-(34) appears to be quite cumbersome since there exists in general a different set of coefficients δA_m^{pq} and δB_m^{pq} for each cylinder pq. To this end, note that every double summation term appearing in Eq. (30)-(34) is in fact expressible as a discrete three-dimensional Fourier convolution. Thus, it can be expected that the solution procedure for the coefficients δA_m^{pq} and δB_m^{pq} be greatly simplified by introducing the Fourier transforms

$$\delta B_m(\theta,\phi) = \sum_p \sum_q \delta B_m^{pq}\, e^{ip\theta}\, e^{iq\phi} \tag{51}$$

and

$$\delta A_m(\theta,\phi) = \sum_p \sum_q \delta A_m^{pq}\, e^{ip\theta}\, e^{iq\phi}. \tag{52}$$

In fact, combining Eq. (30)-(34) and (43)-(52), it can be shown that

$$\begin{aligned}
&\sum_{m=1}^{\infty} F_m(\theta,\phi)\,\delta A_m(\theta,\phi) - \left[a^2 F_2(\theta,\phi) - \frac{H(\theta,\phi)}{(1-e^{i\theta})(1-e^{i\phi})}\right]\frac{\delta B_1(\theta,\phi)}{2i} - \sum_{m=2}^{\infty}\left[\frac{\overline{F_{m-1}(-\theta,-\phi)}}{(m-1)}\right]\frac{\overline{\delta B_m(-\theta,-\phi)}}{2i} \\
&+ \left[\ln a^2 + \frac{L(\theta,\phi)}{(1-e^{i\theta})(1-e^{i\phi})}\right]\frac{\overline{\delta B_1(-\theta,-\phi)}}{2i} - \sum_{m=2}^{\infty}\left[m\,a^2 F_{m+1}(\theta,\phi) - G_m(\theta,\phi)\right]\delta B_m(\theta,\phi) = \\
&\qquad - \delta s_{m0}\frac{B_1^0}{2i}\left[-2a^2 F_1(\theta,\phi) - 2a^2 F_1(0,0) + G_2(\theta,\phi) + G_2(0,0)\right] \\
&\qquad - \sum_{m=1}^{\infty} m\,\delta s_{m0} A_m^0\left[F_{m+1}(\theta,\phi) + (-1)^m F_{m+1}(0,0)\right] + \overline{\delta s_{m0}}\frac{B_1^0}{2i}\left[F_1(\theta,\phi) + F_1(0,0)\right] \\
&\qquad - \sum_{m=2}^{\infty}\frac{B_m^0}{2i}\left\{m\,\delta s_{m0}\left[G_{m+1}(\theta,\phi) + (-1)^{m-1}G_{m+1}(0,0) - a^2(m+1)\left[F_{m+2}(\theta,\phi) + (-1)^{m+1}F_{m+2}(0,0)\right]\right]\right. \\
&\qquad\qquad \left. - \overline{\delta s_{m0}}\left[F_m(\theta,\phi) + (-1)^{m-1}F_m(0,0)\right]\right\} \\
&\qquad - \sum_{m=2}^{\infty}\frac{\overline{B_m^0}}{2i}\,\overline{\delta s_{m0}}\left[\overline{F_m(-\theta,-\phi)} + (-1)^{m-1}\overline{F_m(0,0)}\right] - \overline{\delta s_{m0}}\frac{\overline{B_1^0}}{2i}\left[\overline{F_1(-\theta,-\phi)} + \overline{F_1(0,0)}\right] \\
&\qquad\qquad - \delta s_{m0}\frac{\overline{B_1^0}}{2i}\left[F_1(\theta,\phi) + F_1(0,0)\right] \qquad (53) \\
&\sum_{m=1}^{\infty}\left[a^t\binom{-m}{t}F_{m-t}(\theta,\phi)\right]\delta A_m(\theta,\phi) + \sum_{m=2}^{\infty} a^t\left[\left[\binom{-m}{t}G_{m-t}(\theta,\phi) + a^2\binom{-m}{t+1}F_{m-t+1}(\theta,\phi)\right]\frac{\delta B_m(\theta,\phi)}{2i}\right. \\
&\left. - \frac{1}{t\,a^t}\frac{\overline{\delta B_{t+1}(-\theta,-\phi)}}{2i} + \left[(-1)^t a^t G_{t+1}(\theta,\phi) + (-1)^{t+1}a^{t+2}F_{t+2}(\theta,\phi)\right]\frac{\delta B_1(\theta,\phi)}{2i} - \frac{(-a)^t}{t}F_t(\theta,\phi)\frac{\overline{\delta B_1(\theta,\phi)}}{2i}\right] = \\
&- \delta s_{m0}\sum_{m=1}^{\infty}\left[\binom{-m}{t}a^t A_m^0\left[F_{m-t+1}(\theta,\phi) + (-1)^{m-t}F_{m-t+1}(0,0)\right] - (-a)^t\frac{B_1^0}{2i}\left[(t+1)\delta s_{m0}\left[G_{t+2}(\theta,\phi) + (-1)^t G_{t+2}(0,0)\right]\right.\right. \\
&\left.\left. - a^2(t+2)\,\delta s_{m0}\left[F_{t+3}(\theta,\phi) + (-1)^t F_{t+3}(0,0)\right] - \overline{\delta s_{m0}}\left[F_{t+1}(\theta,\phi) + (-1)^t F_{t+1}(0,0)\right]\right.\right.
\end{aligned}$$

$$- \sum_{m=2}^{\infty} \begin{Bmatrix} -m \\ l \end{Bmatrix} a^l \frac{B_m^0}{2i} \left[(m+l)\, \delta s_{00} \left\{ G_{m+l,1}(\theta,\phi) + (-1)^{m+l-1} G_{m+l,1}(0,0) \right\} - \overline{\delta s_{00}} \left\{ F_{m+l}(\theta,\phi) + (-1)^{m+l-1} F_{m+l}(0,0) \right\} \right]$$

$$+ a^2 \begin{Bmatrix} -m \\ l+1 \end{Bmatrix} \delta s_{00} (m+l+1) \left\{ F_{m+l+2}(\theta,\phi) + (-1)^{m+l+1} F_{m+l+2}(0,0) \right\} - (-a)^l \frac{\bar{B}_1^0}{2i} \delta s_{00} \left\{ F_{l+1}(\theta,\phi) + (-1)^l F_{l+1}(0,0) \right\} \tag{54}$$

$$\frac{\delta A_1(\theta,\phi)}{a} + \sum_{m=1}^{\infty} a\, F_m(\theta,\phi) \frac{\delta B_m(\theta,\phi)}{2i} + \sum_{m=1}^{\infty} a\, \overline{F_m(-\theta,-\phi)} \frac{\overline{\delta B_m(-\theta,-\phi)}}{2i}$$

$$= - a\, \delta s_{00} \left[\sum_{m=1}^{\infty} \frac{B_m^0}{2i} m \left\{ F_{m+1}(\theta,\phi) + (-1)^m F_{m+1}(0,0) \right\} \right]$$

$$- a\, \overline{\delta s_{00}} \left[\sum_{m=1}^{\infty} \frac{\bar{B}_m^0}{2i} m \left\{ \overline{F_{m+1}(-\theta,-\phi)} + (-1)^m \overline{F_{m+1}(0,0)} \right\} \right] \tag{55}$$

$$\frac{1}{a^2} \delta A_2(\theta,\phi) - \sum_{m=2}^{\infty} \left[\frac{m\, a^2}{2} \overline{F_{m+1}(-\theta,-\phi)} \right] \frac{\overline{\delta B_m(-\theta,-\phi)}}{2i} + \frac{\delta B_1(\theta,\phi)}{2i} - \left[\frac{a^2}{2} \overline{F_2(-\theta,-\phi)} \right] \frac{\overline{\delta B_1(-\theta,-\phi)}}{2i}$$

$$= \overline{\delta s_{00}} \sum_{m=1}^{\infty} \frac{\bar{B}_m^0}{2i} \frac{m\,(m+1)\, a^2}{2} \left\{ \overline{F_{m+2}(-\theta,-\phi)} + (-1)^{m+1} \overline{F_{m+2}(0,0)} \right\} \tag{56}$$

and

$$\frac{1}{a^l} \delta A_l(\theta,\phi) + \frac{1}{a^{l-2}} \frac{\delta B_{l-1}(\theta,\phi)}{2i} - \sum_{m=2}^{\infty} \left[\begin{Bmatrix} -m+1 \\ l \end{Bmatrix} \frac{a^l}{(m-1)} \overline{F_{m+l-1}(-\theta,-\phi)} \right] \frac{\overline{\delta B_m(-\theta,-\phi)}}{2i}$$

$$- \frac{(-a)^l}{l} \overline{F_l(-\theta,-\phi)} \frac{\overline{\delta B_1(-\theta,-\phi)}}{2i} = \overline{\delta s_{00}} \left[(-a)^l \frac{\bar{B}_1^0}{2i} \left\{ \overline{F_{l+1}(-\theta,-\phi)} + (-1)^l \overline{F_{l+1}(0,0)} \right\} \right.$$

$$\left. + \sum_{m=2}^{\infty} \begin{Bmatrix} -m+1 \\ l \end{Bmatrix} a^l \frac{(m+l-1)}{(m-1)} \frac{\bar{B}_m^0}{2i} \left\{ \overline{F_{m+l}(-\theta,-\phi)} + (-1)^{m+l-1} \overline{F_{m+l}(0,0)} \right\} \right] \tag{57}$$

where

$$F_m(\theta,\phi) = \sum_{\substack{r,s \\ (r,s)\neq(0,0)}} \frac{1}{s_{rs}^m} e^{ir\theta} e^{is\phi} \qquad m = 1,\ldots \tag{58}$$

and

$$G_m(\theta,\phi) = \sum_{\substack{r,s \\ (r,s)\neq(0,0)}} \frac{\bar{s}_{rs}}{s_{rs}^m} e^{ir\theta} e^{is\phi} \qquad m = 2,\ldots \tag{59}$$

$$H(\theta,\phi) = \sum_{r,s} \left[\frac{\bar{s}_{rs}}{s_{rs}} - \frac{\bar{s}_{(r-1)s}}{s_{(r-1)s}} - \frac{\bar{s}_{r(s-1)}}{s_{r(s-1)}} + \frac{\bar{s}_{(r-1)(s-1)}}{s_{(r-1)(s-1)}} \right] e^{ir\theta} e^{is\phi} \tag{60}$$

$$L(\theta,\phi) = \sum_{r,s} \ln \left| \frac{s_{rs}\, s_{(r-1)(s-1)}}{s_{(r-1)s}\, s_{r(s-1)}} \right|^2 e^{ir\theta} e^{is\phi}. \tag{61}$$

Note in Eq. (60) and (61) that the terms $\frac{\bar{s}_{rs}}{s_{rs}}$ and $\ln \left| s_{rs} \right|^2$ are ignored if $(r,s)=(0,0)$. Further, the convention on the order of summation, already discussed in connection with the flow past a regular array, is also selected here. Finally, note from Eq. (50) and (51), that

$$\delta B_1(0,0) = 0. \tag{62}$$

STABILITY ANALYSIS

The solution of Eq. (53)-(57) provides a representation of the coefficients δB_ν and of the associated function $\delta B_1(\theta,\phi)$ in the form

$$\delta B_\nu = \alpha_\nu\, \delta s_{00} + \beta_\nu\, \overline{\delta s_{00}} \tag{63}$$

$$-\sum_{m=2}^{\infty}\binom{-m}{l}a^{l}\frac{B_m^0}{2i}\left[(m+l)\,\delta s_{00}\left\{G_{m+l}(\theta,\phi)+(-1)^{m+l-1}G_{m+l}(0,0)\right\}-\overline{\delta s_{00}}\left\{F_{m+l}(\theta,\phi)+(-1)^{m+l-1}F_{m+l}(0,0)\right\}\right.$$
$$\left.+a^{2}\binom{-m}{l+1}\delta s_{00}(m+l+1)\left\{F_{m+l+2}(\theta,\phi)+(-1)^{m+l+1}F_{m+l+2}(0,0)\right\}\right]-(-a)^{l}\frac{\bar{B}_l^0}{2i}\delta s_{00}\left\{F_{l+1}(\theta,\phi)+(-1)^{l}F_{l+1}(0,0)\right\} \tag{54}$$

$$\frac{\delta A_1(\theta,\phi)}{a}+\sum_{m=1}^{\infty}a\,F_m(\theta,\phi)\frac{\delta B_m(\theta,\phi)}{2i}+\sum_{m=1}^{\infty}a\,\overline{F_m(-\theta,-\phi)}\,\frac{\overline{\delta B_m(-\theta,-\phi)}}{2i}$$
$$=-a\,\delta s_{00}\left[\sum_{m=1}^{\infty}\frac{B_m^0}{2i}\,m\left\{F_{m+1}(\theta,\phi)+(-1)^{m}F_{m+1}(0,0)\right\}\right]$$
$$-a\,\overline{\delta s_{00}}\left[\sum_{m=1}^{\infty}\frac{\bar{B}_m^0}{2i}\,m\left\{\overline{F_{m+1}(-\theta,-\phi)}+(-1)^{m}\overline{F_{m+1}(0,0)}\right\}\right] \tag{55}$$

$$\frac{1}{a^2}\,\delta A_2(\theta,\phi)-\sum_{m=2}^{\infty}\left[\frac{m\,a^2}{2}\overline{F_{m+1}(-\theta,-\phi)}\right]\frac{\overline{\delta B_m(-\theta,-\phi)}}{2i}+\frac{\delta B_1(\theta,\phi)}{2i}-\left[\frac{a^2}{2}\overline{F_2(-\theta,-\phi)}\right]\frac{\overline{\delta B_1(-\theta,-\phi)}}{2i}$$
$$=\overline{\delta s_{00}}\sum_{m=1}^{\infty}\frac{\bar{B}_m^0}{2i}\,\frac{m\,(m+1)\,a^2}{2}\left[\overline{F_{m+2}(-\theta,-\phi)}+(-1)^{m+1}\overline{F_{m+2}(0,0)}\right] \tag{56}$$

and

$$\frac{1}{a^{l}}\,\delta A_l(\theta,\phi)+\frac{1}{a^{l-2}}\,\frac{\delta B_{l-1}(\theta,\phi)}{2i}-\sum_{m=2}^{\infty}\left[\binom{-m+1}{l}\frac{a^{l}}{(m-1)}\overline{F_{m+l-1}(-\theta,-\phi)}\right]\frac{\overline{\delta B_m(-\theta,-\phi)}}{2i}$$
$$-\frac{(-a)^{l}}{l}\overline{F_l(-\theta,-\phi)}\,\frac{\overline{\delta B_1(-\theta,-\phi)}}{2i}=\overline{\delta s_{00}}\left[(-a)^{l}\frac{\bar{B}_l^0}{2i}\left\{\overline{F_{l+1}(-\theta,-\phi)}+(-1)^{l}\overline{F_{l+1}(0,0)}\right\}\right.$$
$$\left.+\sum_{m=2}^{\infty}\binom{-m+1}{l}a^{l}\,\frac{(m+l-1)}{(m-1)}\,\frac{\bar{B}_m^0}{2i}\left\{\overline{F_{m+l}(-\theta,-\phi)}+(-1)^{m+l-1}\overline{F_{m+l}(0,0)}\right\}\right] \tag{57}$$

where

$$F_m(\theta,\phi)=\sum_{\substack{r,s\\(r,s)\neq(0,0)}}\frac{1}{s_{rs}^{m}}\,e^{is\theta}\,e^{ir\phi}\qquad m=1,\ldots \tag{58}$$

and

$$G_m(\theta,\phi)=\sum_{\substack{r,s\\(r,s)\neq(0,0)}}\frac{\bar{s}_{rs}}{s_{rs}^{m}}\,e^{is\theta}\,e^{ir\phi}\qquad m=2,\ldots \tag{59}$$

$$H(\theta,\phi)=\sum_{r,s}\left[\frac{\bar{s}_{rs}}{s_{rs}}-\frac{\bar{s}_{r(s-1)}}{s_{r(s-1)}}-\frac{\bar{s}_{(r-1)s}}{s_{(r-1)s}}+\frac{\bar{s}_{(r-1)(s-1)}}{s_{(r-1)(s-1)}}\right]e^{is\theta}\,e^{ir\phi} \tag{60}$$

$$L(\theta,\phi)=\sum_{r,s}\ln\left|\frac{s_{rs}\,s_{(r-1)(s-1)}}{s_{(r-1)s}\,s_{r(s-1)}}\right|^{2}e^{is\theta}\,e^{ir\phi}. \tag{61}$$

Note in Eq. (60) and (61) that the terms $\frac{\bar{s}_{rs}}{s_{rs}}$ and $\ln\left|\frac{s_{rs}}{s_{rs}}\right|^{2}$ are ignored if $(r,s)=(0,0)$. Further, the convention on the order of summation, already discussed in connection with the flow past a regular array, is also selected here. Finally, note from Eq. (50) and (51), that

$$\delta B_1(0,0)=0. \tag{62}$$

STABILITY ANALYSIS

The solution of Eq. (53)-(57) provides a representation of the coefficients δB_l^{rs} and of the associated function $\delta B_1(\theta,\phi)$ in the form

$$\delta B_l^{rs}=\alpha^{rs}\,\delta s_{00}+\beta^{rs}\,\overline{\delta s_{00}} \tag{63}$$

and

$$\delta B_1(\theta,\phi) = \alpha(\theta,\phi)\,\delta s_{00} + \beta(\theta,\phi)\,\overline{\delta s_{00}}. \tag{64}$$

The variation of the force exerted by the fluid on the fiber rs due to the motion of the cylinder 00 can thus be expressed as

$$\delta F^{rs} = 4\,i\,\pi\,\mu\,\delta B_1^{rs} = (4\,i\,\pi\,\mu\,\alpha^{rs})\,\delta s_{00} + (4\,i\,\pi\,\mu\,\beta^{rs})\,\overline{\delta s_{00}} \tag{65}$$

Relying on the superposition principle discussed in the previous section, it is found that the variation of the force exerted on the cylinder is due to the motion of all cylinders, is

$$\delta F_{rs} = \sum_p \sum_q \left[(4\,i\,\pi\,\mu\,\alpha^{(r-p)(s-q)})\,\delta s_{pq} + (4\,i\,\pi\,\mu\,\beta^{(r-p)(s-q)})\,\overline{\delta s_{pq}} \right]. \tag{66}$$

Separating the real and imaginary components, it can be shown that the above relation can be rewritten in the form

$$\begin{bmatrix} \delta F_x^{rs} \\ \delta F_y^{rs} \end{bmatrix} = \sum_p \sum_q \begin{bmatrix} f_{11}^{(r-p)(s-q)} & f_{21}^{(r-p)(s-q)} \\ f_{12}^{(r-p)(s-q)} & f_{22}^{(r-p)(s-q)} \end{bmatrix} \begin{bmatrix} \delta x_{pq} \\ \delta y_{pq} \end{bmatrix} \tag{67}$$

where

$$\delta s_{pq} = \delta x_{pq} + i\,\delta y_{pq} \tag{68}$$

$$f_{11}^{pq} = -4\,\pi\,\mu \left[Img(\alpha^{pq}) + Img(\beta^{pq}) \right] \tag{69}$$

$$f_{12}^{pq} = 4\,\pi\,\mu \left[Re(\beta^{pq}) - Re(\alpha^{pq}) \right] \tag{70}$$

$$f_{21}^{pq} = 4\,\pi\,\mu \left[Re(\alpha^{pq}) + Re(\beta^{pq}) \right] \tag{71}$$

$$f_{22}^{pq} = 4\,\pi\,\mu \left[Img(\beta^{pq}) - Img(\alpha^{pq}) \right] \tag{72}$$

In the above relations, the notations $Img(z)$ and $Re(z)$ designate the real and imaginary parts of a complex number z.

It is seen from Eq. (67) that the fluid act as a "series of springs" since the forces are proportional to the displacements. For stability, the stiffness matrix must only possess eigenvalues with positive real parts. These eigenvalues, denoted in the sequel by λ and their corresponding eigenvectors $\left[\ldots \delta x_{pq}\ \delta y_{pq}\ \delta x_{p(q+1)}\ \delta y_{p(q+1)} \ldots \right]^t$ satisfy the following equations

$$\sum_p \sum_q \begin{bmatrix} f_{11}^{(r-p)(s-q)} & f_{21}^{(r-p)(s-q)} \\ f_{12}^{(r-p)(s-q)} & f_{22}^{(r-p)(s-q)} \end{bmatrix} \begin{bmatrix} \delta x_{pq} \\ \delta y_{pq} \end{bmatrix} = -\lambda \begin{bmatrix} \delta x^{rs} \\ \delta y^{rs} \end{bmatrix} \tag{73}$$

For all r and s, note that the left-hand side of the above condition represents a discrete two-dimensional Fourier convolution. Thus, introducing the Fourier transforms

$$\delta x(\theta,\phi) = = \sum_r \sum_q \delta x_{pq}\ e^{ip\theta}\ e^{iq\phi} \tag{74}$$

$$\delta y(\theta,\phi) = = \sum_r \sum_q \delta y_{pq}\ e^{ip\theta}\ e^{iq\phi} \tag{75}$$

$$f_{11}(\theta,\phi) = = \sum_r \sum_q f_{11}^{pq}\ e^{ip\theta}\ e^{iq\phi} = 2\,\pi\,\mu\,i \left[\alpha(\theta,\phi) + \beta(\theta,\phi) - \overline{\alpha(-\theta,-\phi)} - \overline{\beta(-\theta,-\phi)} \right] \tag{76}$$

and similarly

$$f_{12}(\theta,\phi) = = 2\,\pi\,\mu \left[\beta(\theta,\phi) - \alpha(\theta,\phi) - \overline{\alpha(-\theta,-\phi)} + \overline{\beta(-\theta,-\phi)} \right] \tag{77}$$

$$f_{21}(\theta,\phi) = = 2\,\pi\,\mu \left[\alpha(\theta,\phi) + \beta(\theta,\phi) + \overline{\alpha(-\theta,-\phi)} + \overline{\beta(-\theta,-\phi)} \right] \tag{78}$$

$$f_{22}(\theta,\phi) = = 2\,i\,\pi\,\mu \left[\alpha(\theta,\phi) - \beta(\theta,\phi) - \overline{\alpha(-\theta,-\phi)} + \overline{\beta(-\theta,-\phi)} \right] \tag{79}$$

it is found that Eq. (73) reduces to the 2x2 eigenvalue problem

$$\begin{bmatrix} f_{11}(\theta,\phi) & f_{21}(\theta,\phi) \\ f_{12}(\theta,\phi) & f_{22}(\theta,\phi) \end{bmatrix} \begin{bmatrix} \delta x(\theta,\phi) \\ \delta y(\theta,\phi) \end{bmatrix} = -\lambda \begin{bmatrix} \delta x(\theta,\phi) \\ \delta y(\theta,\phi) \end{bmatrix}. \tag{80}$$

The eigenvalue λ must be such that a nontrivial solution of Eq. (80) exists. This is achieved when

$$\lambda = -\frac{1}{2}\left[f_{11}(\theta,\phi) + f_{22}(\theta,\phi)\right] \pm \frac{1}{2}\left[\left(f_{11}(\theta,\phi) - f_{22}(\theta,\phi)\right)^2 + 4 f_{12}(\theta,\phi) f_{21}(\theta,\phi)\right]^{\frac{1}{2}} \tag{81}$$

NUMERICAL RESULTS

In order to illustrate the above theoretical development, two square arrays have been considered; the first one is unstaggered with a distance between fibers of $\sqrt{2}$ while the second one is staggered at 45° with a unit distance between fibers. In order to numerically simulate the specific order of summation associated with Eq. (41), (42) and (58)-(61), the domain of the indices p and q was selected to be $(p,q) \in [-10,10]\times[-5000,5000]$. A good matching with the theoretical results of Drummond and Tahir (1984) was obtained.

Shown in Fig. 2-6 are contour plots of the values of the eigenvalues corresponding to fiber radii, 0.1, 0.2 and 0.4 which reveal that the array is unstable for all of the cases considered. Note that the magnitude of the most negative eigenvalue increases as the fiber diameter increases, or equivalently as the density of fibers increases.

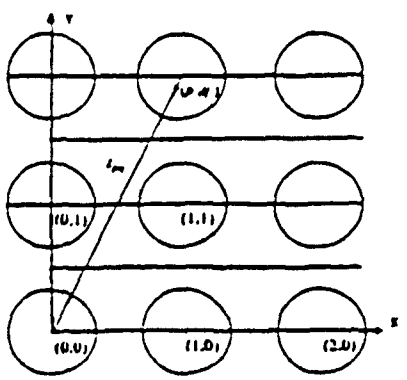

Fig.1 Geometry

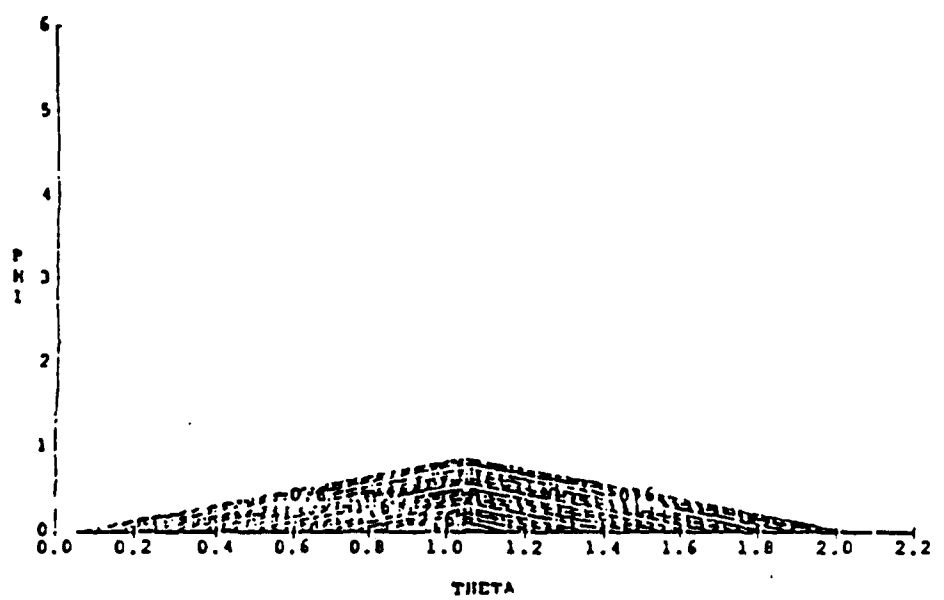

Fig. 2 Contour plot of lowest eigenvalue, staggered, a=0.2

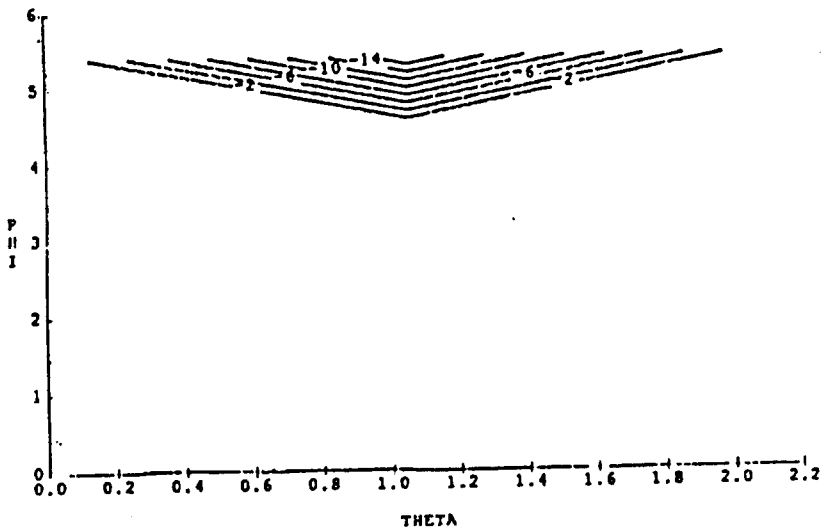

Fig. 3 Contour plot of lowest eigenvalue, staggered, a=0.4

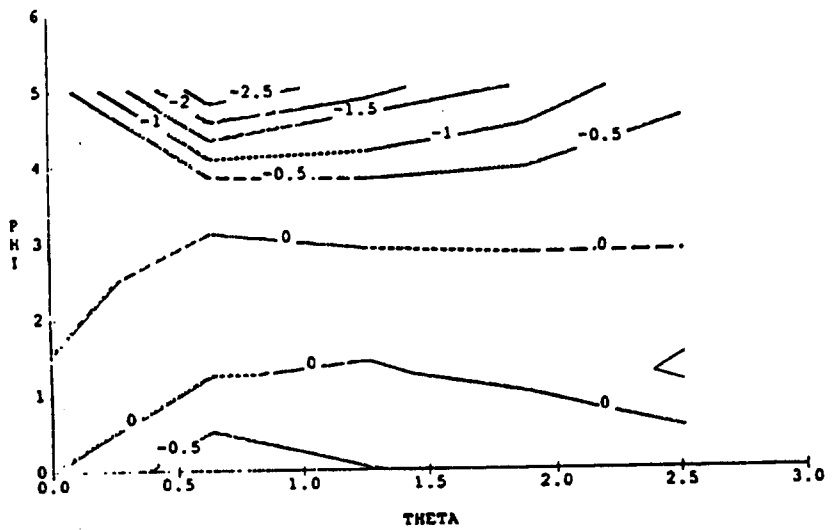

Fig. 4 Contour plot of lowest eigenvalue, staggered, a=0.1

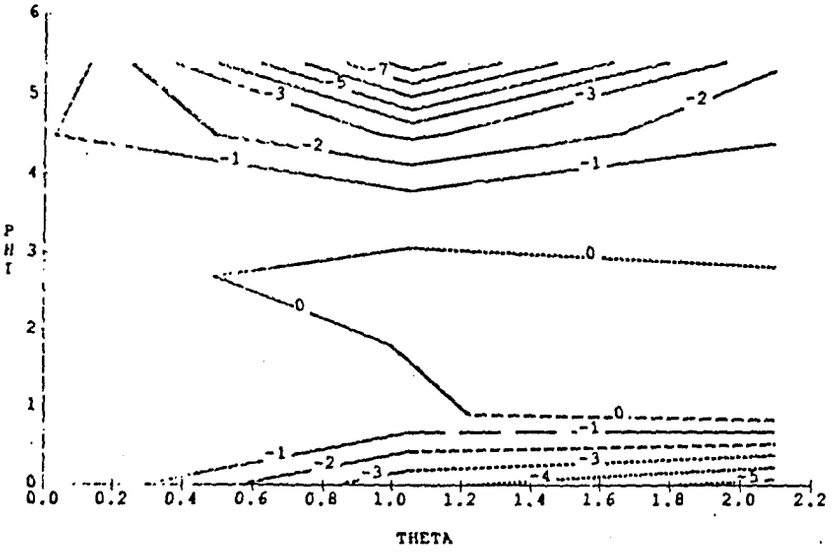

Fig. 5 Contour plot of lowest eigenvalue, staggered, a=0.2

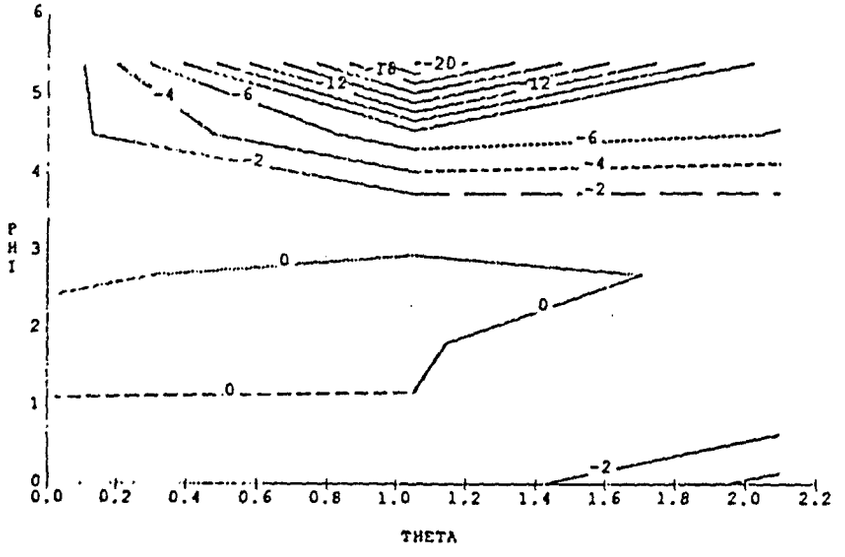

Fig. 6 Contour plot of lowest eigenvalue, staggered, a=0.4

CONCLUSIONS

In an attempt to explain the phenomenon of fiber clustering in thermoplastics, the low Reynolds number flow through an array of rigid cylinders (modeling the fibers) has been investigated. Specifically, the present study emphasized the determination of the forces exerted by the viscous fluid (the resin) on the cylinders for an arbitrary array. These results were then used to study the stability of a slightly imperfect square array of fibers. The stability analysis reveals that

(1) within the assumption of low Reynolds number, the stability of the array of fibers is independent of both the flow velocity and the fluid viscosity.

(2) the array of fibers is unstable, that is, small deviations of the fiber locations from a perfectly regular square, staggered or unstaggered, array will lead with time to a disordered arrangement of fibers.

(3) the magnitude of the most negative eigenvalue which quantifies the rate at which the disorder grows, increases with the concentration of fibers.

(4) the value of the most negative eigenvalue and the corresponding mode of instability do not appear to vary substantially with the staggering.

ACKNOWLEDGEMENTS

The support of this work by a grant of the US Army Research Office, Engineering and Science Division, Structural Mechanics Branch is gratefully acknowledged.

REFERENCES

Chen, S.S., Fujita, K., and Au-Yang, M.K., 1990, *Flow Induced Vibration - 1990 -*, Proceedings of the 1990 Pressure Vessels and Piping Conference, Nashville, TN, June 17-21, ASME, Publication PVP-189.

Conca, C., Planchard, J., and Vanninathan, M., 1990, "Limits of the Resonance Spectrum of Tube Arrays Immersed in a Fluid," *Journal of Fluids and Structures*, Vol. 4, pp. 541-558.

Drummond, J.E., and Tahir, M.I., 1984, "Laminar Viscous Flow Through Regular Arrays of Parallel Solid Cylinders," *International Journal of Multiphase Flow*, Vol. 10, No. 5, pp. 515-540.

Gordon, D., 1978, "Numerical Calculations of Viscous Flow Fields Through Cylinder Arrays," *Computers and Fluids*, Vol. 6, pp. 1-13.

Happel, J., and Brenner, H., 1973, *Low Reynolds Number Hydrodynamics*, Noordhoff, Leyden.

Hasimoto, H., 1959, "On the Periodic Fundamental Solutions of the Stokes Equations and their Application to Viscous Flow Past a Cubic Array of Spheres," *Journal of Fluid Mechanics*, Vol. 5, pp. 317-328.

Hjellming, L.N., and Walker, J.S., 1990, "Motion of Continuous Fibers through a Newtonian Resin for High Fiber Volume Fraction," *Journal of Composite Materials*, Vol. 24, pp. 853-878.

Kirsch, A.A., and Fuchs, N.A., 1967, "The Fluid Flow in a System of Parallel Cylinders Perpendicular to the Flow Direction at Small Reynolds Numbers," *Journal of the Physical Society of Japan*, Vol. 22, No. 5, pp. 1251-1255.

Kuwabara, S., 1959, "The Forces Experienced by Randomly Distributed Parallel Circular Cylinders or Spheres in a Viscous Flow at Small Reynolds Numbers," *Journal of the Physical Society of Japan*, Vol. 14, No. 4, pp. 527-532.

Miyagi, T., 1958, "Viscous Flow at Low Reynolds Numbers Past an Infinite Row of Equal Circular Cylinders," *Journal of the Physical Society of Japan*, Vol. 13, No. 5, pp. 493-496.

Sangani, A.S., and Acrivos, A., 1982, "Slow Flow Past Periodic Arrays of Cylinders with Application to Heat Transfer," *International Journal of Multiphase Flow*, Vol. 8, No. 3, pp. 193-206.

Tamada, K., and Fujikawa, H., 1957, "The Steady Two Dimensional Flow of Viscous Fluid at Low Reynolds Numbers Passing Through an Infinite Row of Equal Parallel Circular Cylinders," *Quarterly Journal of Mechanics and Applied Mathematics*, Vol. 10, Part 4, pp. 425-432.

Tamada, K., and Fujikawa, H., 1959, "The Steady Flow of Viscous Fluid at Low Reynolds Numbers Passing Obliquely Through a Plane Grid Made by Equal Parallel Circular Cylinders," *Journal of the Physical Society of Japan*, Vol. 14, No. 2, pp. 202-216.

White, F.M., 1974, *Viscous Fluid Flow*, McGraw-Hill.

AMD-Vol. 150/AD-Vol. 32, Damage Mechanics in Composites
ASME 1992

CURING INDUCED MICROCRACKS IN POLYMER MATRICES

Kaushik Mallick and Dusan Krajcinovic
Department of Mechanical and Aerospace Engineering
Arizona State University
Tempe, Arizona

ABSTRACT

The objective of the present two-scale model describing the evolution of the connectivity, stresses and temperatures in a polymerizing thermoset slab is to estimate the damage incurred during a typical cure cycle. The mean-field (macro-scale) part of the model couples equations of heat transfer, rate of chemical reactions (governing formation and rupture of crosslinks) and visco-elastic deformation in the slab. The micromechanical part of the model explores the influence of the disordered microstructure on the stress concentrations and rupture of overloaded bonds. Two parts of the model are intrinsically coupled through the fraction of existing bonds.

INTRODUCTION

Mechanical response of polymer matrix composites, and ultimately their strength, is strongly affected by the residual stress and submicro- and micro-defects induced during the curing process. The magnitude of residual stresses and the size of micro-defects depend on the chemical process, thermal gradients and stresses developed during the polymerization. Consequently, optimization of the curing process, i.e. minimization of the performance limiting birth defects, is undeniably an important task with far reaching consequences. However, the inherent complexity of the phenomenon, coupling exothermic chemical reactions, heat transfer and the damage evolution resulting from the attendant emergence of the stress and strain fields, defies easy solutions. The complexity is augmented by the disordered and evolving (time dependent) microstructure of the polymeric matrix and its effect on the local fluctuations of stresses.

A majority of the already existing phenomenological continuum models are, with a varying degree of rigor and success, focused on the determination of the mean-field (volume averaged) estimates of the macro-stress and temperature. However, the mere fact that a resin specimen survived the curing process in a single piece implies that the (average) rupture strength of the specimen exceeded the mean-field curing stresses at all times. Yet the inevitable presence of the ubiquitous microcracks, attributable to the chemical and thermal shrinkage, is a convincing testimony to the fact that the stress fluctuations did exceed the rupture strength of the polymer network *locally* at some time of the polymerization process. Indeed, the gossamer architecture (Zallen, 1983) of the newly formed gel backbone is replete with defects of all sizes and shapes. Hence, substantial stress concentrations must be expected during the early stage of the curing process as a rule rather than as

an exception. Further evolution of the damage nucleated just beyond the sol to gel transition can subsequently occur as a result of thermal shrinkage during the cooling phase of the curing process (Guz', et al., 1988).

The objective of this study is to provide a first stage in the development of an analytical model describing, ever so roughly, a set of coupled physico-chemical processes referred to as polymerization. More specifically, the analyses are focused on the competing mechanisms of chemical reactions during which the crosslinks are formed and the mechanical causes of crosslink ruptures. Primary interest of this study centers on the influence of these processes on the mechanical performance of the polymer and its residual strength. In view of many assumptions and simplifications, introduced into the model at this stage of its development, no pretense is made with regard to the numerical accuracy. Rather than fitting a particular curve for a particular resin subjected to a particular curing process, the primary focus of this study is placed on the replication of the dominant trends in mechanical behavior during the polymerization process of a generic thermoset resin.

KINETICS OF THE POLYMERIZATION PROCESSING THERMOSET RESINS

Polymerization is a complex process during which the colliding polyfunctional monomers react by crosslinking and form geometrically irregular three-dimensional networks. On the specimen or macro-scale the material during this process changes it phase from a viscous fluid to a glassy solid. On the micro-scale the same process is observed as a change in connectivity as the colliding monomers crosslink into m-mers. The exothermic reaction of crosslinking is accompanied by chemical (cure) shrinkage.

The early models of polymerization can be divided into two classes. One class of these models emphasized diffusion limited aggregation. The mean-field description of the m-mer growth model is, in this class of models, based on the Smoluchowski kinetic rate equation (for a lucid discussion of these models see Martin and Adolf, 1991). Despite their success in replicating the time dependence of the m-mers these models do not involve spatial correlations (shapes of m-mers and the spatial distribution of microdefects). As such these models are of limited use in the present case in view of the objectives of this study.

The second class of models (de Gennes, 1976, Herrmann, et al., 1983, Leyvraz, 1990, etc.) simulates the polymerization process by a bond percolation on a lattice. According to this model monomers are placed (actually fixed in nodes of a selected lattice). The bonds are subsequently allowed to form in a random sequence until the backbone (infinite cluster or gel) emerges when the fraction of formed crosslinks p reaches the percolation threshold p_c. The geometrical form (or type) of the lattice depends on the functionality of the monomers. Though deceptively simple and conceptually alluring, the model, nevertheless, has at least two deficiencies. Firstly, monomers are rather mobile at low levels of the connectivity p (prior to the formation of the gel) and can hardly be modeled as being fixed in nodes of a lattice. Secondly, the distance between monomers are measured in Angstroms. Consequently, the defects in these monomer lattices (measured by multiples of distances between monomers) are submicroscopic and, therefore, much too small to be of concern as stress concentrators or potential nuclei of micro-defects.

Both of these shortcomings were resolved in the polymerization kinetics model suggested by Martin and Wilcoxon (1989). According to this model the early stages of the polymerization process are dominated by diffusion limited aggregation of mobile monomers into nodules (or aggregates). This aggregation occurs simultaneously at many points within the melt. The growth of this nodules is governed by the Smoluchowski rate equation. These nodules grow exponentially with time until they fill the entire space and become practically immobile. At this point their radii become equal to the spatial correlation length ξ (proportional to the probability that two monomers, belonging to the same cluster are separated by the distance r).

The second phase of the polymerization process, according to Martin and Wilcoxon (1989), is dominated by crosslinking of virtually immobile nodules into larger clusters of nodules. Hence,

considering nodules as "renormalized" monomers fixed spatially into lattice nodes, the second phase of the polymerization process may, indeed, be simulated as the bond percolation on lattice. Assuming that bonding will take place only between the closest neighbors the cubic lattice represents both the simplest and most appealing choice. The nodule diameter is typically between 0.02 and 0.08 μm (Mijovic and Tsay, 1981, Martin and Wilcoxon, 1989), (i.e. at least two orders of magnitude larger than monomers itself). Consequently the voids and defects in the lattice will be measured in micrometers. As the nodule clusters become larger, an "infinite" macromolecule (gel) emerges spanning the entire specimen and endowing it with an initially minuscule shear strength (or more rigorously specimen shear stiffness). The spanning gel is still encapsulated by the surrounding viscous fluid referred to as sol. The stiffness is the second derivative of the Gibbs' energy with respect to the stress (Krajcinovic, et al., t.a.). Thus, the described sol to gel transition can be classified as the second-order phase transition. Shear compliance (or its inverse shear stiffness) of the specimen exhibits singular behavior at the sol to gel (or phase) transition. The fraction of the existing bonds between neighboring clusters will be labeled by p and the percolation threshold (at which gel emerges) by p_c. Physically, the sol to gel transition is a transition in connectivity from the short range connectivity of isolated nodule clusters to the long range connectivity of the gel. In defining the characteristic length the conventional spatial correlation function ξ must be replaced by the connectivity correlation length R_z defined as the z-average cluster radius.

The stresses attributable to chemical shrinkage are negligible prior to the sol to gel transition. As long as the nodules may move as rigid bodies the stresses associated with shrinkage of chain links connecting individual monomers cannot be substantial. At the percolation threshold $p = p_c$ both the stresses in individual links and the strength of the polymer are equal to zero. As the fraction p of the bonds connecting adjacent nodules increases beyond the percolation threshold p_c both the stresses and the strength start growing. The average (mean-field) stresses $\overline{\sigma}$ depend only on the lattice connectivity p and temperature T. They can be estimated using appropriate mean-field models (Martin and Adolf , 1990, Mallick and Krajcinovic, 1992). As already suggested, the mean-field stresses $\overline{\sigma}$ should at all times (and all p between p_c and 1) be smaller than the specimen strength if a polymer is to survive the curing process.

However, in the phase of the curing process just beyond the percolation threshold the gel geometry is very irregular, i.e the lattice is inundated by voids of all sizes and shapes. The attendant stress concentrations should and do exceed the mean-field values by an order of magnitude and more. These local stresses can be sufficiently large to cause rupture of some of the bonds subjected to largest stresses. Rupture of these highly stressed bonds relieves the stresses but at the same time represents the nucleus of the defects attributable to the curing process. In extreme cases the macro-failure may be attributed to these "birth" defects.

The classification of the sol-to-gel transition as a second order phase transition (see Zallen, 1983, Stauffer and Aharoni, 1992, etc) is not only of academic significance. Much more importantly this means that the process of crosslinking of nodules can, indeed, be simulated by the bond percolation problem on a lattice. This in turn means that this apparently random process exhibits certain universal trends robust to the details of microstructure and actual crosslinking sequence.

The universal trends of the sol-to-gel transition are reflected in the universality of the crosslinking level $p = p_c$ (where p is the fraction of the crosslink, or the probability that a given crosslink exists) at the percolation (connectivity) threshold. Additionally, the singularity of the shear compliance at the percolation threshold scales as $|p = p_c|^T$ (Martin and Adolf, 1991). The shear compliance is the order parameter since it exists only for $p \geq p_c$. Also $|p = p_c|$ is the proximity parameter. The scaling exponent T depends only on the dimensionality while the critical connectivity at the percolation threshold p_c depends on the dimensionality and the coordination number (number of closest neighbors) of the lattice.

ANALYTICAL MODEL

Mean-Field Model

According to the present experience the thermosetting resins such as epoxies can develop significant stresses during cure. These stresses principally arise from the shrinkage caused by chemical reactions in the material (Rozenberg and Irzhak, 1991, Korotkov et. al, 1991, etc.). A number of experimental and analytical studies have been devoted in the past to the estimation of cure stresses in polymer matrix composites (Hahn and Pagano, 1976, Loos and Springer, 1983, Bogetti and Gillespie, 1989, etc.). These studies focused on the formulation of continuum phenomenological models needed to determine the evolution of the elastic modulus of the gelling material with the degree of cure. In reality, the visco-elasticity of the crosslinked polymers is much more complex than assumed in these models. The viscosity can be traced not only to the changing connectivity p (loosely related to the degree of cure) but also the dynamics of the polymer chains (reptation, etc.) within the network. However, since the incipient gel is a self-similar structure, a change in the degree of cure essentially results in a mere change in scale of the cluster size. Thus, with a suitable rescaling of time, it is possible to derive a universal relationship for the time-dependent viscoelastic behavior of the curing polymer referred to as the time-cure superposition principle (Adolf and Martin, 1990).

To illustrate the salient aspects of the problem consider a polymer slab of constant thickness $2h_o$ infinitely extended in the (x, z) plane. The surfaces of the slab $y = \pm h_o$ are stress free and exposed to the temperature (controlled in the autoclave) which does not change with respect to x and z coordinates. Accordingly, both the temperature and the mean-field stresses are functions of the time t and coordinate y (defining the position across the slab thickness) only. Extension of the model to more complicated geometries is conceptually, if not computationally, simple.

The heat conduction problem is governed by the well known partial differential equation (Loos and Springer 1983, Ciriscioli and Springer, 1990, Mallick and Krajcinovic, 1992)

$$\frac{\partial(\rho S T)}{\partial t} = \frac{\partial}{\partial y}\left[k\frac{\partial T}{\partial y}\right] + \rho H_T \frac{\partial p}{\partial t} \tag{1}$$

The second term on the right-hand side of (1) is the contribution of the heat liberated in the exothermic reactions (crosslinking). The density ρ, thermal conductivity k and the specific heat S are assumed to be constant (independent of the degree of connectivity and temperature) for the duration of the process. Also, H_T is the total exothermic heat energy generated during the course of the reaction.

The differential equation governing the rate of the change of bonds in the percolation lattice is often concealed in the literature as the equation of the chemical kinetics (Kenny, 1988, Mallick and Krajcinovic, 1992, etc.). However, in most of these cases the rate equation is not complete. Change in the number of bonds connecting nodules, occupying the sites of the lattice, results from the competition of two simultaneous chemical processes. One process, typically considered in the literature, consist of the formation of bonds through chemical reactions between two adjacent nodules. The second process, often neglected in ventures of this kind, consists of the rupture of the highly stressed existing bonds.

Assuming the considered chemical reaction to be of first-order, the rate at which the bonds form must be proportional to the number of potential sites at which they can form. The total fraction of these potential sites must be equal to the fraction of the missing links $(1 - p)$. The coefficient of proportionality reflects the fact that some of the collisions (occurring between two monomers with inadequate kinetic energy) will not be effective. Thus, the proportionality factor (rate constant) must be defined as an exponential function of the activation energy U_o and temperature T leading to an Arrhenius type of equation. The rate at which the bonds rupture presents a less enjoyable task since it also depends on the unknown stress $\bar{\sigma}$ in the bond. The rate at which the bond rupture must be

proportional to the density of the existing bonds $p = \frac{N_t}{N}$ where N_t is the existing and N the total number of bonds in the lattice at $p = 1$. Thus, the total change in the density of bonds is

$$\frac{\partial p}{\partial t} = \left\{\frac{A_o}{t_o}\exp\left(-\frac{U_o}{k_B T}\right)\right\}(1-p) - \sum_{i=1}^{N_t}\frac{1}{N}\left\{\frac{A_o}{t_o}\exp\left(-\frac{U_o - \gamma\sigma_i}{k_B T}\right)\right\} \qquad (2)$$

In (2) $t_o = 10^{-13}$ sec is the period of free thermal vibrations of an atom , $k_b = 1.38 \cdot 10^{-23}$ J /°K is the Boltzmann's constant and A_o is a rate constant for the reaction. The bar above the symbol denotes average over the (x, z) plane. The quantity can only depend on y and t. The sum in (2) is taken over all existing bonds N_t. The basic problem with the equation (2) is that the stress in the i-th link σ_i may, and as a rule will, substantially differ from the mean-field estimate $\overline{\sigma}$. Assuming that all links which will rupture in a given instant of time are subjected to the same (high) stress $\sigma_i \approx q\overline{\sigma}$ where q is the stress concentration (or overload) factor the differential equation (2) may be recast into a more palatable form

$$\frac{\partial p}{\partial t} \approx \left\{\frac{A_o}{t_o}\exp\left(-\frac{U_o}{k_B T}\right)\right\}(1-p) - \left\{\frac{A_o}{t_o}\exp\left(-\frac{U_o - \gamma\overline{\sigma}}{k_B T}\right)\right\}p \qquad (3)$$

The coefficient γ (often referred to as the activation volume) embodies the bond stiffness and the stress concentration factor q. The accuracy of the expression (3) can be expected to be quite good as the connectivity p approaches unity. However, the stress concentrations will be quite severe in the period during which the emerging gel is of very irregular geometry.

Since all slab boundaries are free of stresses and assuming that the dead weight is negligible the only non vanishing macro-stresses (equal to each other) are $\overline{\sigma}_x$ and $\overline{\sigma}_z$ As shown in (Mallick and Krajcinovic, 1992) the constitutive relationship of the material relating the average (mean-field) stresses and the rate of change of eigenstrains $\overline{\varepsilon}^*$ is

$$\overline{\sigma}_x(y,t) + \frac{4}{3K}\int_o^t \frac{\partial G(y,\chi-\chi')}{\partial \chi}\overline{\sigma}_x(y,t')\,dt' = -6\int_o^t G(y,\chi-\chi')\frac{\partial \overline{\varepsilon}^*}{\partial t'}dt' \qquad (4)$$

where G is the cure and time dependent shear modulus and χ the reduced time variable defined on the basis of the time-cure superposition principle (Adolf and Martin, 1990)

$$\chi(t) = c\int_o^t \{p(t) - p(t')\}^4\,dt' \qquad (5)$$

In (5) c is a constant. Furthermore, in (4) $\overline{\varepsilon}^*$ is the isotropic eigenstrain in the material due to chemical shrinkage and thermal dilatation $\overline{\varepsilon}^* = \overline{\varepsilon}_{th} - \overline{\varepsilon}_{sh}$. During the chemical reaction two reacting monomers reduce their distance in order to attain the equilibrium position. As a result, the molecular chain link experiences chemical shrinkage. The chemical shrinkage in the slab is proportional to the number of formed bonds , i.e. the p above the gel point

$$\overline{\varepsilon}_{sh} = \overline{\varepsilon}_f \frac{p - p_c}{1 - p_c} \qquad (6)$$

where $\bar{\varepsilon}_f$ is the final shrinkage strain at the end of the cure ($p=1$). The thermal strain is $\varepsilon_{th} = \alpha (T - T_C)$ with α being the thermal expansion coefficient for the material, while $T = T_C$ at the percolation threshold. In deriving the above equations it was assumed that the bulk modulus of the material is independent of the connectivity p, i.e. that the polymer response to hydrostatic stresses is independent of the sol content. Hence, the material is assumed to behave viscoelastically when subjected to shear stresses, and elastically in hydrostatic state of stress (Lee and Rogers, 1963).

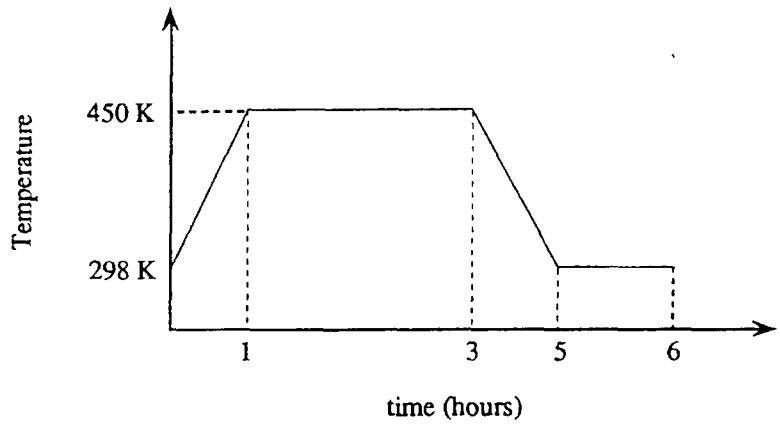

Fig.1 Variation of autoclave temperature with time

The system consisting of the differential equations (1) and (3) and the non-homogeneous integral equation (4) are coupled and hence cannot be soved analytically in a closed form. The mean-field estimate for the temperature T, connectivity p and the stress $\bar{\sigma}$ can be obtained numerically at an arbitrary time t and position y by discretizing the time scale into finite time steps (Mallick and Krajcinovic, 1992). Results of these computations, performed for the curing cycle shown in Fig. 1, are displayed in Figs. 2 and 3. As expected the average stresses are largest at the middle of the slab. They increase during the entire cure cycle and their spatial gradient remains more or less unchanged with time. The rate at which the stresses grow is slow at the beginning of the cure cycle. However, the stress magnitude increases significantly after the sol-gel transition.

Lattice Model

The mean-field estimates of the temperatures and the stresses present just the first step in the analysis of cure induced defects. Local failure of the material is, obviously, predetermined by the local, rather than average, stresses. However, determination of local stresses within a severely disordered microstructure is by no means a trivial task. In fact, computation of local stresses can be done only by discretizing the slab. In the present case the discretization of the slab into a network of nodules connected by bonds has already been discussed in the context of the percolation model of the polymerization kinetics. The slab will be approximated by a stack of uncoupled two-dimensional, finite, plane square lattices embedded in (x, z) planes. Since the slab is considered to be infinitely extended in the x and z directions, variations of displacements in these two directions are zero and $\bar{\varepsilon}_x = \bar{\varepsilon}_z = 0$. Consequently,

$$\bar{\varepsilon} * L_x + \bar{u}_x = 0 \quad \text{and} \quad \bar{\varepsilon} * L_z + \bar{u}_z = 0 \tag{7}$$

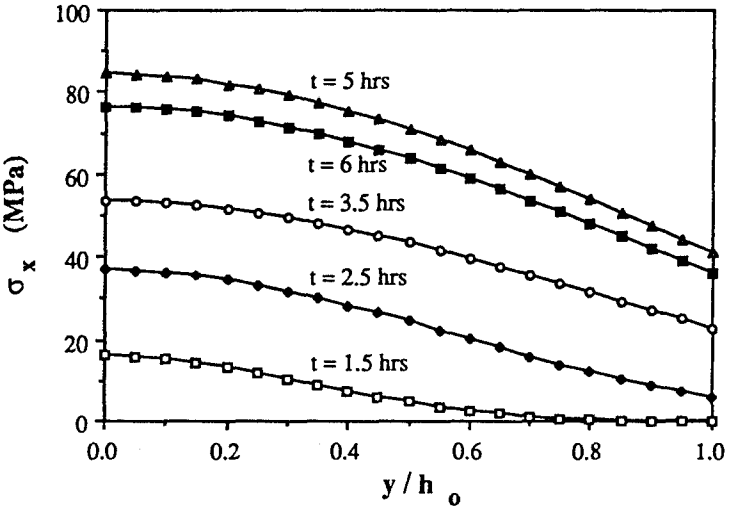

Fig.2 Variation of curing stresses with time across the thickness of the resin slab

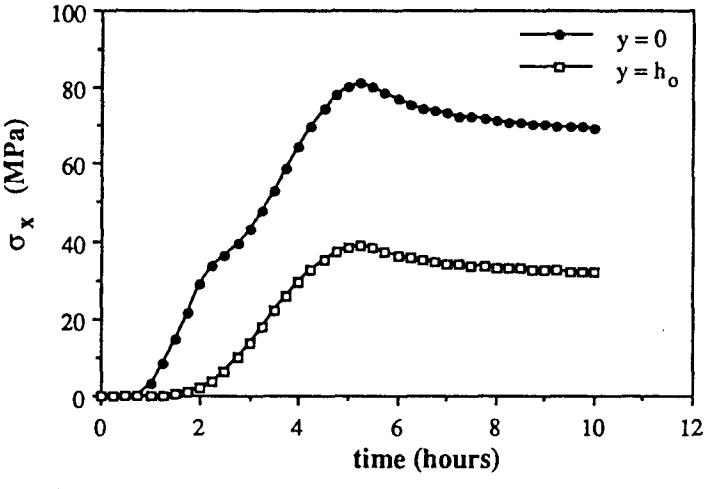

Fig.3 Evolution of stresses with time at the midplane $y=0$ and on the surface $y=h_o$ of the slab.

where $\bar{\varepsilon}^*$ is the average eigenstrain (resulting from chemical and thermal shrinkage). Also, L_x and L_z are the lengths of the network in x and z directions. Finally $\bar{u}_x$ and $\bar{u}_z$ are the displacements imposed on the boundaries $x = L_x$ and $z = L_z$ to satisfy the conditions $\bar{\varepsilon}_x = \bar{\varepsilon}_z = 0$ (assuming $x = 0$ and $z = 0$ are fixed). In the current analysis $L_x = L_z = L$ such that

$$\bar{u}_x = \bar{u}_z = \bar{u} = -\bar{\varepsilon} * L = -\bar{\varepsilon} * N\ell \qquad (8)$$

In (8) $L = N\ell$ where N is the lattice size and ℓ is the bond length (internodular distance).

At first glance it seems that the central-force lattice (truss) is the simplest and computationally least expensive alternative. However, as indicated in Beale and Srolovitz (1988) the dilution of trusses leads to internal instabilities of the central-force lattice resulting in a response not typical of real materials. Moreover, the behavior of the lattice in the neighborhood of the percolation point is dominated by the bending effects (see, for example, the discussion in Sahimi, 1986). It should also be remembered that the percolation lattice is obtained by renormalization, i.e. that the sites are occupied by nodules rather than individual monomers. Thus, the bonds between two adjacent nodules are not single atomic bonds but bundles of bonds which are indeed endowed by flexural strength and stiffness. Thus, the frame seems to be the simplest trouble-free discretization available. In this approximation the bonds are approximated by beams which are able to transmit bending moments, transverse and axial loads.

Rate Model of Rupture

In a disordered microstructure fracture is a statistical event described by probabilistic laws (Kausch, 1987). Load and temperature to which a specimen is subjected activates a multitude of processes resulting in the change of its microstructure. It is obvious that it is not possible to predict with any certainty the onset of a particular molecular event at a particulate time and location. However, the events such as rupture can be described probabilistically leading to reasonably good estimates.

The rate theories of fracture (Regel, et al., 1974, Kausch, 1987, etc.) are based on the premise that the rupture of a particular bond is controlled by temperature and stress in an equipolent manner. More specifically, it is assumed that the rupture is not an instantaneous event. The stress serves merely to lower the energy barrier (activation energy) while the failure occurs as a result of spikes in the thermal energy associated with synergisms in the chaotic motion of atoms. The experimental measurements of the time to rupture t_r of tensile specimens made of polycrystalline solids, single crystals and polymers are fitted well by the exponential expression (Regel, et al., 1974)

$$t_r = t_o \exp\left(\frac{U_o - \gamma\bar{\sigma}}{k_b T}\right) \qquad (9)$$

using the same notation as in (2). The term $\gamma\bar{\sigma}$ represents the work of the stress in the bond which reduces the potential barrier U_0. The expression (9) is derived for uniaxial tension of a specimen, i.e. a homogeneous state of stress. In the case of a link in bending instead of the global criterion it becomes necessary to consider the rupture of the cross-section subjected to maximum stress. Thus, instead of (9) the time to rupture can be estimated from

$$t_r = t_o \exp\left(\frac{U_o - \max(M_i\theta_i)}{k_b T}\right) \qquad i=1,2 \qquad (10)$$

In (10) M_i are the bending moments and θ_i are the angular rotations at the two ends of the beam.

Numerical Simulations on the Lattice

The discrete part of the proposed computational model includes the following steps:

(a) The process is started at time $t = 0$ when the individual nodules are disconnected. Links are added randomly to the system connecting the nearest neighbor nodules placed into nodes of a regular square lattice. In this regime ($0 < p < p_c$) the lattice does not possess any shear stiffness. It is

assumed that shrinkage stresses are local and very small during this phase leaving the network structure unperturbed.

(b) At the gel point ($p = p_c$) the infinite cluster of links traverses the lattice endowing it with shear stiffness and strength. Starting from this point the formation of new bonds will result in shrinkage strains and stresses within the gel (backbone) cluster.

The state of lattice at $t = t_1$ is defined by p_1, T_1 and $\overline{\sigma}_1$. To determine the temporal change of state during a short interval of time Δt it is necessary to compute the increments Δp, ΔT and $\Delta\overline{\sigma}_1$, solving the system of equations (1), (3) and (4). However, the rupture of links depends on local rather than average stresses. In other words the second term on the right hand side of the equation (3) provides only a rough estimate of the number of ruptured links. To compute a better estimate it is necessary to determine local stresses σ_i in links through the stress analysis of the lattice (frame).

(c) For a selected time interval Δt, the state variables p_2, T_2 and $\overline{\sigma}_2$ are computed for the state of the lattice at $t_2 = t_1 + \Delta t$. At this time, the incremental displacement imposed on the boundary of the network due to shrinkage can be computed from (8)

$$\Delta\overline{u}(y,t_2) = \left[\overline{\varepsilon}_f\left\{\frac{\Delta p(y,t_2)}{1-p_c}\right\} - \alpha\Delta T(y,t_2)\right]N\ell \qquad (11)$$

where $\Delta p = p_2 - p_1$, $\Delta T = T_2 - T_1$. The nodes on $x = 0$ and $z = 0$ are fixed to preserve symmetry. The nodes on $x = L$ and $z = L$ are attached to rigid walls which are subjected to the displacement $\Delta\overline{u}$ as determined in (11).

(d) The angular rotations (θ_i, θ_j) and the bending moments M_i and M_j at the ends of each link (ij) are determined using the methods of conventional frame analysis. The equations of equilibrium are solved by the conjugate gradient method (Golub and Van Loan, 1989). The average forces in the links are computed from the mean field stresses $\overline{\sigma}$ multiplied by the tributary area (ℓ^2). The maximum stress in a link is computed from the greater of the bending moments at its two ends, M_i and M_j.

(e) The mean time to rupture t_r^k is computed for each bond k from the expression (10). Bonds are then visited in ascending order of their time to rupture. The probability of failure of the bond k within the time step Δt is computed from

$$p_{kr} = 1 - \exp\left(-\frac{\Delta t}{t_r^k}\right) \qquad (12)$$

The rupture of a link is decided on the basis of a simple lottery. For each link k, a random number p_k is chosen such that $0 \le p_k \le 1$. The bond k ruptures if $p_k > p_{kr}$. A ruptured link is removed permanently from the system. The load it was carrying is redistributed to the surviving links relaxing the system to the state of minimum energy.

(f) After all the bonds in the network have been visited, the bond breaking process is stopped. The total number of ruptured links in the current time step is computed and compared with the estimate defined by the second term on the right hand side of equation (3). If the difference is large, the time step is reduced, the predictor is corrected and steps (c)-(e) repeated.

(g) The simulation is terminated when the probabilities of failure of all bonds in the network become negligible.

RESULTS OF NUMERICAL SIMULATIONS

The numerical values for polyethylene were used in the simulation (Termonia et al., 1985, Regel, 1974) in absence of the appropriate data for the thermosetting resins. In particular, E = 300 GPa, $\gamma = 3.65 \times 10^{-30}$ m and $U_o = 2.2 \times 10^{-19}$ J. The constant A_o in (3) was taken as 1.32×10^{-4} sec to replicate the cure kinetics of the resin Hercules 3506. The thickness of the beams, a, was assumed to be 5×10^{-9} m and the lattice spacing ℓ was taken as 2×10^{-8} m (Martin and Wilcoxon, 1989). The constant c in (5) was taken as 3.16 (Mallick and Krajcinovic, 1992).

Figures 4 and 5 show the results of numerical simulations on a 12 x 12 lattice for two different locations in the slab : (a) the surface ($y = h_o$) and (b) the mid-plane ($y = 0$). The average force, the maximum force and the ratio between the maximum force and the average force (i.e. the stress concentration) are plotted vs. time in Figs. 4(a) and (b). Although the average force is small just beyond the gel point, the stress concentration is very large. This results from the fact that the just formed infinite cluster has an irregular structure. The constituent beams resist the shrinkage deformation by flexure subjecting some of the bonds within the gel to very high bending moments. With the progress of the reaction more bonds are added to the structure and the network becomes more ordered. As p tends to 1 (perfect frame) the beams will resist the shrinkage displacement in axial mode with no bending at all. The rate of increase of shrinkage strain decreases with time as well. Consequently, the stress concentration reduces monotonically and the rate of growth of the maximum force diminishes significantly as the reaction nears its completion. The maximum force is significantly higher in the middle of the slab than on its surface. This is attributable to the fact that the center experiences a higher rate of crosslinking, locking in higher residual stresses at a stage when the network is still very irregular and sparse.

Figs. 5 (a) and (b) show the changes of the fraction of reacted, existing and ruptured bonds in the network with cure time. The rates of growth of these fractions diminish as the cure progresses. After the gel surpasses the critical regime, the rate of increase of shrinkage strain and consequently the energy term $M_i\theta_i$ in (10) becomes negligible. In addition, as the temperature of the lattice starts to descend to room temperature, the time to rupture for the bonds increases significantly. Consequently, the adaptive time step of the simulation can be increased as well. The simulation is terminated when the probability of rupture of the most highly stressed bond becomes negligible. The fraction of ruptured bonds reaches a saturation level near the end of the cure process. It is important to notice that the damage is much larger in the middle of the slab where it cannot be easily detected.

It is also observed from Figs 5 (a) and (b) that the fraction of broken bonds is considerably higher in the center of the slab ($y=0$) than at the surface ($y=h_o$). This can be explained from the following two facts : (1) the rate of addition of bonds in the center of the slab is higher, resulting in a higher rate of shrinkage strain; a larger fraction of bonds are subjected to high bending moments and hence susceptible to failure in the center of the slab, and, (2) the center of the slab attains a higher temperature due to the exothermic nature of the chemical reaction, reduces the time to rupture for individual bonds and enhancing the probabilities of their rupture. Higher temperature also results in a higher thermal shrinkage effect in the center of the slab.

The results of the simulation, although executed on a relatively small size of lattice, brings out the essential features of damage evolution that is to be expected in the post-gel regime. The maximum forces occur inside the network where the stress concentrations are high. It can be postulated that the micro cracks originate from a small avalanche of failures of these hot bonds located in a close neighborhood. The concentration, distribution and the shape of these defect clusters are likely to determine the strength and integrity of the cured specimen.

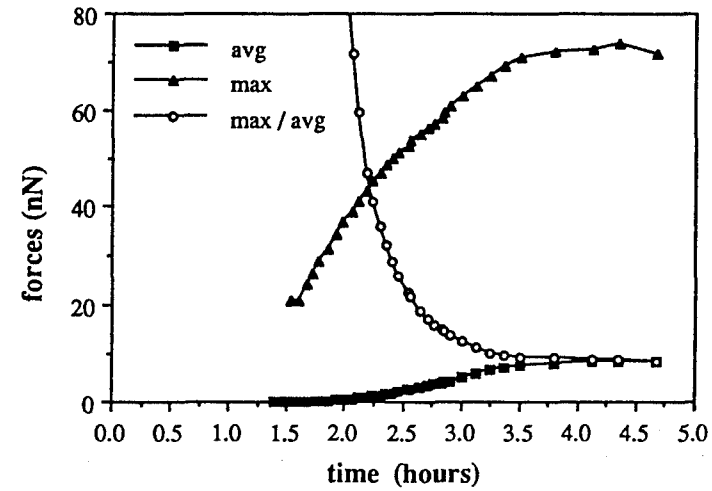

(a)

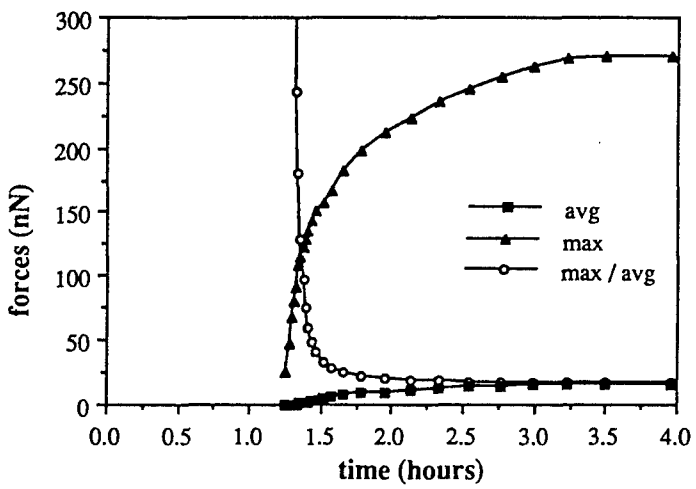

(b)

Fig.4 Variation of the average and maximum force with time for a polymer network at : (a) the surface and (b) the center of the slab

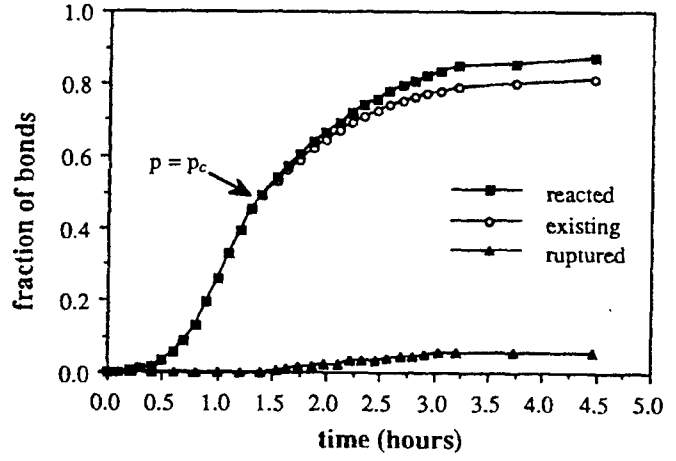

(a)

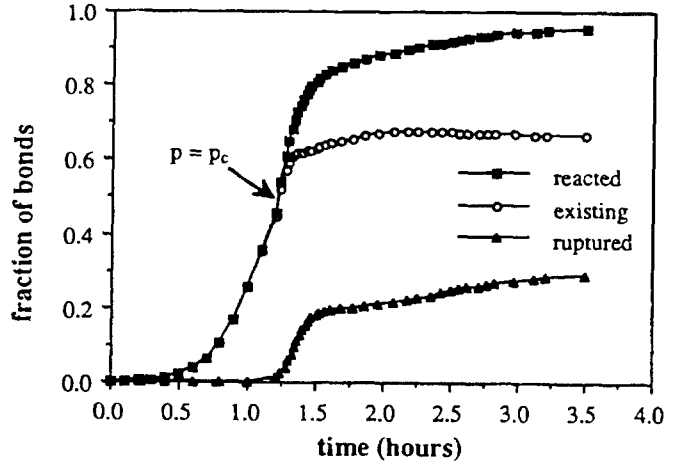

(b)

Fig. 5 Growth of the fraction of reacted, ruptured and existing crosslinks in a polymer network at : (a) the surface and (b) the center of the slab

SUMMARY AND CONCLUSIONS

The basic premise of this study is that the estimates of average (macro or mean-field) values of stresses and temperatures during the gelation of thermoset resins do not suffice to determine the initial damage ("birth defects"). The damage attributable to the curing process is directly and

inherently related to large fluctuations in the stress and temperature fields and the level of the microstructural disorder.

The principal variables defining the considered processes are temperature, stress and the state of the connectivity (related to the degree of cure). The source of the stresses are gradients in temperature and chemical shrinkage associated with the formation of the crosslinks. The attendant change of volume can be defined by means of eigenstrains. In the mean-field approximation the volume averaged values of these variables can be determined solving the heat transfer equation, rate of the chemical reaction equation and the inhomogeneous integral equation relating macro-stresses and eigenstrains. These three equations are intrinsically coupled since the shear modulus depends on the connectivity (fraction of existing bonds p) and the rate of the bond formation on the energy barrier (i.e. temperature and stress).

During the early stages of the gel formation the microstructure of the polymer slab is of very irregular shape replete with voids and crack-like defects in a variety of sizes and shapes. The determination of the stress concentrations in such an irregular solid is a non-trivial task. This task is further complicated by the non-deterministic geometry of the microstructure and distribution of damage. Within this study the problem of the determination of stress concentration in the diluted solid is simulated by the bond percolation on a quadratic lattice.

At this point of the development the proposed model has all the earmarks of a feasibility study. All equations on both scales are written and the problem is conceptually put together into a coherent, but obviously not final or computationally most efficient, form. As a first try the three-dimensional problem is reduced to two-dimensions approximating the solid by a stack of two-dimensional lattices. Some other, less important but not far reaching, simplifications were made for computational efficiency. Nevertheless, even in its nascent form the proposed model shows all advantages of statistical modeling and percolation theory in applications to elasticity problems characterized by the disordered structure.

ACKNOWLEDGMENT

The research on which this paper is based was made possible by the research grant from the U.S. Army Research Office, Engineering Science Division, Structural Mechanics Branch to the Arizona State University.

REFERENCES

Adolf, D., and Martin, J. E., 1990, "Time-Cure Superposition During Crosslinking", *Macromolecules*, Vol. 23, pp. 3700-3704.

Bogetti, T. A., and Gillespie, W., Jr., 1989, "Process-Induced Stress and Deformation in Thick-Section Thermosetting Composite Laminates", In *21st International SAMPE Technical Conference*, Atlantic City, N.J.

Ciriscioli, P. R., and Springer, G.S., 1990, *Smart Autoclave Cure of Composites*, Technomic, Lancaster, PA.

deGennes, P. G., 1976, "On a Relation Between Percolation Theory and the Elasticity of Gels", *Journal de Physique Letters*, Vol. 37., pp. L1- L2.

Golub, G. H. and Van Loan, C. F. , 1989, *Matrix Computations*, 2nd edition, The Johns Hopkins University Press, Baltimore.

Guz', A. N., Tomashevskii, V.T., Shul'ga, N.A. and Iakovlev, V.S., 1988, *Technological Stresses and Deformations in Composite Materials*, Vischa Shkola Publ., Kiev, Ukraine.

Hahn, H.T., and Pagano, N.J., 1976, "Curing Stresses in Composite Laminates", *Journal of Composite Materials*, Vol. 10, pp. 266-277.

Herrmann, H. J., Stauffer, D., and Landau, D. P., 1983, "Computer Simulation of a Model for Irreversible Gelation", *Journal of Physics A* , Vol. 16., pp. 1221-1239.

Kausch, H. H., 1987, *Polymer Fracture*, Springer, Berlin.

Kenny, J. M., 1988, "Computer Modeling of the Processing of Advanced Epoxy Based Composites", in *Computer Aided Design in Composite Material Technology*, Springer-Verlag, New York.

Korotkov, V. N., Chekanov, Y. A. and Rozenberg, B. A., 1991, "Defect Formation in Curing Epoxy in a Rigid Vessel", *Journal of Materials Science Letters*, Vol. 10, pp. 896-899.

Krajcinovic, D., Lubarda, V. and Sumarac, D., t.a., "Some Fundamental Aspects of Brittle Cooperative Phenomenon - Mean Field Model", submitted for publication.

Lee, E. H., and Rogers, T. G., 1963, "Solution of Viscoelastic Stress Analysis Problems Using Measured Creep or Relaxation Functions", *Journal of Applied Mechanics*, Vol. 34, pp. 127-133.

Leyvraz, F., 1990, "Exact Relations Between Kinetic Gelation and Percolation", *Journal of Physics. A*, Vol. 23, pp. 987-998.

Loos, C. A., and Springer, G. S., 1983, "Curing of Epoxy Matrix Composites", *Journal of Composite Materials*, Vol. 17, pp. 135-169.

Mallick, K. and Krajcinovic, D., 1992, "Cure Induced Inelastic Deformation in Thermosetting Polymers", AMD -Vol. 132, MD- Vol. 30, *Recent Advances in Damage Mechanics and Plasticity*, ASME 1992.

Martin, J. E., and Adolf, D., 1990, "Constitutive Equation for Cure-Induced Stresses in a Viscoelastic Material", *Macromolecules*, Vol. 23, pp. 5014-5019.

Martin, J. E., and Adolf, D., 1991, "The Sol-Gel Transition in Chemical Gels", *Annual Reviews of Physical Chemistry*, Vol. 42, pp. 311-339.

Martin, J. E., and Wilcoxon, J. P., 1989, "Spatial Correlations and Growth in Dilute Gels", *Physical Review A*, Vol. 39, pp. 252-258.

Mijovic, J. and Tsay, L., 1981, "Correlations between Dynamic Mechanical Properties and Nodular Morphology of Cured Epoxy Resins", *Polymer*, Vol. 22, pp. 902-906.

Regel, V.R., Slutsker, A. I. and Tomashevskii, E. E., 1974, *Kinetic Theory of the Strength of Solids*, Nauka, Moscow, 1974.

Rozenberg, B. A. and Irzhak, V. I., 1991, "The Role of Mechanical Phenomena During the Formation of Network Polymers", *Macromolecular Chemistry*, Vol. 45, pp. 127-135.

Sahimi, M., 1986, "Relation between the Critical Exponent of Elastic Networks and the Conductivity and Geometrical Exponents", *Journal of Physics C*, Vol. 19, pp. L79-L83.

Stauffer, D. and Aharoni, A., 1992, *Introduction to Percolation Theory*, 2nd edition, Taylor and Francis, London.

Termonia, Y., Meakin, P. and Smith, P., 1985, "Theoretical Study of the Influence of the Molecular Weight on the Maximum Tensile Strength of Polymer Fibers", *Macromolecules*, Vol. 18, pp. 2246-2252.

Zallen, R., 1983, *The Physics of Amorphous Solids*, Wiley, New York, NY.

3. Madhukar, M. S. and L. T. 1990. "Effect of Fiber-Matrix Adhesion on the Longitudinal Compressive Properties of Graphite/Epoxy Composites," *Proceedings of the Fifth Technical Conference of the American Society for Composites*, pp. 849–858.
4. Pagano, N. J. and G. P. Tandon. 1988. "Elastic Response of Multi-Directional Coated-Fiber Composites," *Composites Science and Technology*, 31:273–293.
5. Ghosn, L. J. and B. A. Lerch. 1989. "Optimum Interface Properties for Metal Matrix Composites," *NASA Technical Memorandum 102295*, August.
6. Arnold, S. M. and T. E. Wilt. 1992. "Influence of Engineered Interfaces on Residual Stresses and Mechanical Response in Metal Matrix Composites," *NASA Technical Memorandum 105438*, March.
7. Carman, G. P., R. C. Averill, K. L. Reifsnider and J. N. Reddy. 1992. "Optimization of Fiber Coatings to Minimize Stress Concentrations in Composite Materials," submitted to *Journal of Composite Materials*, March.
8. Tryson, L. D. and J. L. Kardos. 1981. "The Use of Ductile Innerlayers in Glass Fiber Reinforced Epoxies," *36th Annual Conference, Reinforced Plastics/Composites Institute. The Society of the Plastics Industry, Inc.*, February, Session 2-E, pp. 1–5.
9. Carman, G. P., J. J. Lesko, A. Razvan and K. L. Reifsnider. 1993. "Model Composites: A Novel Approach for the Evaluation of Micromechanical Behavior," *Composite Materials: Fatigue and Fracture (4th Symposium ASTM), ASTM STP 1156*, W. W. Stinchcomb and N. E. Ashbaugh, eds., Philadelphia: American Society for Testing and Materials, pp. 381–400.
10. Carman, G. P. 1991. *Micromechanics of Finite Length Fiber in Composite Materials*, Ph.D. Dissertation, Virginia Polytechnic Institute and State University, December.
11. Raghava, R., R. M. Caddell and G. S. Y. Yeh. 1973. "The Macroscopic Yield Behavior of Polymers," *Journal of Materials Science*, 8:225–232.
12. Caddell, R. M., R. S. Raghave and A. G. Atkins. 1974. "Pressure Dependent Yield Criteria for Polymers," *Materials Science and Engineering*, 13:113–129.
13. Silano, A. A., S. K. Bhateja and K. D. Pae. 1974. "Effects of Hydrostatic Pressure of the Mechanical Behaviour of Polymers: Polyurethane, Polyoxymethylene, and Branched Polyethylene," *Intern. J. Polymeric Mater.*, 3:117–131.
14. Matsushige, S. V., S. V. Radcliffe and E. Baer. 1975. "The Mechanical Behaviour of Polystyrene under Pressure," *Journal of Materials Science*, 10:833–845.
15. Silano, A. A., K. D. Pae and J. A. Sauer. 1977. "Effects of Hydrostatic Pressure on Shear Deformation of Polymers," *Journal of Applied Physics*, 48(10):4076–4083.

Fiber Clustering: A Comparison of Two Resin Flow Models

MARC P. MIGNOLET*
Department of Mechanical and Aerospace Engineering
Arizona State University
Tempe, AZ 85287-6106

(Received June 8, 1993)
(Revised January 20, 1994)

ABSTRACT: The present paper provides a comparative analysis of the potential of two different resin flow models, the Ideal Fibre-Reinforced fluid and the Stokes' flow model, to account for fiber clustering. It is shown that both of these models represent well the resin flow during different periods of the curing process. On that basis, it is shown that fiber clustering occurs early in the curing process when viscosity is still low. Then, as time increases, the resin becomes more viscous and prevents any further relative motions of the fibers.

KEY WORDS: fiber clustering, Ideal Fibre-Reinforced fluid, Stokes' flow.

INTRODUCTION

THE ACCURATE PREDICTION of the physical properties of a fiber-reinforced composite material given the corresponding properties of the fibers and of the resin, and the characteristics of the cure cycle has long been recognized as a very difficult task. Although many breakthroughs have been made in the last decade, there still remains some challenging issues, such as the determination of the factors that control the buckling, wrinkling, and clustering of fibers during curing. In a series of recent papers [1,2], the occurrence of the first two anomalies has been investigated by analyzing the stability of transverse and longitudinal flows of an Ideal Fibre-Reinforced fluid [3,4]. The goal of the present paper is to assess the applicability of this fiber-resin model to the prediction of the clustering of fibers and to compare the findings with the results of a similar study based on a Stokes' flow model [5]. For completeness, the major assumptions underlying both the Ideal Fibre-Reinforced fluid and the Stokes' flow models will first be reviewed.

*Associate Professor.

0021-9983/94/15 1467-13 $6.00/0

THE IDEAL FIBRE-REINFORCED FLUID MODEL

Assumptions and Governing Equations

Following Hull, Rogers and Spencer [1,2] assume that the fibers are continuously distributed in the resin. Further, denote by $a_r(\underline{x},t)$, $r = 1,2,3$, the 3 components of the unit vector $\underline{a}(\underline{x},t)$ specifying the direction of the tangent to the axis of the fiber located at time t at $\underline{x} = (x_1,x_2,x_3)$. Similarly, $u_r(\underline{x},t)$, $r = 1,2,3$, designates the 3 components of the velocity vector of a fluid particle located at $\underline{x}$. Then, considering the resin to be incompressible, it is found that

$$\frac{\partial u_r}{\partial x_r} = \frac{\partial u_1}{\partial x_1} + \frac{\partial u_2}{\partial x_2} + \frac{\partial u_3}{\partial x_3} = 0 \tag{1}$$

Note that the conventional indicial notation, in which a repeated index implies summation, has been used.

Further, it is assumed that the fibers convect with the resin during the flow or equivalently that a fiber remains surrounded by the same fluid element at all times. This condition can mathematically be expressed as

$$\frac{\partial a_r}{\partial t} + u_s\frac{\partial a_r}{\partial x_s} = a_s\frac{\partial u_r}{\partial x_s} \tag{2}$$

Moreover, the fibers are modeled as inextensible elements. Then, denoting by D the deformation tensor such that

$$D_{rs} = \frac{1}{2}\left[\frac{\partial u_r}{\partial x_s} + \frac{\partial u_s}{\partial x_r}\right] \tag{3}$$

it is found that

$$a_r D_{rs} a_s = 0 \tag{4}$$

Following Reference [3], the constitutive equation for the Ideal Fibre-Reinforced fluid is expressed in the form

$$\sigma_{rs} = -p\delta_{rs} + Ta_r a_s + 2\eta_T D_{rs} + 2(\eta_L - \eta_T)[a_r a_q D_{qs} + a_s a_q D_{qr}] \tag{5}$$

where σ, p, and T denote respectively the stress tensor, the pressure in the fluid, and the tension in the fiber at a space location $\underline{x}$ at time t. Further, the symbols η_L and η_T designate the longitudinal and transverse shear viscosities.

Finally, the linear momentum equation describes the evolution of the stress tensor as

$$\frac{\partial \sigma_{rs}}{\partial x_s} = \varrho\left[\frac{\partial u_r}{\partial t} + u_s\frac{\partial u_r}{\partial x_s}\right] \tag{6}$$

where ϱ denotes the density of the resin.

Fiber Clustering Risk—Stability Analysis

In an earlier analysis of the fiber clustering problem [5], to be reviewed in the next section, it had been shown that this phenomenon could be traced to a lack of stability of arrays of fibers through which resin flows. Surprisingly, it was shown that small misalignments of the fibers in doubly periodic, staggered or unstaggered, arrays would grow, hence increasing the disorder in the arrays. This conclusion had been drawn by modeling the fibers as rigid cylinders and the resin as a viscous Newtonian fluid whose velocity field satisfies Stockes' equation. It is now desired to perform a similar stability analysis by relying on the Ideal Fibre-Reinforced fluid model and to compare the results with the findings of the earlier study [5].

Stability analyses are often conducted in two steps. First, the characteristics of the base flow, i.e. velocity and pressure fields, forces applied, etc., are determined by solving the governing equations. Then, small changes in these flow characteristics are assumed to be present and the temporal evolution, i.e. growth or decay, of these perturbations is derived. Clearly, the system is stable if all perturbations die out as $t \to \infty$.

Motivated by a previous study of clustering [5], the present analysis will focus on the stability of a uniform flow perpendicular to the axes of the fibers. This base flow is then characterized by the velocity field

$$\underline{u} = \underline{u}^{(o)} = (v,0,0) \tag{7}$$

where v is a constant and by

$$\underline{a} = \underline{a}^{(o)} = (0,1,0) \tag{8}$$

for all $\underline{x}$ and t. Clearly, such a flow satisfies Equations (1)–(6) with

$$D_{rs} = D_{rs}^{(o)} = 0 \qquad r,s = 1, 2 \text{ or } 3 \tag{9}$$

and

$$\sigma_{rs} = \sigma_{rs}^{(o)} = -p^{(o)}\delta_{rs} + T^{(o)}\delta_{r2}\delta_{s2} \tag{10}$$

where $p^{(o)}$ and $T^{(o)}$ are constants.

To assess the stability of the flow of an Ideal Fibre-Reinforced fluid given by

Equations (7)-(10), small changes in some or all variables $\underline{u}$, $\underline{a}$, p, D_{rs} and σ_{rs} will now be introduced. Since the formation of clusters does not perturb the direction of the fibers, it will be assumed that the vector $\underline{a}$ is unchanged or, equivalently, that Equation (8) remains valid for the flow past a clustered array of fibers. Perturbations of the velocity and pressure fields are however expected so that

$$u_r(\underline{x},t) = u_r^{(o)}(\underline{x},t) + u_r'(\underline{x},t) \tag{11}$$

and

$$p(\underline{x},t) = p^{(o)}(\underline{x},t) + p'(\underline{x},t) \tag{12}$$

where it is assumed that

$$|u_r'(\underline{x},t)| \ll v \quad \text{and} \quad |p'(\underline{x},t)| \ll |p^{(o)}(\underline{x},t)| \tag{13}$$

The stability of the uniform flow given by Equations (7)-(10) can then be assessed by determining the temporal evolution of the disturbances $u_r'(\underline{x},t)$ and $p'(\underline{x},t)$. To this end, note that Equations (2) and (8) imply that all three components of the velocity are independent of x_2. Using this observation in conjunction with Equations (5) and (6) leads to the conclusion that neither p nor $\partial T/\partial x_2$ does vary with x_2. Further, note that a non-zero value of $\partial T/\partial x_2$ would lead to an infinite fiber tension at $x_2 = \pm\infty$. Thus, one must enforce

$$\frac{\partial T}{\partial x_2} = 0 \tag{14}$$

Then, the most general velocity field that is consistent with Equation (8) satisfies the partial differential equations

$$-\frac{\partial p}{\partial x_r} + \eta_T\left[\frac{\partial^2 u_r}{\partial x_1^2} + \frac{\partial^2 u_r}{\partial x_3^2}\right] = \varrho\left[\frac{\partial u_r}{\partial t} + u_1\frac{\partial u_r}{\partial x_1} + u_3\frac{\partial u_r}{\partial x_3}\right] \quad r = 1,3 \tag{15}$$

$$\eta_L\left[\frac{\partial^2 u_2}{\partial x_1^2} + \frac{\partial^2 u_2}{\partial x_3^2}\right] = \varrho\left[\frac{\partial u_2}{\partial t} + u_1\frac{\partial u_2}{\partial x_1} + u_3\frac{\partial u_2}{\partial x_3}\right] \tag{16}$$

which correspond to Equations (5) and (6), and the incompressibility condition, Equation (1) or equivalently

$$\frac{\partial u_1}{\partial x_1} + \frac{\partial u_3}{\partial x_3} = 0 \tag{17}$$

Introducing Equations (11) and (12) in the governing Equations (15)-(17) and

keeping only the first terms in the perturbations $u_r'(\underline{x},t)$ and $p'(\underline{x},t)$, it is found that

$$-\frac{\partial p'}{\partial x_r} + \eta_T\left[\frac{\partial^2 u_r'}{\partial x_1^2} + \frac{\partial^2 u_r'}{\partial x_3^2}\right] = \varrho\left[\frac{\partial u_r'}{\partial t} + v\frac{\partial u_r'}{\partial x_1}\right] \quad r = 1,3 \tag{18}$$

$$\eta_L\left[\frac{\partial^2 u_2'}{\partial x_1^2} + \frac{\partial^2 u_2'}{\partial x_3^2}\right] = \varrho\left[\frac{\partial u_2'}{\partial t} + v\frac{\partial u_2'}{\partial x_1}\right] \tag{19}$$

and

$$\frac{\partial u_1'}{\partial x_1} + \frac{\partial u_3'}{\partial x_3} = 0 \tag{20}$$

The solution of Equations (18)-(20) corresponding to the initial and boundary conditions

$$p_0'(\underline{x}) = [p'(\underline{x},t)]_{t=0} \tag{21a}$$

$$u_{r0}'(\underline{x}) = [u_r'(\underline{x},t)]_{t=0} \tag{21b}$$

$$\lim_{x_s \to \pm\infty} p'(\underline{x},t) = 0 \text{ for all } t \text{ and } s = 1,3 \tag{22a}$$

$$\lim_{x_s \to \pm\infty} u_r'(\underline{x},t) = 0 \text{ for all } t, r = 1,2,3 \text{ and } s = 1,3 \tag{22b}$$

describes the evolution in space and time of a perturbation in the flow that appeared at $t = 0$ and thus will permit the assessment of the stability of the flow given by Equations (7)-(10). The unboundedness of the domain $(x_1,x_3) \in (-\infty,\infty) \times (-\infty,\infty)$, the boundary conditions (22) and the linearity of the governing Equations (18)-(20) suggest the use of the Fourier transform technique. Specifically, the velocity and pressure field, $u_r'(\underline{x},t)$ and $p'(\underline{x},t)$, can be expressed as a superposition of elementary solutions of the form

$$u_r'(\underline{x},t) = \mathrm{Re}[u_r^{\alpha\gamma}(t)\exp(i\alpha x_1 + i\gamma x_3)] \qquad r = 1,2,3 \tag{23}$$

and

$$p'(\underline{x},t) = \mathrm{Re}[p^{\alpha\gamma}(t)\exp(i\alpha x_1 + i\gamma x_3)] \tag{24}$$

for all values of $(\alpha,\gamma) \in (-\infty,\infty) \times (-\infty,\infty)$. Introducing the assumed solution, Equations (23) and (24), in Equations (18)-(20) leads to 4 first-order coupled ordinary differential equations in $u_r^{\alpha\gamma}(t)$ and $p^{\alpha\gamma}(t)$. The linearity of these relations with respect to the functions $u_r^{\alpha\gamma}(t)$ and $p^{\alpha\gamma}(t)$ indicates that the

solution can be written in the form

$$u_r^{(\gamma)}(t) = u_{r0}^{(\gamma)} \exp(\lambda_r^{(\gamma)} t) \tag{25}$$

and

$$p^{(\gamma)}(t) = p_0^{(\gamma)} \exp(\lambda^{(\gamma)} t) \tag{26}$$

for some constants $u_{r0}^{(\gamma)}$, $p_0^{(\gamma)}$, $\lambda_r^{(\gamma)}$ and $\lambda^{(\gamma)}$. The eigenvalue problem that results from the introduction of Equations (23)–(26) in Equations (18)–(20) has the solution

$$\lambda^{(\gamma)} = \lambda_1^{(\gamma)} = \lambda_3^{(\gamma)} = -\frac{\eta_T}{\varrho}[\alpha^2 + \gamma^2] - iv\alpha \tag{27}$$

and

$$\lambda_2^{(\gamma)} = -\frac{\eta_L}{\varrho}[\alpha^2 + \gamma^2] - iv\alpha \tag{28}$$

The analysis of Equations (23)–(28) indicates that a perturbation in the uniform flow of an Ideal Fibre-Reinforced fluid propagates in the x_1 direction at the flow velocity v. More importantly, Equations (27) and (28) demonstrate that each of the Fourier components, Equations (23) and (24) are *damped* since

$$\mathrm{Re}\{\lambda^{(\gamma)}\} = \mathrm{Re}\{\lambda_1^{(\gamma)}\} = \mathrm{Re}\{\lambda_3^{(\gamma)}\} = -\frac{\eta_T}{\varrho}[\alpha^2 + \gamma^2] \leq 0 \tag{29}$$

and

$$\mathrm{Re}\{\lambda_2^{(\gamma)}\} = -\frac{\eta_L}{\varrho}[\alpha^2 + \gamma^2] \leq 0 \tag{30}$$

Thus, any perturbation to the uniform flow [Equations (7)–(10)] dies out, or equivalently the fibers will return to their original configuration as $t \to \infty$. Clearly then, there is no fiber clustering in an Ideal Fibre-Reinforced fluid.

STOKES' FLOW MODEL

Assumptions and Governing Equations

In the context of the manufacturing of composite materials, it is found that a low mean velocity, v, a high kinematic viscosity, ν, and a small diameter of the fibers, d, lead to a very small value of the Reynolds number based on the diameter of the fibers. The theory of linear creeping flows thus represents an appropriate framework for the present analysis. Neglecting all inertia terms, it is found that the continuity and momentum equations reduce to Equation (1) and

$$\mu \frac{\partial^2 u_r}{\partial x_j \partial x_j} = \frac{\partial p}{\partial x_r} \qquad r = 1,2,3 \tag{31}$$

where the symbol μ denotes the dynamic viscosity. Introducing the vorticity vector $\underline{\omega}$ as

$$\underline{\omega} = \mathrm{curl}\ \underline{u} \quad or \quad \omega_r = \epsilon_{rsk} \frac{\partial u_k}{\partial x_s} \qquad r = 1,2,3 \tag{32}$$

it is readily shown that Equation (31) reduces to

$$\frac{\partial^2 \omega_r}{\partial x_j \partial x_j} = 0 \qquad r = 1,2,3 \tag{33}$$

Proceeding as in the previous section, it can be argued that the clustering of the fibers does not produce any flow along the fibers. It is thus sufficient, to analyze the stability of the uniform flow given by Equation (7), to only consider velocity perturbations in the x_1 and x_3 directions, or equivalently, to set $u_2 = 0$. For such two-dimensional flows, the vorticity vector possesses only one non-zero component, ω_3 which can be seen from Equation (33) to admit a representation of the form

$$\omega_3(z) = \sum_{m=1}^{\infty} (B_m r^{-m} e^{-im\theta} + \bar{B}_m r^{-m} e^{im\theta}) = \sum_{m=1}^{\infty} \left(\frac{B_m}{z^m} + \frac{\bar{B}_m}{\bar{z}^m} \right) \tag{34}$$

where the parameters B_m are constant complex numbers and $z = x_1 + ix_3 = re^{i\theta}$. Note finally that the overbar designates the operation of complex conjugation. The complex velocity $W(z) = u_1 - iu_3$ corresponding to Equation (34) can be shown to be [5]

$$W(z) = \frac{1}{2i} \left[\sum_{m=2}^{\infty} \left(\frac{B_m \bar{z}}{z^m} - \frac{\bar{B}_m}{(m-1)\bar{z}^{m-1}} \right) + B_1 \frac{\bar{z}}{z} + \bar{B}_1 \ln \bar{z} \right]$$

$$+ \sum_{m=0}^{\infty} \frac{A_m}{z^m} + \frac{1}{2i} \bar{B}_1 \ln z \tag{35}$$

where A_m, $m = 0, \ldots$ are arbitrary complex constants. The singularity displayed by the flow field [Equation (35)] at $z = 0$ is clearly inadmissible unless that point does not belong to the fluid domain. More precisely, it can be argued

that this point must coincide with the center of one of the fibers. Symmetry considerations dictate, however, that no one fiber has a privileged role in the analysis. Thus, there must be a singularity of the flow field [Equation (35)] at the center of each fiber and

$$W_{array}(z) = \sum_p \sum_q W(z - s_{pq}) \tag{36}$$

In the above relation, the double summation over the fiber indices p and q extends over the entire array and s_{pq} denotes, as in Figure 1, the complex number associated with the position vector of the fiber in the pth column and the qth row.

The determination of the values of the complex coefficients A_m^{pq} and B_m^{pq} corresponding to each of the fibers is accomplished by enforcing no-slip boundary conditions on the circumference of each of the fibers and by specifying the mean velocity of the flow through the array. Once these coefficients are known, it is quite simple to determine the pressure field and the forces exerted on the fibers. In particular, it can be shown that the force acting on the fiber pq can be expressed as [6]

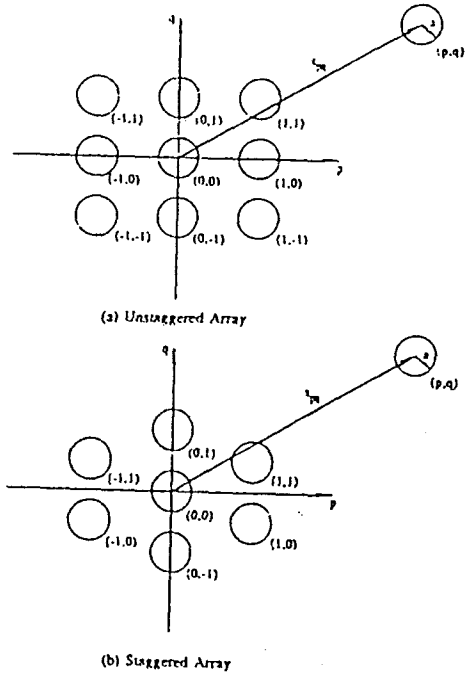

Figure 1. Array geometry: (a) unstaggered array and (b) staggered array.

$$F^{pq} = F_1^{pq} + iF_3^{pq} = 4i\pi\mu B_1^{pq} \tag{37}$$

Fiber Clustering Risk—Stability Analysis

To assess the stability of the array of fibers, it is necessary as in the previous section to first determine the characteristics of the base flow, i.e., the velocity and pressure fields, the forces exerted on the fibers, etc., or more succinctly, the values of the coefficients A_m^{pq} and B_m^{pq}. The flow past a perfectly regular array is obtained by enforcing that all fibers play the same role or equivalently that

$$A_m^{pq} = A_m^{(0)} \quad \text{and} \quad B_m^{pq} = B_m^{(0)} \quad \text{for } (p,q) \in (-\infty,\infty) \times (-\infty,\infty) \tag{38}$$

for some complex numbers $A_m^{(0)}$, $m = 0,1,2,\ldots$, and B_m^{pq}, $m = 1,2,3,\ldots$. Clearly, these coefficients are not arbitrary, they must be selected to satisfy the boundary conditions. These constraints lead to an infinite set of linear algebraic equations for the complex numbers $A_m^{(0)}$ and $B_m^{(0)}$ which can be solved by standard techniques (see Reference [5] for more details).

The second step of the present stability analysis consists in the study of the effects of small perturbations of the base problem. Since the focus of this investigation is on predicting the onset of clustering, the effect of small misalignments of the fibers will be determined. To this end, assume that the fibers are located at the points $s'_{pq} = s_{pq} + \delta s_{pq}$ where the symbol s_{pq} denotes the position of the fiber (p,q) in the regular array while δs_{pq} represents its small mispositioning. Introducing this relation in the no-slip boundary conditions and linearizing the resulting relations provides a first order approximation of both the flow parameters A_m^{pq} and B_m^{pq} corresponding to an irregular array and the associated forces being exerted on the fibers as a result of their mispositioning (see Reference [5] for a detailed presentation of the pertinent equations). It is found in particular that the components, δF_1^{rs} and δF_3^{rs}, of the small change δF^{rs} of the force acting on the fiber rs due to the mispositioning $\delta s_{pq} = \delta x_{1,pq} + i\delta x_{3,pq}$ can be expressed as

$$\begin{bmatrix} \delta F_1^{rs} \\ \delta F_3^{rs} \end{bmatrix} = \sum_{p,q} \begin{bmatrix} f_{11}^{(r-p)(s-q)} & f_{13}^{(r-p)(s-q)} \\ f_{31}^{(r-p)(s-q)} & f_{33}^{(r-p)(s-q)} \end{bmatrix} \begin{bmatrix} \delta x_{1,pq} \\ \delta x_{3,pq} \end{bmatrix} \tag{39}$$

where f_{ij}^{rs}, $i,j = 1,3$, are the contributions to the force acting on the fiber rs corresponding to unit mispositionings $\delta x_{1,00}$ and $\delta x_{3,00}$, respectively. Note that these components are readily computed from the perturbed coefficients B_1^{pq} using Equation (37).

It is seen from Equation (39) that the fluid acts as a "series of springs" since the forces are proportional to the displacements. For stability, the corresponding stiffness matrix must only possess eigenvalues with positive real parts. These eigenvalues, denoted in the sequel by λ, must be such that

$$\delta F_1^{rs} = -\lambda \delta x_{1,rs} \quad \text{and} \quad \delta F_3^{rs} = -\lambda \delta x_{3,rs} \tag{40}$$

for all r and s. At this point, note that the right-hand side of Equation (39) can

be viewed as discrete two-dimensional Fourier convolutions of the sequences f_{ij}^{pq} and $\delta x_{i,pq}$. Thus, introducing the discrete Fourier transforms

$$\delta x_1(\theta,\phi) = \sum_{p,q} \delta x_{1,pq} e^{ip\theta} e^{iq\phi}; \quad \delta x_3(\theta,\phi) = \sum_{p,q} \delta x_{3,pq} e^{ip\theta} e^{iq\phi} \tag{41}$$

and similarly for the force components f_{ij}^{pq}, it is found that Equations (39) and (40) reduce to the 2 × 2 eigenvalue problem

$$\begin{bmatrix} f_{11}(\theta,\phi) & f_{13}(\theta,\phi) \\ f_{31}(\theta,\phi) & f_{33}(\theta,\phi) \end{bmatrix} \begin{bmatrix} \delta x_1(\theta,\phi) \\ \delta x_3(\theta,\phi) \end{bmatrix} = -\lambda \begin{bmatrix} \delta x_1(\theta,\phi) \\ \delta x_3(\theta,\phi) \end{bmatrix} \tag{42}$$

Given values of the Fourier variables θ and ϕ, with $(\theta,\phi) \in [0,2\pi] \times [0,2\pi]$, two values $\lambda_1(\theta,\phi)$ and $\lambda_2(\theta,\phi)$ are obtained by solving the eigenvalue problem Equation (42). Then, the array is stable if and only if

$$\lambda_i(\theta,\phi) \geq 0 \quad i = 1,3 \quad \text{and} \quad (\theta,\phi) \in [0,2\pi] \times [0,2\pi] \tag{43}$$

In Reference [5], a series of staggered and unstaggered arrays have been considered and the above procedure has been followed to obtain two-dimensional contour plots of the eigenvalues $\lambda(\theta,\phi)$. One such typical plot is shown in Figure 2 for an unstaggered array and $a = 0.2$ while the distance between the center of the fibers is unity. The analysis of the many cases treated has revealed that

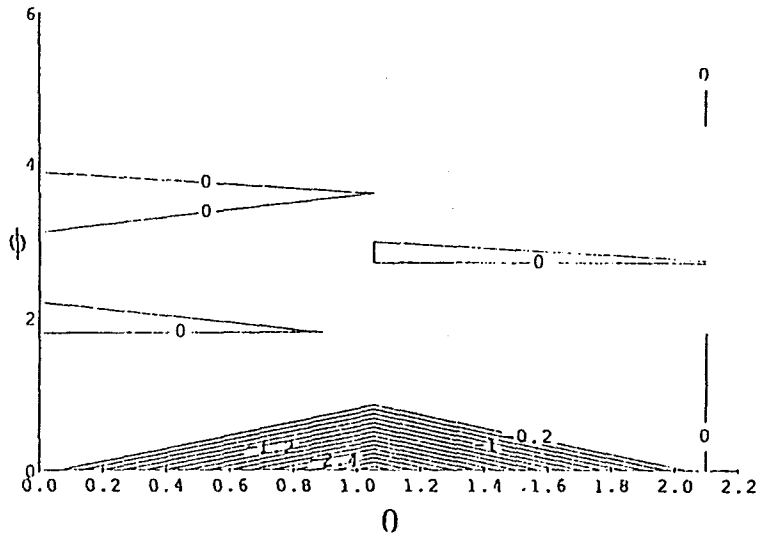

Figure 2. Contour plot of the lowest eigenvalue, unstaggered array, a = 0.2.

1. The array of fibers is unstable, that is, small deviations of the fiber locations from a perfectly regular square, staggered or unstaggered, array will lead in time to a disordered arrangement of fibers.
2. The magnitude of the most negative eigenvalue, which quantifies the rate at which the disorder grows, increases with the concentration of fibers.
3. The value of the most negative eigenvalue and the corresponding mode of instability do not appear to vary substantially with the staggering.
4. The dominant mode of instability, corresponding to the most negative eigenvalue, appears to be independent of both fiber concentration and staggering for moderate to high fiber concentrations and corresponds to $\phi = 0$ or (2π) and $\theta \approx 1.1$.

COMPARISON OF THE TWO MODELS

Although the two flow models that have been discussed in this paper appear to be quite different, they share at least two important properties, namely the incompressibility of the fluid [Equation (1)], and the existence of the uniform two-dimensional base flow given by Equation (7). Similarities in the stability analysis also exist. Note in particular that the assessment of the stability is not achieved in the physical domain but rather in the frequency domain obtained by Fourier transformation over the spatial variables x_1 and x_3. This finding indicates that experimental observations of the clustering phenomenon would probably be most revealing after Fourier transformation over the space domain.

The most important conclusion that can however be drawn from the comparison is that the two models disagree on the stability of the array of fibers; the Ideal Fibre-Reinforced model predicts the array to be stable while it is unstable according to the Stokes' flow model. This opposition in findings must clearly be associated with a basic difference in the properties of the fluid in the two models.

One such difference is the treatment of the inertia terms which are ignored in the Stokes' model but are kept in the Ideal Fibre-Reinforced fluid formulation and appear on the right-hand side of Equation (6). Note however that the signs of the real parts of the complex numbers $\lambda^{\alpha r}$ and $\lambda^{\beta r}$, $r = 1,2,3$ [Equations (29) and (30)], do not depend on the value of the density ϱ so that the presence or absence of the inertia terms in the fluid model should not affect the assessed stability of the array.

It is then concluded that the source of the disparity lies in the treatment of the dynamics of the fibers, which are convecting with the fluid in the Ideal Fibre-Reinforced model but move separately from it in the Stokes' flow formulation. In fact, this conclusion could have been expected by considering Figure 3; it is not possible for the resin to convect with the fibers *and* stay incompressible as the fibers move from their original configuration [Figure 3(a)] to their place within a cluster [Figure 3(b)]. Thus, the inability of the Ideal Fibre-Reinforced fluid model to yield an unstable array or equivalently, to account for fiber clustering, is directly associated with the assumption (2), i.e., that the fibers convect with the fluid.

This conclusion does not imply that the Ideal Fibre-Reinforced model cannot

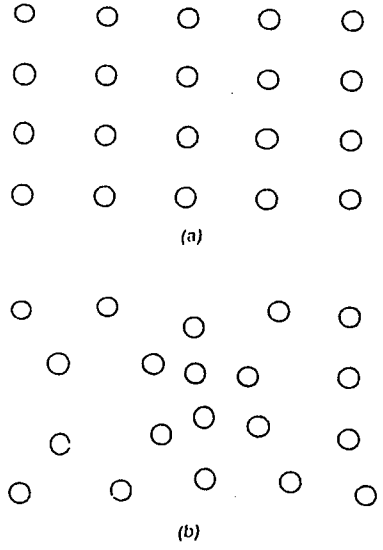

Figure 3. Regular and clustered arrays of fibers: (a) regular array of fibers and (b) clustered array of fibers.

accurately represent the resin flow, it only indicates that it does not do so *when fiber clustering occurs.* In fact, the hypothesis of convection of the fibers with the flow is certainly justified near the gel point where the viscosity is so large that separating a fiber from its surrounding resin would require a very large force. In the earlier part of the curing process, however, viscosity may slow down relative motions of the fibers with respect to the resin but cannot prevent them.

It is then concluded from these observations that fiber clustering must occur early in the curing process when the resin may, as suggested in Reference [7] and done in Reference [5], be modeled as a Newtonian fluid. Further, as the cure proceeds, the viscosity increases, the non-Newtonian character of the resin appears [7], and the fluid flow becomes stable, i.e., the fibers are "trapped" in their configuration.

ACKNOWLEDGEMENTS

The support of this work by the grant DAAL03-91-G0030 of the US Army Research Office, Engineering and Science Division, Structural Mechanics Branch, is gratefully acknowledged.

REFERENCES

1. Hull, B. D., T. G. Rogers and A. J. M. Spencer. 1991. *Composites Manufacturing*, 2:185–191.
2. Hull, B. D., T. G. Rogers and A. J. M. Spencer. 1992. *J. Non-Newtonian Fluid Mechanics*, 43:325–349.

3. Balasubramanyam, R., R. S. Jones and A. B. Wheeler. 1989. *Composites*, 20:33–37.
4. Rogers, T. G. 1991. In *Inelastic Deformation of Composite Materials*, G. J. Dvorak, ed., New York, NY: Springer-Verlag, pp. 653–674.
5. Mignolet, M. P. 1992. In *Recent Advances in Damage Mechanics and Plasticity*, J. W. Ju, ed., New York, NY: ASME Press, pp. 173–185.
6. Miyagi, T. 1958. *J. Physical Society of Japan*, 13:493–496.
7. Bartlett, C. J. 1978. *SPE Annual Technical Conference*, pp. 638–640.

AMD-Vol. 185, Damage Mechanics in Composites
ASME 1994

CREEP RUPTURE OF POLYMERS

Dusan Krajcinovic
Department of Mechanical and Aerospace Engineering
Arizona State University
Tempe, Arizona

Kaushik Mallick
All Plastics and Fiberglass
Mobile, Alabama

ABSTRACT

The objective of this paper is the inquiry into the high temperature rupture of polymers. The inquiry is of qualitative nature with little pretense in regard to numerical accuracy and fit of some set of experimental data. Instead the paper addresses some of the fundamental issues of the high temperature failure of polymer specimens in tension with emphasis on the microstructural disorder, question of scale and the random nature of the rupture process. Paper discusses a simple mean-field model (appropriate for oriented thermoplastics), Monte Carlo simulations on lattices and multifractal formalism needed to deal with crosslinked networks of resins. By allowing a simple solution the mean-field model serves as an illustration of some of the aspects of the rate theory of rupture. Two latter models provide an evidence of the effects of the specimen size on the time to rupture and the stress concentrations on the onset of the tertiary creep.

INTRODUCTION

This short study focuses on the determination of the time to rupture of polymer specimens subjected to high temperatures and modest stress level. Inelastic deformation is associated with the sequential scission of molecular chains. At low stress levels and high temperature the scission of molecular chains is attributed to spatial and temporal fluctuations of temperature reflecting the chaotic atomic motion. Consequently, the rupture patterns are random rendering the conventional, deterministic fracture mechanics failure criteria if not entirely inapplicable then at least suspect. The second problem is to relate the events on the atomic level (physics of the long and/or crosslinked molecular chains) to the macro-response and the creep rupture of the specimen itself. on the micro-scale a resin can be represented as a crosslinked network. Geometrically, a lattice seems to be an appropriate model of the microstructure. To render this discretization objective it is necessary to keep the characteristic microstructural length as the

resolution length of the model. This requires incredibly large lattices which are unsuitable for the numerical simulations. Multifractal formalism is used in this case to enable analyses of stress fluctuations in large lattices and provide reasonable estimates of their time to rupture in function of the applied mean-field stress, average temperature, initial damage and specimen size.

KINETIC CRITERIA OF LINK RUPTURE

Atoms of a molecular chain subjected to temperatures above absolute zero perform chaotic motion about their equilibrium positions. The intensity of this motion is directly proportional to the temperature and the disorder level (degree to which the atoms are "frozen" into the micro-structural network). The stable motion of a single atom, interacting with its neighbors, can be visualized as a motion of a sphere near the bottom of a potential well. The well depth, i.e. the distance between the bottom of the well and its rim, represents the energy barrier related to the attractive component of the interatomic force. At low temperatures the motion of the sphere is stable, i.e. if the sphere is forced away from its equilibrium position (bottom of the well) it will return to it within a finite period of time upon the removal of the external force. Occasionally, the energy imparted to an atom by its vibrating neighbors will be sufficiently large to drive it over the rim of the well causing in the process rupture of the interatomic bonds. Kinetic energy of the vibrating atoms is directly proportional to the interatomic forces and temperature. The probability of the rupture of the interatomic bonds is proportional to the force (stress) carried by the bond and the temperature caused by chaotic vibration of its neighbors. A model based on this concept is, therefore, often referred to as stress/temperature driven (Curran, et al. 1987).

Rupture can also be viewed as a chemical reaction during which the molecular chains are severed and atoms dissociated from the surface of a solid. The kinetic theory of rupture can, therefore, be developed within the framework of the rate theory of chemical reactions (collision theory). The adjective kinetic, characterizing this class of rupture models, indicates that the conditions leading to the rupture of atomic bonds are deduced from the motion of atoms. The governing rupture parameters explicitly depend on the time. Moreover since the atomic motion is random the ensuing criteria are stochastic.

In absence of the electrolytic effects the process of chemical dissociation is purely a thermal phenomenon. Temperature is a measure of the intensity with which the atoms, forming the atomic lattice, change their relative positions. Thus, the temperature is by inference an integral and essential part of the process of fracture. Since the motion of atoms is chaotic the temperature exhibits large spatial and temporal fluctuations on the atomic scale. The resultant of interatomic forces acting upon an atom is in a great majority of cases not sufficient to cause an atom to dissociate from its neighbors. However, since the number of atoms is very large a non-zero probability always exists that the chaotic motion will create a "resonance" condition in which the interactive forces on a small fraction of atoms align themselves to provide a large unbalanced force collinear with the normal to the surface of the solid. The kinetic energy imparted to these atoms may suffice to cause their "activation" or dissociation. These events correspond to large amplitudes of spatially localized temperature fluctuations. Fracture is, therefore, in essence a thermally activated process (Glasstone, et al. 1941, Regel', et al. 1974, Kausch 1987 or Krausz and Krausz 1988, etc.). The kinetics of the scission process is determined by probability that the peaks of the thermal energy exceed strength of the links of the molecular network keeping individual atoms of the chain within the potential well.

Skipping the details of the derivation (available in the above cited literature) it suffices to write down the expression for the average time to rupture of a single link of a molecular chain

$$t_r = t_o \exp\left(\frac{U_o - fu}{k_b T}\right) \tag{1}$$

In (1) U_O (Kcal/mole) is the sublimation energy (the work necessary to displace an atom from its equilibrium position to infinity), k_bT is the average energy of thermal vibration of atoms near the bottom of the potential well, where $k_b = 1.38\ 10^{-16}$ (erg/°K) is the Boltzmann constant and T (°K) the absolute temperature. Furthermore, ($t_o \approx 10^{-12} s$) is the period of the free vibration of an atom. Also, f and u are the force to which a link is subjected and its elongation. The Arrhenius (exponential) factor can be interpreted as the average number of oscillations performed by an atom about its equilibrium position prior to its dissociation from the molecular chain (scission). The difference $U_o - fu$ is the height of the energy barrier (depth of the potential well) which must be exceeded by the imparted thermal energy for a link to rupture.

MEAN-FIELD MODEL OF A BUNDLE OF CHAINS

As a simplest model consider a loose bundle of parallel, highly oriented chains resembling the crystalline region of a thermoplastic polymer such as polyethylene. Without making further attempts in the direction of providing a more realistic model of the actual microfibrilar microstructure of thermoplastic polymers (see Regel', et al 1974, Kausch 1987, et.) it will be assumed that all chains are taut and that they equally share in supporting the resultant F of the externally applied tensile tractions. Only the elongation in the direction of the of the resultant F is allowed. In other words, the parallel bar model (Krajcinovic and Silva 1982, Krajcinovic, et al. 1993, etc.) with a democratic load sharing rule is selected as the simplest approximation of crystalline region of a polymer. The time to rupture of each link is defined by (1).

Within the loose bundle, parallel bar model (mean field) approximation the external force F is equally shared by all extant (surviving) links. Consider the case when the resultant of the externally applied tensile tractions F is constant. Denote by N the number of links in the undamaged system. Even though the externally applied force F on the system is in a classical creep test held constant the forces in links f increase with time as the number of ruptured links n increases. The force carried by each extant link is in this approximation (Regel', et al. 1974) equal to

$$f(t) = \frac{F}{N - n(t)} = \frac{F}{N_t(t)} = \frac{F}{N[1 - D(t)]} \tag{2}$$

where $N_t(t) = N - n(t)$ is the number of extant bars carrying the external tensile force F = const.. In (2) the symbol D is used to denote the damage parameter which is here taken as being the ratio between the number of ruptured links and the initial number links, i.e.

$$D(t) = \frac{n(t)}{N} = \frac{N - N_t(t)}{N} = 1 - \frac{N_t(t)}{N} \tag{3}$$

The elongation $u(t)$ of the (i.e. its displacement in the direction of the applied force) system is

$$u(t) = \frac{F}{\bar{K}(t)} = \frac{F}{N_t(t)k} = \frac{F}{K[1-D(t)]} \tag{4}$$

where $\bar{K}(t) = N_t(t)k$ is the effective stiffness of the system and k=const. the stiffness of a link.

Introduce further the expressions for the force f_o carried by a single link in an undamaged system and the elongation u_o of the undamaged system

$$f_o = \frac{F}{N} \quad and \quad u_o = \frac{F}{K} = \frac{u}{1-D} = u\frac{N}{N_t} \tag{5}$$

and the time to rupture of a link not subjected to a mechanical force

$$t_r^o = t_o \exp\left(\frac{U_o}{k_b T}\right) \tag{6}$$

Using the above introduced parameters the time to rupture of a link (1) can be rewritten as

$$\tau_r = \frac{t_r}{t_r^o} = \exp\left[-\Delta\tilde{U}_o\left(\frac{N}{N_t}\right)^2\right] \quad where \quad \Delta\tilde{U}_o = \frac{f_o u_o}{k_b T} \tag{7}$$

The rate at which the links rupture (dN_t / dt) must be directly proportional to the number of surviving links N_t and inversely proportional to the period t_r which separates two subsequent spikes of thermal energy of magnitude $(U_o - fu)$. Thus,

$$\frac{dN_t}{dt} = -\frac{N_t}{t_r} \tag{8}$$

Final expression for the time rate of change of the damage can now be derived by combining the two above equations and representing the resulting expression in terms of the damage variable D. After relatively simple manipulations it follows that

$$t_r = t_r^o \exp\left(-\frac{N}{aN_t^2}\right) \tag{9}$$

The differential equation defining the time rate of the evolution of damage is finally derived by combining the rate equation (8) and the expression for the time to rupture (9). Hence,

$$d\tau = \exp\left[-\Delta\tilde{U}_o\left(\frac{1}{1-D}\right)^2\right]\frac{dD}{(1-D)} \tag{10}$$

Corresponding initial conditions are that at t=0 the damage D is absent as well.

In addition to the nonlinear ordinary differential equation (10) specifying the rate of damage evolution it is usually necessary to determine the displacement (elongation) u of the system (for

a constant force F)

$$\frac{du}{d\tau} = \frac{F}{K(1-D)^2}\frac{dD}{d\tau} \tag{11}$$

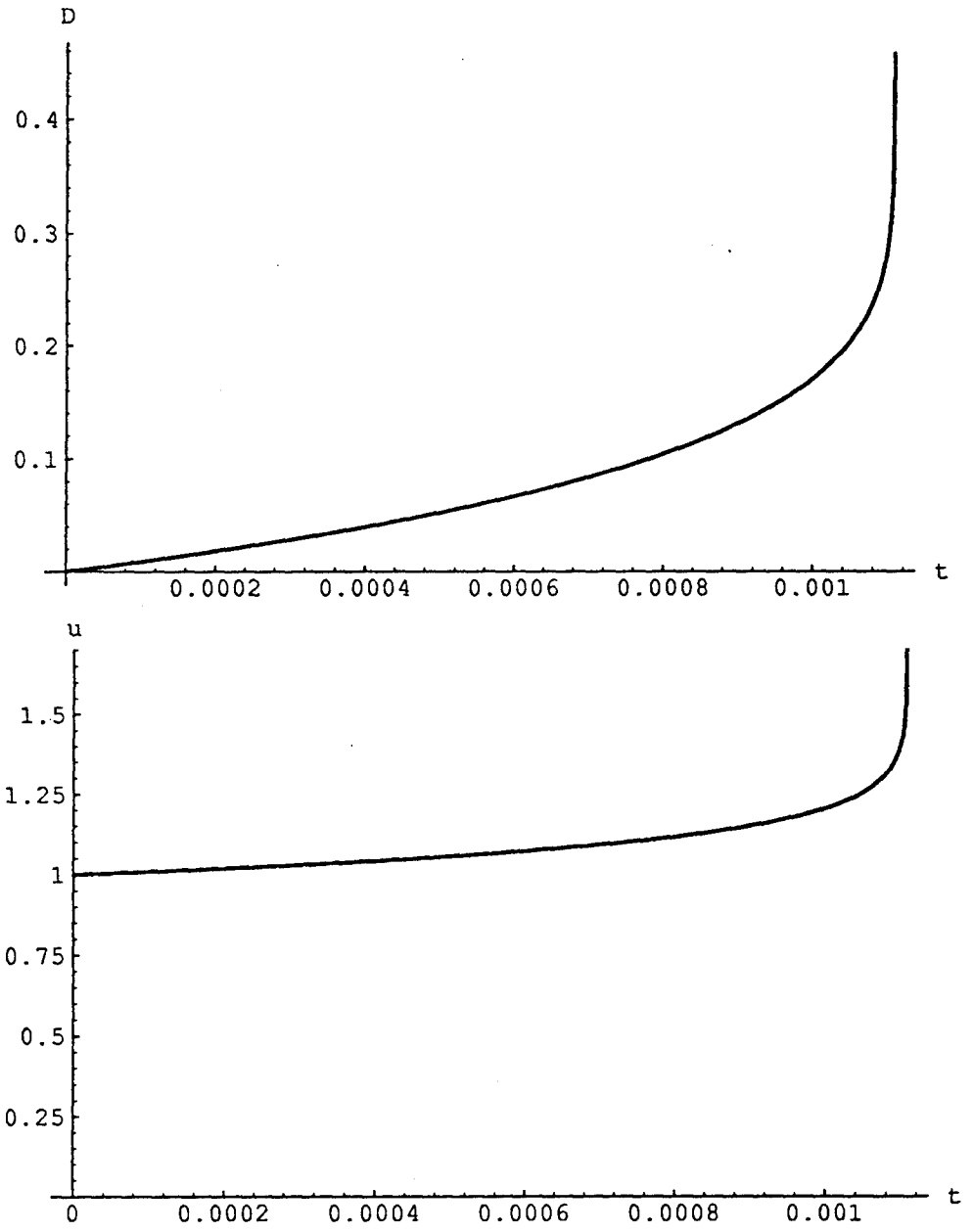

Fig. 1. Damage evolution and system elongation as a function of time.

For purpose of illustration take $U_o = 2 \cdot 10^{-19} N \cdot m$ and define the contribution of the mechanical load to the decrease of the energy barrier as a fraction of its initial height by $f_o u_o = \alpha U_o$ (where $0 \le \alpha < 1$). The increase of the damage and system elongation (chain stretch) with time for α=0.1 are plotted in Fig.1 against the time. The plots in Fig.1 clearly demonstrate the familiar trademarks of the traditional secondary and tertiary creep deformations. If the stress is increased by 2.5 times (α=0.25) the time to rupture decreases by $6 \cdot 10^4$ times.

LATTICE SIMULATIONS

The so-called effective continuum and/or mean-field models are based on the assumption that the defect density is reasonably small and that the direct interaction of adjacent defects represents a second order effect. More specifically, it is assumed that the local stress field in the vicinity of each defect is equal to the average, far-field stress field. As a result all spatial correlations, leading to stress concentrations, are eliminated from considerations. The accuracy and the applicability of this popular class of methods in estimates of the rupture thresholds and rupture modes is at best questionable. Unfortunately, a rigorous, analytical determination of the local fluctuations of stresses attributable to the direct interaction of randomly spaced defects of complex and irregular geometry remains an elusive goal.

Lattice simulations of the rupture processes in disordered continua, developed in the last decade by statistical physicists, proved to be quite successful in modeling of the type of failure of current interest. Microstructure of epoxy resins emphasizes a network consisting of a set of aggregates (nodes) interconnected by links in form of crosslinked molecular chains (Martin and Wilcoxon 1989). The diameter of these aggregates ranges from 0.01 to 0.1 μm. Exact geometry of the lattice depends primarily on the functionality of the monomers.

Assume that a particular epoxy microstructure can be, in a two-dimensional approximation, modeled by a triangular lattice. Assume also that the activation energy of each link are identical. The simulation is in this case quite simple (Termonia, et al. 1985, Mallick and Krajcinovic 1992). The probability of rupture of the i-th link within a time interval Δt is

$$p_i^{(r)}(t \in \Delta t) = t_o^{-1} \exp\left(-\frac{U_o - f_i \Delta \ell_i}{k_b T}\right)\Delta t \qquad (12)$$

since the rate of rupture of links is inversely proportional to their time to rupture (1). In (12) f_i and $\Delta \ell_i$ are the force carried by the i-th link and its elongation (stretch). Original (unstrained) length of all links is ℓ. The sign of the product $f_i \Delta \ell_i$ is taken as positive if the force is tensile and negative if it is compressive. This is consistent with the fact that the height of the rupture energy barrier is decreased by tensile and increased by compressive forces.

The initial step in the lattice simulation consists of the determination of the forces in the links of the lattice at t=0. Lattice is subjected to uniaxial tension in vertical direction. To facilitate the simulations the lattice is provided by two rigid bus-bars needed to distribute the load evenly to the lattice. Periodic conditions are prescribed on lateral sides to avoid shape effect. Forces in links are computed from conventional truss analyses. Once the forces acting on each link and link elongation are computed the probabilities of their rupture is determined from (12). The time period Δt (upper bound) during which at least one link must rupture is obtained from (12) as the inverse of the cumulative probability

$$\left[\sum_{i=1}^{N_f(t)} t_o^{-1} \exp\left(-\frac{U_o - f_i \Delta \ell_i}{k_b T}\right)\right]^{-1} \leq \Delta t \qquad (3)$$

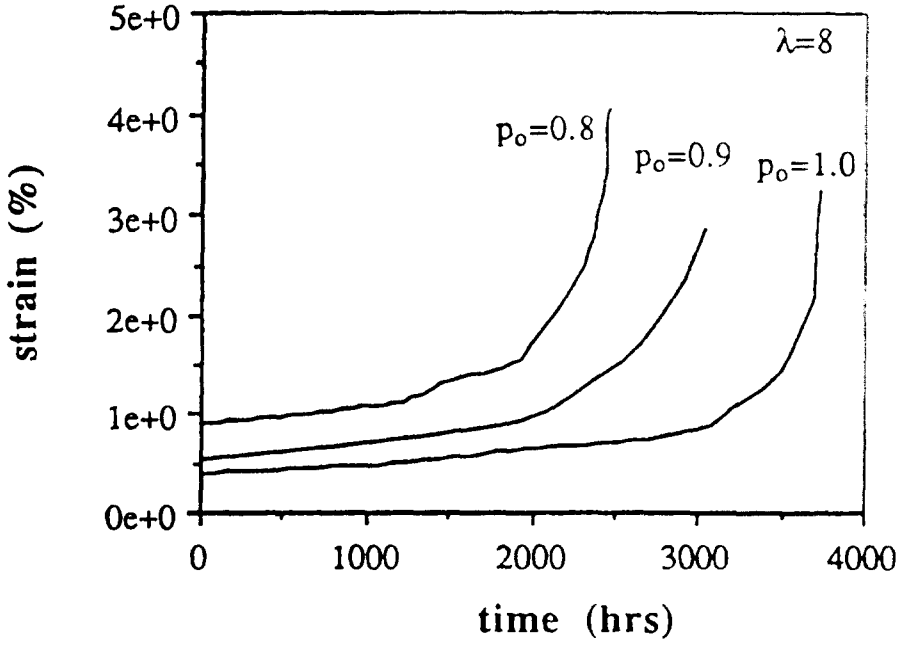

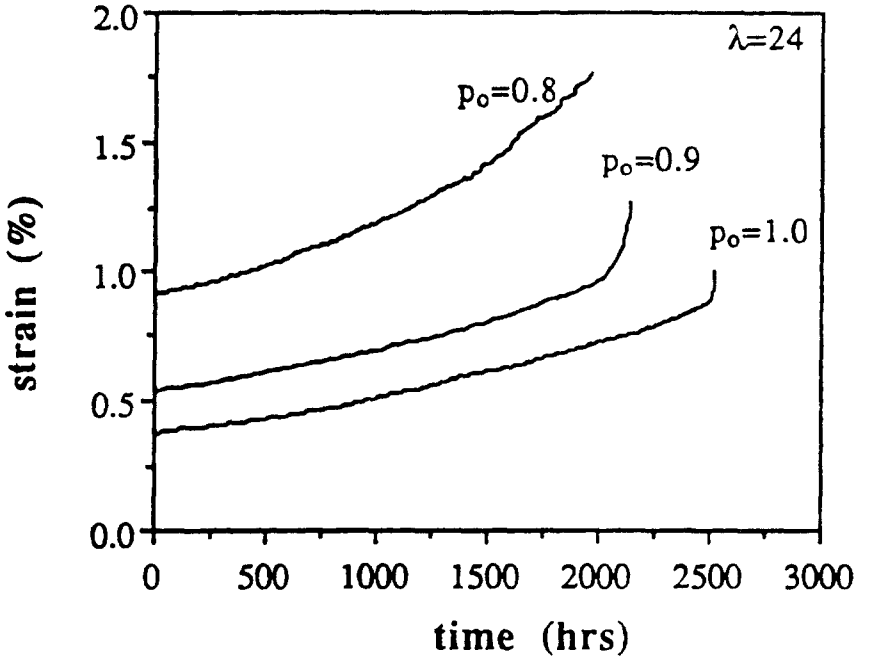

Fig.2. Strain vs. time for two lattices of different sizes for different initial damage.

A link can rupture well before the maximum Δt, computed from (13) by using the equality sign, expires. Keeping time interval Δt well below the upper limit will significantly increase the simulation accuracy. A link which ruptures is now determined by a Monte Carlo lottery. Ruptured link is removed from the lattice, the lattice is relaxed and new equilibrium state computed. The next step in simulations is performed using the newly computed forces in the links of a lattice which is not any more perfect. Links adjacent to the removed links carry larger loads. Hence, the stress concentrations attributed to defects is accounted for using truss analyses. Failure occurs at the state at which the diluted lattice ceases to be able to transmit the applied (constant) mechanical tractions. Time to rupture is computed adding all time steps (13).

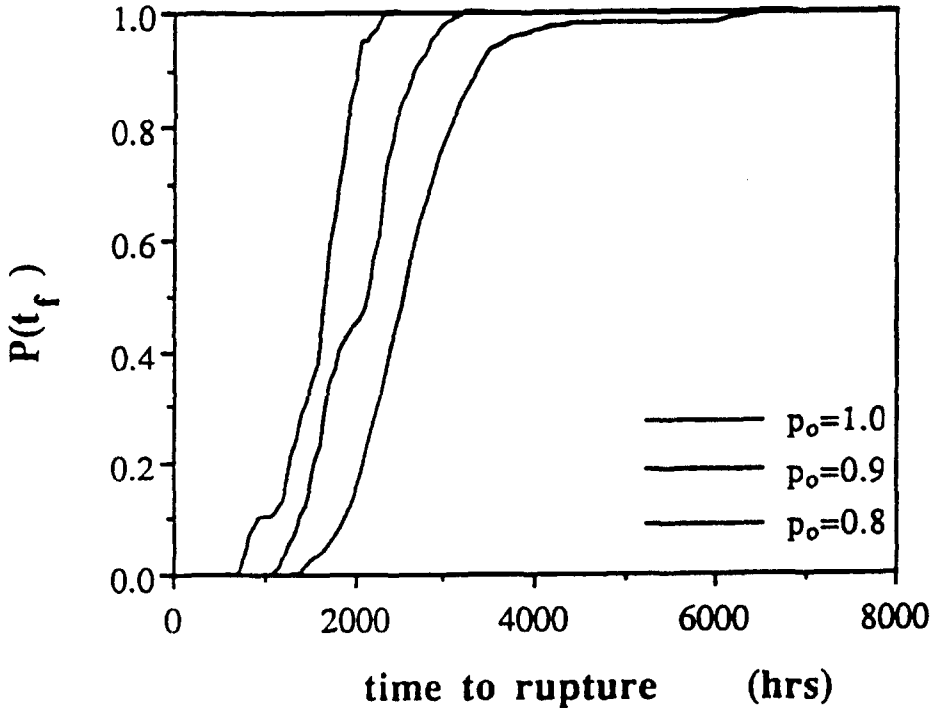

Fig.3. Cumulative probability distribution function of time to rupture vs. time to rupture.

Numerical simulations were performed using the following input data (taken mostly from the cited literature) $\ell = 5 \cdot 10^{-8} m$, $U_o = 2.19 \cdot 10^{-19} N \cdot m$, $E = 2.76 GPa$, $\sigma = 2.76 MPa$ and $T = 0.8 T_g$, where E is the elastic modulus, σ=const. the externally applied tensile stress and $T_g = 403^{\circ} K$ the glass transition temperature. The size of the lattice in the direction of the applied loads is denoted by L. These input data are roughly characteristic of the commercially available resin diglycidyl ether of bisphenol A (DGEBA). To minimize the computational effort the time interval Δt is determined using the equality sign in (13). The curves shown below are computed averaging over 500 samples of the smallest lattice size $\lambda = L / \ell = 8$, 100 samples for λ=16 and 50 samples for λ=24. The number of samples on largest lattice size λ=32 were too few to provide reasonably smooth averages. The plots of strain vs. time is shown for three different initial dilutions (1-p) in Fig.2a-b. The onset of the tertiary creep is marked by the sharp change of the gradient in the curves in Fig.2. Cumulative probability distribution $P(t)$ for the time to rupture for the case λ=24 is ploted in Fig.3. Curves for other sizes are quite similar. In both Fig.2 and Fig.3 symbol p_o is used to denote the fraction of links present at the initiation of the

simulation. Thus, $p_o = 1$ characterizes a perfect (undamaged) lattice. As expected the influence of the initial defects manifests itself only in the translation of the plotted curves.

It is interesting that the effective stiffness of the lattice is a linear function of the dilution $q = 1 - p$, where q can also be interpreted as the probability that a link is ruptured. Linear dependence of the effective stiffness on the dilution (fraction of ruptured links) q is independent of the lattice size λ and persists well beyond the defect concentrations for which this could have been expected. This conclusion is consistent to one deduced three years ago by Krajcinovic and Basista (1991). Independence of effective stiffness on specimen size is of significance for the selection of the damage parameter on the macro (or specimen) scale, i.e. interpretation of the test data and their relation with field measurements on actual structures.

MULTIFRACTAL FORMALISM

Numerical simulations illustrated in the preceding section have a somewhat insidious and serious shortcoming. The expressions derived in two preceding sections are based on the considerations on the molecular level. As a result the resolution length must be equal to the distance between two aggregates, i.e. to $\ell = 5 \cdot 10^{-8} m$. Hence, to consider a two dimensional specimen it is necessary to have $4 \cdot 10^{10}$ nodes per each cm^2 of the specimen. This obviously represents an impossible task even if the fastest available computers are available. A possible alternative, which is very often pursued, is to use a coarser discretization. The links in this lattice do not have a clear physical significance and the determination of the material parameters is relegated to fitting some data with adjustable "constants". Moreover, no hierarchical discretization (including finite element method) is objective since the direct interaction is allowed only between the defects belonging to the same "finite element". As a rule results obtained by any discretization of this type are mesh sensitive.

A much more reliable set of results can be derived using the multifractal formalism discussed in Krajcinovic and Mallick (to appear) based on the methods developed by Hansen and Roux (1988), Roux and Hansen (1989) and many others. A rather lengthy and involved derivation is based on the fact that the rate at which the links are ruptured are equal to the sum of the individual probabilities

$$\frac{dq}{dt} = \frac{1}{N} \sum_{i=1}^{N_i(t)} \frac{1}{t_o} \exp\left(- \frac{U_o - f_i \delta_i}{k_b T} \right) = \frac{1}{t_o} \exp\left(- \frac{U_o}{k_b T} \right) \sum_{n=0}^{\infty} \frac{1}{n!} M_n(\Phi) \tag{14}$$

where $M_n(\Phi)$ is the n-th statistical moment of the distribution of free energies $p(\Phi_i = f_i \delta_i)$. Using the property of self-similarity at the percolation threshold the n-th statistical moment can be written (for a constant stress ensemble in the considered case) as

$$M_n(\Phi) = \int_o^{\infty} \Phi^n p(\Phi) d\Phi \propto \lambda^{z(n)} \tag{15}$$

In contrast to fractals the exponents $z(n)$ are different for different n.

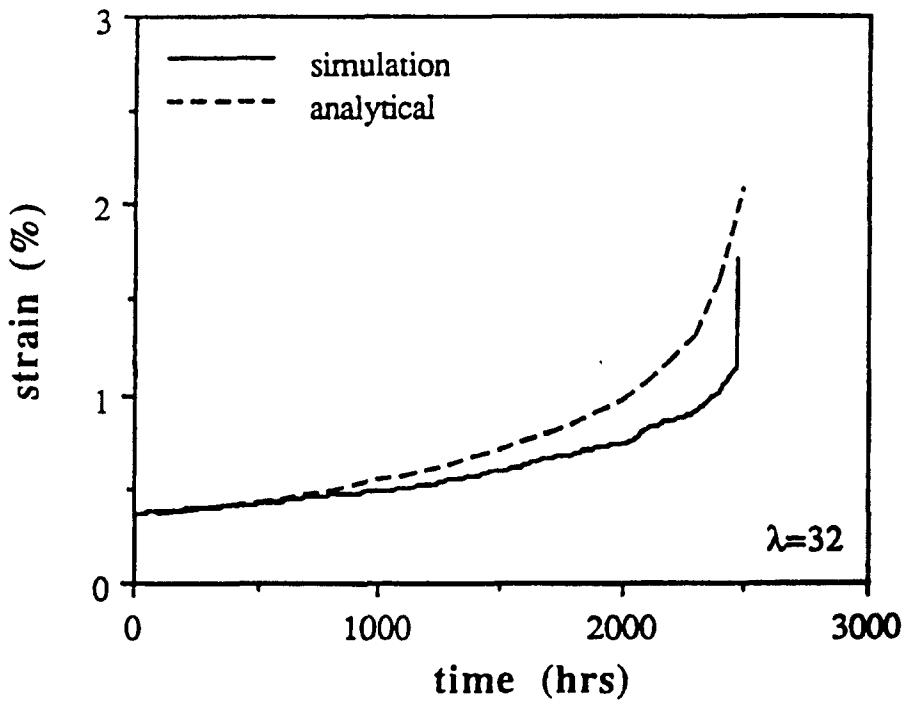

Fig.4. Strain vs. time. Comparison of numerical simulations and multifractal formalism

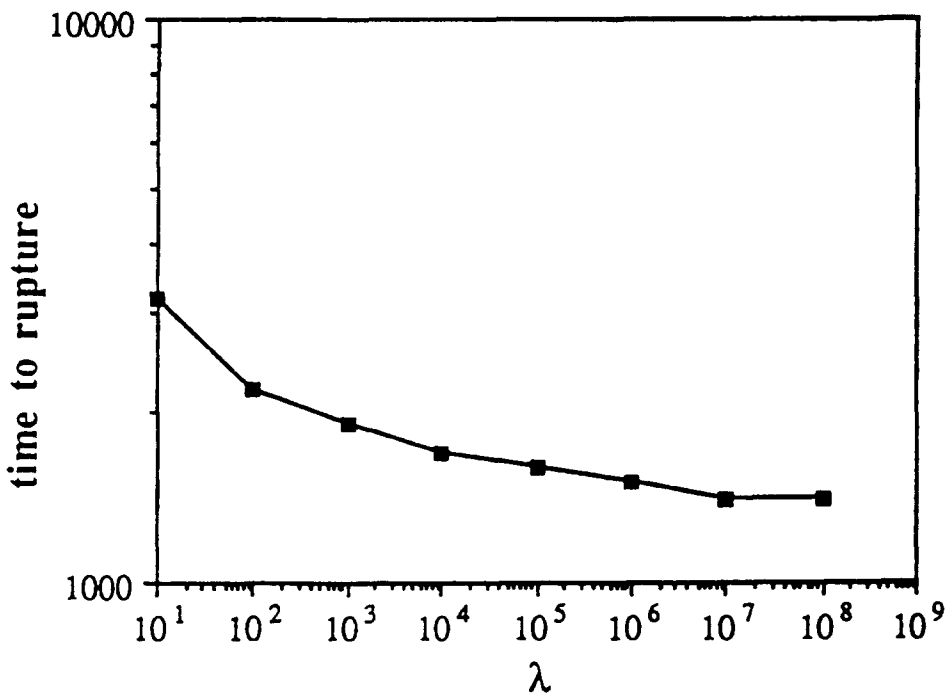

Fig.5. Time to creep rupture as a function of specimen size

Leaving the details of the derivation for a subsequent paper it seems interesting to highlight at least some of the preliminary results. The plot of the strain vs. time using multifractal formalism and numerical simulations for a large lattice λ=32 is shown in Fig.4. At this point it is not evident whether the discrepancy between the results should be attributed to a rather coarse simulations (using equality in the determination of the time interval in (13)) or to some other cause. It is interesting, that despite persistent discrepancies in the latter part of the secondary creep phase, the time to rupture determined by the two compared methods were uniformly close. The time to rupture vs. the specimen size, computed on the basis of the multifractal formalism, is plotted in Fig.5. As expected the initial drop in time to rupture with increase of specimen size is rather dramatic. As the size becomes larger the size effect becomes less pronounced.

SUMMARY AND CONCLUSIONS

The presented study of the creep rupture of polymers emphasizes three important aspects: (a) influence of the temperature on rupture of molecular chains, (b) role of the microstructural disorder, (c) random character of the rupture process and (d) the effect of the specimen size. The study is qualitative in nature and ensuing conclusions must be interpreted as a rough guidance into the physics of the phenomenon. Each of those four issues has a strong influence on the creep deformation in general and the rupture threshold in particular. The conventional models based on mean-field analyses of homogenized continua, deterministic rupture (or damage evolution) criteria and arbitrary discretizations do not address either of these issues. Introduction of many adjustable parameters or non-physical idealizations of the constitutive laws (including at least some of the micro-polar models) may, indeed, provide means to fit a set of test data but will not go very far in providing a better understanding of the deformation process. It seems reasonably to conclude that the large scatter of experimental data is not a nuisance or a result of poorly conducted tests but a reflection of the four essential aspects of the problem listed above.

ACKNOWLEDGMENT

The authors would like to express their gratitude for the financial support in form of a research grant from the U.S. Army Research Office, Engineering Science Division to Arizona State University which made this work possible.

REFERENCES

Curran, D.R., Seaman, L., and Shockey, D.A., 1987, "Dynamic Failure of Solids", *Physics Reports*, Vol. 147, No. 5 & 6, pp. 253-388.

Glasstone, S., Laidler, K.J., and Eyring, H., 1941, *The Theory of Rate Processes*, McGraw-Hill, New York, NY.

Hansen, A., and Roux, S, 1988, "Multifractality in Elastic Percolation", *J. Stat. Physics*, Vol. 53, pp. 759-771.

Kausch, H.-H., 1987, *Polymer Fracture*, Springer Verlag, Berlin, Germany.

Krajcinovic, D. and Basista, M., 1991, "Rupture of Central-Force Lattices Revisited", *J. Phys. I*, Vol. 1, pp. 241-245.

Krajcinovic, D., Lubarda, V., and Sumarac, D., 1993, "Some Fundamental Aspects of the Brittle Cooperative Phenomena - Effective Continua Methods", *Mech. of Materials*, Vol. 15, pp. 99-115.

Krajcinovic, D., and Mallick, K., to appear, "Chemo-Mechanics of the Process Induced

Damage Evolution in Thermosets, Part I and II".

Krajcinovic, D., and Silva, M.A.G., 1982, "Statistical Aspects of the Continuous Damage Theory", *Int. J. Solids Structures*, Vol. 18, pp. 551-562.

Krausz, A.S., and Krausz, K., 1988, *Fracture Kinetics of Crack Growth*, Kluwer Acad. Publ., Dordrecht, The Netherlands.

Mallick, K., and Krajcinovic, D., 1992, "Curing Induced Microcracks in Polymer Matrices", *Damage Mechanics in Composites*, D.H. Allen and D.C. Lagoudas, eds., AMD-Vol. 150, AD-Vol. 32, ASME Publ., pp.141-154.

Martin, J.E., and Wilcoxon, J.P., 1989, "Spatial Correlations and Growth in Dilute Gels", *Phys. Rev. A*, Vol. 39, pp. 252-258.

Regel', V.R., Slutsker, A.I., and Tomashevskii, E.E., 1974, *Kinetic Theory of Strength of Solids*, Nauka, Moscow (in Russian).

Roux, S., and Hansen, A., 1989, "Off-Threshold Multifractality in Percolation", *Europhys. Lett.*, Vol. 8, pp. 729-734.

Termonia, Y., Meakin, P., and Smith, P., 1985, "Theoretical Study of the Influence of the Molecular Weight on the Maximum Tensile Strength of Polymer Fibers", *Macromolecules*, Vol. 18, pp. 2246-2252.

IUTAM Symposium on "Size-Scale Effects in the Failure Mechanisms of Materials and Structures" A. Carpinteri, Ed.

DAMAGE INCURRED DURING THE POLYMERIZATION OF THERMOSETS

D. KRAJCINOVIC
Arizona State University, Tempe, AZ, USA

Abstract

The proposed analytical model for the determination of the damage incurred during the polymerization (curing) of thermoset resins is based on the consideration of the interaction of heat transfer, chemical reaction and mechanical deformation. Consideration is focused on the molecular, micro and continuum (macro) scale. Proposed model illustrates the fundamental importance of the microstructural disorder on the curing process. A short discussion of characteristic lengths, characterizing the microstructure, provides often neglected criteria for the selection of appropriate models. The analytical model are illustrated with a simple problem of damage evolution in an infinitely extended slab of resin.

Keywords: Damage mechanics, polymers, gelation, order-disorder transition, percolation, size and scale effects.

1. Introduction

Principal objective of this paper is to illustrate the fundamental aspects of relationships which exists between the events observed on: (a) molecular, (b) micro and (c) macro (continuum) scales. The basic premise of this study is that an appropriate description of the microstructural disorder is an absolute necessity in analytical modeling of this class of problems. Selection of analytical model must be based on the relative magnitude of the characteristic lengths which describe the state of the order of the microstructure.

The effect of the disorder on the macro response (transport properties) of the system is of largest importance when the concentration of micro-defects is large. A curing polymer is characteristic of this class of processes since it, by definition, passes through the connectivity or sol-to-gel transition. At low values of the degree of cure (i.e. while the sol phase percolates) the system is a fluid with a progressively increasing viscosity. The deformation of the solid fragments (clusters) is entropic in nature since it occurs in absence of strain energy accumulation. At the sol to gel

(phase or elastic percolation) transition the solid phase (gel) percolates through the system. The curing slab acquires shear stiffness and the further deformation occurs in enthalpic mode involving stresses, strains and storage of elastic energy in the crosslinked gel cluster. Stresses in the system are attributable to the chemical and thermal shrinkage of the slab and spatial and temporal fluctuations of the temperature.

2. Polymerization Process

At the onset of curing (i.e. at zero degree of cure) a system consist of individual monomers (single molecules) and initiators. Low temperatures restrict the mobility of monomers and prevent chemical reactions. The mobility of monomers in the bath is increased as the temperature in the autoclave is raised. The ensuing physico-chemical process is known as the polymerization. Curing of thermosets is a complex process during which a fraction of colliding poly-functional m-mers which are endowed with a sufficient kinetic energy, react and bond together into large molecular chains. During advanced stages of the curing process individual molecular chains crosslink into large three-dimensional networks of irregular geometry and topology which provide stiffness (resistance to deformation).

Emergence of stresses in a crosslinked network during curing is attributed to eigenstrains caused by thermal and chemical shrinkage and temperature gradients. Thermal shrinkage occurs during the cooling cycle. Chemical shrinkage reflects the reduction of distance between reacting n-mers during the formation of a bond. Since the collisions between n-mers and k-mers are random events the distribution of eigenstrains is random both in spatial and temporal sense. Local fluctuations of thermal, stress and strain fields are further magnified by the disordered (gossamer) geometry of the ramified network of polymer chains. Consequently, even though the average stresses just beyond the sol to gel transition may be relatively modest the stress concentrations suffice to cause nucleation of sub-microcracks and microcracks. The presence of the ubiquitous process induced damage in polymers [1-3] is a testimony to the effect that the disorder has on the damage evolution.

Newer models of polymerization, supported by the electron microscope studies [4], lend support to the premise that the physics and chemistry of gelation is governed by a sequence of a kinetic (aggregation) and an equilibrium (percolation) process. In its initial stage polymerization is dominated by the mobility of monomers forming a multitude of aggregates suspended in the sol phase percolating through the specimen. System deforms as a viscous fluid. Topologically, the structure of each aggregate resembles a Cayley tree as suggested by the Flory-Stockmayer theory. The diameter of the aggregates typically reaches 0.01 to 0.1 μm [5] before they run out of "free volume" exhausting their "molecular maneuverability and macroscopic fluidity" [6]. At this point aggregates are too large and too densely packed to be able to change their position without deforming and displacing the neighboring aggregates. At this point the process crosses over from aggregation to that of bond percolation characterized by a random formation of bonds between the stationary aggregates (which assume the role of renormalized monomers fixed in the sites of a three-dimensional lattice).

During the percolation stage of the polymerization process "stationary" aggregates

link together by bonds. These aggregate clusters form networks which grow larger with time. At a given connectivity between individual aggregates the divergence of the so-called correlation or coherence length ξ (defined as the length beyond which the cluster sizes are exponentially rare) indicates the emergence of the infinite (spanning) cluster (gel molecule) of interconnected aggregates having a finite shear stiffness. Physically, the aggregates flocculate and as $\xi \to \infty$ the flocculated phase forms the infinite network or gel. On the macro- (or slab) scale, the percolation threshold $\xi \to \infty$, or sol to gel transition, is discerned by a very steep increase of the viscosity of the system. The attendant immobilization of the curing mass is reflected in the attainment of the shear strength and stiffness. The actual elastic percolation threshold is therefore defined as the connectivity $p = p_{ce}$ at which the infinite (spanning) cluster emerges on the renormalized lattice (with aggregates as nodes). Topology of the lattice is defined by the functionality of monomers. The distance between the sites is set by the diameter of the aggregates at the crossover from the aggregation to the percolation phase.

Final changes in material properties take place when the temperature is decreased to the glass transition level. Above the glass transition temperature polymers behave as a viscoelastic solid. At temperature below the glass transition temperature the conformation (entropic) changes of the molecular chain geometry become difficult and each chain locks in a given conformation.

3. Characteristic Lengths

Typical analytical models of micromechanics are based on the universally used but not always acknowledged assumption that the considered material is statistically homogeneous on some scale which is much smaller than the smallest linear size of the specimen. This assumption is seldom questioned under the guise that the defect concentration is small. In the considered case, characterized by a large micro-structural disorder in the vicinity of the sol to gel (connectivity) transition this assumption is obviously not applicable.

The above offered description of the process and the distinction between the micro and macro scales are purely qualitative. A precise quantitative distinction between the scales involves several characteristic lengths. The first length ℓ defines distance between the aggregates at the point at which they become immobilized (i.e. at the crossover between the aggregation and percolation regimes). At first glance it appears that the length ℓ is not important from the point of view of stress analysis since the stresses are negligible before the gel molecule forms (prior to the point at which the solid acquires shear strength). However, the length ℓ is important since it defines the intrinsic length of the sub-microcracks nucleated by the rupture of a single link connecting two adjacent aggregates. Hence, the length ℓ is the intrinsic microstructural length and must be selected as the resolution length (mesh size) to render micromechanical analyses objective (mesh independent).

The linear specimen size L is the second characteristic length which must be introduced since the fracture strength is an extrinsic property of brittle solids (reflected by the conventional size effect). In certain cases the strength or toughness of disordered solids may also exhibit shape effect. In these cases a single length is

not sufficient to characterize the strength of the specimen.

Finally, the correlation length ξ, defined as a maximum length over which the clusters of interconnected aggregates are exponentially rare, is not only important in its own right but is crucial in the process of the selection of the analytical model. Somewhat less precisely the correlation length can also be defined as the mean distance between the two sites belonging to the same cluster. The correlation length is typically defined in function of the connectivity p of the network. The connectivity p is defined as the fraction of links formed between the aggregates during the percolation phase of the process. At the percolation threshold (sol to gel transition $p = p_{ce}$) of an infinite lattice the correlation length ξ tends to infinity, i.e. spans the system by connecting two sides of the specimen. Hence, at the percolation threshold the only evolving characteristic length is lost and the microstructural geometry is rendered self-similar. Infinite cluster is a random, physical fractal which is statistically self-similar. In other words the probability density function of the considered medium property does not exhibit spatial fluctuations. In the asymptotic neighborhood of the percolation threshold (with p slightly in excess of p_{ce}) the range of the self similarity is finite. At lengths less then ξ the geometry appears to be statistically the same as at the percolation threshold. On the scales larger than ξ the network appears to be statistically homogeneous. Thus, the correlation length represents the upper bound below which the cluster is self-similar. The property of self-similarity, reflected in the universality of the scaling laws and percolation threshold p_{ce}, will be repeatedly used in the sequel to this part of the paper.

In micromechanical models it is necessary to relate the actual random, inhomogeneous and piece-wise discontinuous solid with an equivalent effective continuum. The mapping between two media is based on the establishment of the equivalence of the properties and fields in a point of the effective continuum and the corresponding properties of the actual solid averaged over a volume of the material enveloping the considered material point. The smallest volume of the material for which this correspondence can be established, at a given goodness-of-fit, is defined as the representative volume element. The material properties are, therefore, the properties of the representative volume element with a linear size L_r.

Having defined characteristic length and their influence on the homogeneity of the system it becomes possible to determine the range of the validity of methods of analysis. The utility of the effective continuum methods is limited to the case when the defects in the lattice are small, i.e. when the largest defects can be comfortably tucked into the representative volume element. The *MMM* (micro, meso, macro) principle of Hashin [7] can be cast into a more explicit form of an inequality

$$\hat{\xi} << L_r << L \tag{1}$$

where $\hat{\xi}$ and L_r are the linear sizes of the largest defect cluster and the representative volume element. Concentration of defects must be small enough to: (a) render the direct defect interactions a second order effect and (b) reduce the probability of finding a large cluster of connected microcracks to negligible levels. At the incipient percolation transition the condition (1) is not satisfied since the defects percolate through the specimen, i.e. since the size of the defect cluster is singular $\hat{\xi} \to \infty$..

Second of two conditions, related to interaction of the adjacent defects, is also not satisfied in the neighborhood of the percolation threshold rendering the conventional continuum theories and micromechanical models based on the effective continuum (mean-field) theory at best imprecise and vague and at worst inapplicable.

In summary, in the neighborhood of the percolation threshold

$$p \to p_{ce}^{+} \quad and \quad \hat{\xi} \to \infty \tag{2}$$

the geometry and topology of the microstructure is statistically self-similar. Within this range percolation models provide good estimates of the macro response. At modest connectivities p for which a small enough representative volume element exists, such that inequalities (1) are satisfied, solid is statistically homogeneous over a small enough volume needed to render the mean field theories applicable. The macro response within the crossover regime separating the self-similar and macro-homogeneous regime depends not only on the defect density but also on the direct interaction between closely spaced micro-defects. In most cases the determination of the macro response within the crossover regime does not admit elegant analytical solutions. This type of problem is typically approached using numerical simulations and introducing switching (or blending) functions which in two limits blend into self-consistent and percolation solutions [8].

4. Continuum Model

Most of the existing literature [3, 9--11] etc. related to the curing problem focuses on the formulation of local continuum models. Based on the dubious premise that all of the processes depend primarily on the average stresses and strains these models are applicable only when the microstructure is rather homogenous and the stress concentrations negligible. As demonstrated above this is by no means true in the case of polymerization. The geometry of the gel molecule is all but regular, presence of the correlation length renders the solid intrinsically non-local and the rupturing sequence of links is a random process. However, for computational efficiency it is necessary to formulate the continuum model as a general framework relating average stresses, strains and temperature on the specimen scale. This, in fact, is the objective of this part of the paper.

The process of heat conduction is governed by the partial differential equation of diffusion type [12-14] etc.

$$\frac{\partial}{\partial t}(\rho C_p \bar{T}) = \frac{\partial}{\partial x_i}\left(K_t \frac{\partial \bar{T}}{\partial x_i}\right) + \frac{\rho H_t}{2\sqrt{\chi}} \frac{\partial \chi}{\partial t} \tag{3}$$

In general, density ρ, thermal conductivity K_t and the specific heat C_p depend on the extent of the reaction (i.e. the connectivity). Total exothermic heat energy H_t generated during the course of the reaction is assumed to be a constant for a specified resin

and curing regime. The second term on the right hand side of (3) represents the heat liberated during the exothermic reaction of bond formation. The parameter $\chi(y,t)$ represents the fraction of molecular bonds (probability that a given bond between two molecules exists) and is, for a simple polyesterification reaction, related to the degree of cure $\alpha(y,t)$, defined as the probability of finding an individual monomer, by the expression derived in [15] for a simple poly-esterification reaction as

$$\chi = \alpha^2 \tag{4}$$

Relation (4) is crucial for experimental verification of the model since the degree of cure α can be measured using scanning calorimetry methods. Another parameter used in percolation models to quantify the connectivity is p is defined as the probability of finding a link connecting two aggregates. However, this parameter cannot be measured. The parameters $p(y,t)$ and $\chi(y,t)$ are linearly proportional suggesting the following relationship satisfying asymptotic behavior at percolation threshold

$$p = \frac{\chi - \chi_s}{1-\chi_s} H(1-\chi_s) \tag{5}$$

In (5) $H(x)$ stands for the Heaviside functional while χ_s is defined as a fraction of monomer bonds at which the aggregates become mobile and the process crosses over from aggregation to bond percolation. The expression (5) preserves the asymptotic behavior (scaling law) of p and χ in the neighborhood of the percolation threshold. The need for the relation (5) is further emphasized by the fact that during the aggregation phase of the process $p = 0$. Distinction existing between the three parameters (χ, α, p), defining the connectivity of the gel network, has neither been fully recognized nor appreciated in the existing mechanics literature.

The equation of the rate of chemical reactions can be derived from the collision theory. Rate at which the bonds are formed depends on the probability that two molecules, having sufficient kinetic energy to overcome the repelling forces, will collide and react in a unit of time. This probability is, according to the Boltzmann-Maxwell statistic [16] given in form of the Arrhenius dependence on the temperature T and activation energy U. Thus, the probability that a bond will be formed during the collision is proportional to $\exp(-U / k_b T)$ where k_b is the Boltzmann constant. Activation energy U is defined as the difference between the sublimation energy U_o and the free energy Φ stored in a link of the network.

The rate of the accrual of links in the renormalized network was derived in [14, 17] in the form of an ordinary differential equation

$$\frac{dp}{dt} = \frac{1}{t_o}\exp\left(-\frac{U_o}{k_b T}\right)(1-p) - \frac{1}{N}\sum_{i=1}^{N}\frac{1}{t_o}\exp\left(-\frac{U_o - \Phi_i}{k_b T}\right) \qquad p > p_{ce} \tag{6}$$

First and second terms on the right hand side of the expression (6) defines the rate at which the links between the aggregates are formed and ruptured, respectively. Equation (6) can be rewritten in a simpler form as

$$\frac{dp}{dt} = \frac{1}{t_o}\exp\left(-\frac{U_o}{k_b T}\right)(1-p-w) \tag{7}$$

The parameter w can be cast into a more convenient form [17] as

$$w = \sum_{n=o}^{\infty} \frac{1}{n!} M_n(\varphi) \tag{8}$$

where

$$M_n(\varphi) = \int_o^{\infty} \varphi^n \tilde{p}(\varphi) d\varphi \tag{9}$$

is the n-th statistical moment of the distribution of the normalized free energy $\varphi = \Phi / k_b T$ stored in the individual links of the gel network.

Finally, it is necessary to derive the equation relating the macro (average) stress in the slab and the eigenstrain related to the thermal and chemical shrinkage. The well known expressions for the relaxation of polymers due to the changes in the conformations of the molecular chains associated with the disentaglements and diffusion of segments [18] must be changed to accommodate the changing connectivity $p(t,y)$ of the network. The character of the viscoelasticity is determined by the vibratory motion of individual chain segments and the free length of chains between two adjacent crosslinks. The characteristic time of relaxation depends on the state of connectivity and the frictional effects which inhibit changes of conformations.

Continuum theory of the viscoelastic response of crosslinked polymers based on the Rouse and Zimm models and the reptation dynamics was recently developed in [4, 19]. Elastic properties of a curing polymer change with the extent of crosslinking (growing degree of cure α). Realizing that the change in the degree of cure α results in the change of scale (defined by the change in the correlation length ξ) [19] suggested a redefined time to account for the proportionality between the relaxation time of a cluster and its size. The ensuing time-cure superposition model approximates the viscoelastic deformation of curing polymers by a sequence of states corresponding to discrete times defining the extent of the chemical reaction.

Considering a slab infinitely extended in horizontal direction (xz plane), free of tractions at the bottom and top surfaces and neglecting the body forces, the integral equation for the only non-vanishing components $\sigma_x(y,t) \equiv \sigma_z(y,t)$ of the macro (volume averaged) stress tensor can be derived in the following form [17]

$$\frac{1}{2}\sigma_x(y,t)+\int_o^t G_\infty[p(s)]\left\{\frac{2}{3K[p(s)]}\frac{d\sigma_x(y,s)}{ds}+3\frac{d\bar{\varepsilon}^*(y,s)}{ds}\right\}ds+\int_o^t \varepsilon_y^{eff}(s)\frac{dG_\infty[p(s)]}{ds}ds$$

$$+\int_o^t G_r[t-s,p(s)]\left\{\frac{2}{3K[p(s)]}\frac{d\sigma_x(y,s)}{ds}+3\frac{d\bar{\varepsilon}^*(y,s)}{ds}\right\}ds=0 \qquad (10)$$

where $G_r(p,t)$, $G_\infty(p)$ are the equilibrium and relaxation shear moduli, $K(p)$ the bulk modulus and

$$\bar{\varepsilon}^* = \bar{\varepsilon}_{th} - \bar{\varepsilon}_{sh} = \alpha(T-T_{ce}) - \frac{p-p_{ce}}{1-p_{ce}}\bar{\varepsilon}_f \qquad (11)$$

the volume average of the eigenstrain due to the total shrinkage attributable to the chemical reaction and temperature. In (11) α, T_{ce} and $\bar{\varepsilon}_f$ are the coefficient of thermal expansion, temperature at the percolation threshold and the final extent of shrinkage at the termination of the cure process ($p=1$). Finally,

$$e_{ij}^{eff}(s) = \int_o^s \Gamma_r[s-u,p(u)]\frac{\partial e_{ij}(u)}{\partial u}du \qquad (12)$$

is the effective strain tensor which couples the memory effects of the relaxation and the equilibrium moduli of the curing polymer [19]. The non-dimensional (normalized) relaxation modulus in (12) is defined by the ratio

$$\Gamma_r(s) = \frac{G_r(s)}{G_r(0)} \qquad (13)$$

Details of the derivation are available in [17].

In summary, a rational determination of macro (volume averaged) stresses and strains in a curing resin slab requires solution of three coupled equations (3), (7) and (10) governing exothermic heat conduction, rate of chemical reactions and mechanical deformation. Boundary conditions require that the temperature at the traction free surfaces $y=\pm h$ (where $2h$ is the slab thickness) is equal to the autoclave temperature. Initially, at $t=0$ the stresses are equal to zero and the connectivity is equal to the connectivity at the elastic percolation threshold $p(t=0)=p_{ce}$.

Three governing equations in three unknown functions $\sigma_x(y,t)$, $T(y,t)$, $p(y,t)$ are coupled both directly and indirectly through the parameters which depend on the connectivity p. The determination of the effective parameters using micromechanical models such as mean field and percolation theories is a well understood problem. A much more insidious coupling occurs in equation (7). The rate at which the links of the renormalized network rupture depends not only on the zero-th (i.e. average stress) but on all other moments of the distribution of forces (internal energies) in the

network as well. Consequently, the considered problem cannot be solved using the conventional mean field models of micromechanics.

5. Micromechanical Considerations

The material parameters in the heat conduction equations do not exhibit singular behavior in the neighborhood of the percolation threshold. In fact they change only slightly and to simplify the derivation they will be considered as being constants. Furthermore, it will be assumed that the bulk modulus changes with the connectivity in a manner defined by the self consistent approximation, i.e. that in tension

$$\frac{K(p)}{K_o} = \frac{p - p_{ce}}{1 - p_{ce}} \qquad p_{ce} \le p \le 1$$

and (14)

$$K = 0 \qquad p \le p_{ce}$$

Expressions (4) ignore finer points of the scaling laws in the asymptotic neighborhood of the percolation threshold and the interaction of defects in the crossover regime. A more sophisticated form for $K(p)$ can be derived using blending functions [8] but the gain will be minimal since the accent is on the shear strains.

At the percolation threshold (gel point) the shear modulus (i.e. stiffness) of the slab is, by definition, equal to zero. As a consequence of similarity the shear stiffness is expected to follow a universal power law immediately after the slab passes through the gel point. This expectation was, indeed, observed in experiments (summarized in [4]) in which a polymer at gel point was subjected to an oscillating strain field of constant amplitude. The divergence of the viscosity and the equilibrium shear modulus in the asymptotic vicinity of the gel point is defined by the scaling laws [19]

$$\eta \propto |p_{ce} - p|^{-k} \qquad \text{and} \qquad G \propto |p_{ce} - p|^{z} \tag{15}$$

Universal exponents in (15) are $z = d\nu \cong 8/3$ and $0 \le k \le 4/3$, where ν is the exponent for the correlation length ξ. As the connectivity p is increased beyond the percolation threshold the clusters size increases. Large clusters diffuse slower than the small ones. Thus, the degree of the cure is reflected in the change of the scale. The actual time must be renormalized dividing it by the longest relaxation time τ_z which dominates the dynamics of the of molecular chains. The longest relaxation time is defined as a time needed for a chain of length ξ to diffuse through its own radius. Written in the following form

$$\tau_z = \int_o^\infty tGT(t)dt \Big/ \int_o^\infty GT(t)dt = \frac{\eta}{G_\infty} \propto |p - p_{ce}|^{-(z+k)} \tag{16}$$

the longest relaxation time also represents the time at which the response crosses over from a simple to a complex viscoelastic regime. Accounting for the fact that the decay crosses over form the power law to an exponential law as the time t approaches the longest relaxation time the expression for the relaxation shear modulus for the bulk polymer melt was specified by [19] as

$$G_r(t) \propto \frac{\eta}{\tau_z}\left(\frac{\tau_z}{t}\right)^{2/3} \exp\left[-\left(\frac{\tau_z}{t}\right)^{0.4}\right] \qquad p < p_{ce}$$

and (17)

$$G_r(t) = CG_\infty\left(\frac{\tau_z}{t}\right)^{2/3} \exp\left[-\left(\frac{t}{\tau_z}\right)^{0.4}\right] \qquad p > p_{ce}$$

where C is a constant which depends on the shear modulus of the glassy phase.

The first of the two expressions (17) is applicable to the system in which the fluid phase (sol) percolates, i.e. for a viscous fluid with a vanishing equilibrium shear modulus. The second of two expressions, representing the statement of the cure-superposition principle, is valid for a system in which the solid phase (gel) percolates. The shear resistance is provided by the infinite cluster (gel) which dominates the deformation process. The simple scaling law (17) was shown to replicate the experimental data with a surprising accuracy [4, 19] which persists well into the mean field regime.

Finally, it is necessary to determine the stiffness of the links connecting aggregates (sites of the renormalized lattice). Each of these links represents a network formed by several molecular chains crosslinked to each other. On the molecular (chain) scale the deformation modes of a single chain include: change of conformation (segment rotation or gauche-trans transformation), cavitation, slip and/or chain scission [2]. To determine the "stiffness" of a chain it suffices to consider only the change of conformation and its effect on the flexibility. A stretching polymer chain passes through a sequence of a discrete equilibrium (minimum free energy) states which correspond to different conformations. In the course of stretching process very little energy is stored in the bonds. The change in the free energy is almost entirely attributed to the decrease in entropy (probability of corresponding conformational states). The deformation process of the described type belongs to the class of entropic elasticity. If the force on a single free and highly deformable links is maintained for a long time the chain reverts to its most probable conformation converting the excess energy into heat.

The stiffness of a single chain can be determined analytically only for small deformations of freely jointed single chains. In all other cases determination of the link stiffness requires simplifying assumptions. Force-displacement relation in a crosslinked chain network combines the competing effects of elastic stretching (enthalpic effects) and conformation changes (entropic effects). A crosslinked network is both dissipative and energy storing. Assuming the deformation to be small it can again be assumed that the force-elongation relation remains linear but the spring stiffness is not a constant.

Consider a crosslinked network consisting of N_c chains each of which is formed of

n_s segments. The average free energy stored in a segment of i-th link is $\bar{\phi}_i(p) = \Phi_i / [N_c n_s(p)]$. Free energy stored in the link can be estimated assuming that: all chains have the same length and that the end-to-end distances of each chain are defined by Maxwell probability density function [20]. Subject to these assumptions the average free energy stored in a segment of the i-th crosslinked network connecting two neighboring aggregates is

$$\bar{\phi}_i(p) = \frac{\Phi_i}{N_c n_s(p)} \approx \frac{3k_b T}{2n_s(p)\ell^2} r^2 \tag{18}$$

where ℓ is the average distance between the aggregates and $n_s(p)$ the average number of segments in a chain. As the number of segments in a crosslinked network increases during curing the free energy decreases while the activation energy increases. The rate of rupture of links connecting the aggregates rupture (8) is now

$$w = \sum_{n=0}^{\infty} \frac{1}{n!} \int_o^{\infty} \varphi^n \tilde{p}(\varphi) d\varphi \quad \textit{where} \quad \varphi = \frac{\bar{\phi}}{k_b T} \tag{19}$$

Normalized free energy φ in (19) is redefined in view of the postulated rupture process of radicalized chains. The mechanical energy stored in the link serves only to lower the energy barrier through its contribution to the free energy (in form of the internal energy). The increase of the temperature does not only decrease the argument of the exponential function in (6). It also increases the free energy through the entropy term and the rate of formation of free radicals (reducing the time needed for the rupture of a link caused by the scission of a single chain). Hence, the rupture of links connecting the adjacent aggregates is a random process due to the non-deterministic nature of the spatial and temporal fluctuations of thermal energy.

Formation of a crosslinked connection (link) between two adjoining aggregates is not instantaneous. Thus, the link "stiffness" varies with time during its formation. Link rupture is a much more rapid process of chemical dissociation which is also not instantaneous. Since the time needed to form and rupture a link is still short compared to the cure duration it will be assumed that the spring stiffness remains constant from its formation to its rupture and that the link rupture is instantaneous. These assumptions are entirely consistent with the selected resolution length according to which events on molecular scale are smoothed out.

6. Distribution of the Free Energy in the Lattice

Distribution of forces (and energy stored) in the links of the renormalized lattice can be determined using numerical simulations. However, for a lattice analysis to be objective the resolution (bond) length ℓ must be equal to the inherent characteristic length of the microstructure (size of the nucleated sub-microcracks). In the present case, the characteristic microstructural length is equal to the average distance between the adjacent aggregates at the crossover from aggregation to percolation. The initial length of the sub-microcracks [1,2], nucleated in the course of the rupture of a single link, is on the order of $\ell \approx 0.1\mu m$. Thus, to preserve the objectivity, a cubic lattice

occupying a cube with a volume of only 1 cm^3 should be modeled by a lattice having 10^{15} nodes rendering objective simulations impractical if not impossible.

Analytical methods based on the self-similarity of the gel cluster geometry near the percolation transition provide the only feasible alternative. The mass (total length of all constituent links) of the spanning cluster is a statistical fractal. However, different subsets of the cluster (formed by links storing equal free energy) have different fractal dimensions. Structures of this type are referred to as multifractal and are often formed by random multiplicative processes .

Assuming that the considered slab can be approximated by a deck of lattices the distribution of energy stored in the links can be determined using the multifractal formalism developed in [21, 22] Skipping the details available in [17] the expressions for the statistical moments (9) scale in the vicinity of the gel point as

$$M_n(\varphi) = \sum_j \left(\sqrt{\Phi_j}\right)^n \propto \lambda^{y(n)} \quad \text{where} \quad \lambda = L/\ell \tag{20}$$

Each statistical moment scales with a different exponent $y(n)$ which do not depend on the specimen size. However, expression (20) incorporates the scale effect through the parameter λ. The expressions for the exponents can be derived for the percolation transition and the period for which $p > p_{ce}$. After a rather long derivation the exponents in (20) can be written as

$$y(n) \approx \left(\frac{1-p}{1-p_{ce}}\right)^m [-1.25 + 1.03n + 0.87\exp(-1.35n)] \tag{21}$$

where m is a positive integer. Finally, the expression for the rate at which the links rupture (8) becomes

$$w = \sum_{n=0}^{\infty} \frac{1}{n!}\left(\frac{\overline{\phi}_{avg}}{k_b T}\right)^n C_1^{1-n}\lambda^{y(n)} \quad \text{where} \quad \overline{\phi}_{avg} = \int_0^{\infty} \overline{\phi}\tilde{p}(\overline{\phi})d\overline{\phi} \tag{22}$$

where the constant C_1 must be determined from simulations.

7. Illustrative Example

Using data for the DGEBA epoxy resin and the curing regime shown in Fig. 1a it was now possible to solve the problem by numerical integration of the derived system of equations (3), (7) and (10), with effective material parameters defined in Section 5 and the rate of link ruptures by (22). Figs.1a,b show that the damage accumulates (link rupture) before the cooling starts. Thus, as conjectured in [3], the damage incurred during the polymerization is attributable to the chemical rather than thermal shrinkage. Furthermore, comparing curves with triangles it becomes obvious that the damage is much larger in the middle of the slab than on the free surfaces.

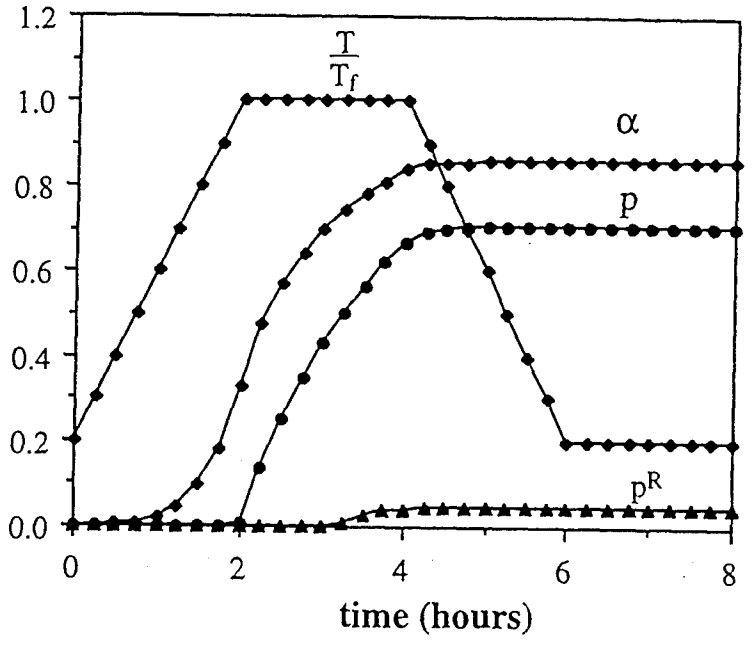

(a)

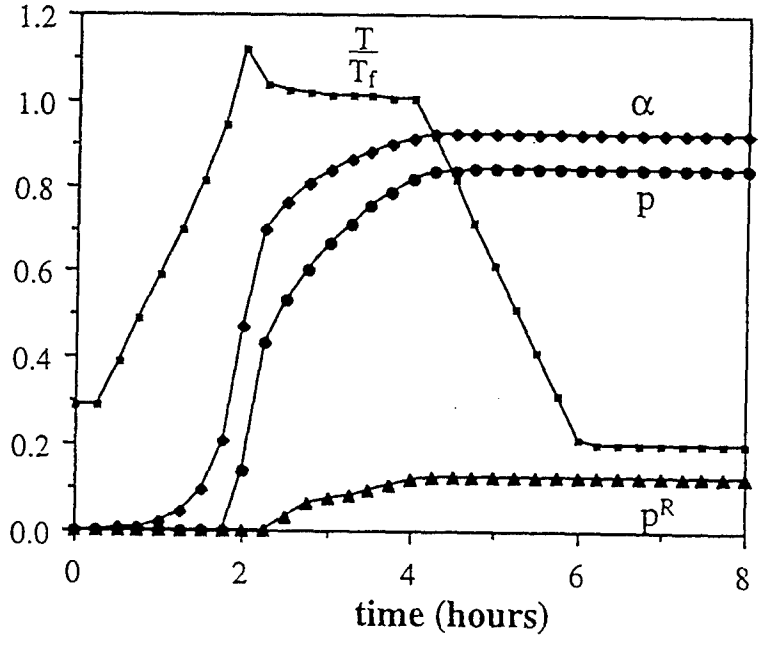

Fig.1. Evolution of the normalized temperature, degree of cure (α), connectivity p and fraction of ruptured links (p^R) at: (a) surface of the slab and (b) slab mid-plane.

8. Summary and Conclusions

The proposed model for the determination of the damage incurred in thermoset resins during polymerization: (a) encompasses three scales, (b) couples equations of chemical reaction rate, heat transfer and mechanical deformation and (c) clearly identifies all material parameters. It also considers microstructural disorder and its effect on the rupturing process. Consideration of the relative magnitude of characteristic lengths indicate that other methods are not applicable to this problem.

Simplifying assumptions introduced for purposes of illustration can be readily removed at some expense of the tractability. However, even in its current form the proposed model represent a radical change of basic concepts by emphasizing the essential role of microstructural disorder on the evolution of process induced damage.

9. Acknowledgement

The author gratefully acknowledges the financial support rendered by the research grant from U.S. Army Research Office, Engineering Science Division to the Arizona State University which made this work possible.

10. References

1. Kuksenko, V.S. and Tamuzs, V.P., (1981), *Fracture Micromechanics of Polymer Materials*, M. Nijhoff Publ., Boston, MA.
2. Kausch, H.-H., (1987), *Polymer Fracture*, Springer-Verlag, Berlin, Germany.
3. Guz', A.N., V.T. Tomashevskii, N.A. Shul'ga and V.S. Iakovlev, (1988), *Technological Stresses and Deformations in Composite Materials,* Vischa Shkola Publ., Kiev, Ukraine.
4. Martin, J.E., Adolf, A. and Wilcoxon, J.P., (1989), Viscoelasticity near the sol-gel transition, *Physical Review A.*, Vol. 39, pp. 1325-32.
5. Martin, J.E. and Wilcoxon, J.P., (1989), Spatial correlations and growth in dilute gels, *Physical Review A*, Vol. 39, pp. 252-8.
6. Zallen, R., (1983), *The Physics of Amorphous Bodies*, Wiley, New York, NY.
7. Hashin, Z., (1983), Analysis of composite materials - a survey, *Journal of Applied Mechanics*, Vol. 50, pp. 481-505.
8. Thorpe, M.F. and Jasiuk, I., (1992), New results in the theory of elasticity for two-dimensional composites, *Proceedings of Royal Society of London*, Vol. A 438, pp. 531-544.
9. Hahn, H.T. and Pagano, N.J., (1976), Curing stresses in composite laminates, *Journal of Composite Materials*, Vol. 10, pp. 266-77.
10. Li, N. and Barber, J.H., (1989), Residual stresses in castings with axi-symmetric solidification, *Engineering Science Reprints*, 26th Annual technical Meeting of the Society of Engineering Sciences, Ann Arbor, MI.
11. Bogetti, E.G. and Gillespie, W. Jr., (1989), Process-induced stress and deformation in thick-section thermosetting composite laminates, *Reprints of 21st International SAMPE Technical Conference*, Atlantic City, NJ.

12. Mallick, K. and D. Krajcinovic, (1992a), Cure induced inelastic deformation in thermosetting polymers, in: *Recent Advances in Damage Mechanics and Plasticity*, (ed. J.W. Ju), ASME Publication, AMD-Vol. 132, MD-Vol. 30, New York, NY., pp. 159-72.
13. Ciriscioli, P.R. and G.S. Springer, (1990), *Smart Autoclave Cure of Composites*, Technomics, Lancaster, PA.
14. Mallick, K. and D. Krajcinovic, (1992b), Curing induced microcracks in polymer matrices, in: *Damage Mechanics in Composites*, (eds. D.H. Allen and D.C. Lagoudas), ASME Publication, AMD-Vol. 150, AD-Vol. 32, pp. 141-54.
15. Stockmayer, W.H., (1943), Theory of molecular size distribution and gel formation in branched chain polymers, *The Journal of Chemical Physics*, Vol. 11, pp. 45-55.
16. Glasstone, S., Laidler, K.J. and Eyring, H., (1941), *The Theory of Rate Processes*, McGraw-Hill Book Co., New York, NY.
17. Krajcinovic, D. and Mallick, K., (in print), Micromechanics of the process induced damage evolution in thermosets, *J.ournal of Mechanics and Physics of Solids*.
18. Meares, P., (1965), *Polymers*, D. Van Nostrand Company Ltd., New York, NY.
19. Adolf, D. and Martin, J.E., (1990), Time-cure superposition during cross-linking, *Macromolecules*, Vol. 23, pp. 3700-4.
20. Farris, R.J., (1971), The stress-strain behavior of mechanically degradable polymers, in: *Polymer Networks - Structure and Mechanical Properties*, (eds. A.J. Chompff and S. Newmann), Plenum Press, New York, NY.
21. Hansen, A. and Roux, S., (1988), Multifractality in elastic percolation, *Journal of Statistical Physics*, Vol. 53, pp. 759-71.
22. Roux, S. and Hansen, A., (1989), Off-threshold multifractality in percolation, *Europhysics Letters*, Vol. 8, pp. 729-34.

Journal of Mechanics and Physics of Solids (to appear).

MICROMECHANICS OF THE PROCESS INDUCED DAMAGE EVOLUTION IN THERMOSETS

Dusan Krajcinovic and Kaushik Mallick[1]
Mechanical and Aerospace Engng., Arizona State University
Tempe, AZ 85287-6106

ABSTRACT

Present study focuses on the formulation of a micromechanically based analytical model of the evolution of damage in thermoset resins during cure. Study emphasizes the effect of the microstructural disorder on the macro response. To avoid introduction of arbitrary fitting constants and parameters the problem is considered on three different length scales. The proposed model consists of a system of equations governing the exothermic chemical reaction, heat transfer and deformation. Effective properties of the solid and distribution of stresses are determined using non-traditional micromechanical models.

I. INTRODUCTION

The principal objective of this study is to formulate a rational analytical model needed to determine the damage accumulated in resins during the cure. Considerations of events on the molecular and micro scales emphasizes the necessity for an appropriate description of damage evolution which depends on all statistical moments of the distribution of stresses in the disordered microstructure of the resin near the sol-gel transition. This study indicates the arbitrariness of the continuum models which neglect the disorder of the resin microstructure near the sol to gel transition. Consideration of relations between the characteristic lengths, intrinsic to the evolving microstructure, underlines the limitations of traditional (mean field) methods of micromechanics used for the determination of the effective material parameters and stresses in the vicinity of the phase transition.

---

[1] Currently: All Plastics & Fiberglass, Mobile, AL 36608

II. POLYMERIZATION PROCESS

Polymerization of thermosets is a complex process during which the initial sol (viscous fluid) transforms into a gel (intricate network of crosslinked aggregates). When heated in autoclave monomers of a dilute solution diffuse and collide. A fraction of colliding monomers, which are endowed with a sufficient kinetic energy, react and bond together into progressively larger chains. This process, occurring at many sites simultaneously, generates many fractal aggregates consisting of entangled molecular chains [MARTIN and ADOLF (1991)]. Topologically, the structure of each aggregate resembles a Cayley tree as suggested by the Flory-Stockmayer theory. The diameter of the aggregates typically reaches 0.01 to 0.1 μm [MARTIN and WILCOXON (1989)] before they run out of "free volume" exhausting their "molecular maneuverability and macroscopic fluidity" [ZALLEN, (1983)]. At this point aggregates become too large to be able to change their position without deforming and displacing the neighboring aggregates. Accordingly, the process crosses over to that of the bond percolation which is characterized by a random formation of bonds between the stationary aggregates (which assume the role of renormalized monomers fixed in the sites of a three-dimensional lattice).

During the percolation stage of the polymerization process aggregates linked together by bonds form clusters which grow larger with time. At a well defined threshold value of the fraction of links connecting individual aggregates, the correlation length (defined as the length beyond which the cluster sizes are exponentially rare) diverges $\xi \to \infty$ reflecting the emergence of the infinite (spanning) cluster (gel molecule) of interconnected aggregates. On the macro scale, the percolation threshold $\xi \to \infty$, or sol to gel transition, is discerned by a very steep increase of the viscosity of the system and in the attainment of the shear strength and stiffness. The actual elastic percolation threshold is defined as the connectivity $p = p_{ce}$ at which the infinite (spanning) cluster emerges on the renormalized lattice. Final changes in material properties take place when the temperature is decreased to the glass transition level. At this point each chain locks into a given conformation rendering further conformational (entropic) changes

difficult [COWIE (1991)]. A conceptual scheme of the sequence of events is sketched in Fig.1.

Curing induced stresses in a crosslinked network are attributed to eigenstrains caused by thermal and chemical shrinkage and temperature gradients. Chemical shrinkage reflects the reduction of distance between reacting m-mers during the formation of a bond. Since the collisions between n-mers and k-mers are random events the distribution of eigenstrains is spatially and temporally random. Thermal shrinkage occurs during the cooling cycle. Local fluctuations of stress and strain fields are magnified by the disordered geometry of the ramified network of polymer chains. Thus, even though the average stresses just beyond the sol to gel transition may be relatively modest the stress concentrations are sufficient to cause nucleation of sub-microcracks and microcracks. Ubiquity of the process induced damage in polymers [KUKSENKO and TAMUZS (1981), KAUSCH (1987) and GUZ', et al. (1988)] is a testimony to the effect of disorder on damage evolution.

III. CHARACTERISTIC LENGTHS

The described polymerization process and the distinction between the micro and macro scales are purely qualitative. A precise quantitative distinction between the scales requires consideration of several characteristic lengths. The first of these lengths ℓ defines distance between the aggregates at the point at which they become immobilized (at the crossover between the aggregation and percolation regimes). At a first glance it appears that the length ℓ is not important for stress analysis since the stresses are negligible prior to the formation of the gel molecule (before the solid acquires shear strength). However, the length ℓ is important since it defines the intrinsic length of the sub-microcracks [KUKSENKO and TAMUZS (1981)] nucleated by the rupture of a single link connecting two adjacent aggregates. Hence, length ℓ is an intrinsic microstructural length. Assuming that the smallest microcrack of interest is of the size of the space between two aggregates ℓ must be selected as the resolution length to render micromechanical analyses objective (mesh independent).

The linear specimen size L is also a characteristic length since the fracture strength is an

extrinsic property of brittle solids (reflected by the conventional size effect).

The correlation length ξ, defined as a maximum length over which the clusters of interconnected aggregates are exponentially rare [ISICHENKO (1992)], is not only important in its own right but is crucial in the process of the selection of the analytical model. The correlation length $\xi(p)$ is defined as a function of the connectivity p of the network. The connectivity p is defined as the fraction of links formed between the aggregates during the percolation phase of the process. At the percolation threshold (sol-gel transition $p = p_{ce}$) of an infinite lattice the correlation length ξ tends to infinity, by spanning the system and connecting two sides of the specimen. Hence, at the percolation threshold the only evolving characteristic length is lost and the microstructural geometry is rendered self-similar. Infinite cluster is a random, physical fractal which is statistically self-similar. In other words the probability density function of the considered property of this cluster does not exhibit spatial fluctuations. In the asymptotic neighborhood of the percolation threshold (with p slightly in excess of p_{ce}) the range of the self similarity is finite. At lengths less then ξ the geometry appears to be statistically the same as at the percolation threshold (i.e. self-similar). On the scales larger than ξ the network is statistically homogeneous. Thus, the correlation length represents the upper bound below which the cluster is self-similar. The property of self-similarity, reflected in the universality of the scaling laws and percolation threshold p_{ce}, will be repeatedly used in the sequel to this part of the paper.

In micromechanical models it is necessary to relate the actual random, inhomogeneous and piece-wise discontinuous solid with an equivalent effective continuum. The mapping between two media is based on the establishment of the equivalence of the properties and fields in a point of the effective continuum and the corresponding properties of the actual solid averaged over a volume of the material enveloping the considered material point. The smallest volume of the material for which this correspondence can be established, at a given goodness-of-fit, is defined as the representative volume element. The material properties are, therefore, the properties of the representative volume element with a linear size L_r.

Having defined characteristic length and their influence on the homogeneity of the system it

becomes possible to determine the range of the validity of methods of analysis. The utility of the effective continuum methods is limited to the case when the defects in the lattice are small, i.e. when the largest defects can be comfortably tucked into the representative volume element. The domain within which the *MMM* (micro, meso, macro) principle of [HASHIN (1983)] and mean field models are valid can be cast into an explicit form of an inequality

$$\hat{\xi} << L_r << L \tag{1}$$

where $\hat{\xi}$ is the correlation length of the defects (defined as cluster of missing links between the aggregates forming the lattice nodes). Concentration of defects must also be small enough to: (a) render the direct defect interactions a second order effect and (b) reduce the probability of finding a large cluster of connected microcracks to negligible levels. At the incipient sol-gel transition the condition (1) is not satisfied since the defects percolate through the specimen, i.e. since the size of the largest defect cluster is singular $\hat{\xi} \to \infty$ (or $\hat{\xi} \to L$ in a finite lattice). Second of two conditions, related to the interaction of adjacent defects, is also not satisfied in the neighborhood of the percolation threshold rendering the conventional continuum theories and micromechanical models based on the effective continuum (or mean-field) theory inapplicable.

In summary, in the neighborhood of the percolation threshold

$$p \to p_{ce}^{+} \quad and \quad \hat{\xi} \to \infty \tag{2}$$

the geometry and topology of the microstructure is statistically self-similar. Within this range percolation models provide good estimates of the macro response. At modest connectivities p for which a small enough representative volume element exists, such that inequalities (1) are satisfied, solid is statistically homogeneous over a small enough volume needed to render the mean field theories applicable. The macro response within the crossover regime separating the self-similar and macro-homogeneous regime depends not only on the defect density but also on the direct interaction between the closely spaced micro-defects. Determination of macro response within the crossover regime does not admit elegant analytical solutions. This type of problem is typically approached using numerical simulations and introducing switching functions which in two limits blend into self-consistent and percolation solutions [THORPE and JASIUK (1992)].

IV. CONTINUUM MODEL

Most of the existing literature [LEVITSKY and SCHAFFER (1974), HAHN and PAGANO (1976), GUZ', et al. (1988), LI and BARBER (1989), BOGETTI and GILLESPIE (1989), MALLICK and KRAJCINOVIC (1992a), etc.] related to the curing problem is focused on the formulation of local continuum models. Based on the premise that all of the processes depend primarily on the average stresses and strains these models are applicable only when the microstructure is macro homogenous and the effect of the stress concentrations on the macro response negligible. This is by no means true in the considered case. The geometry of the gel cluster is all but regular. Absence of macro homogeneity renders the solid intrinsically non-local and the rupturing sequence of links is a random process. However, for computational efficiency it is necessary to formulate the continuum model as a general framework relating average stresses, strains and temperature on the specimen scale. At $p \to 1$ the equations of this model refer to an effective solid statistically homogenous over length $L_r << L$. Near the percolation threshold $p \to p_c^+$ these equations and parameters refer to the specimen, i.e. gel cluster.

IV.1. *Heat Conduction*

Process of heat conduction is governed by the partial differential equation of diffusion type [CIRISCIOLI and SPRINGER (1990), MALLICK and KRAJCINOVIC (1992a, 1992b), etc.]

$$\frac{\partial}{\partial t}(\rho C_p \bar{T}) = \frac{\partial}{\partial x_i}\left(K_t \frac{\partial \bar{T}}{\partial x_i}\right) + \frac{\rho H_t}{2\sqrt{\chi}} \frac{\partial \chi}{\partial t} \qquad (i = 1, 2, 3) \qquad (3)$$

In general, density ρ, thermal conductivity K_t and the specific heat C_p depend on the extent of the reaction. Total exothermic heat energy H_t generated during the reaction is assumed to be a constant for a specified resin and curing regime. Second term on the right hand side of (3) represents the heat liberated during the exothermic reaction of bond formation. The parameter $\chi(y,t)$ represents the fraction of molecular bonds (probability that a given bond between two

molecules exists) and is, for a simple polyesterification reaction, related to the degree of cure $\alpha(y,t)$ by the expression derived in STOCKMAYER (1943)

$$\chi = \alpha^2 \tag{4}$$

Relation (4) is crucial for experimental verification of the model since the degree of cure α can be measured using scanning calorimetry methods [DUSI, et al. (1987)]. Another parameter used in percolation models to quantify the connectivity, i.e. the probability of finding a link connecting two aggregates, is p. This parameter cannot be directly measured. The parameters $p(y,t)$ and $\chi(y,t)$ are linearly proportional suggesting the following relationship that satisfies asymptotic behavior at percolation threshold

$$p = \frac{\chi - \chi_s}{1 - \chi_s} H(1 - \chi_s) \tag{5}$$

In (5) $H(x)$ stands for the Heaviside function while χ_s is defined as a fraction of monomer bonds at which the aggregates cease to be mobile and the process crosses over from aggregation to bond percolation. The expression (5) preserves the asymptotic behavior of p and χ in the neighborhood of the percolation threshold. The need for this relation is further emphasized by the fact that during the aggregation phase of the process $p = 0$. The distinction existing between the three parameters (χ, α, p), which define various aspects of the connectivity of the gel network, has neither been fully recognized nor appreciated in the existing literature.

IV.2. *Kinetic of the Chemical Reaction of Bonding*

The equation of the rate of chemical reactions can be derived from the collision theory. The rate at which the bonds are formed depends on the probability that two m-mers, having sufficient kinetic energy to overcome the molecular repelling forces, will collide and react within a unit of time. ,According to the Boltzmann-Maxwell statistic [GLASSTONE, et al. (1941), etc.] this probability assumes the form of the Arrhenius dependence on the temperature T and activation energy U. The probability that a bond will be formed during the collision is proportional to

$\exp(-U/k_bT)$ where k_b is the Boltzmann constant. Activation energy U is defined as the difference between the sublimation energy U_o and the free energy Φ, i.e.

$$U = U_o - \Phi = U_o - (W - TS) \tag{6}$$

The difference $U_o - \Phi$ represents the energy barrier, i.e. the energy which must be supplied for a bond between two aggregates to either form or rupture [REGEL', et al. (1974) or KRAUSZ and KRAUSZ (1988)]. The free energy Φ represents the difference between the internal energy W and the product of the absolute temperature T and entropy S.

The net rate at which the links between the aggregates are formed during the percolation phase is equal to the difference between the rates at which they form and rupture. The probability that a link will form in a unit of time is, according to the Maxwell-Boltzmann statistics, equal to $t_o^{-1}\exp(-U_o/k_bT)$, where t_o is the period of the free thermal vibration of an atom. On the other hand the probability that a link will fail in a unit of time is $t_o^{-1}\exp[-(U_o-\Phi_i)/k_bT]$. The probability that a link will fail depends on the free energy it stores. Hence, the probability of rupture changes from one link to the other. The net rate of the link accrual [MALLICK and KRAJCINOVIC (1992b)] is, therefore, equal to

$$\frac{dp}{dt} = \frac{1}{t_o}\exp\left(-\frac{U_o}{k_bT}\right)(1-p) - \frac{1}{N}\sum_{i=1}^{N}\frac{1}{t_o}\exp\left(-\frac{U_o-\Phi_i}{k_bT}\right) \qquad p > p_{ce} \tag{7}$$

where N is the total number of links in the undamaged lattice (formed by aggregates as sites), p and (1-p) the fractions of extant and absent links between aggregates, respectively. Expression (7) assumes that the reaction is simple, i.e. that it does not involve "reaction loops". Equation (7) can be appropriately adjusted for a given reaction type. It is interesting that the second term on the right hand side of (7) was not introduced by GUZ', et al. (1988) and BOGETTI and GILLESPIE (1989) even though they also considered the cure induced damage.

The number of links that will rupture within the time interval (0,t) can be obtained integrating the second term on the right hand side of (7)

$$p_r(t) = \int_o^t \frac{1}{N(s)} \sum_{i=1}^{N_t(s)} \frac{1}{t_o} \exp\left(-\frac{U_o - \Phi_i(s)}{k_b T(s)} \right) ds \tag{8}$$

Thus, the equation (7) can be rewritten in a compact form as

$$\frac{dp}{dt} = \frac{1}{t_o} \exp\left(-\frac{U_o}{k_b T} \right) (1 - p - w) \tag{9}$$

where

$$w = \int_o^\infty \exp\left(\frac{\Phi}{k_b T} \right) \tilde{p}(\Phi) d\Phi \tag{10}$$

with $\tilde{p}(\Phi)$ being the probability density function of free energies stored in individual links. Expanding the exponential function in the argument of the integral in (10) into an infinite Taylor series it follows that

$$w = \int_o^\infty \sum_{n=o}^\infty \frac{1}{n!} \left(\frac{\Phi}{k_b T} \right) \tilde{p}(\Phi) d\Phi = \sum_{n=o}^\infty \frac{1}{n!} \int_o^\infty \left(\frac{\Phi}{k_b T} \right)^n \tilde{p}\left(\frac{\Phi}{k_b T} \right) d\left(\frac{\Phi}{k_b T} \right) = \sum_{n=o}^\infty \frac{1}{n!} M_n(\varphi) \tag{11}$$

where

$$M_n(\varphi) = \int_o^\infty \varphi^n \tilde{p}(\varphi) d\varphi \tag{12}$$

is the n-th statistical moment of the distribution of the normalized free energy $\varphi = \Phi / k_b T$ stored in the individual links of the gel network. Hence the rate at which links rupture depends on all statistical moments of the force distribution in a disordered network. This alone makes this both different from and much more complicated than a typical micromechanical problem.

IV.3. *Stresses in the Curing Slab*

Finally, it is necessary to derive the equation relating the macro (average) stress in the slab and the eigenstrains related to the thermal and chemical shrinkage. The well known expressions

for the relaxation of polymers due to the changes in the conformations of molecular chains associated with the disentaglements and diffusion of segments [MEARES (1965)] must be changed to accommodate the changing connectivity p(t,x) of the network. The character of the viscoelasticity is determined by the vibratory motion of individual chain segments and the free length of chains between two adjacent crosslinks. The characteristic time of relaxation depends on the state of connectivity and the frictional effects which inhibit changes of conformations.

Continuum theory of the viscoelastic response of crosslinked polymers based on the Rouse and Zimm models and the reptation dynamics was recently developed in [MARTIN, et al. (1989)]. Elastic properties of a curing polymer change with the extent of crosslinking (growing degree of cure α). Realizing that the change in the degree of cure α results in the change in scale (defined by the change in the correlation length ξ) ADOLF and MARTIN (1990) suggested a redefined time to account for the proportionality between the relaxation time of a cluster and its size. The ensuing time-cure superposition model approximates the viscoelastic deformation of curing polymers by a sequence of states corresponding to discrete times defining the extent of the chemical reaction.

The relaxation components of the strain tensor for a material with constant equilibrium shear and bulk moduli are usually written in the form of a hereditary integral [MEARES (1965), RABOTNOV (1977)]. During a curing process the connectivity $p(x_i,t)$ is not a constant. Hence, the ratio between the rate of the relaxation and the rate of cure changes. Immediately after the emergence of the gel the extent of crosslinking is very small, the gel disordered and the relaxation times very long compared to the cure time. At advanced stages of the curing process the free lengths of the polymer chains become much shorter. Consequently, the rate at which the stress in the chains relaxes becomes small in comparison to the rate of cure.

In a general case of an arbitrary ratio between the rates of relaxation and cure, MARTIN and ADOLF (1990) suggested that the equilibrium component of the deviatoric shear stress can be written in form of the following expression

$$s_{ij}^{\infty}(t) = 2\int_{o}^{t} G_{\infty}[p(s)]\frac{\partial e_{ij}(s)}{\partial s}ds + 2\int_{o}^{t} e_{ij}^{eff}(s)\frac{\partial G_{\infty}[p(s)]}{\partial s}ds \tag{13}$$

where s_{ij}, e_{ij} are the components of the deviatoric stress and strain tensor. Also, e_{ij}^{eff} is the effective deviatoric strain tensor which couples the memory effects of the relaxation and the equilibrium moduli of the curing polymer [MARTIN and ADOLF (1990)] defined by

$$e_{ij}^{eff}(s) = \int_{o}^{s} \Gamma_r[s-u, p(u)]\frac{\partial e_{ij}(u)}{\partial u}du \tag{14}$$

The shear modulus is defined as usual by a sum of the equilibrium and relaxation moduli $G(p,t) = G_{\infty}(p) + G_r(p,t)$. The non-dimensional (normalized) relaxation modulus in (14) is defined by the ratio

$$\Gamma_r(s) = \frac{G_r(s)}{G_r(0)} \tag{15}$$

It can be shown that the general constitutive expression (13) tends to proper behavior at two limits of the ratio between the rate of cure and the chain relaxation times.

The available experimental data related to hereditary materials indicate that the volumetric deformation is elastic, i.e. that the bulk modulus does not change appreciably during a viscoelastic deformation [RABOTNOV (1977)]. This assumption is generally accepted on the face value [MUKI and STERNBERG (1961), etc.] even though in the present case it is not clear that the reptation effects are absent in tension. Assuming that the viscous effects are negligible the bulk modulus is only a function of the connectivity p. The corresponding constitutive law which relates the hydrostatic stresses and strains is then

$$\sigma_{kk}(t) = \int_{o}^{t} 3K[p(s)]\frac{\partial}{\partial s}[\varepsilon_{kk}(s) - 3\bar{\varepsilon}^{*}(s)]ds \tag{16}$$

where $\bar{\varepsilon}^{*}(s)$ is the volume averaged isotropic eigenstrain in the material due to the thermal dilatation $\bar{\varepsilon}_{th}$ and the chemical shrinkage $\bar{\varepsilon}_{sh}$. By definition, volume averaged chemical shrinkage is directly proportional to the number of links formed between the aggregates such that

$$\bar{\varepsilon}^{*} = \bar{\varepsilon}_{th} - \bar{\varepsilon}_{sh} = \alpha(T - T_{ce}) - \frac{p - p_{ce}}{1 - p_{ce}}\bar{\varepsilon}_{f} \tag{17}$$

where α, T_{ce} and $\bar{\varepsilon}_{f}$ are the coefficient of thermal expansion, temperature at the elastic percolation threshold and the final extent of the shrinkage at the cure end (p =1).

To simplify the computations consider a weightless resin slab of constant thickness $2h_o$ infinitely extended in the (x,z) plane. Temperature on the traction free slab faces $y = \pm h_o$ is equal to the autoclave temperature $T_a(t)$ which is a known function of time

$$T = T_a(t) \qquad @\, y = \pm h_o \tag{18}$$

In absence of externally applied surface tractions (which are typically too small to be of consequence) all volume averaged macro-parameters such as the average temperature T, stress σ and strain ε are only a function of time and coordinate y. The only non-vanishing stresses and strains are $\sigma_x \equiv \sigma_z$ and ε_y. The final integral equation for the macro (volume averaged) stress in the viscoelastic slab with changing connectivity can be, after some rather cumbersome manipulations, cast into the following form

$$\frac{1}{2}\sigma_x(y,t) + \int_o^t G_\infty[p(s)]\left\{\frac{2}{3K[p(s)]}\frac{d\sigma_x(y,s)}{ds} + 3\frac{d\bar{\varepsilon}^{*}(y,s)}{ds}\right\}ds + \int_o^t \varepsilon_y^{eff}(s)\frac{dG_\infty[p(s)]}{ds}ds$$
$$+ \int_o^t G_r[t-s, p(s)]\left\{\frac{2}{3K[p(s)]}\frac{d\sigma_x(y,s)}{ds} + 3\frac{d\bar{\varepsilon}^{*}(y,s)}{ds}\right\}ds = 0 \tag{19}$$

The initial conditions are that at $t = 0$, stresses $\sigma_x = \sigma_z = 0$ are equal to zero, while $T = T_{ce}$ and $p = p_{ce}$.

The system of three coupled equations (3), (9) and (19), subject to mentioned boundary and initial conditions, in terms of three volume averaged variables σ, T and p, suffices for the determination of connectivity, stresses, strains and temperature in the slab for a given regime of autoclave temperatures. As already stated this conclusion implies that the term (11), i.e. the effective properties and the exact distribution of forces in the renormalized network, can be determined at any connectivity p.

V. MICROMECHANICAL CONSIDERATIONS

Material parameters in (3), (9) and (19) are, in fact, effective parameters derived by averaging over the representative volume element. As such they can be determined either by using mean-field considerations (if the criteria for homogeneity (1) are satisfied) or applying the arguments of the percolation theory (if the geometry and topology of the specimen are self-similar). In addition to the material parameters it is necessary to determine the elastic properties of the links of the renormalized lattice which connect the adjacent aggregates.

V.1. *Stiffness and Rupture Strength of a Link Connecting Two Aggregates*

Each of the links of the renormalized lattice represents itself a network formed by several molecular chains crosslinked to each other. On the molecular scale the deformation modes of a single chain include: change of conformation (segment rotation or gauche-trans transformation), cavitation, slip and/or chain scission [KAUSCH (1987)]. To determine the "stiffness" of a chain it suffices to consider only the change of conformation and its effect on the flexibility. A stretching polymer chain passes through a sequence of a discrete equilibrium (minimum free energy) states which correspond to different conformations. In the course of stretching process very little energy is stored in the bonds. The change in the free energy is almost entirely attributed to the decrease in entropy (diminishing probability of corresponding conformational states). The deformation process of the described type belongs to the class of entropic elasticity. If the force on a single free and highly deformable links is maintained for a long time the chain reverts to its most probable conformation converting the excess energy into heat.

The stiffness of a single chain can be determined analytically only for small deformations of freely jointed single chains. In all other cases determination of the link stiffness requires simplifying assumptions. Force-displacement relation in a crosslinked chain network combines the competing effects of elastic stretching (enthalpic effects) and conformation changes (entropic

effects). A crosslinked network is both dissipative and energy storing. Nevertheless, at small deformations the force-elongation relation remains linear but the spring stiffness is not a constant.

Consider a crosslinked network consisting of N_c chains each of which is formed of n_s segments. The average free energy stored in a segment of i-th link is $\overline{\phi}_i(p) = \Phi_i / [N_c n_s(p)]$. Free energy stored in the link can be estimated assuming that: all chains have the same length and that the end-to-end distances of each chain are defined by the Maxwell probability density function [PEREPECHKO (1981)]. Subject to these assumptions the average free energy stored in a segment of the i-th crosslinked network connecting two neighboring aggregates is

$$\overline{\phi}_i(p) = \frac{\Phi_i}{N_c n_s(p)} \approx \frac{3k_b T}{2n_s(p)\ell^2} r^2 \tag{20}$$

where ℓ is the average distance between the aggregates and $n_s(p)$ the average number of segments in a chain. As the number of segments in a crosslinked network increases during curing the free energy decreases and the activation energy increases. The rate of rupture of links connecting the aggregates rupture (10) is now

$$w = \sum_{n=0}^{\infty} \frac{1}{n!} \int_o^{\infty} \varphi^n \tilde{p}(\varphi) d\varphi \qquad where \qquad \varphi = \frac{\overline{\phi}}{k_b T} \tag{21}$$

where $\tilde{p}(\varphi)$ is the probability density function of the distribution of free energy stored in lattice links. Normalized free energy φ in (21) is redefined in view of the postulated rupture process of radicalized chains. Mechanical energy stored in a link serves only to lower the energy barrier through its contribution to the free energy. The increase of the temperature does not only decrease the argument of the exponential function in (7). It also increases the free energy through the entropy term and the rate of formation of free radicals (reducing the time needed for the rupture of a link caused by the scission of a single chain). Hence, the rupture of links connecting the adjacent aggregates is a random process due to the non-deterministic nature of the spatial and temporal fluctuations of thermal energy.

Formation of a crosslinked connection (link) between two adjoining aggregates is not

instantaneous. Thus, the link "stiffness" varies with time during its formation. Link rupture is a much more rapid process of chemical dissociation which is also not instantaneous. Since the time needed to form and rupture a link is still short compared to the cure duration it will be assumed that the spring stiffness remains constant from its formation to its rupture and that the link rupture is instantaneous. These assumptions are entirely consistent with the selected resolution length according to which events on molecular scale are smoothed out.

V.2. *Elastic Moduli*

The material parameters in the heat conduction equation do not exhibit singular behavior in the neighborhood of the percolation threshold. In fact they change only slightly and to simplify the derivation they will be considered as being constants [TWARDOWSKI, et al. (1993)]. Additionally, it will be assumed that the bulk modulus changes with the connectivity in a manner defined by the self consistent approximation, i.e. that in tension

$$\frac{K(p)}{K_o} = \frac{p - p_{ce}}{1 - p_{ce}} \qquad p_{ce} \le p \le 1$$

where K_o is the bulk modulus of the glassy phase and (22)

$$K = 0 \qquad p \le p_{ce}$$

Expressions (22) ignore finer points of the scaling laws in the asymptotic neighborhood of the percolation threshold and the interaction of defects in the crossover regime [SAHIMI (1986)]. A more sophisticated expression for $K(p)$ can be derived using blending functions [THORPE and JASIUK (1992)] but the gain in accuracy will be minimal since the crossover region is typically very short [FENG, et al. (1985)].

At the percolation threshold the shear stiffness of the slab is, by definition, equal to zero. As a consequence of similarity the shear stiffness is expected to follow a universal power law immediately after the slab passes through the gel point. This expectation was, indeed, observed in experiments (summarized in [MARTIN, et al. (1989)]) in which a polymer at gel point was subjected to an oscillating strain field of constant amplitude. The divergence of the viscosity and

the equilibrium shear modulus in the asymptotic vicinity of the gel point is defined by the scaling laws [ADOLF and MARTIN (1990)]

$$\eta \propto |p_{ce} - p|^{-k} \qquad \text{and} \qquad G \propto |p_{ce} - p|^{z} \tag{23}$$

Universal exponents in (23) are $z = d\nu \cong 8/3$ and $0 \le k \le 4/3$, where d is the dimensionality and ν the exponent for the correlation length ξ. As the connectivity p is increased beyond the percolation threshold the clusters grow in size. Large clusters diffuse slower than the small ones. Thus, the degree of the cure is reflected as the change of the scale. Actual time must be renormalized dividing it by the longest relaxation time τ_z which dominates the dynamics of the of molecular chains. The longest relaxation time is defined as a time needed for a chain of length ξ to diffuse through its own radius. The longest relaxation time

$$\tau_z = \int_o^\infty tGT(t)dt \Big/ \int_o^\infty GT(t)dt = \frac{\eta}{G_\infty} \propto |p - p_{ce}|^{-(z+k)} \tag{24}$$

also represents time at which the response crosses over from a simple to a complex viscoelastic regime. Accounting for the fact that the decay crosses over form the power law to an exponential law as the time t approaches the longest relaxation time the expression for the relaxation shear modulus for the bulk polymer melt was specified by ADOLF and MARTIN (1990) as

$$G_r(t) = CG_\infty \left(\frac{\tau_z}{t}\right)^{2/3} \exp\left[-\left(\frac{t}{\tau_z}\right)^{0.4}\right] \qquad p > p_{ce} \tag{25}$$

where C is a constant which depends on the shear modulus of the glassy phase. Expression (25), which represents the statement of the cure-superposition principle, is valid for a system in which the solid phase (gel) percolates. The shear resistance is provided by the infinite cluster (gel) which dominates the deformation process. The simple scaling law (25) was shown to replicate the experimental data with a surprising accuracy [MARTIN, et al. (1989), ADOLF and MARTIN (1990)] which persists well into the mean field regime.

VI. DISTRIBUTION OF THE FREE ENERGY IN THE LATTICE

VI.1. *Distribution of Forces in Links in the Neighborhood of the Percolation Threshold*

Determination of the entire distribution of forces in links of the renormalized lattice, needed to compute the rate at which the links rupture from (11), is by far the most difficult aspect of the problem. At the percolation threshold gel cluster is very disordered. Forces in cutting (red) links can easily be two orders of magnitude larger than averages. Lattice simulations represent a popular strategy for the determination of the forces in individual links. For example, the distribution of the free energy stored in individual links of 32x32 planar triangular central-force lattice, determined for several different realizations of the same statistics using conventional methods of structural mechanics, is plotted in form of a binned histogram in Fig.2a. The same distribution averaged over 100 realizations is plotted in Fig.2b. Tail end of the distribution, i.e. number of links storing large free energies, changes significantly from one physical realization to the other and strongly depends on the lattice size $L = \lambda \ell$ (where ℓ is the link length). Moreover, the probability to find a link carrying a large force will increase with the size of the lattice. These two aspects (referred to as the mesh sensitivity) are especially important since the objective modeling of typical resin specimens would require very large lattices which are unsuitable for repeated simulations needed to form a statistically representative sample.

For a lattice analysis to be objective the resolution (bond) length ℓ must be equal to the inherent characteristic length of the microstructure (size of the nucleated sub-microcracks). In the present case, the characteristic microstructural length is equal to the average distance between the adjacent aggregates at the crossover from aggregation to percolation. The initial length of the sub-microcracks [KUKSENKO and TAMUZS (1981), KAUSCH (1987)], nucleated in the course of the rupture of a single link, is of the order of $\ell \approx 0.1\,\mu m$. Thus, to preserve the objectivity, a cubic lattice occupying a cube with a volume of only 1 cm^3 should be modeled by a lattice having 10^{15} nodes rendering direct simulations [such as those by TERMONIA, et al. (1985)] impractical if not impossible. A lattice is a true model of a microstructure only if: (a) the link length ℓ is equal to the distance between two adjacent aggregates, (b) the force-elongation

relation in a link is defined by (20) and (c) its type is defined by the functionality of the monomers. Lattices with link lengths which are orders of magnitude larger than ℓ are approximations which will in this case lead to erroneous results.

According to the expression (11) the rate at which links rupture is dependent on the distribution of energies stored in individual links which is defined by an infinite series of statistical moments $M_n(\varphi)$. Assuming that all links have identical stiffness k it follows that the energy stored in links is $2\Phi_i = kf_i^2$. With the help of the identity $\tilde{p}\left(\sqrt{\Phi}\right)d\left(\sqrt{\Phi}\right) = \tilde{p}(\Phi)d\Phi$ the above described problem may be reformulated in terms of the forces carried by individual links. Since the forces in links of the network in the asymptotic neighborhood of the percolation transition are attributable primarily to the chemical shrinkage the probability of finding a large compressive force in a link is negligible. In the considered slab only the links in the (x,z) plane are subjected to substantial tensile forces. Hence, to simplify the analyses further the actual three-dimensional lattice is approximated by a stack of parallel two-dimensional triangular central-force lattices in (x,z) planes. Consideration of three dimensional lattices does not present conceptual problems but is, nevertheless, computationally few orders of magnitude more time consuming. Therefore, it seems reasonable to focus on the two-dimensional problems first.

Consider first the distribution of forces in links of a two-dimensional lattice the neighborhood of the percolation threshold. The mass of the spanning cluster (zero-th moment) scales with the lattice size as λ^D where $(D = 91/48)$. As a result of its highly ramified structure most of the links of the spanning cluster do not carry any load. Within the node-link-blob picture, these cantilevered links (dangling ends) account for a large part of the spanning cluster mass. Only a fraction of the links belonging to the spanning cluster can store free energy. Links that carry non-zero loads form the spanning cluster backbone. The mass of the backbone is proportional to

$$\sum_{f=0^+}^{\infty} n(f,L) \propto \lambda^{D_b} \tag{26}$$

where $D_b = 1.62 \pm 0.02$ (in two dimensions) is also a universal exponent. The cutting (or red) links connecting the blobs carry largest loads. The number of cutting links scales as $\lambda^{1/\nu}$ where

($\nu = 4/3$) [CONIGLIO (1981)]. The universality of these scaling laws and exponents (D, D_b, ν) is the consequence of self-similarity (as the correlation length $\xi \to \infty$) of the lattice geometry in the neighborhood of the percolation threshold. The ultimate task is to determine the number of links $n(f,\lambda)$ carrying different forces f in a lattice of size $\lambda = L/\ell$ which is geometrically represented by a binned histogram of forces in links. Statistical moments of the distribution of forces in the neighborhood of the percolation transition are defined by

$$M_k(\lambda) = \sum f^k n(f,\lambda) \approx \int_o^\infty f^k n(f,\lambda) df \propto \lambda^{z(k)} \tag{27}$$

In contrast to fractals (such as mass of the backbone) each statistical moment of the distribution of forces in links scales with a different exponent. Computation of the rate at which links rupture (11) is reduced to determination of the set of size-independent exponents $z(k)$ (k=0,1,...,∞).

Instead of performing repeated numerical simulations on lattices to determine $z(k)$ in (27) it is much more efficient to make use of the existing data for the current transmitting fuse networks [HANSEN (1990), ROUX and HANSEN (1990), etc.] and establish an analytical transition between fuse and elastic networks [HANSEN and ROUX (1988)]. Consider, therefore, first a fuse network for which

$$[M_k(\lambda)]_c = \sum i^k n_c(i,\lambda) \approx \int_o^1 i^k n_c(i,\lambda) di \propto \lambda^{x_c(k)} \tag{28}$$

where $n(i,\lambda)$ is the number of links carrying current i. The subscript "c" indicates a constant current ensemble, i.e. a set of networks carrying the identical current. The product $i^k n(i,\lambda)$ is very small at both limits ($i = 0,1$) (since the number of cutting links is very small) and peaks at an intermediate value of current i_k. Hence, the integral in (28) may be estimated using the method of steepest descent or saddle point [see de ARCANGELIS (1988), HANSEN (1990) or STAUFFER and AHARONI (1992)] as

$$M_k \approx n(i_k,\lambda) i_k^k \tag{29}$$

The current i_k at which the integrant in (28) peaks is given by extremum condition

$$\left.\frac{d\{\ln[n(i,\lambda)]\}}{d[\ln(i)]}\right|_{i=i_k} = -k \tag{30}$$

At the percolation threshold every function is expected to scale as a power law. Hence

$$i_k^2 \propto \lambda^{-a(k)} \quad and \quad n(i_k,\lambda) \propto \lambda^{f(k)} \tag{31}$$

Substituting (31) into (29) and comparing the ensuing expression with (27) it follows that

$$x(k) = f(k) - ka(k) \tag{32}$$

The exponents in power laws (31) are then

$$a(i,\lambda) = -\frac{dx}{dk} = -\frac{\ln(i)}{\ln(\lambda)}, \qquad f(i,\lambda) = x(k) + ka(k) = \frac{\ln[n(i,\lambda)]}{\ln(\lambda)} \tag{33}$$

Parameter $a(i,\lambda)$, referred to as the Lipschitz-Hoelder exponent [PYRAK-NOLTE, et al. (1992)], defines the spatial distribution of currents. Function $f(i,\lambda)$ is the fractal dimension of the support of current distribution. As shown in HANSEN (1990) and STAUFFER and AHARONI (1992) the exponents (33) are indeed independent of the lattice size λ. Consequently, the graphs in the (f,a) space computed for different lattice sizes λ do collapse on a single, master curve. The function $f[a(k)]$ (33.b), representing an infinite series of exponents $x_c(k)$, is referred to as the multifractal spectrum, and is as universal as the scaling laws (exponents). A straight line with slope (-k) is tangent to the curve $f(a)$ at point a_k defined by (33) which provides the main contribution to the k-th statistical moment (29). Hence, the apex of the curve in Fig.3 corresponds to the zero-th statistical moment $f[a(k=0)] = D_b$. The point of the curve with a vertical tangent $f[a(k \to \infty)] = 1/\nu$ corresponds to the statistics which is dominated by the cutting crosslinks. It can be shown that the curve (33) is strictly convex [HANSEN (1990)].

Even though the analytical expression for the scaling exponent $x_c(m)$ is not available the simulations in HANSEN (1990) can be fitted by the following expression

$$x_c(m) = 0.75 + 0.87e^{-0.676m} \tag{34}$$

Exponents computed from (34) satisfy the analytical results for the required limits as $m \to 0$ (mass of the backbone), $(m \to \infty)$ mass of cutting links and the lattice conductivity (m = 2).

Extensive numerical simulations in support of the above discussed representation of the

multifractal spectrum make a compelling argument for its utility in the determination of the distribution of currents in a fuse networks. However, the elastic percolation in central force lattices and conduction percolation in fuse networks represents two different universal classes. Thus, the multifractal spectrum (34) cannot and does not apply to elastic percolation problems.

Consider now a lattice of size $L = \lambda\ell$ subjected to tractions applied at its boundaries. As a result of the vectorial nature of the equilibrium conditions the forces in cutting links can be much larger than the applied forces and can, in the limit, tend to infinity. Assuming that the k-th moment of the distribution of the square root of the energy stored in the lattice links scales as a multifractal (similar to (28)) it follows that

$$[M_k]_f = \sum_j \left(\sqrt{\Phi_j}\right)_f^k \equiv \int_o^\infty \left(\sqrt{\Phi_j}\right)_f^k n\left(\sqrt{\Phi_j}, \lambda\right)_f d\left(\sqrt{\Phi_j}\right) \propto \lambda^{y_f(k)} \tag{35}$$

It is reasonable to conjecture that the transition rule between two universal classes can be inferred on the basis of the relation existing between the scaling exponents for the effective compliance $y_f(2)$ and resistance $x_c(2)$. Using the results summarized in SAHIMI (1986) it follows that

$$y_f(2) = x_c(2) + 2 \tag{36}$$

The HANSEN and ROUX (1988) conjecture consists of assuming that the relation (36), which is true for the second moments, will remain valid for all moments of the two distributions. Scaling exponents of two distributions (27) and (35) are assumed to be related as if (36) is true for all n

$$y_f(n) = x_c(n) + n \tag{37}$$

Subscript "f" stands for the constant externally applied force ensemble.

Consider a two-dimensional, elastic, central-force network and denote by F, X and $\overline{S}$ the external tensile forces applied at two opposite ends of the network, corresponding elongation and effective compliance of the network, respectively. Observed network is near the percolation threshold. Total elastic energy stored within the gel cluster is for unit stiffness of individual links

$$\frac{1}{2}F^2\bar{S}=\frac{1}{2}\sum\left(\sqrt{\Phi}\right)^2 \tag{38}$$

where Φ is the free energy of a crosslink and with sum extended over all crosslinks forming the gel backbone. For a constant unit force $F = 1$, the effective compliance of the gel cluster (second moment of the free energy distribution) scales for a constant force ensemble as

$$\bar{S}=[M_2]_f=\sum\left(\sqrt{\Phi}\right)_f^2 n\left(\sqrt{\Phi},\lambda\right)_f \cong \int_o^\infty \left(\sqrt{\Phi}\right)_f^2 n\left(\sqrt{\Phi},\lambda\right)_f d\left(\sqrt{\Phi}\right) \propto \lambda^{y_f(2)} \tag{39}$$

Next task is to perform the transition from the constant force to the constant free energy ensemble. The total free energy is equal to $\Phi = F^2\bar{S}/2$, where the effective network compliance $\bar{S}$ is constant during entropic deformation only at small "strains". Thus, for a constant force $F=1$ it follows that

$$[M_k]_{ee}=\bar{S}^{k-2}[M_k]_f \tag{40}$$

where the subscript "*ee*" refers to the elastic energy ensemble. From (39) and (40) it follows that

$$y_{ee}(k)=y_f(k)-\frac{k}{2}y_f(2) \tag{41}$$

In the present case the control parameter is the energy density. Since the total energy of the lattice scales as λ^d (where the dimensionality d=2), using (37) and (41) it finally follows that

$$y_{ed}(k)=y_f(k)+k-\frac{k}{2}y_f(2)=x_c(k)-\frac{k}{2}x_c(2) \tag{42}$$

where subscript "ed" refers to a constant energy density.

The expression for the scaling exponents for all statistical moments of the distribution of free energy stored in links, derived from (34) and (42), has the following form

$$y_{ed}(n)=0.75+0.51n+0.87e^{-0.676n} \tag{43}$$

where as required $y_{ed}(0)=D_b=1.62$ and $y_{ed}(2)=2$ (since F=1).

The analytical expression for the multifractal spectrum is from (33.a)

$$f[a(n)]=1.51-1.48a+0.87(0.87-1.7a)\log(0.87-1.7a) \tag{44}$$

The multifractal spectrum $f(\alpha)$ vs. α, defined by (44), is plotted in the Fig. 4.

The scaling law (44) for the statistical moments of the energy stored in the links of the

network is based on the conjecture (37) and should be verified by numerical simulations on lattices. This task was undertaken by HANSEN and ROUX (1988) who performed extensive simulations on triangular central force lattices ranging in size from 30x30 to 80x80 nodes. The results predicted by the multifractal formalism were in very close agreement with numerical simulations for all low order moments (up to n=4). Errors of about 15% for n=5 should have been expected in view of the relatively small lattices and modest statistical samples (only 50 realizations on largest lattices). In summary, the proposed multifractal formalism describes the microstructural disorder in the neighborhood of the percolation threshold with a remarkable combination of accuracy and simplicity.

VI.2. *Distribution of Forces in the Links in the Off-Threshold States*

The lattice disorder, and the attendant fluctuations of forces in crosslinks about the mean value, is largest in the asymptotic neighborhood of the percolation (connectivity) transition. However, at this stage the mean force in the network is minimum (almost zero). Thus, largest stress concentrations may take place at larger connectivities p. To establish the phase of the curing process during which the microcracks are most likely to nucleate and grow it is necessary to extend the derived multifractal scaling laws to the off-threshold states ($p > p_{ce}$).

As a first step consider an infinitely large lattice $\lambda \to \infty$ which contains a relatively small fraction of ruptured links (i.e. a state $p \to 1$ far away from the percolation threshold). The distribution of the energy stored in links becomes fractal (dependent on the average mass of extant links - mean field case) such that for $p \to 1$ the distribution of energy stored in links is

$$n(\sqrt{\Phi}, \lambda, p \to 1) \propto \lambda^{f_o} \tag{45}$$

where $f_o = 2$ since the number of links storing energy must scale as the "volume" of the considered two-dimensional network. In a perfect (undiluted) network the scalar quantity $\sqrt{\Phi}$ (free energy density) is independent of the network size. Thus, since

$$\sqrt{\Phi} \propto \lambda^{a_o} \tag{46}$$

it follows that $a_o = 0$ at $p = 1$. Consequently, in an undamaged lattice the multifractal spectrum

collapses on a single point (a_o, f_o) in the space of the rescaled energy and energy distribution (independent of the length scale). To determine the distribution of energies stored in individual links of the lattice in an off-threshold state it is necessary to define the rule governing the gradual evolution of the scaling exponents from the state $(a_o = 0, f_o = 2)$ in a pristine lattice $(p = 1)$ to the multifractal spectrum (42) at the elastic percolation threshold $(p = p_{ce})$. At an arbitrary state $(1 \geq p \geq p_{ce})$ energy distribution in the elastic networks can be described by scaling laws [ROUX and HANSEN (1989), HANSEN, et al. (1991)] as

$$n(\sqrt{\Phi}, \lambda, p) \propto \lambda^{F(\beta)} \quad and \quad \sqrt{\Phi}(\lambda, p) \propto \lambda^{\beta} \tag{47}$$

The function $F(\beta)$ reflects the multifractal nature of the distribution of forces in the critical state. In the pristine state all diagonals of a triangular central-force lattice carry the same force, and the distribution of forces shrinks to a single point. In critical state (elastic percolation) the distribution of forces ranges from zero (dangling ends) to very large magnitudes (cutting links). The band-width of the force distribution increases gradually in proportion to the accumulated damage (decreasing connectivity p). In order to define the relation between the band-width of the force distribution growth and the increasing disorder ROUX and HANSEN (1989) and HANSEN, et al. (1991) introduced an intensive thermodynamic variable

$$\zeta = \frac{\ln(\xi)}{\ln(\lambda)} \tag{48}$$

which plays the role of the control parameter (instead of the number of ruptured links) or "time". The corresponding intensive thermodynamic flux is

$$\beta(\zeta) = \zeta a \tag{49}$$

Statistically (49) defines the band-width of the distribution of free energies stored in the links of the lattice. This band-width depends on the lattice size and current connectivity p.

The respective intensive histogram is

$$F[\beta(\zeta), \zeta] = 2 - \zeta[2 - f(a)] \tag{50}$$

Evolution of the multifractal spectrum with the change of the connectivity p is plotted in Fig.4.

The final expression for the scaling law for the histograms of links binned with respect to the energy they store can be derived combining expressions (44), (47) and (49) in the form

$$F[\beta(\zeta),\zeta]=2-\zeta\left[0.49+1.48\frac{\beta}{\zeta}+0.87\left(0.87-1.7\frac{\beta}{\zeta}\right)\ln\left(0.87-1.7\frac{\beta}{\zeta}\right)\right] \tag{51}$$

An approximate analytical expression for the multifractal spectrum (constant energy density ensemble) can be derived using the Legendre transformation (33) and (43, 51) in the form

$$y_{ed}(n,p)=2-\zeta(p)[1.25-0.512n-0.87\exp(-0.676n)] \tag{52}$$

For current purposes it suffices to notice that the scaling law (47), with (52) fully determines all statistical moments of the distribution of energy stored in each link in both critical and off-critical states (i.e. for each $p_{ce}\le p\le 1$ and arbitrary lattice size λ). In conjunction with equation (19) these expressions provide the needed background for the determination of an analytical solution for the rate at which the crosslinks rupture during the curing process in a two-dimensional central-force network of arbitrary size.

In all cases of practical importance (when the linear size of the slab exceeds few millimeters) the networks must be very large. The probability distribution density function of the energy stored in crosslinks can then be written dividing the distribution of energy by the total surface area of the network as

$$\tilde{p}\left(\Phi^{1/2},\lambda,p\right)=C_1\frac{n\left(\Phi^{1/2},\lambda,p\right)}{\lambda^2}=C_1\lambda^{F(\beta)-2} \tag{53}$$

where C_1 is the non-dimensional amplitude which characterizes the backbone mass. The n-th statistical moment of the above given probability density function $\tilde{p}(\Phi,\lambda,p)$ is then

$$[M_n]=\int_o^\infty \Phi^n\tilde{p}(\Phi)d\Phi\propto\lambda^{z(n)} \tag{54}$$

Exponents of the scaling law for the moments of the statistical distribution of energy stored in the crosslinks of the central-force network can be derived substituting the identity $\tilde{p}(\Phi)d\Phi\equiv\tilde{p}(\Phi^{1/2})d(\Phi^{1/2})$ into (35) and comparing the result with (54) in the form

$$z(n)=y(2n)-2 \tag{55}$$

Using (52) in (55) it finally follows that

$$z(n,p)=\zeta(p)[-1.25+1.03n+0.87\exp(-1.35n)] \tag{56}$$

The exponents of the scaling law for the statistical moments of the distribution of energy stored in crosslinks depends on the correlation length ξ and connectivity p implicitly through the parameter ς in (56). However, the dependence of the correlation length on the fraction of extant crosslinks (connectivity of the lattice) p is different in the mean field and percolation regimes. For present purposes it seems reasonable to use an approximate expression

$$\zeta(p) = \left(\frac{1-p}{1-p_{ce}}\right)^m \tag{57}$$

which smoothly interpolates range between the limits $x(p = p_{ce}) = 1$ and $x(p = 1) = 0$. Exponent m in (57) is an adjustable constant taken as an integer larger than unity.

The expression (54) for the moments of the energy distribution can now be rewritten as

$$M_n = C_1 C_2^n \lambda^{z(n)} \tag{58}$$

Two constants C in (58) are estimated from the first two moments of the energy distribution

$$M_o = \int_o^\infty \tilde{p}(\Phi)d\Phi = p_b = C_1\lambda^{z(o)} \qquad M_1 = \int_o^\infty \Phi\tilde{p}(\Phi)d\Phi = \Phi_{avg} = C_1 C_2 \lambda^{z(1)} \tag{59}$$

where p_b is the number of bonds (mass) in the backbone and Φ_{avg} the average energy stored in the bonds of the backbone. Since the energy density Φ / λ^2 is an intensive property from (58) it follows that $z(1) = 0$. Final expression for all statistical moments follows form (58, 59)

$$M_n = C_1^{1-n}\Phi_{avg}^n \lambda^{z(n)} \tag{60}$$

Parameter C_1 is determined by fitting numerical simulations [MALLICK (1993)] for the first statistical moment (which is not nearly as sensitive the higher moments).

Rate at which the links rupture (11) can finally be rewritten in view of (60) as

$$w = \sum_{n=0}^{\infty} \frac{1}{n!}\left(\frac{\bar{\phi}_{avg}}{k_b T}\right)^n C_1^{1-n}\lambda^{z(n)} \quad \textit{where} \quad \bar{\phi}_{avg} = \int_0^\infty \bar{\phi}\tilde{p}(\bar{\phi})d\bar{\phi} \tag{61}$$

The rate of link accrual can now be determined analytically from the expression (7), in conjunction with (56, 57, 61), for any specimen size λ., without time consuming numerical simulations.

VII. ILLUSTRATIVE EXAMPLE

Utility of the above formulated model can be illustrated on the example of the epoxy resin known as diglycidyl ether of bisphenol A (DGEBA). Material parameters for the selected resin were taken from LOOS and SPRINGER (1983), BOGETTI and GILLESPIE (1989) as: conductivity K_T=0.167 W/(m K), resin density ρ= 1.26·10^3 kg/m^3, specific heat C_p=1.26·10^3 KJ/(kg K), heat of reaction H_T= 474 KJ/kg, coefficient of thermal expansion α_t = 6.2·10^{-5} (1/°C), final shrinkage strain ε_f= 0.02, equilibrium shear modulus of the fully cured resin $G_\infty(p=1)$= 1.06·10^3 MPa and the equilibrium Poisson's ratio $\nu_\infty = 0.3$. The activation energy of the resin was assumed to be U_o=2·10^9 J [REGEL', et al. (1974), TERMONIA, et al. (1985)]. The period of molecular vibration t_o= 10^{-12} sec was assumed to be temperature independent [TERMONIA, et al. (1985)]. The autoclave temperature regime is shown in Fig.2 of this paper. The temperatures are T_o=25°C, T_f=125°C while the times are t_1=2 hrs, t_2=4 hrs. and t_3=6 hrs..

The average diameter of polymer aggregates was assumed to be 300 Å and the distance between the aggregate centers ℓ=0.05 μm [ERATH and ROBINSON (1963, MIJOVIC and TSAY (1981)]. Slab thickness and length were taken to be $2h$=1 cm and L=0.5 m, respectively. Consequently, in order to keep the resolution length as being equal to the size of the distance separating two aggregates the number of links in one row should be $\lambda = L/\ell = 10^7$. This illustrates the magnitude of the numerical effort associated with mesh-independent numerical simulations on lattices. The rigidity percolation threshold of the fcc lattice was taken as $p_{ce} = 0.5$ [FENG, et al. (1985)]. The degree of cure α_c at the gel point is found to occur between 0.55 and 0.8 [PLAZEK and FRUND (1990)]. Thus, $0.3 < \chi_{ce} < 0.64$. In computations it was assumed that $\chi_{ce} \approx 0.55$.

The evolution of temperature, degree of connectivity and fraction of ruptured links with time are depicted in Fig.5 at the surface and the mid-plane of the slab. From the plotted data the rate of damage evolution and growth is most pronounced during the period at which $T = T_f$ characterized by rapid increase of the degree of cure. Hence, damage evolution depends almost entirely on the reaction rate (chemical shrinkage) as hypothesized in GUZ', et al. (1988). Only an

insignificant fraction of total damage can be attributed to thermal shrinkage associated with the cooling cycle in the autoclave. The variation of the degree of cure across the slab thickness is plotted in Fig.6. Variation of the viscoelastic (average or mean-field) normal stresses across the slab thickness during cure are shown in Fig.7. Largest stresses occur at the mid-plane of the slab. Variation of average stresses at the surface and mid-plane of the slab as a function of time are plotted in Fig.8.

The dominant role of stress concentrations (attributable to excessive disorder) in damage evolution is obvious from the fact that the link rupture rate within the interval ($t > 4$ *hrs.*), in which the stress is largest, is insignificant. In fact, significant microcracking occurs in the interval ($2 > t > 4$ *hrs.*) during which the magnitude of average stresses is below 20% of maximum value. This result alone proves that the application of traditional mean field models in this case leads to wrong conclusions. From the performed computations it is also obvious that most of the damage occurs away from the slab surface making its detection difficult. The cure induced damage levels of approximately 10% at the mid-plane and average damage levels of half of that severity is consistent with the available data.

VIII. SUMMARY AND CONCLUSIONS

The proposed analytical model for the determination of the damage incurred in thermoset resins during polymerization: (a) encompasses three scales (molecular, micro and macro), (b) couples equations of chemical reaction rate, heat transfer and mechanical equilibrium and (c) clearly identifies all material parameters. Moreover, the proposed model considers the microstructural disorder and suggest a potent analytical method for the determination of the stress concentrations characteristic of the disordered microstructures. A simple discussion of the relative magnitudes of three characteristic lengths demonstrates that the conventional micromechanical models, based on the effective continuum (or mean-field) theory, would not be applicable in the considered case. Polymerization of resins is, in fact, a paradigm of this class of problems since the microstructure must by definition pass through the percolation threshold

characterized by large disorder and entropic deformation processes. It is well known that the mean field estimates of the scaling laws for macro parameters and defect distribution are in substantial error in the neighborhood of the percolation (sol to gel) transition.

The proposed modes is based on a proper equation for the rate of chemical reactions (7) which, in contrast to existing models, includes the rate at which the links rupture (rate of damage evolution). Moreover, this equation is cast into a form which: (a) demonstrates the dependence of the rate of damage evolution on the stress concentrations in the disordered microstructure and (b) allows application of the multifractal formalism. The parameters of the effective solid are determined in the mean-field and the self-similar regimes. Constitutive relation for the solid (19) was derived on the basis time-cure superposition model of stress relaxation in viscous materials with changing connectivity proposed by ADOLF and MARTIN (1990). Effect of the micro-structural disorder is introduced through the material parameters and the distribution of forces within the diluted lattice.

One of the principal objectives of this work was to emphasize the fact that the damage during curing must be attributed to the large stress concentrations which take place because of the strongly disordered microstructural geometry and large spatial and temporal fluctuations of temperature. This fact alone separates this model from those available in the literature. Using this approach it was shown that the damage evolution is a random process which depends not only on the stresses but also on the temperature fluctuations. Moreover, damage accumulation and patterns depend not only on the average stress but even more so on the extreme stresses (stress concentrations in a disordered lattice). In fact, computations (Figs. 5 and 8) indicate that the mean field (effective properties) models will always lead to erroneous conclusions. Microstructural disorder and attendant stress concentrations are, therefore, dominant aspects of system near the phase transition. Consequently, the conventional fracture mechanics criteria, derived for enthalpic deformation processes, should be replaced by the non-deterministic criteria of the kinetic theory which fully recognizes the effect of the disorder. The application of the non-deterministic models of the kinetic rupture theory are further justified by the fact that they are

applied at the scale of molecular chains at which the bond rupture can be interpreted as the chemical reaction of the bond dissociation. Finally, the proposed model provides a rational estimate of the size effect through the parameter λ in the expression (60).

At this stage of the development the proposed model was for numerical efficiency based on several assumptions which can be readily eliminated if so desired. The transition to three dimensional lattices is one of assumptions which will require non-trivial further considerations. Further validation and verification of the model and a more precise identification of some of the parameters will require adequate experimental studies. In summary, the proposed theory represent a radical change of some of the basic concepts of micromechanical modeling by acknowledging the essential role of the disorder in damage evolution. As such the proposed model is not merely an incremental improvement of the existing continuum and micromechanical models based on averaging (or homogenization).

V. ACKNOWLEDGEMENT

The authors gratefully acknowledge the research grant from the U.S. Army Research Office, Engineering Science Division, Structural Mechanics Branch to Arizona State University which made the research on which this paper is based possible. The authors also acknowledge helpful consultations with Dr. Marc Mignolet of Arizona State University.

VI. REFERENCES

Adolf, D. and Martin, J.E. (1990), Time-Cure Superposition During Crosslinking, *Macromolecules*, Vol. 23, pp. 3700-3704.

Bogetti, T.A., and Gillespie, W. Jr., (1989), Process Induced Stress and Deformation in Thick-Section Thermosetting Composite Laminates, Reprints of 21 Int. SAMPE Tech Conf., Atlantic City, NJ.

Ciriscioli, P.R. and Springer, G.S., (1990), *Smart Autoclave Cure of Composites*, Technomics, Lancaster, PA.

Coniglio, A., (1981), Cluster Structure near the Percolation Threshold, *J. of Physics A*, Vol. 15, pp. 3829-3844.

Cowie, J.M.G., (1991), *Polymers: Chemistry and Physics of Modern Materials*, Chapman and Hall, New York, NY.

de Arcangelis, L., (1988), Fractals and Multifractals in Physics, Ch. II in: *Disorder and Mixing*, E. Guyon, J. Nadal and Y. Pomeau, Eds., pp. 31-41, NATO ASI Series, Vol. 152, Kluwer Publ.., Boston, MA.

Dusi, M.R., Lee, W.I., Ciriscioli, P.R. and Springer, G.S., (1987), Cure Kinetics and Viscosity of Fiberite 976 Resin, *J. of Composite Materials*, Vol. 21, pp. 243-261.

Erath, E.H. and Robinson, M., (1963), Colloidal Particles in the Thermosetting Resins, *J. of Polymer Science C*, pp. 65-76.

Feng, S., Thorpe, M.F. and E. Garboczi, (1985), Effective-Medium Theory of Percolation on Central-Force Lattices, *Phys. Rev. B*, Vol. 31, pp. 276-280.

Glasstone, S., Laidler, K.J. and Eyring, H., (1941), *The Theory of Rate Processes*, McGraw-Hill Book Co., New York, NY.

Guz', A.N., Tomashevskii, V.T., Shul'ga, N.A. and Iakovlev, V.S., (1988), *Technological Stresses and Deformations in Composite Materials*, Vischa Shkola Publ., Kiev, Ukraine.

Hahn, H.T. and Pagano, N.J., (1976), Curing Stresses in Composite Laminate, *J. of Composite Materials*, Vol. 10, pp. 266-277.

Hansen, A., (1990), Disorder, in: *Statistical Models for Fracture of Disordered Media*, H.J. Herrmann and S. Roux, Eds., pp. 115-158, North Holland, Amsterdam, The Netherlands.

Hansen, A. and Roux, S., (1988), Multifractality in Elastic Percolation, *J. of Statistical Physics*, Vol. 53, pp. 759-771.

Hansen, A., Roux, S. and Hinrichsen, E.L., (1990), Annealed Model for Breakdown Processes, *Europhys. Lett.*, Vol. 13, pp. 517-522.

Hashin, Z., (1983), Analysis of Composite Materials - a Survey, *J. Appl. Mech.*, Vol. 50, pp. 481-505.

Isichenko, M.B., (1992), Percolation, Statistical Topography and Transport in Random Media, *Rev. of Modern Physics*, Vol. 64, pp. 961-1043.

Kausch, H.-H., (1987), Polymer Fracture, *Springer Verlag*, Berlin, Germany.

Krausz, A.S. and Krausz, K., (1988), *Fracture Kinetics of Crack Growth*, Kluwer Acad. Publ., Dordrecht, The Netherlands.

Kuksenko, V.S. and Tamuzs, V.P., (1981), *Fracture Micromechanics of Polymer Materials*, M. Nijhoff Publ., Boston, MA.

Levitsky, M. and Schaffer, B.W., (1974), Thermal Stresses in Chemically Hardening Elastic Media with Application to Molding Process, *J. Appl. Mech.*, Vol. 41, pp. 647-651.

Li, N. and Barber, J.H., (1989), Residual Stresses in Castings with Axisymmetric Solidification, *Engineering Science Reprints*, 26th Annual Technical Meeting of the Society of Engineering Sciences, Ann Arbor, MI.

Loos, C.A. and Springer, G.S., (1983), Curing of Epoxy Matrix Composites, *J. of Comp. Materials*, Vol. 17, pp. 135-169.

Mallick, K., (1993), *Process Defects in Polymers*, Ph.D. Thesis, Mechanical and Aerospace Engng, Arizona State University, Tempe, AZ.

Mallick, K. and Krajcinovic, D., (1992a), Cure Induced Inelastic Deformation in Thermosetting Polymers, in: *Recent Advances in Damage Mechanics and Plasticity*, (ed. J.W. Ju), ASME Publ., AMD-Vol. 132, MD-Vol.30, pp. 159-172, New York, NY.

Mallick, K. and Krajcinovic, D., (1992b), Curing Induced Microcracks in Polymer Matrices, in: *Damage Mechanics in Composites*, (eds. D.H. Allen and D.C. Lagoudas), ASME Publ., AMD-Vol. 150, MD-Vol.32, pp. 141-154, New York, NY.

Martin, J.E. and Adolf, D., (1990), Constitutive Equations for Cure-Induced Stresses in a Viscoelastic Material, *Macromolecules*, Vol. 23, pp. 5014-5019.

Martin, J.E. and Adolf, D., (1991), The Sol-Gel Transition in Chemical Gels, *Annual Reviews of Physical Chemistry*, Vol. 42, pp. 311-339.

Martin, J.E., Adolf, D. and Wilcoxon, J.P., (1989), Viscoelasticity Near the Sol-Gel

Transition, *Phys. Review A*, Vol. 39, pp. 1325-1332.

Martin, J.E. and Wilcoxon, J.P., (1989), Spatial Correlations and Growth in Dilute Gels, *Phys. Rev. A*, Vol. 39, pp. 252-258.

Meares, P, (1965), *Polymers*, D. Van Nostrand Co., Ltd., New York, NY.

Mijovic, J. and Tsay, L., (1981), Correlations Between Dynamic Mechanical Properties and Nodular Morphology of Cured Epoxy Resins, *Polymer*, Vol. 20, pp. 1095-1107.

Muki, R. and Sternberg, E., (1961), On Transient Thermal Stresses in Viscoelastic Materials with Temperature-Dependent Properties, *J. Appl. Mech.*, Vol. 28, pp. 193-207.

Perepechko, I.I., (1981), *An Introduction to Polymer Physics*, Mir Publ., Moscow, Russia.

Plazek, D.J. and Frund, Z.N. Jr., (1990), Epoxy Resins (DGEBA); The Curing and Physical Aging Process, *J. of Polymer Science*, Vol. 28, pp. 431-448.

Pyrak-Nolte, L.J., Myer, L.R. and Nolte, D.D., (1992), *Fractures: Finite-size Scaling and Multifractals*, PAGEOPH, Vol. 138, pp. 679-706.

Rabotnov, Yu.Yu., (1977), *Elements of the Hereditary Solid Mechanics*, Nauka, Moscow.

Regel', V.R., Slutsker, A.I. and Tomashevskii, E.E., (1974), *Kinetics Theory of Strength of Solids*, Nauka, Moscow, Russia.

Roux, S. and Hansen, A., (1989), Off-Threshold Multifractality in Percolation, *Europhys. Lett.*, Vol. 8, pp. 729-734.

Sahimi, M., (1986), Relation Between the Critical Exponents of Elastic Percolation Networks and the Conductivity and Geometrical Exponents, *J. Physics C: Solid State Physics*, Vol. 19, pp. L79-L83.

Stauffer, D. and Aharoni, A., (1992), *Introduction to Percolation Theory*, 2nd Edition, Taylor and Francis, London, UK.

Stockmayer, W.H., (1943), Theory of Molecular Size Distribution and Gel Formation in Branched Chain Polymers, *The J. of Chemical Physics*, Vol. 11, pp. 45-55.

Termonia, Y., Meakin, P. and Smith, P., (1985), Theoretical Study of the Influence of the Molecular Weight on The Maximum Tensile Strength of Polymer Fibers, *Macro-*

molecules, Vol. 18, pp. 2246-2252.

Thorpe, M.F. and Jasiuk, I., (1992), New Results in the Theory of Elasticity for Two-Dimensional Composites, *Proc. Royal Soc. London*, Vol. A 438, pp. 531-544.

Twardowski, T.E., Lin, S.E. and Geil, P.H., (1993), Curing in Thick Composite Laminates: Experiments and Simulations, *J. of Comp. Materials*, Vol. 27, pp. 216-250.

Zallen, R., (1983), *The Physics of Amorphous Bodies*, J. Wiley & Sons, New York, NY.

FIGURE CAPTIONS:

Fig. 1: Phases of the polymerization process in resins.

Fig. 2: Distribution of the free energy in the links of a 32x32 triangular central-force lattice near the percolation threshold (p=0.67) obtained by numerical simulations: (a) four different realizations and (b) distribution averaged over 100 realizations.

Fig. 3: Multifractal spectrum $f(a)$ vs a at the percolation threshold for the case of the constant energy density ensemble.

Fig. 4: Evolution of the multifractal spectrum $F(\beta)$ vs. β for a growing connectivity p.

Fig. 5: Evolution of the normalized temperature (T/T_f), degree of cure (α), average connectivity density p and density of fractured links p^R with time at: (a) external slab surface and (b) slab midplane.

Fig. 6: Variation of the degree of cure (α) with time across the slab thickness.

Fig. 7: Variation of the average normal stresses $(\overline{\sigma}_{xx}, \overline{\sigma}_{zz})$ with time across the slab thickness.

Fig. 8: Variation of the average normal stresses $(\overline{\sigma}_{xx}, \overline{\sigma}_{zz})$ with time at the surface and mid-plane of the slab.

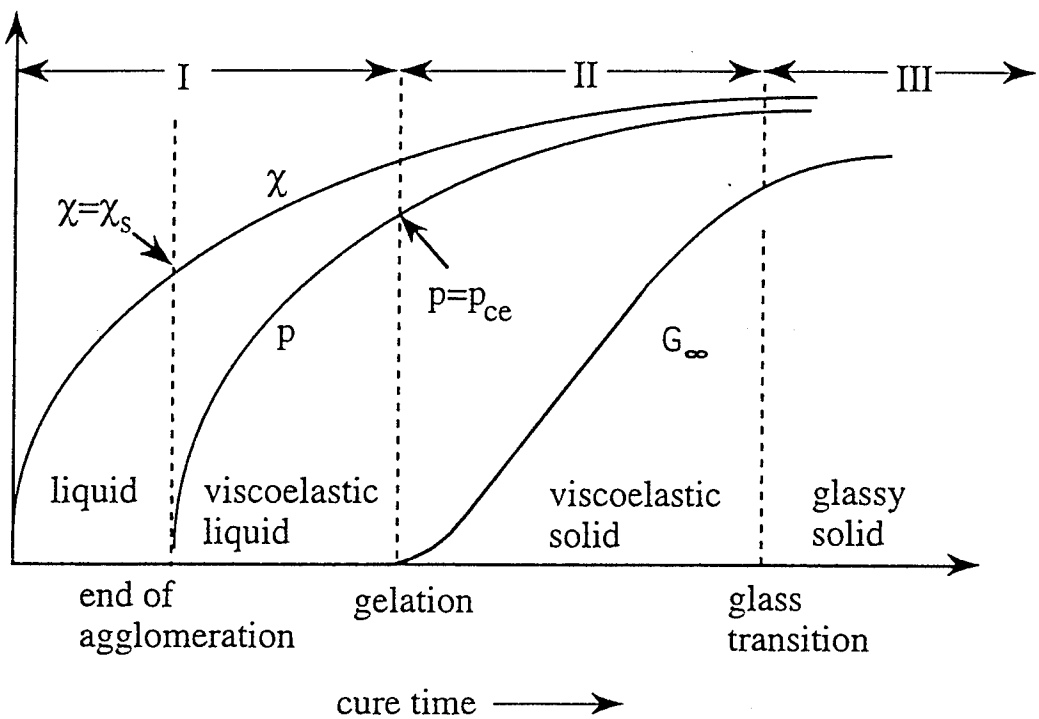
I
II
III
χ
χ=χs
p=pce
p
G∞
liquid
viscoelastic liquid
viscoelastic solid
glassy solid
end of agglomeration
gelation
glass transition
cure time

Fig. 1.

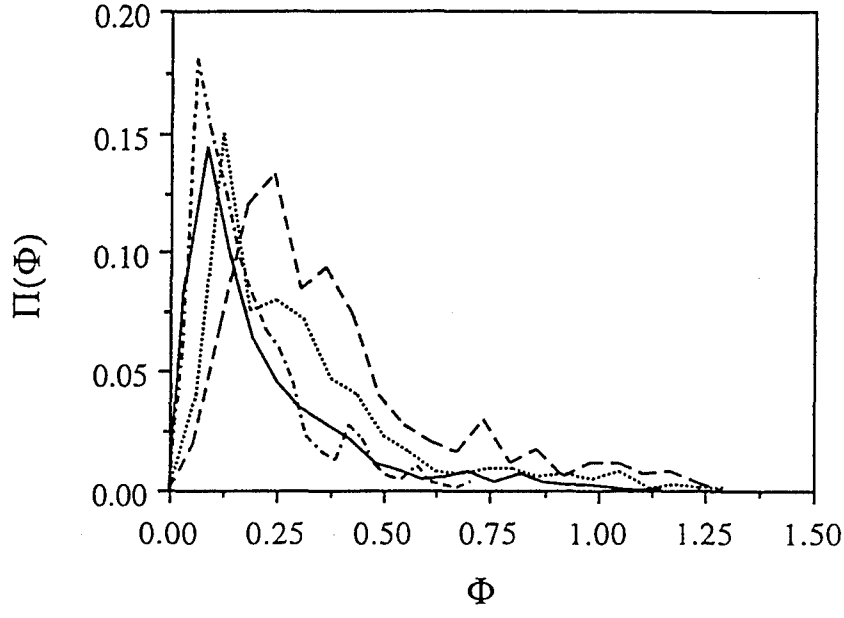
0.20
0.15
0.10
0.05
0.00
Π(Φ)
0.00
0.25
0.50
0.75
1.00
1.25
1.50
Φ

(a)

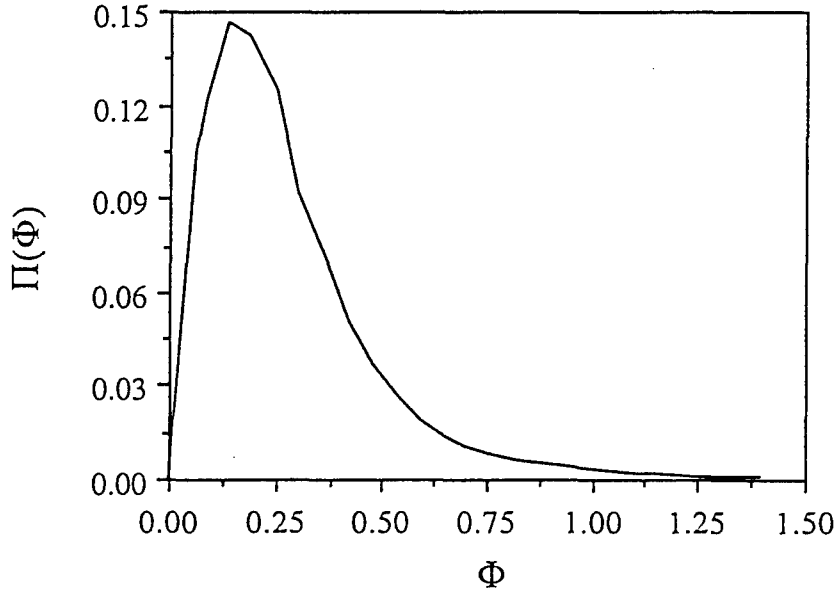
0.15
0.12
0.09
0.06
0.03
0.00
Π(Φ)
0.00
0.25
0.50
0.75
1.00
1.25
1.50
Φ

(b)

Fig.2.

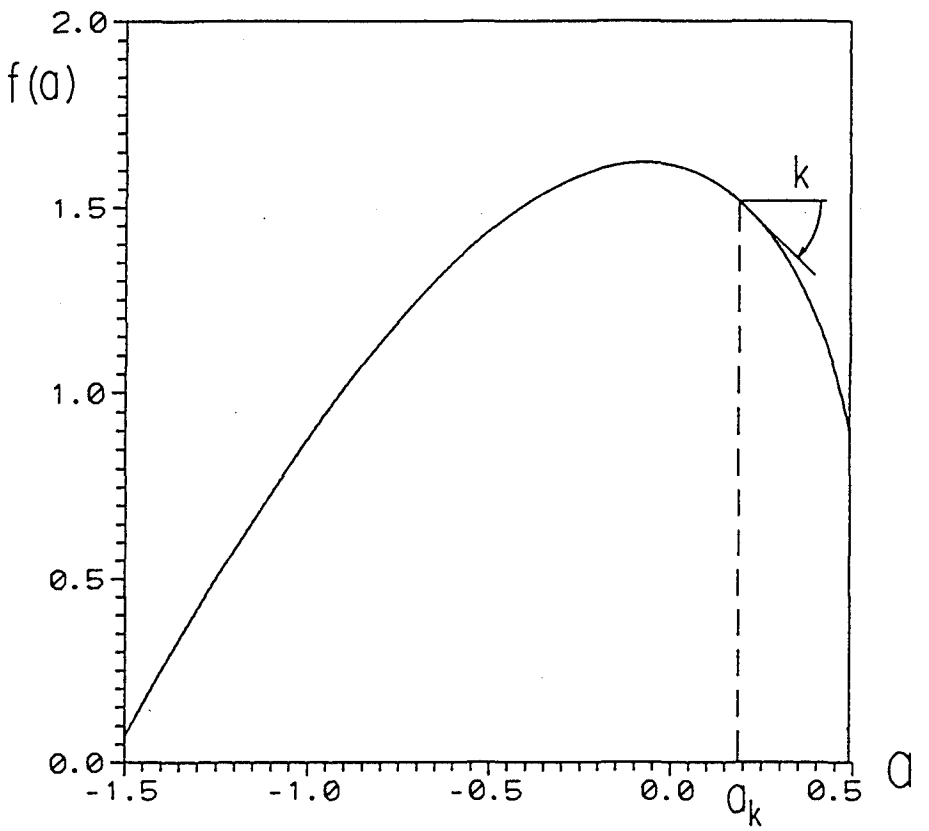

Fig. 3.

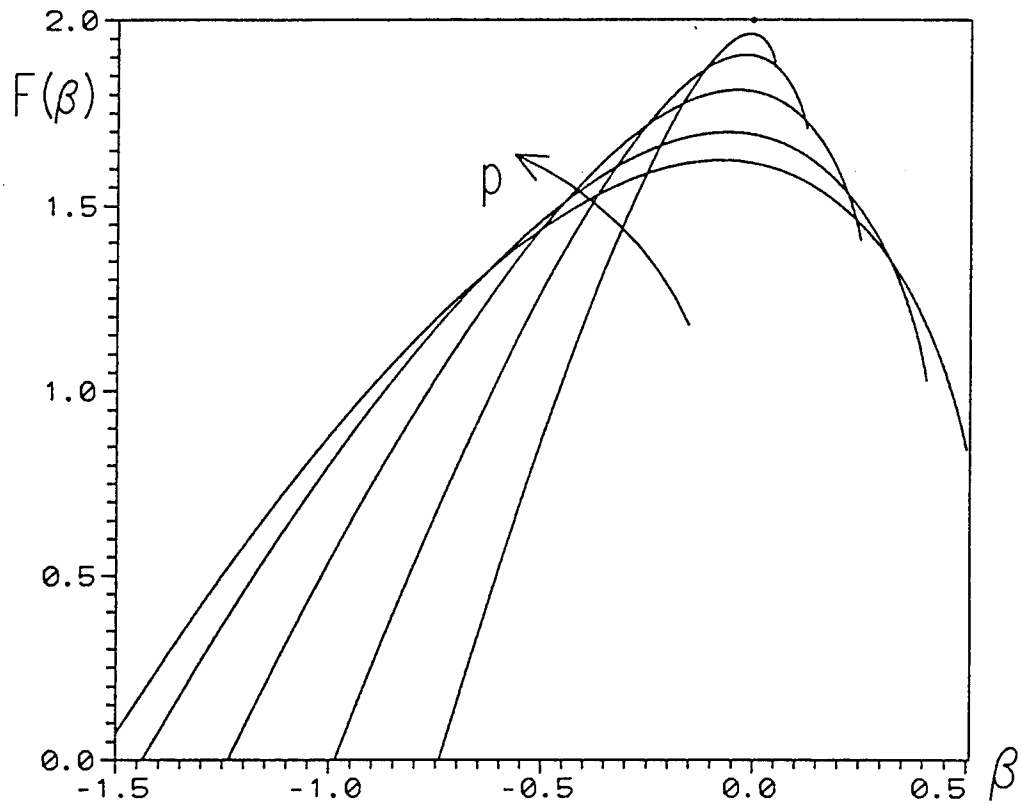

Fig. 4.

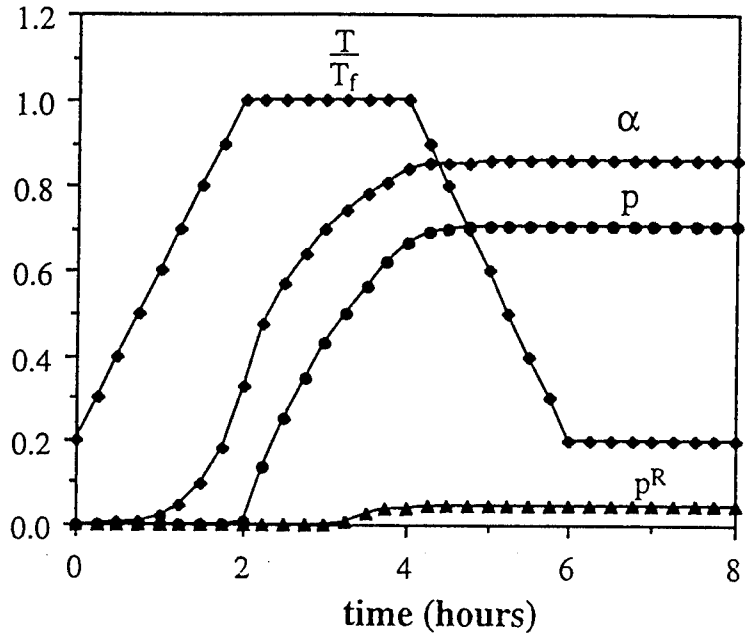
1.2
1.0
0.8
0.6
0.4
0.2
0.0
T/Tf
α
p
pR
0
2
4
6
8
time (hours)

(a)

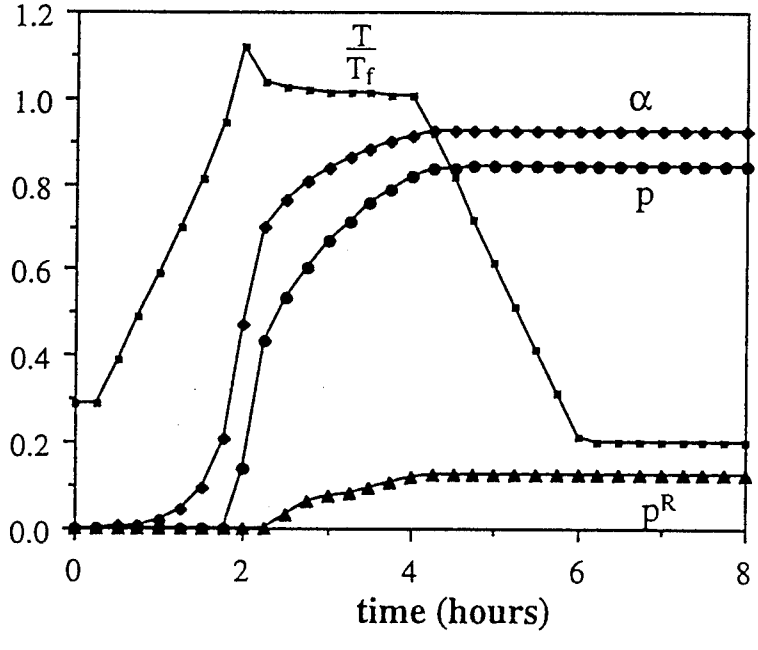
1.2
1.0
0.8
0.6
0.4
0.2
0.0
T/Tf
α
p
pR
0
2
4
6
8
time (hours)

(b)

Fig. 5.

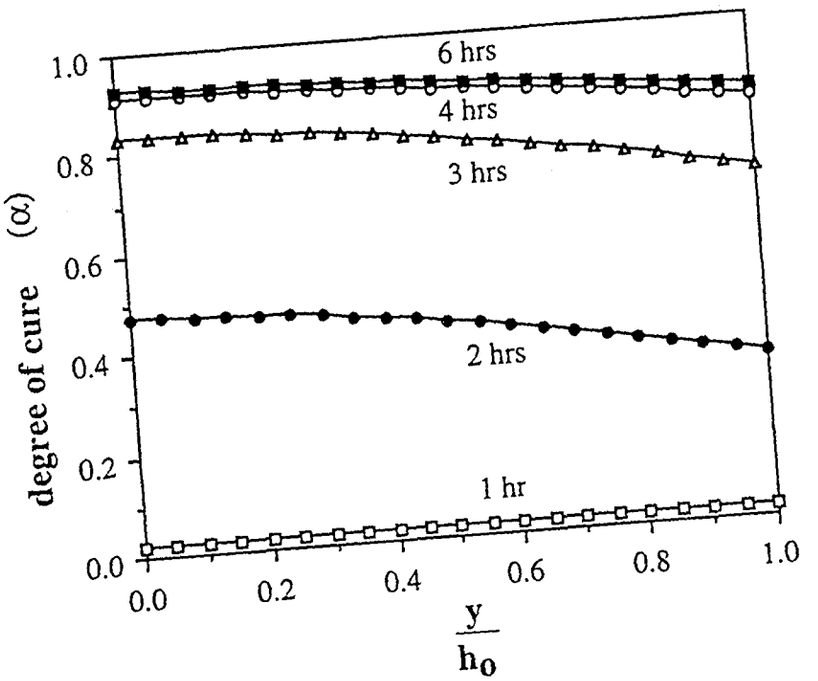
6 hrs
4 hrs
3 hrs
2 hrs
1 hr
1.0
0.8
0.6
0.4
0.2
0.0
degree of cure (α)
0.0
0.2
0.4
0.6
0.8
1.0
y
h0

Fig. 6

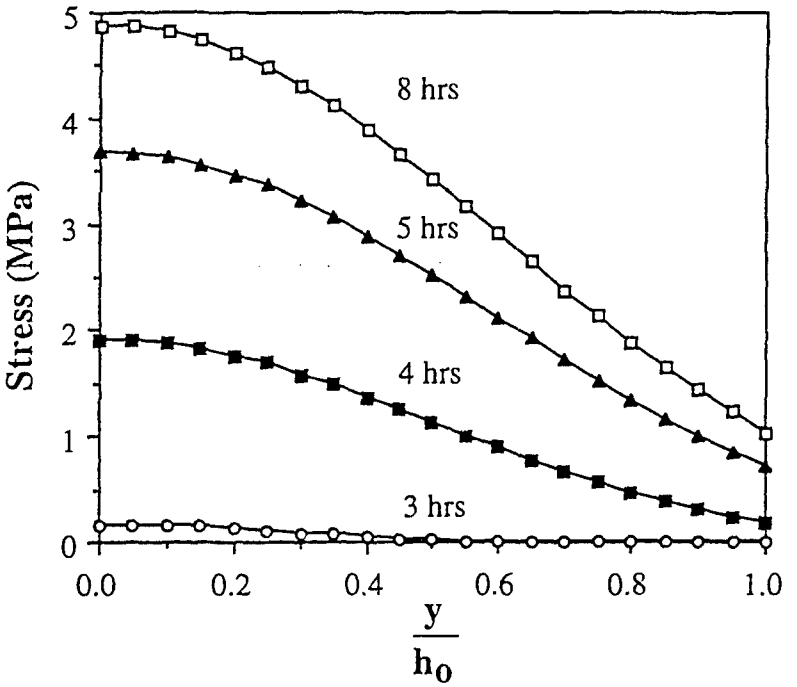

Fig. 7.

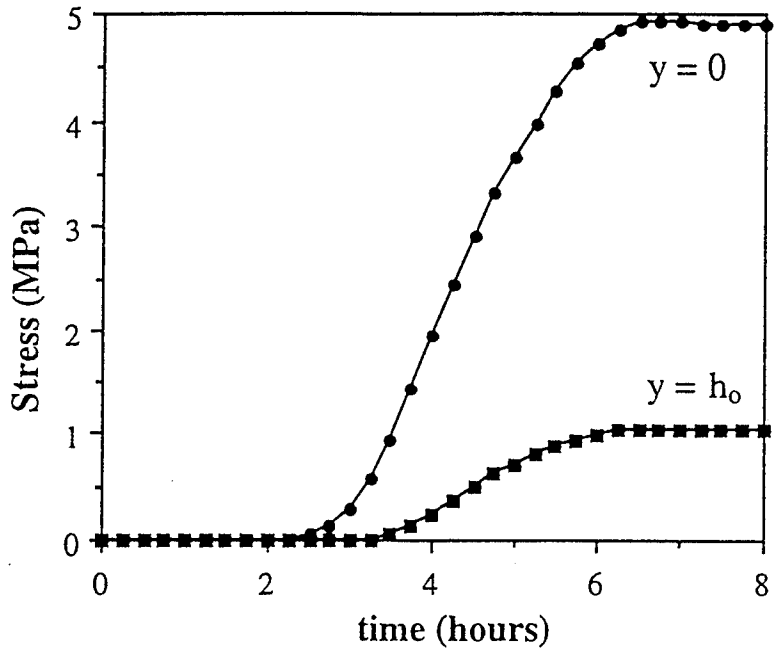

Fig. 8.

Pergamon

Int. J. Solids Structures Vol. 31, No. 21, pp. 2951–2964, 1994

0020–7683/94 $7.00 + .00

0020–7683(94)00067–0

AN ANALYSIS OF LARGE-STRAIN DAMAGE ELASTOPLASTICITY

V. A. LUBARDA

Department of Mechanical and Aerospace Engineering, Arizona State University, Tempe, AZ 85287-6106, U.S.A.

(*Received* 3 *September* 1993; *in revised form* 12 *April* 1994)

Abstract—The elastoplastic constitutive analysis which utilizes the model of multiplicative decomposition of the deformation gradient into its elastic and plastic parts has been mainly developed and applied to elastically isotropic materials, which remain isotropic during the process of plastic deformation. This paper extends the application of the model to materials that change their elastic properties during the deformation process as a result of the material degradation and the corresponding damage. The exact kinematic and kinetic analysis of the finite deformations leads to an additive decomposition of the total strain rate into its elastic, damage and plastic constituents. The general structure of the expression for the damage strain rate is derived, valid for utilized damage tensors of any order. The analysis of elastoplastic deformation of elastically anisotropic materials without damage is also presented, with the application to transversely isotropic materials. The relationships between the elastic and plastic strain rates and the components of the multiplicative decomposition and their rates are also given.

1. INTRODUCTION

Let $\mathscr{B}_0$ be the initial, undeformed configuration of a considered material sample, and $\mathscr{B}_t$ its deformed configuration obtained by a specified loading program from the initial to current time t. Assume that a loading is beyond the elastic limit, so that inelastic deformation processes take place, pertinent to internal structure and composition of the considered material. For example, if the material is a ductile metal, inelasticity is caused by the dislocation motion and related micromechanisms occurring within a metal polycrystalline structure. For a brittle material, such as rock or concrete, inelastic deformation is a consequence of the evolution of internal crack structure, i.e. the initiation and propagation of microfractures within the material sample. Whatever the cause of inelasticity is, let $\mathbf{F}$ be the deformation gradient that maps the infinitesimal material element $\mathrm{d}\mathbf{X}$ from its initial configuration to its current configuration $\mathrm{d}\mathbf{x}$, i.e. $\mathrm{d}\mathbf{x} = \mathbf{F}\mathrm{d}\mathbf{X}$. Both the initial $\mathbf{X}$ and the current $\mathbf{x}$ locations of the material particle are referred to the same, fixed set of the rectangular coordinate axes. Introduce next the intermediate reference configuration $\mathscr{P}_t$ by elastic distressing the current configuration $\mathscr{B}_t$ to zero stress. Therefore, defined configuration differs from the initial configuration by residual (plastic) deformation, and from the current configuration by reversible (elastic) deformation. If $\mathrm{d}\mathbf{p}$ is the material element in $\mathscr{P}_t$, corresponding to its configuration $\mathrm{d}\mathbf{x}$ in $\mathscr{B}_t$, then $\mathrm{d}\mathbf{x} = \mathbf{F}_e\mathrm{d}\mathbf{p}$, where $\mathbf{F}_e$ denotes the deformation gradient associated with elastic loading from $\mathscr{P}_t$ to $\mathscr{B}_t$. Introducing also the deformation gradient of the transformation $\mathscr{B}_0 \to \mathscr{P}_t$, by $\mathrm{d}\mathbf{p} = \mathbf{F}_p\mathrm{d}\mathbf{X}$, the multiplicative decomposition of deformation gradient follows (Lee, 1969):

$$\mathbf{F} = \mathbf{F}_e\mathbf{F}_p. \tag{1}$$

$\mathbf{F}_e$ is customarily called elastic, and $\mathbf{F}_p$ plastic part of the total deformation gradient $\mathbf{F}$. For inhomogeneous deformations, only $\mathbf{F}$ is the true deformation gradient, whose components are the partial derivatives $\partial\mathbf{x}/\partial\mathbf{X}$. In contrast, the mappings $\mathscr{P}_t \to \mathscr{B}_t$ and $\mathscr{B}_0 \to \mathscr{P}_t$ are not, in general, continuous one-to-one mappings, so that $\mathbf{F}_e$ and $\mathbf{F}_p$ are not defined as the gradients of the respective mappings (which may not exist), but as the point functions (local deformation gradients). In the case when elastic distressing to zero stress ($\mathscr{B}_t \to \mathscr{P}_t$) is not physically achievable due to the onset of reverse inelastic deformation before the zero stress

is reached (which often occurs at advanced stages of deformation due to anisotropic hardening and strong Bauschinger effects in ductile metals, or due to the incomplete frictional back-sliding of the crack faces in brittle rocks), the intermediate configuration can be conceptually introduced by virtual distressing to zero stress, locking all inelastic structural changes that would occur during the actual distressing.

Deformation gradients $\mathbf{F}_e$ and $\mathbf{F}_p$ are not uniquely defined, because arbitrary local material element rotations superposed to unstressed state give alternate intermediate configurations. However, if the material is elastically isotropic and remains such during the inelastic deformation, preserving its elastic properties, the elastic strain energy ψ_e per unit unstressed volume is an isotropic function of the right Cauchy–Green elastic deformation tensor $\mathbf{C}_e = \mathbf{F}_e^T\mathbf{F}_e$, i.e. $\psi_e(\mathbf{Q}\mathbf{C}_e\mathbf{Q}^T) = \psi_e(\mathbf{C}_e)$. Here, $\mathbf{Q}$ is an orthogonal tensor corresponding to arbitrary rigid-body rotation superposed to the unstressed state (superscript T denotes the transpose). The elastic stress response from $\mathscr{P}_t \to \mathscr{B}_t$ is, therefore, not influenced by the nonuniqueness of intermediate configuration and is given by the well-known isotropic finite elasticity law (Truesdell and Noll, 1965)

$$\boldsymbol{\sigma} = \frac{2}{|\mathbf{F}_e|}\mathbf{B}_e\frac{\partial\psi_e(\mathbf{B}_e)}{\partial\mathbf{B}_e}. \tag{2}$$

In eqn (2), the strain energy (per unit unstressed volume) ψ_e is an isotropic function of the left Cauchy–Green elastic deformation tensor $\mathbf{B}_e = \mathbf{F}_e\mathbf{F}_e^T$, $|\ |$ denotes the determinant and $\boldsymbol{\sigma}$ is the Cauchy stress tensor. This structure of elasticity law was used in a series of papers on the elastoplastic constitutive equations by Lee and his coworkers (Lee, 1969; Lubarda and Lee, 1981; Agah-Tehrani *et al.*, 1987), by Lubarda (1991a, 1994) and Lubarda and Shih (1994).

Few attempts were made to extend the analysis based on the multiplicative decomposition to materials that are elastically anisotropic in its initial (underformed) configuration, or to materials that develop elastic anisotropy during a course of inelastic deformation (Dafalias, 1985; Lubarda, 1991b). In fact, since in most elaborations it was assumed that elastic properties are not influenced by the previous inelastic processes, which is an unacceptable assumption in many cases of engineering importance, the usefulness of the decomposition was seriously questioned (Nemat-Nasser, 1982). The difficulty was partly related to the nonuniqueness of the unstressed configuration, its consequences on the anisotropic elastic response, and anticipated mathematical difficulties that may arise in proper handling of the analysis. This paper is, consequently, devoted to the generalization of the existing constitutive analysis, based on the multiplicative decomposition, to materials that change their elastic properties during the inelastic deformation process, and exhibit the damage–elastoplastic response. The general formulation is presented, restricted to isothermal and time-independent material behavior.

2. DESCRIPTION OF ANISOTROPIC ELASTIC RESPONSE

Consider an intermediate configuration $\mathscr{P}_t$ obtained by distressing the current configuration $\mathscr{B}_t$ to zero stress. Assume that the material in configuration $\mathscr{P}_t$ is elastically anisotropic, either because it was initially anisotropic, or because it has developed elastic anisotropy during the previous inelastic deformation (for example, due to the grain rotations in a polycrystalline metal sample and the consequent crystallographic texture, or due to anisotropic crack progression in the brittle rock samples). Therefore, let $\mathscr{D}$ denote a set of the symmetric tensor variables of various orders (scalars, second-order, fourth-order tensors, etc.), attached to the current configuration $\mathscr{B}_t$, which appropriately account for the degradation of elastic material properties and their directional changes, accumulated during the previous inelastic deformation. The variables $\mathscr{D}$ will be referred to as the damage variables. For example, in modeling inelastic behavior with infinitesimal elastic component of strain, the current (degraded) fourth-order elastic stiffness tensor can be selected as an appropriate damage tensor (Dougill, 1983). Ortiz (1985) has used the current elastic

compliance tensor as the damage tensor in his study of inelastic behavior of concrete [see also Lubarda and Krajcinovic (1993, 1994a)].

Even if there is no degradation of elastic material properties, the tensor variables $\mathscr{D}$ can be introduced to properly and conveniently describe the state of initial elastic anisotropy of the material [structural tensors (Boehler, 1987)]. For example, in the case of transverse isotropy with the axis of isotropy in the current configuration $\mathscr{B}_t$ coincident with the direction $\mathbf{n}$, the structural tensor is the second-order tensor $\mathscr{D} = \mathbf{n} \otimes \mathbf{n}$. For orthotropic material with the principal directions of orthotropy coincident with the directions $\mathbf{n}_1$, $\mathbf{n}_2$, $\mathbf{n}_3$, the structural tensors are $\mathbf{n}_1 \otimes \mathbf{n}_1$, $\mathbf{n}_2 \otimes \mathbf{n}_2$ and $\mathbf{n}_3 \otimes \mathbf{n}_3 = \mathbf{I} - \mathbf{n}_1 \otimes \mathbf{n}_1 - \mathbf{n}_2 \otimes \mathbf{n}_2$ ($\mathbf{I}$ denotes the second-order unit tensor and $\otimes$ the outside tensor product). The structural tensors corresponding to a general elastic anisotropy can be similarly formed and are given in Boehler (1987).

The introduced damage variables can only change during continuing inelastic deformation but remain unaltered during elastic unloading or reverse elastic loading, except for the elastic embedding which convects them together with the material. Therefore, the damage variables $\mathscr{D}$ in the current configuration $\mathscr{B}_t$ become the variables $\hat{\mathscr{D}}$ in the intermediate configuration, induced from $\mathscr{D}$ by elastic deformation $\mathbf{F}_e$. For example, for the second-order damage tensor, the induced tensor can be defined by a transformation of the weighted contravariant or covariant type, i.e.

$$\hat{\mathscr{D}} = |\mathbf{F}_e|^m \mathbf{F}_e^{-1} \mathscr{D} \mathbf{F}_e^{-T} \quad \text{or} \quad \hat{\mathscr{D}} = |\mathbf{F}_e|^{-m} \mathbf{F}_e^T \mathscr{D} \mathbf{F}_e, \tag{3}$$

where m is the weight and (-1) denotes the inverse. For the fourth-order damage tensor, the corresponding induced tensor is

$$\hat{\mathscr{D}} = |\mathbf{F}_e|^m \mathbf{F}_e^{-1} \otimes \mathbf{F}_e^{-1} \mathscr{D} \mathbf{F}_e^{-T} \otimes \mathbf{F}_e^{-T} \quad \text{or} \quad \hat{\mathscr{D}} = |\mathbf{F}_e|^{-m} \mathbf{F}_e^T \otimes \mathbf{F}_e^T \mathscr{D} \mathbf{F}_e \otimes \mathbf{F}_e. \tag{4}$$

For example, the second tensor in eqn (4) has the components

$$\hat{\mathscr{D}}_{ijkl} = |\mathbf{F}_e|^{-m} (F_{i\alpha}^e)^T (F_{j\beta}^e)^T \mathscr{D}_{\alpha\beta\gamma\delta} F_{\gamma k}^e F_{\delta l}^e. \tag{5}$$

To describe the elastic response of anisotropic material at the current state of deformation and material damage, the strain energy ψ per unit initial volume is assumed to be given by

$$\psi = \psi(\mathbf{C}_e, \hat{\mathscr{D}}). \tag{6}$$

Note that $\psi = |\mathbf{F}_p| \psi_e$, where ψ_e is the elastic strain energy per unit unstressed volume in the intermediate configuration. Since the unit of unstressed volume contains a varying amount of mass during the deformation process whenever plastic deformation is compressible, so that $|\mathbf{F}_p| \neq 1$, the strain energy ψ per unit initial volume is introduced in eqn (6), as it always refers to a fixed amount of mass.

Since the material response is independent of the superposed rotation to intermediate-unstressed configuration, eqn (6) has to be an isotropic scalar function of the set of all its arguments, i.e. $\mathbf{C}_e$ and $\hat{\mathscr{D}}$. For example, if the set $\mathscr{D}$ consists of the second-order tensors $\mathscr{D}_2$ and the fourth-order tensors $\mathscr{D}_4$, the isotropy of ψ requires that for every orthogonal transformation $\mathbf{Q}$,

$$\psi(\mathbf{Q}\mathbf{C}_e\mathbf{Q}^T, \mathbf{Q}\hat{\mathscr{D}}_2\mathbf{Q}^T, \mathbf{Q} \otimes \mathbf{Q}\,\hat{\mathscr{D}}_4\,\mathbf{Q}^T \otimes \mathbf{Q}^T) = \psi(\mathbf{C}_e, \hat{\mathscr{D}}_2, \hat{\mathscr{D}}_4). \tag{7}$$

Note that under the superposed rotation $\mathbf{Q}$ of the intermediate configuration, $\mathscr{D}$ does not change, as it is defined with respect to the current configuration. Since $\mathbf{F}_e$ changes to $\mathbf{F}_e\mathbf{Q}^T$, from eqn (3) it follows that $\hat{\mathscr{D}}_2$ changes to $\mathbf{Q}\hat{\mathscr{D}}_2\mathbf{Q}^T$. An analogous change rule applies to the fourth-order damage tensor $\hat{\mathscr{D}}_4$, as utilized in eqn (7).

The theory of isotropic scalar and tensor functions of several tensor arguments has been extensively studied in the literature. A comprehensive treatment of various important

issues has been presented by Spencer (1971, 1987) and Boehler (1977, 1987). There the integrity basis for the considered functions are derived mainly for the vector and second-order tensor arguments. Betten (1982, 1987, 1992) has also considered the functions that depend on the second- and fourth-order tensors and construction of their individual and joint invariants. For example, if $\hat{\mathscr{D}}$ in eqn (6) is a single second-order symmetric tensor, ψ can be represented as a polynomial of its irreducible integrity basis consisting of the following invariants:

$$(\mathbf{C}_e:\mathbf{I}),(\mathbf{C}_e:\mathbf{C}_e),(\mathbf{C}_e^2:\mathbf{C}_e),(\hat{\mathscr{D}}:\mathbf{I}),(\hat{\mathscr{D}}:\hat{\mathscr{D}})$$
$$(\hat{\mathscr{D}}^2:\hat{\mathscr{D}}),(\mathbf{C}_e:\hat{\mathscr{D}}),(\mathbf{C}_e:\hat{\mathscr{D}}^2),(\mathbf{C}_e^2:\hat{\mathscr{D}}),(\mathbf{C}_e^2:\hat{\mathscr{D}}^2). \tag{8}$$

In eqn (8), (:) stands for the inner (trace) product of the second-order tensors. The integrity basis can be written for any finite set of second-order tensors. Spencer (1971) provides a list of invariants and the integrity bases for the polynomial scalar functions dependent on one to six second-order tensor arguments. For general (not necessarily polynomial) functions, the integrity bases are replaced by the function bases, which, in general, contain fewer terms than the corresponding integrity bases. For example, the function bases of the general scalar function dependent on an arbitrary number of second-order tensors are composed of the traces of the products of all unordered combinations of only one, two and three tensorial arguments (Boehler, 1977).

The construction of the integrity bases for the second- and fourth-order symmetric tensors is a more difficult task. Some of the individual and joint invariants are listed below [for the more complete list, refer to Betten (1987, 1992)]:

$$\hat{\mathscr{D}}::(\mathbf{I}\otimes\mathbf{I}),(\hat{\mathscr{D}}::\mathbf{II}),(\hat{\mathscr{D}}::\hat{\mathscr{D}})$$
$$\hat{\mathscr{D}}::(\mathbf{C}_e\otimes\mathbf{C}_e),(\mathbf{I}:\hat{\mathscr{D}}:\mathbf{C}_e^2),(\mathbf{C}_e:\hat{\mathscr{D}}):(\hat{\mathscr{D}}:\mathbf{C}_e). \tag{9}$$

In eqn (9), **II** is the fourth-order unit tensor, while :: designates the trace, so that for the two fourth-order tensors **A** and **B**, $\mathbf{A}::\mathbf{B}=A_{ijkl}B_{ijkl}$. The trace of the fourth-order tensor **A** and the second-order tensor **C** is the second-order tensor $\mathbf{A}:\mathbf{C}$, with the components $A_{ijkl}C_{kl}$.

In general, the stress response from the intermediate to current configuration is given by

$$\boldsymbol{\sigma}=\frac{2}{|\mathbf{F}_e|}\mathbf{F}_e\frac{\partial\psi_e}{\partial\mathbf{C}_e}\mathbf{F}_e^{\mathrm{T}}, \tag{10}$$

which is independent of the rigid-body rotation superposed to the intermediate configuration. This clearly follows since $\boldsymbol{\sigma}$ does not change under the superposed rotation **Q** of the intermediate configuration, while $\mathbf{F}_e$ changes to $\mathbf{F}_e\mathbf{Q}^{\mathrm{T}}$, and $\mathbf{C}_e$ to $\mathbf{Q}\mathbf{C}_e\mathbf{Q}^{\mathrm{T}}$. More detailed discussion of the objectivity issues in the formulation of elastoplasticity theory by using the multiplicative decomposition of the deformation gradient is presented by Lubarda (1991a).

Expressing the strain energy ψ_e per unit unstressed volume in terms of the strain energy ψ per unit initial volume, eqn (10) can be rewritten as

$$\boldsymbol{\tau}=2\mathbf{F}_e\frac{\partial\psi(\mathbf{C}_e,\hat{\mathscr{D}})}{\partial\mathbf{C}_e}\mathbf{F}_e^{\mathrm{T}}, \tag{11}$$

where $\boldsymbol{\tau}=|\mathbf{F}|\boldsymbol{\sigma}$ is the Kirchhoff stress and $\psi=|\mathbf{F}_p|\psi_e$ is the strain energy per unit initial volume. In the rate-type constitutive analysis considered in this paper, it will be useful to start the analysis with the finite elasticity law [eqn (11)], even when intended application is to material behavior with infinitesimal elastic components of strain.

3. RATE-TYPE ANALYSIS

To derive the rate-type constitutive equations of the damage–elastoplastic material behavior, apply first the material time derivative (designated by the superimposed dot) to both sides of eqn (11). By an appropriate and straightforward rearrangement of the terms, it follows that

$$\dot{\boldsymbol{\tau}} = (\dot{\mathbf{F}}_e\mathbf{F}_e^{-1})\boldsymbol{\tau} + \boldsymbol{\tau}(\dot{\mathbf{F}}_e\mathbf{F}_e^{-1})^T + 2\mathbf{F}_e\left(\frac{\partial^2\psi}{\partial\mathbf{C}_e\otimes\partial\mathbf{C}_e}:\dot{\mathbf{C}}_e\right)\mathbf{F}_e^T + 2\mathbf{F}_e\left(\frac{\partial^2\psi}{\partial\mathbf{C}_e\otimes\partial\hat{\mathscr{D}}}:\dot{\hat{\mathscr{D}}}\right)\mathbf{F}_e^T. \tag{12}$$

In view of eqn (11), which gives the stress $\boldsymbol{\tau}$ as a function of $\mathbf{F}_e$ and $\hat{\mathscr{D}}$, the last term on the right-hand side of eqn (12) can be written in a compact form as

$$2\mathbf{F}_e\left(\frac{\partial^2\psi}{\partial\mathbf{C}_e\otimes\partial\hat{\mathscr{D}}}:\dot{\hat{\mathscr{D}}}\right)\mathbf{F}_e^T = \frac{\partial\boldsymbol{\tau}}{\partial\hat{\mathscr{D}}}:\dot{\hat{\mathscr{D}}}. \tag{13}$$

In eqn (13), $\partial\boldsymbol{\tau}/\partial\hat{\mathscr{D}}$ designates the partial derivative of the stress expression (11) with respect to $\hat{\mathscr{D}}$, at constant $\mathbf{F}_e$. Further, since

$$\dot{\mathbf{C}}_e = 2\mathbf{F}_e^T(\dot{\mathbf{F}}_e\mathbf{F}_e^{-1})_s\mathbf{F}_e, \tag{14}$$

where the subscript s designates the symmetric part, the third term on the right-hand side of eqn (12) can be written as

$$2\mathbf{F}_e\left(\frac{\partial^2\psi}{\partial\mathbf{C}_e\otimes\partial\mathbf{C}_e}:\dot{\mathbf{C}}_e\right)\mathbf{F}_e^T = \boldsymbol{\Lambda}_e:(\dot{\mathbf{F}}_e\mathbf{F}_e^{-1})_s. \tag{15}$$

Here, $\boldsymbol{\Lambda}_e$ is the fourth-order tensor with the rectangular components

$$\Lambda^e_{ijkl} = 4F^e_{im}F^e_{jn}\frac{\partial^2\psi}{\partial C^e_{mn}\partial C^e_{pq}}F^e_{kp}F^e_{lq}. \tag{16}$$

Substitution of eqns (13) and (15) into eqn (12) therefore gives

$$\dot{\boldsymbol{\tau}} = (\dot{\mathbf{F}}_e\mathbf{F}_e^{-1})\boldsymbol{\tau} + \boldsymbol{\tau}(\dot{\mathbf{F}}_e\mathbf{F}_e^{-1})^T + \boldsymbol{\Lambda}_e:(\dot{\mathbf{F}}_e\mathbf{F}_e^{-1})_s + \frac{\partial\boldsymbol{\tau}}{\partial\hat{\mathscr{D}}}:\dot{\hat{\mathscr{D}}}. \tag{17}$$

To proceed further with the rate-type constitutive analysis, consider the velocity gradient in the current configuration at time t, defined by $\mathbf{L} = \dot{\mathbf{F}}\mathbf{F}^{-1}$. Introducing the multiplicative decomposition of the deformation gradient [eqn (1)], the velocity gradient can be expressed as

$$\mathbf{L} = \dot{\mathbf{F}}_e\mathbf{F}_e^{-1} + \mathbf{F}_e(\dot{\mathbf{F}}_p\mathbf{F}_p^{-1})\mathbf{F}_e^{-1}. \tag{18}$$

The strain rate $\mathbf{D}$ and the spin $\mathbf{W}$ are given by the symmetric and antisymmetric parts of $\mathbf{L}$:

$$\mathbf{D} = (\dot{\mathbf{F}}_e\mathbf{F}_e^{-1})_s + [\mathbf{F}_e(\dot{\mathbf{F}}_p\mathbf{F}_p^{-1})\mathbf{F}_e^{-1}]_s \tag{19}$$

$$\mathbf{W} = (\dot{\mathbf{F}}_e\mathbf{F}_e^{-1})_a + [\mathbf{F}_e(\dot{\mathbf{F}}_p\mathbf{F}_p^{-1})\mathbf{F}_e^{-1}]_a. \tag{20}$$

Writing $\dot{\mathbf{F}}_e\mathbf{F}_e^{-1}$ as the sum of its symmetric and antisymmetric parts, and using eqn (20) to express the antisymmetric part, one has

$$\dot{\mathbf{F}}_e\mathbf{F}_e^{-1} = (\dot{\mathbf{F}}_e\mathbf{F}_e^{-1})_s + \mathbf{W} - \omega. \tag{21}$$

For convenience, the tensor ω in eqn (21) denotes the spin

$$\omega = [\mathbf{F}_e(\dot{\mathbf{F}}_p\mathbf{F}_p^{-1})\mathbf{F}_e^{-1}]_a. \tag{22}$$

Substitution of eqn (21) into eqn (17) consequently gives

$$\overset{\circ}{\tau} = \mathscr{L}_e : (\dot{\mathbf{F}}_e\mathbf{F}_e^{-1})_s + \frac{\partial\tau}{\partial\hat{\mathscr{D}}} : \dot{\hat{\mathscr{D}}} + \tau\omega - \omega\tau, \tag{23}$$

where

$$\overset{\circ}{\tau} = \dot{\tau} - \mathbf{W}\tau + \tau\mathbf{W} \tag{24}$$

represents the Jaumann derivative of the Kirchhoff stress τ. The material derivative of the Kirchhoff stress appearing on the right-hand side of eqn (24) is $\dot{\tau} = |\mathbf{F}|(\dot{\sigma} + \sigma\,\mathrm{tr}\mathbf{D})$, where tr denotes the trace.

The fourth-order tensor of the instantaneous elastic moduli $\mathscr{L}_e$, appearing in eqn (23), has the rectangular components given by

$$\mathscr{L}^e_{ijkl} = \tfrac{1}{2}(\delta_{ik}\tau_{jl} + \delta_{il}\tau_{jk} + \tau_{ik}\delta_{jl} + \tau_{il}\delta_{jk}) + 4F^e_{im}F^e_{jn}\frac{\partial^2\psi}{\partial C^e_{mn}\partial C^e_{pq}}F^e_{kp}F^e_{lq}, \tag{25}$$

where δ_{ij} denotes the Kronecker delta. In view of the introduced isotropy of the strain energy function ψ, it is easily shown that the components [eqn (25)] are independent of the superposed rotation of the intermediate configuration. In other words, any one from infinitely many by rotation differing deformation gradients $\mathbf{F}_e$ when substituted into eqn (25), gives the same values of the instantaneous elastic moduli. In metals the elastic moduli are usually far greater than the applied stresses and the two fourth-order tensors, whose components are given by eqns (16) and (25), are approximately equal to each other.

4. THE RATES OF DAMAGE TENSORS

Consider first $\hat{\mathscr{D}}$ to be the second-order damage tensor. The material time derivative of the induced tensor of the contravariant type, $\hat{\mathscr{D}} = |\mathbf{F}_e|^m\mathbf{F}_e^{-1}\mathscr{D}\mathbf{F}_e^{-\mathrm{T}}$, is

$$\dot{\hat{\mathscr{D}}} = |\mathbf{F}_e|^m\mathbf{F}_e^{-1}\overset{\bullet e}{\mathscr{D}}\mathbf{F}_e^{-\mathrm{T}}, \tag{26}$$

where

$$\overset{\bullet e}{\mathscr{D}} = \dot{\mathscr{D}} - (\dot{\mathbf{F}}_e\mathbf{F}_e^{-1})\mathscr{D} - \mathscr{D}(\dot{\mathbf{F}}_e\mathbf{F}_e^{-1})^{\mathrm{T}} + m\mathscr{D}\,\mathrm{tr}\,(\dot{\mathbf{F}}_e\mathbf{F}_e^{-1}) \tag{27}$$

is the corresponding (Oldroyd/Truesdell type) convected derivative, relative to the velocity gradient $\dot{\mathbf{F}}_e\mathbf{F}_e^{-1}$. If the induced tensor of the covariant type is used, i.e. $\hat{\mathscr{D}} = |\mathbf{F}_e|^{-m}\mathbf{F}_e^{\mathrm{T}}\mathscr{D}\mathbf{F}_e$, one has

$$\dot{\hat{\mathscr{D}}} = |\mathbf{F}_e|^{-m}\mathbf{F}_e^{\mathrm{T}}\overset{\bullet e}{\mathscr{D}}\mathbf{F}_e^{-\mathrm{T}}, \tag{28}$$

where

$$\overset{\circ}{\mathscr{Q}}^{e} = \dot{\mathscr{Q}} + \mathscr{Q}(\dot{\mathbf{F}}_e\mathbf{F}_e^{-1}) + (\dot{\mathbf{F}}_e\mathbf{F}_e^{-1})^T\mathscr{Q} - m\mathscr{Q}\,\mathrm{tr}\,(\dot{\mathbf{F}}_e\mathbf{F}_e^{-1}) \tag{29}$$

is the corresponding (Cotter–Rivlin/Truesdell type) convected derivative, associated with the covariant transformation. Substitution of either eqn (26) or (28) into the second term on the right-hand side of expression (23) therefore gives

$$\frac{\partial\tau}{\partial\hat{\mathscr{Q}}} : \dot{\hat{\mathscr{Q}}} = \frac{\partial\tau}{\partial\mathscr{Q}} : \overset{\circ}{\mathscr{Q}}^{e}. \tag{30}$$

It should be observed that the introduced convected derivatives [eqns (27) and (29)] are not uniquely defined because the unstressed intermediate configuration is specified only to within an arbitrary rigid-body rotation, so that the velocity gradient $\dot{\mathbf{F}}_e\mathbf{F}_e^{-1}$, used in eqns (27) and (29), is not uniquely defined either. However, in some applications it may be convenient to specify the intermediate configuration uniquely, on the basis of some additional physical structure, explicitly introduced in the considered material model and pertinent to its internal structure and the deformation modes. For example, in the crystal plasticity (Asaro, 1983), the rotation of the intermediate configuration is uniquely specified by requiring that the basic crystalline (lattice) structure always has the same orientation relative to the fixed reference frame [isoclinic intermediate configuration, in the terminology of Mandel (1971, 1973)]. In this case, the velocity gradient $\dot{\mathbf{F}}_e\mathbf{F}_e^{-1}$ is uniquely defined and represents the sum of the lattice strain rate and the lattice spin. Physically, it is the discontinuous slip of the material over the active slip planes that causes the lattice orientation to be convected by the lattice and not by the material itself.

On the other hand, in some applications it may be more appropriate to introduce the convected derivative as the derivative observed in the reference frame that deforms with the material, i.e. relative to the material velocity gradient $\mathbf{L} = \dot{\mathbf{F}}\mathbf{F}^{-1}$. For example, in brittle materials like brittle rocks, the change of elastic properties occurs due to propagation of the crack-like defects through the material, which convects them with itself during the deformation process. Therefore, by using eqn (18) to eliminate $(\dot{\mathbf{F}}_e\mathbf{F}_e^{-1})$, eqn (26) can be rewritten as

$$\hat{\mathscr{Q}} = |\mathbf{F}_e|^m\mathbf{F}_e^{-1}\dot{\mathscr{Q}}\mathbf{F}_e^{-T} + (\dot{\mathbf{F}}_p\mathbf{F}_p^{-1})\hat{\mathscr{Q}} + \hat{\mathscr{Q}}(\dot{\mathbf{F}}_p\mathbf{F}_p^{-1})^T - m\hat{\mathscr{Q}}\,\mathrm{tr}\,(\dot{\mathbf{F}}_p\mathbf{F}_p^{-1}), \tag{31}$$

where

$$\dot{\hat{\mathscr{Q}}} = \dot{\mathscr{Q}} - \mathbf{L}\mathscr{Q} - \mathscr{Q}\mathbf{L}^T + m\mathscr{Q}\,\mathrm{tr}\mathbf{L}. \tag{32}$$

Similarly, eqn (28) can be rearranged as

$$\dot{\hat{\mathscr{Q}}} = |\mathbf{F}_e|^{-m}\mathbf{F}_e^T\dot{\mathscr{Q}}\mathbf{F}_e - \hat{\mathscr{Q}}(\dot{\mathbf{F}}_p\mathbf{F}_p^{-1}) - (\dot{\mathbf{F}}_p\mathbf{F}_p^{-1})^T\hat{\mathscr{Q}} + m\hat{\mathscr{Q}}\,\mathrm{tr}(\dot{\mathbf{F}}_p\mathbf{F}_p^{-1}), \tag{33}$$

where

$$\dot{\hat{\mathscr{Q}}} = \dot{\mathscr{Q}} + \mathscr{Q}\mathbf{L} + \mathbf{L}^T\mathscr{Q} - m\mathscr{Q}\,\mathrm{tr}\mathbf{L}. \tag{34}$$

Substitution of either eqn (31) or (33) into the second term on the right-hand side of expression (23) now gives

$$\frac{\partial\tau}{\partial\hat{\mathscr{Q}}} : \dot{\hat{\mathscr{Q}}} = \frac{\partial\tau}{\partial\mathscr{Q}} : \dot{\mathscr{Q}} + \mathscr{A} : (\dot{\mathbf{F}}_p\mathbf{F}_p^{-1}). \tag{35}$$

When eqn (31) is used, the fourth-order tensor $\mathscr{A}$ is defined by

$$\mathscr{A}:(\dot{\mathbf{F}}_p\mathbf{F}_p^{-1})=\frac{\partial\tau}{\partial\hat{\mathscr{D}}}:[(\dot{\mathbf{F}}_p\mathbf{F}_p^{-1})\hat{\mathscr{D}}+\hat{\mathscr{D}}(\dot{\mathbf{F}}_p\mathbf{F}_p^{-1})^T-m\hat{\mathscr{D}}\,\mathrm{tr}(\dot{\mathbf{F}}_p\mathbf{F}_p^{-1})]. \tag{36a}$$

If eqn (33) is used, eqn (36a) is replaced by

$$\mathscr{A}:(\dot{\mathbf{F}}_p\mathbf{F}_p^{-1})=-\frac{\partial\tau}{\partial\hat{\mathscr{D}}}:[\hat{\mathscr{D}}(\dot{\mathbf{F}}_p\mathbf{F}_p^{-1})+(\dot{\mathbf{F}}_p\mathbf{F}_p^{-1})^T\hat{\mathscr{D}}-m\hat{\mathscr{D}}\,\mathrm{tr}(\dot{\mathbf{F}}_p\mathbf{F}_p^{-1})]. \tag{36b}$$

It should be pointed out that, although in this section the damage tensors were assumed to be the second-order tensors, the structure of expressions (30)–(35) remain the same for any introduced higher-order symmetric damage tensors. This is illustrated for the fourth-order tensors in the Appendix of this paper.

5. IDENTIFICATION OF ELASTIC AND DAMAGE STRAIN RATES

Substituting expression (30) into eqn (23) it follows

$$\overset{\circ}{\tau}=\mathscr{L}_e:(\dot{\mathbf{F}}_e\mathbf{F}_e^{-1})_s+\frac{\partial\tau}{\partial\mathscr{D}}:\overset{\bullet e}{\mathscr{D}}+\tau\omega-\omega\tau. \tag{37}$$

If eqn (35) rather than eqn (30) is used, one has

$$\overset{\circ}{\tau}=\mathscr{L}_e:(\dot{\mathbf{F}}_e\mathbf{F}_e^{-1})_s+\frac{\partial\tau}{\partial\mathscr{D}}:\dot{\mathscr{D}}+\mathscr{A}:(\dot{\mathbf{F}}_p\mathbf{F}_p^{-1})+\tau\omega-\omega\tau. \tag{38}$$

Concentrating attention first to the case when eqn (37) applies, it is next shown that the strain rate $(\dot{\mathbf{F}}_e\mathbf{F}_e^{-1})_s$ consists of three parts: elastic strain rate $\mathbf{D}_e$, damage strain rate $\mathbf{D}_d$ and an additional part denoted by Δ, such that

$$(\dot{\mathbf{F}}_e\mathbf{F}_e^{-1})_s=\mathbf{D}_e+\mathbf{D}_d+\Delta. \tag{39}$$

Indeed, substitution of eqn (39) into eqn (37) gives

$$\overset{\circ}{\tau}=\mathscr{L}_e:\mathbf{D}_e+\mathscr{L}_e:\mathbf{D}_d+\frac{\partial\tau}{\partial\mathscr{D}}:\overset{\bullet e}{\mathscr{D}}+\mathscr{L}_e:\Delta+\tau\omega-\omega\tau. \tag{40}$$

Since the instantaneous elastic moduli tensor $\mathscr{L}_e$ and its inverse, the instantaneous elastic compliance tensor $\mathscr{L}_e^{-1}$, possess required symmetry and reciprocity properties

$$(\mathscr{L}_e^{-1})_{ijkl}=(\mathscr{L}_e^{-1})_{ijlk}=(\mathscr{L}_e^{-1})_{jikl}=(\mathscr{L}_e^{-1})_{klij}, \tag{41}$$

it follows that $\mathscr{L}_e^{-1}:\overset{\circ}{\tau}$ is derivable from the elastic rate potential $\phi_e=\frac{1}{2}\mathscr{L}_e^{-1}:(\overset{\circ}{\tau}\otimes\overset{\circ}{\tau})$ as its gradient $\partial\phi_e/\partial\overset{\circ}{\tau}$. Therefore,

$$\mathbf{D}_e=\mathscr{L}_e^{-1}:\overset{\circ}{\tau} \tag{42}$$

gives the reversible strain increment, that is recovered in a hardening material upon unloading of the Jaumann stress increment associated with $\overset{\circ}{\tau}$. Further, it is natural to define the damage strain rate $\mathbf{D}_d$ as the strain rate associated with progressive degradation of the material elastic properties, as represented by the change of damage variables $\mathscr{D}$. Hence, the damage strain rate $\mathbf{D}_d$ has to be directly related to the rate of change tensor $\overset{\bullet e}{\mathscr{D}}$. Consequently, in view of the previously established relationship [eqn (42)] between $\mathbf{D}_e$ and $\overset{\circ}{\tau}$, it necessarily follows that eqn (40) splits into three equations:

$$\mathscr{L}_e : \mathbf{D}_e = \overset{\circ}{\tau} \tag{43}$$

$$\mathscr{L}_e : \mathbf{D}_d + \frac{\partial \tau}{\partial \mathscr{D}} : \overset{\bullet e}{\mathscr{D}} = \mathbf{0} \tag{44}$$

$$\mathscr{L}_e : \Delta + \tau\omega - \omega\tau = \mathbf{0}. \tag{45}$$

Inversion of eqn (43) gives the elastic strain rate expression (42). Solving eqn (44) for $\mathbf{D}_d$ provides the expression for the damage strain rate

$$\mathbf{D}_d = -\mathscr{L}_e^{-1} : \left(\frac{\partial \tau}{\partial \mathscr{D}} : \overset{\bullet e}{\mathscr{D}} \right) \tag{46}$$

With the evolution equation for the damage rate $\overset{\bullet e}{\mathscr{D}}$ additionally constructed, eqn (46) explicitly gives the damage strain rate $\mathbf{D}_d$. Finally, condition (45) defines the remaining part of the strain rate $(\dot{\mathbf{F}}_e \mathbf{F}_e^{-1})_s$, appearing in eqn (39), i.e.

$$\Delta = -\mathscr{L}_e^{-1} : (\tau\omega - \omega\tau). \tag{47}$$

If eqn (38) is used in place of eqn (37), it is easily shown that the corresponding damage strain rate is defined by

$$\mathbf{D}_d = -\mathscr{L}_e^{-1} : \left(\frac{\partial \tau}{\partial \mathscr{D}} : \dot{\mathscr{D}} \right), \tag{48}$$

while expression (47) is replaced by

$$\Delta = -\mathscr{L}_e^{-1} : [\mathscr{A} : (\dot{\mathbf{F}}_p \mathbf{F}_p^{-1}) + \tau\omega - \omega\tau]. \tag{49}$$

It is clear that the right-hand side of eqn (48) is independent of the superposed rotation to the intermediate configuration, hence for the prescribed $\dot{\mathscr{D}}$ and the known current state of the material, eqn (48) uniquely specifies the damage strain rate $\mathbf{D}_d$. Since $\mathbf{D}_e$ is also uniquely specified, the nonuniqueness of the strain rate $(\dot{\mathbf{F}}_e \mathbf{F}_e^{-1})_s$, associated with a possible superposed rigid-body rotation of the intermediate unstressed configuration, is all contained in the nonuniqueness of the Δ part of this strain rate, given by eqn (49). However, in the subsequent analysis, the Δ part of the strain rate is of no direct interest and its nonuniqueness does not present any problem.

6. PARTITION OF THE STRAIN RATE INTO ITS ELASTIC, DAMAGE AND PLASTIC PARTS

Substituting expression (39) for the strain rate $(\dot{\mathbf{F}}_e \mathbf{F}_e^{-1})_s$ into expression (18) for the total strain rate, it now follows that

$$\mathbf{D} = \mathbf{D}_e + \mathbf{D}_d + \Delta + [\mathbf{F}_e(\dot{\mathbf{F}}_p \mathbf{F}_p^{-1})\mathbf{F}_e^{-1}]_s. \tag{50}$$

Consequently, by defining the plastic strain rate $\mathbf{D}_p$ as

$$\mathbf{D}_p = [\mathbf{F}_e(\dot{\mathbf{F}}_p \mathbf{F}_p^{-1})\mathbf{F}_e^{-1}]_s + \Delta, \tag{51}$$

expression (50) gives the additive decomposition of the total strain rate into its elastic, damage and plastic constituents, i.e.

$$\mathbf{D} = \mathbf{D}_e + \mathbf{D}_d + \mathbf{D}_p. \tag{52}$$

For example, if the material behavior is such that the Ilyushin postulate can be adopted (Ilyushin, 1961), i.e. the nett work done during arbitrary closed strain cycle is positive, provided that inelastic deformation occurred during the cycle, it follows that $\mathbf{D}_p + \mathbf{D}_d = \mathbf{D} - \mathbf{D}_e$ part of the total strain rate is normal to the yield surface in stress space [see eqn (11) of Ilyushin (1961) and the discussion following eqn (16) of Hill (1968)]. If elastic properties are assumed to be uninfluenced by inelastic deformation, the damage strain rate is zero and $\mathbf{D}_p = \mathbf{D} - \mathbf{D}_e$ part of the strain rate is normal to the yield surface.

7. ELASTOPLASTICITY WITHOUT DAMAGE

As a special case of the general formulation presented in the previous sections, consider the elastoplastic deformation of an elastically anisotropic material without a damage. For the sake of simplicity, restrict attention to transversely isotropic material. A similar analysis can be performed in the case of elastic orthotropy or more general anisotropy. Let $\mathbf{n}_0$ be the unit vector parallel to the axis of isotropy in the initial undeformed configuration $\mathscr{B}_0$. In the current elastoplastically deformed configuration $\mathscr{B}_t$ the material is assumed to remain transversely isotropic, with the axis of isotropy parallel to the unit direction $\mathbf{n}$. The corresponding structural tensor is (Boehler, 1987)

$$\mathscr{D} = \mathbf{n} \otimes \mathbf{n}. \tag{53}$$

Due to discontinuous slip and other micromechanisms of plastic deformation, the direction of the isotropy axis is not, in general, convected by the total deformation gradient, i.e. $\mathbf{n} \neq |\mathbf{F}|^{-1}\mathbf{F}\mathbf{n}_0$. It will be convenient in this section to specify the intermediate unstressed configuration $\mathscr{P}_t$ to be isoclinic, so that the direction of the isotropy axis in $\mathscr{P}_t$ is parallel to its direction $\mathbf{n}_0$ in the initial undeformed configuration $\mathscr{B}_0$. Note that the so defined isoclinic configuration is unique to within an arbitrary rigid-body rotation about the axis of isotropy $\mathbf{n}_0$. Since the elastic material response from $\mathscr{P}_t$ to $\mathscr{B}_t$ is not influenced by the rotation about the isotropy axis, this rotation is of no further importance. If $\mathbf{F}_e$ is the deformation gradient from any of the introduced isoclinic configurations to the current configuration, it follows that

$$\mathbf{n} = |\mathbf{F}_e|^{-1}\mathbf{F}_e\mathbf{n}_0. \tag{54}$$

Equation (54) holds because the axis of isotropy can be considered to be embedded in the material during the elastic deformation $\mathbf{F}_e$. The induced structural tensor in the intermediate configuration is, therefore, obtained by the contravariant-type transformation

$$\hat{\mathscr{D}} = |\mathbf{F}_e|^2 \mathbf{F}_e^{-1} \mathscr{D} \mathbf{F}_e^{-T} = \mathbf{n}_0 \otimes \mathbf{n}_0. \tag{55}$$

Since $\hat{\mathscr{D}}$ is a constant tensor, from eqn (26) it follows that $\overset{\circ e}{\mathscr{D}} = \mathbf{0}$, and eqn (46) gives that the damage strain rate is also equal to zero, $\mathbf{D}_d = \mathbf{0}$. This was naturally expected to be the case, because it is assumed that the material remains transversely isotropic, with the unchanged elastic properties.

Consequently, expression (39) reduces to

$$(\dot{\mathbf{F}}_e\mathbf{F}_e^{-1})_s = \mathbf{D}_e + \boldsymbol{\Delta}. \tag{56}$$

Equation (56), together with expression (47) for the $\boldsymbol{\Delta}$ part of the strain rate, provides the explicit relationship between the elastic strain rate $\mathbf{D}_e$ and the constituents $\mathbf{F}_e$ and $\mathbf{F}_p$, and their rates, of the multiplicative decomposition of the deformation gradient $\mathbf{F} = \mathbf{F}_e\mathbf{F}_p$,

$$\mathbf{D}_e = (\dot{\mathbf{F}}_e\mathbf{F}_e^{-1})_s + \mathscr{L}_e^{-1} : (\tau\omega - \omega\tau). \tag{57}$$

The remaining part of the total strain rate is the plastic part

$$\mathbf{D}_p = [\mathbf{F}_e(\dot{\mathbf{F}}_p\mathbf{F}_p^{-1})\mathbf{F}_e^{-1}]_s - \mathscr{L}_e^{-1} : (\tau\omega - \omega\tau). \tag{58}$$

For example, if the material behavior is such that the Ilyushin postulate applies, the plastic strain rate $\mathbf{D}_p$ given by eqn (58) is governed by plastic potential and is normal to the corresponding yield surface in stress space. This follows by applying the Ilyushin postulate to certain finite or infinitesimal strain cycles, as shown by Hill (1968) and Hill and Rice (1973). The interpretation of the expressions analogous to eqns (57) and (58) that arise in the crystal plasticity studies has been given by Hill and Rice (1972), Hill and Havner (1982) and Asaro (1983).

The instantaneous elastic moduli tensor $\mathscr{L}_e$ defined by eqn (25), depends on the elastic deformation gradient $\mathbf{F}_e$, which is here defined relatively to isoclinic intermediate configuration. To determine $\mathbf{F}_e$, we proceed as follows. By the polar decomposition theorem, the elastic deformation gradient $\mathbf{F}_e$ can be expressed as $\mathbf{F}_e = \mathbf{V}_e\mathbf{R}_e$, where $\mathbf{V}_e$ is the elastic stretch and $\mathbf{R}_e$ is the elastic rotation tensor. Since the elastic strain energy ψ_e is an isotropic function of both $\mathbf{C}_e$ and $\hat{\mathscr{D}}$, it follows that

$$\psi_e(\mathbf{C}_e, \hat{\mathscr{D}}) = \psi_e(\mathbf{B}_e, \tilde{\mathscr{D}}). \tag{59}$$

In eqn (59), $\mathbf{B}_e = \mathbf{V}_e^2$ is the left Cauchy–Green elastic deformation tensor, while the rotation induced structural tensor $\tilde{\mathscr{D}}$ is defined by

$$\tilde{\mathscr{D}} = \mathbf{R}_e\hat{\mathscr{D}}\mathbf{R}_e^T = \tilde{\mathbf{n}} \otimes \tilde{\mathbf{n}}, \tag{60}$$

where

$$\tilde{\mathbf{n}} = \mathbf{R}_e\mathbf{n}_0. \tag{61}$$

The stress response (11) can consequently be written as

$$\tau = 2\mathbf{V}_e\frac{\partial\psi(\mathbf{B}_e, \tilde{\mathscr{D}})}{\partial\mathbf{B}_e}\mathbf{V}_e. \tag{62}$$

If the current state and the rotation $\mathbf{R}_e$ are known, eqn (62) gives a one-to-one relationship between the stress tensor τ and the elastic stretch tensor $\mathbf{V}_e = \mathbf{B}_e^{1/2}$. To obtain the elastic rotation $\mathbf{R}_e$, however, additional consideration is needed. For example, if on a certain physical basis an evolution equation for the spin $\boldsymbol{\Omega} = \dot{\mathbf{R}}_e\mathbf{R}_e^{-1}$ is constructed, the rotation $\mathbf{R}_e$ is obtained by the integration of

$$\dot{\mathbf{R}}_e = \boldsymbol{\Omega}\mathbf{R}_e. \tag{63}$$

Note that from eqn (61) the rate of change of the unit vector $\tilde{\mathbf{n}}$ is $\dot{\tilde{\mathbf{n}}} = \boldsymbol{\Omega}\tilde{\mathbf{n}}$. When the rotation $\mathbf{R}_e$ is determined, the elastic deformation tensor is calculated from $\mathbf{F}_e = \mathbf{V}_e\mathbf{R}_e$, where $\mathbf{V}_e$ is calculated from eqn (62). The direction of the axis of isotrophy $\mathbf{n}$ in the current configuration is then found from eqn (54).

8. CONCLUDING REMARKS

We have formulated in this paper the constitutive framework for the analysis of finite elastoplastic deformation in the presence of progressive degradation of the elastic material properties and corresponding damage. This has been accomplished by extending the model of the multiplicative decomposition of deformation gradient, which has previously been

applied almost exclusively to the analysis of elastoplastic deformation of elastically isotropic materials, which remain isotropic during the plastic deformation processes. The exact kinematic and kinetic analysis of the finite deformation leads to the partition of the total strain rate into its elastic, damage and plastic parts. A general structure of the expression for the damage strain rate is derived, valid for introduced symmetric damage tensors of any order. The analysis of elastoplastic deformation of elastically anisotropic materials without damage is also presented, with application to transversely isotropic materials.

The presented work requires several extensions in order to complete the constitutive description of materials that undergo damage–elastoplastic deformation. The most immediate one is a development of the constitutive structure for the evolution equations for the appropriately specified damage variables. The coupling between plasticity and damage, elaboration on the structure of the yield and damage surfaces, existence of inelastic potentials and normality properties, are some of the associated questions also requiring further research. The valuable insight is already available from some of the previous related work, both in metal plasticity and rock and concrete inelasticity, such as Rice (1971), Rudnicki and Rice (1975), Nemat-Nasser (1983), Ortiz (1985), Ashby and Sammis (1990), Voyiadjis and Kattan (1992), Lubarda and Krajcinovic (1994b), etc.

Acknowledgments—The author is grateful for the support provided by the research contract with the Waterways Experiment Station, U.S. Army Corps of Engineers, and the research grant from the U.S. Army Research Office, Engineering Science Division, Structural Mechanics Branch to Arizona State University, which made this work possible.

REFERENCES

Agah-Tehrani, A., Lee, E. H., Mallett, R. L. and Onat, E. T. (1987). The theory of elastic–plastic deformation at finite strain with induced anisotropy modeled as combined isotropic-kinematic hardening. *J. Mech. Phys. Solids* **35**, 519–539.

Asaro, R. J. (1983). Micromechanics of crystals and polycrystals. In *Advances in Applied Mechanics* (Edited by J. W. Hutchinson and T. Y. Wu), Vol. 23, pp. 1–115. Academic Press, New York.

Ashby, M. F. and Sammis, C. G. (1990). The damage mechanics of brittle solids in compression. *Pure Appl. Geophysics* **133**, 489–521.

Betten, J. (1982). Integrity basis for a second-order and a fourth-order tensor. *Int. J. Math. Math. Sci.* **5**, 87–96.

Betten, J. (1987). Invariants of fourth-order tensors. In *Applications of Tensor Functions in Solid Mechanics* (Edited by J. P. Boehler), No. 292, pp. 203–226. Springer-Verlag, Wien.

Betten, J. (1992). Irreduzible invarianten eines tensors vierter stufe. *Z. Angew. Math. Mech.* **72**, 45–57.

Boehler, J. P. (1977). On irreducible representations for isotropic scalar functions. *Z. Angew. Math. Mech.* **57**, 323–327.

Boehler, J. P. (1987). Representation for isotropic and anisotropic nonpolynomial tensor functions. In *Applications of Tensor Functions in Solid Mechanics* (Edited by J. P. Boehler), No. 292, pp. 31–53. Springer-Verlag, Wien.

Dougill, Y. W. (1983). Path dependence and a general theory for the progressively fracturing solid. *Proc. R. Soc. London* **390A**, 341–351.

Dafalias, Y. F. (1985). The plastic spin. *J. Appl. Mech.* **52**, 865–871.

Hill, R. (1968). On constitutive inequalities for simple materials—II. *J. Mech. Phys. Solids* **16**, 315–322.

Hill, R. and Havner, K. S. (1982). Perspectives in the mechanics of elastoplastic crystals. *J. Mech. Phys. Solids* **30**, 5–22.

Hill, R. and Rice, J. R. (1972). Constitutive analysis of elastic–plastic crystals at arbitrary strain. *J. Mech. Phys. Solids* **20**, 401–413.

Hill, R. and Rice, J. R. (1973). Elastic potentials and the structure of inelastic constitutive laws. *SIAM J. Appl. Math.* **25**, 448–461.

Ilyushin, A. A. (1961). On the postulate of plasticity. *Prikl. Mat. Mekh.* **25**, 503–507.

Lee, E. H. (1969). Elastic–plastic deformation at finite strains. *J. Appl. Mech.* **36**, 1–6.

Lubarda, V. A. (1991a). Constitutive analysis of large elasto-plastic deformation based on the multiplicative decomposition of deformation gradient. *Int. J. Solids Structures* **27**, 885–895.

Lubarda, V. A. (1991b). Some aspects of elasto-plastic constitutive analysis of elastically anisotropic materials. *Int. J. Plasticity* **7**, 625–636.

Lubarda, V. A. (1994). Elastoplastic constitutive analysis with the yield surface in strain space. *J. Mech. Phys. Solids* **42**, 931–952.

Lubarda, V. A. and Krajcinovic, D. (1993). Damage tensors and the crack density distribution. *Int. J. Solids Structures* **30**, 2859–2877.

Lubarda, V. A. and Krajcinovic, D. (1994a). Tensorial representation of the effective elastic properties of the damaged material. *Int. J. Damage Mech.* **3**, 38–56.

Lubarda, V. A. and Krajcinovic, D. (1994b). Constitutive structure of the rate theory of damage in brittle elastic solids. *Appl. Math. Comp.* In press.

Lubarda, V. A. and Lee, E. H. (1981). A correct definition of elastic and plastic deformation and its computational significance. *J. Appl. Mech* **48**, 35–40.

Lubarda, V. A. and Shih, C. F. (1994). Plastic spin and related issues in phenomenological plasticity. *J. Appl. Mech.* In press.
Mandel, J. (1971). Plasticité classique et viscoplasticité. *Courses and Lectures No. 97, International Center for Mechanical Sciences*. Springer-Verlag, Udine.
Mandel, J. (1973). Equations constitutives et directeurs dans les milieux plastiques et viscoplastiques. *Int. J. Solids Structures* **9**, 725–740.
Nemat-Nasser, S. (1982). On finite deformation elasto-plasticity. *Int. J. Solids Structures* **18**, 857–872.
Nemat-Nasser, S. (1983). On finite plastic flow of crystalline solids and geomaterials. *J. Appl. Mech.* **50**, 1114–1126.
Ortiz, M. (1985). A constitutive theory for the inelastic behavior of concrete. *Mech. Mater.* **4**, 67–93.
Rice, J. R. (1971). Inelastic constitutive relations for solids: an internal variable theory and its application to metal plasticity. *J. Mech. Phys. Solids* **19**, 433–455.
Rudnicki, J. W. and Rice, J. R. (1975). Conditions for localization of deformation in pressure-sensitive dilatant materials. *J. Mech. Phys. Solids* **23**, 371–394.
Spencer, A. J. M. (1971). Theory of invariants. In *Continuum Physics* (Edited by A. C. Eringen), Vol. I, pp. 239–353. Academic Press, New York.
Spencer, A. J. M. (1987). Isotropic polynomial invariants and tensor functions. In *Applications of Tensor Functions in Solid Mechanics* (Edited by J. P. Boehler), No. 292, pp. 141–169. Springer-Verlag, Wien.
Truesdell, C. and Noll, W. (1965). The nonlinear field theories of mechanics. In *Handbuck der Physik*, Band III/3. Springer-Verlag, Wien.
Voyiadjis, G. Z. and Kattan, P. I. (1992). A plasticity-damage theory for large deformation of solids—I. Theoretical formulation. *Int. J. Engng Sci.* **30**, 1089–1108.

APPENDIX

The expressions for the rates of damage tensors given in Section 4, and for the damage strain rate given in Section 5, were derived by considering the damage tensors $\mathcal{D}$ to be the second-order symmetric tensors. We here show that the same derivation applies when the fourth- or higher-order damage tensors are introduced to adequately describe material degradation during a deformation process. Indeed, the fourth-order induced damage tensor $\hat{\mathcal{D}}$ in the intermediate configuration $\mathscr{P}_r$, corresponding to the fourth-order damage tensor $\mathcal{D}$ in the current configuration $\mathscr{B}_t$, has the covariant-type components

$$\hat{\mathcal{D}}_{ijkl} = |\mathbf{F}_e|^{-m}(F^e_{i\alpha})^{\mathrm{T}}(F^e_{j\beta})^{\mathrm{T}}\mathcal{D}_{\alpha\beta\gamma\delta}F^e_{\gamma k}F^e_{\delta l}. \tag{A1}$$

The material time derivative of eqn (A1) is

$$\dot{\hat{\mathcal{D}}}_{ijkl} = |\mathbf{F}_e|^{-m}(F^e_{i\alpha})^{\mathrm{T}}(F^e_{j\beta})^{\mathrm{T}}\overset{\circ}{\mathcal{D}}{}^{\mathbf{e}}_{\alpha\beta\gamma\delta}F^e_{\gamma k}F^e_{\delta l}, \tag{A2}$$

where $\overset{\circ}{\mathcal{D}}{}^{\mathbf{e}}$ represents a convected derivative of $\mathcal{D}$ relative to the velocity gradient $\dot{\mathbf{F}}_e\mathbf{F}_e^{-1}$. Substituting eqn (A2) into the second term on the right-hand side of the expression (23) therefore gives

$$\frac{\partial\hat{\boldsymbol{\tau}}}{\partial\hat{\mathcal{D}}}:\dot{\hat{\mathcal{D}}} = \frac{\partial\hat{\boldsymbol{\tau}}}{\partial\mathcal{D}}:\overset{\circ}{\mathcal{D}}{}^{\mathbf{e}}, \tag{A3}$$

which is the same structure as that of the previously derived expression (30), valid for the second-order damage tensors.

To derive an expression analogous to eqn (35), eliminate $\dot{\mathbf{F}}_e\mathbf{F}_e^{-1}$ from eqn (18) in terms of the total velocity gradient $\mathbf{L} = \dot{\mathbf{F}}\mathbf{F}^{-1}$, to obtain

$$\begin{aligned}\dot{\hat{\mathcal{D}}}_{ijkl} = |\mathbf{F}_e|^{-m}(F^e_{i\alpha})^{\mathrm{T}}(F^e_{j\beta})^{\mathrm{T}}\dot{\mathcal{D}}_{\alpha\beta\gamma\delta}F^e_{\gamma k}F^e_{\delta l} + m\hat{\mathcal{D}}_{ijkl}\,\mathrm{tr}(\dot{\mathbf{F}}_p\mathbf{F}_p^{-1})\\ -\hat{\mathcal{D}}_{ijku}(\dot{\mathbf{F}}_p\mathbf{F}_p^{-1})_{ul} - \hat{\mathcal{D}}_{iukl}(\dot{\mathbf{F}}_p\mathbf{F}_p^{-1})_{uk} - (\dot{\mathbf{F}}_p\mathbf{F}_p^{-1})^{\mathrm{T}}_{ur}\hat{\mathcal{D}}_{ujkl} - (\dot{\mathbf{F}}_p\mathbf{F}_p^{-1})^{\mathrm{T}}_{ur}\hat{\mathcal{D}}_{uikl}.\end{aligned} \tag{A4}$$

In eqn (A4), $\dot{\mathcal{D}}$ denotes a convected derivative of the fourth-order tensor $\mathcal{D}$, relative to the velocity gradient $\mathbf{L}$, i.e. the derivative observed in the reference frame that deforms with the material in the current configuration $\mathscr{B}_t$. The components of this tensor are

$$\dot{\mathcal{D}}_{\alpha\beta\gamma\delta} = \dot{\mathcal{D}}_{\alpha\beta\gamma\delta} + \mathcal{D}_{\alpha\beta\gamma u}L_{u\delta} + \mathcal{D}_{\alpha\beta u\delta}L_{u\gamma} + L^{\mathrm{T}}_{\beta u}\mathcal{D}_{\alpha u\gamma\delta} + L^{\mathrm{T}}_{\alpha u}\mathcal{D}_{u\beta\gamma\delta} - m\mathcal{D}_{\alpha\beta\gamma\delta}L_{uu}. \tag{A5}$$

Substitution of eqn (A4) into the second term on the right-hand side of the expression (23) then gives

$$\frac{\partial \tau}{\partial \mathcal{D}} : \dot{\mathcal{D}} = \frac{\partial \tau}{\partial \mathcal{D}} : \dot{\mathcal{D}} + \mathcal{A} : (\dot{\mathbf{F}}_p \mathbf{F}_p^{-1}), \tag{A6}$$

with the fourth-order tensor $\mathcal{A}$ defined by an expression similar to eqn (36b), corresponding to the second-order damage tensors. The expression (A6) coincides with the previously derived expression (35). An analogous derivation with the contravariant-type transformation leads to the same conclusion. Consequently, the derivation presented in Section 5 and the structure of the damage strain rate expressions (46) and (48) remain valid if the damage tensors are of the fourth order. The same is true for higher-order tensors, as well.

Int. Conference on Computational Engineering Science, ICES-95

Damage Evolution and Failure Modes

D. Krajcinovic and S. Mastilovic

Arizona State University, Tempe, Arizona, USA

1. INTRODUCTION

A polycrystalline solid is said to deform in a ductile (or plastic) mode if "the material flows through the crystal via dislocation motion, ..., whereas the lattice itself, with the material embedded on it, undergoes elastic deformation and rotation" [1]. It is important to observe that the lattice, its connectivity (density of atomic bonds) and, therefore, the effective elastic parameters do not change during a plastic deformation. Consequently, the residual strain is the only history recording parameter. The inelastic deformation attributed to the damage may be, in a complementary manner, manifested on the macro scale by the change of elastic (effective) parameters or the strain caused by the change of the lattice connectivity. Local discontinuities of the displacement field caused by the rupture of atomic bonds (damage) will, in a perfectly brittle solid, disappear upon unloading to the state of zero stress. Consequently, the damage will not cause residual strains. Thus, the change of the elastic moduli (density of atomic bonds) can be used to represent the thermodynamic flux and will provide a rational measure of the rate of damage accumulation.

The described definition of damage and its effect on the macro response implies averaging in a mean field sense. Underlying assumption of statistical homogeneity is seldom if ever investigated let alone questioned. The objective of this short study is a brief discussion of some limitations of current damage models and associated pitfalls.

2. ESSENTIAL STRUCTURE OF DAMAGE MODELS

The microstructure of a typical engineering material is in a majority of cases disordered. The range of the disorder may vary and the type may be of chemical, geometrical or topological origin. As the damage in form of microcracks accumulates the disorder level progressively increases. Currently available analytical models are almost exclusively of continuum, deterministic and local type. Implicit to this models is: (a) that the statistics of the microstructure is such that the process is on the macro scale reproducible without a large scatter and (b) that the selected state and internal variables and effective parameters are physically identifiable and measurable in tests.

Assuming that the concentration of microcracks and active slip planes is dilute the expression for the macro strain admits, in the infinitesimal strain approximation, the additive form

$$\varepsilon = \mathbf{S}(H):\sigma + \varepsilon^{p} \tag{1}$$

where $\mathbf{S}$ is the effective elastic compliance tensor and ε^{p} the plastic strain. Symbol H is used to denote the set of parameters needed to define the recorded history in thermodynamic sense. Assuming continuity of all tensors in (1) the rate of strain is

$$\dot{\varepsilon} = \mathbf{S}(H):\dot{\sigma} + \dot{\mathbf{S}}(H):\sigma + \dot{\varepsilon}^{p} \tag{2}$$

Three terms on the right hand side of (2) represent the rate of the elastic strain (in a damaged material as defined by the already changed compliance), the rate of strain attributable to the damage increment and the plastic strain rate, respectively.

The effective (overall) compliance of a solid weakened by an ensemble of distributed microcracks and other micro defects can be written in the form of a sum [2]

$$\mathbf{S}(H) = \mathbf{S}_o + \mathbf{S}^*(H) \tag{3}$$

of the compliance of the pristine (undamaged) solid and the compliance associated with the local fluctuations and discontinuities of the displacement fields caused by active micro defects (representing two terms on the right hand side of (3), respectively). The expression for the compliance attributed to the accumulated damage (in form of penny shaped planar microcracks of radius a) can be determined using micromechanical models in form of an integral

$$\mathbf{S}^*(H) = \frac{1}{4\pi}\int_{a^-}^{a^+} p(a)a^3 \int_{\Omega} \mathbf{S}^{(\alpha)}(\mathbf{n},\mathbf{m};\mathbf{S})\rho(\mathbf{n},\mathbf{m})\,da\,d\Omega \tag{4}$$

where $\mathbf{S}^{(\alpha)}(\mathbf{n},\mathbf{m};\mathbf{S})$ is the compliance for a system of microcracks bedded in parallel planes (used here as a Green's function) with normal $\mathbf{n}$ and $\rho(\mathbf{n},\mathbf{m})$ the distribution of the microcrack density with respect to the orientation of their bedding planes. Also, $\mathbf{m}$ defines the normal of an arbitrary plane, Ω the solid angle, $p(a)$ the distribution of microcrack radius sizes and (a^-,a^+) the range within which they change [3].

Analytical quadrature of the integral in (4) is possible only for circular or elliptical planar cracks and in a dilute limit of microcrack density, i.e. when the microcrack interaction is totally neglected. In this case components of the tensor $\mathbf{S}^{(\alpha)}$ depend on the known compliance of the pristine solid $\mathbf{S}_o$. In all other cases each component of $\mathbf{S}^{(\alpha)}$ depends on the unknown components of the overall (effective) compliance tensor $\mathbf{S}^*(H)$ rendering the relation (4) both explicit and implicit. In this case the expression (4) can be, at best, reduced to a system of algebraic equations which defies analytical solutions. Hence, the analytical solution for the overall compliance from (4) is not possible even in the case of the weak interaction, i.e. for the case when the mean field theory and the self consistent or differential models are applicable [4].

In the case when the quadrature (4) is possible the result can be expressed as [5]

$$\mathbf{S}^*(H) = \left\langle Na^3 \right\rangle \sum_{i=1}^{6} c_i \mathbf{I}_i \tag{5}$$

The average value of the product between the number N of microcracks per unit volume and the cube of the crack radius a (in angular bracket), known as the Budiansky, O'Connell parameter [4, 6], is universally accepted as a micromechanically justified measure of damage. Six tensors $\mathbf{I}_i$ represent the irreducible tensor basis of the class of all fourth order tensors which are invariant with respect to the permutations of first and second pair of indices [5]. Finally, six scalars c_i can be determined from the effective (overall) parameters of the solid [5].

Expressions (1) to (5) represent the basis for the micromechanically based constitutive model for materials which deform in a quasi-brittle or brittle-ductile mode. Distribution of the microcrack density $\rho(\mathbf{n},\mathbf{m})$ with respect to the orientation can sometimes be measured using methods of quantitative stereology and is typically

represented using the rosette histograms. Furthermore, these rosette histograms can be approximated by even order tensors [7]. It is interesting that for the determination of the effective compliance (4) a fourth order tensor representation of $\rho(\mathbf{n},\mathbf{m})$ provides an exact (micromechanical) solution [8] in the mean field domain.

3. LIMITATIONS OF THE MEAN FIELD MODELS

Leaving aside for the moment the fact that the distribution of microcracks is seldom known and measurable and that integral in (4) can be integrated analytically only when the microcrack density is dilute, it is essential to examine the conditions under which the mean field constitutive model is physically and geometrically acceptable. Two of these conditions are quite apparent. Firstly, the density of microcracks must be rather dilute since all models based on averaging neglect the direct interaction of the microcracks. Secondly, the relation (5) states that the effective (overall) compliance is invariant to the variations of the number of microcracks per unit volume and the cube of the radius length for which the value of the Budiansky, O'Connell parameter does not change. Finally, all variables and parameters in equations (1) to (5) are volume averages of respective microstructural counterparts. This means that a volume over which the homogenization is performed must exist and must be much smaller than the specimen itself. The last condition may be re-phrased as a requirement that the range over which the solid is statistically homogeneous must be small. Hence, the linear size of the representative volume element must also be small.

The conditions as stated above and in the literature are, to say the least, vague. In order to provide the quantitative measures and rigor to attributes such as dilute, micro, small and short and render the mentioned conditions precise it becomes necessary to introduce the characteristic lengths into considerations.

For example, an effective continuum or mean field model will be applicable, if and only if the following three conditions are met [3]

$$P(L_i > L_d) \to 0 \qquad \max(\xi, L_{c,\max}) << L_{rve} << L$$
$$\left|\frac{\partial \sigma}{\partial x}\right| L_{rve} << |\overline{\sigma}| \tag{6}$$

In (6) L_c, L_d, L_i and L_{rve} are the crack size, distance between cracks, crack interaction range and the linear size of the representative volume element (RVE), respectively. Symbol ξ denotes the correlation length over which the fluctuations of the stress fields created by cracks are correlated. This length, often used in physics of disordered media, is necessary for the proper definition of microcrack clusters and the shear (crack) band. Three conditions (6) require: (a) that the cumulative probability of direct interaction of adjacent microcracks is small, (b) that the largest microcrack or cluster of correlated microcracks is much smaller than the representative volume element which can in turn be comfortably fit into the specimen of size L and (c) that the largest difference of tractions applied at the boundary of the RVE is much smaller than the average traction itself. Third requirement, rarely mentioned and even less frequently considered, is a natural consequence of the fact that the considered models are based on the assumption that the spatial correlation have a negligible effect on the macro response. According to this assumption, which significantly simplifies the model, the exact position of a micro defect within RVE is inconsequential. This condition will place stringent limitations on the size of the RVE in the case of inhomogeneous states of stress and should, in all probability, disqualify the application of these models for the analyses of the process

zone enveloping an atomically sharp tip of a macro-crack. The resolution length ℓ of this model is equal to the linear size L_{rve} of the RVE.

Situation is much simpler in the case of the cell model which replaces a random distribution of defects by a periodic arrangement of equal density (or equal value of the Budiansky, O'Connell parameter). Application of this model requires that

$$L_c \leq L_{cell} << L \tag{7}$$

where the linear size of the cell L_{cell} is constant. The underlying presumptions are:(a) that the resolution length can be infinitely small if the analytical solutions are available or as small as desired if a numerical model is needed and (b) that the model provides a valuable estimate of the effect of the defect interaction on the macro response and macro failure since the defects belonging to adjacent cells may almost touch each other.

However, it is easy to demonstrate that the cell model comes short on these and other expectations. Consider, as an example, a two-dimensional system of parallel slits perpendicular to the direction of tensile tractions. These slits can be arranged into parallel columns by selecting cells of $A_{cell} = (L_x \cdot L_y)$ (where the x axis is parallel to the slit plane). If the length L_x is increased and the length L_y decreased, such that the cell area A_{cell} remains constant, the stress intensity factors will increase and so will the effective compliance. If the cells are compressed in the direction of force and extended in the other direction the effect will be opposite. Thus, the effect of the interaction can be changed at will rendering further analyses non-objective (mesh dependent). Furthermore, the cell model maximizes the smallest distance between the cracks by assuming that they are all equal. It also minimizes the maximum crack length by assuming that they are all equal. As such the cell model overestimates the strength of the damaged solid. Additionally, the self-similar growth of defects is an artifice which also represents a thermodynamically unstable path [9]. Finally, this model predicts simultaneous occurrence of infinitely many percolation thresholds which is also contrary to accepted criteria of a single percolation cluster [10]. It was shown that the cell model overestimates by a factor of two or more the critical density of damage required for the percolation transition. In summary, it seems that the cell model, despite its many computational advantages, is of limited value in the analyses of stress fluctuations in disordered microstructures and for the predictions of macro failure mode and threshold.

4. MACRO RESPONSE

During a brittle deformation process the damage evolves by nucleation of new microcracks, by growth of existing microcracks and/or by combination of two processes. The mode and rate of the damage evolution depends on: (a) state of stress, (b) strain rate, (c) temperature, (d) microstructural disorder and (e) chemical effects. For brevity only the state of the stress and the microstructural disorder will be pursued in this study.

The statement that the tensile stress promotes crack growth is too obvious to be belabored further. Deformation will be, in this case, dominated by the propagation of the critical (largest) defect. It is just as obvious that the crack nucleation is favored by a situation in which a heterogeneous solid is subjected to a long range compressive field. For example, in porous rocks, such as limestone, cracks are nucleated as a result of Hertzian stresses at a contact of two hard grains. However, in absence of long range tensile stresses these microcracks are arrested immediately after their nucleation. As a result these microcracks will be of similar sizes and will be distributed randomly throughout the specimen volume.

Energy barriers in a material with a disordered (heterogeneous) microstructure are in many cases able to arrest the growth of smaller cracks. As a result the damage tolerant materials (such as fiber reinforced resins) will accumulate damage before the macro fracture takes place. On the other side of the spectrum the brittle materials with a homogeneous microstructure will often fail as soon as the first pre-existing defect is destabilized.

Thus, the state of stress may trigger three different macro responses, which will be referred to as: (a) brittle, (b) quasi-brittle, and (c) "ductile". These macro-response are:

(a) A material with a homogeneous microstructure subjected to long range tensile stresses will deform in a linear elastic manner until it fails. Whatever little damage takes place is dominated by the propagation of pre-existing defect. As soon as the nonlinear deformation is initiated a brittle solid ceases to be homogeneous.

(b.1) A damage tolerant material subjected to tensile stresses may accumulate a significant density of microcracks before one of them grows to a size critical in the Griffith's sense. During this process of damage accumulation the specimen stiffness degrades as manifested by the curvature of the stress-strain curve. The material is statistically homogeneous almost until the onset of the failure since the microcracks are small in size during the nucleation dominated phase of the process. Only a very short part of the deformation process preceding the macro failure is dominated by the crack propagation.

(b.2) A weakly confined specimen, made of a material with an inferior cohesive strength, which is subjected to compressive stresses will also accumulate damage up to the point when the fluctuations associated with a cluster of interacting cracks cross over from small to large range. The remarks related to the stress-strain curve, homogeneity and damage accumulation in the cases (b.2) and (b.1) are quite similar.

(c) Damage evolution in a strongly confined specimen made of a material with an inferior tensile strength (such as rock) subjected to a state of stress close to the hydrostatic compression will be dominated by the microcrack nucleation. Nucleated microcracks are immediately arrested by the compressive stress field. Inelastic deformation is attributable to the crack nucleation, crushing, frictional sliding and re-packing (pore collapse). Dislocation slip is in a brittle material, such as polycrystalline ceramics, important primarily as the mechanism for crack nucleation. The accumulated damage may be very large. In comminution processes the microcrack density may exceed the value needed for the onset of the connectivity transition. A brittle material subjected to a hydrostatic compression may harden up to very large strains. Nevertheless, once the connectivity transition is reached the material is disconnected (crushed) becoming unable to carry any tensile or shear stress upon unloading.

5. FAILURE MODES

Failure in a perfectly brittle mode (a) is a statistical event which depends on the distribution of defect sizes. The probability of finding a large crack in a specimen depends not only on its microstructure but also on its size. Hence, the failure threshold is a variate which depends on the constitutive properties of the solid and the specimen size and shape. The failure criterion, in form of a non-deterministic limit curve formulated on the basis of a stability (Griffith's) criterion, must in this case be added to the constitutive description. This type of failure will be referred to as extrinsic or structural.

Failure in a quasi-brittle mode depends on the outcome of the competition of brittle (crack growth) and ductile (crack nucleation) processes. In the case characterized by the presence of tensile stresses (b.1) eventual failure will, in a displacement controlled case, almost always be triggered by the loss of stability of the crack which grew to a critical length. In this case the failure mode is again extrinsic. However, under the force (stress)

controlled conditions macro failure may happen at the peak of the stress-strain curve, i.e. when the effective tangential modulus is reduced to zero. In the (b.2) case the failure may occur by localization, i.e. when a band of closely spaced (but not intersecting) parallel interacting microcracks spans the specimen from one end to the other. In this case the failure mode is again intrinsic since the onset of the localization can be predicted on the basis of the acoustic tensor [11]. This type of failure, known as cooperative phenomena, is related to the order-disorder transition since the fluctuations associated with the shear band extend across the entire system at the onset of the localization. Failure in the ductile mode is obviously intrinsic as well. The material during comminution passes through the percolation (connectivity) transition. The onset of the elastic percolation can be determined from the condition that the effective secant (current) modulus is reduced to zero.

6. SUMMARY

In summary the variety of deformation modes and possible failures during a deformation process characterized by microcracking is much larger than originally estimated. The choice of the model depends on the deformation and failure mode. Homogeneity can almost never be taken from granted and the statistical aspect of the problem must always be considered. As any other continuum theory the damage mechanics can be applied only in the case when the damaged material is statistically homogeneous on a relatively small scale.

ACKNOWLEDGEMENT

The authors would like to express their gratitude for the financial support in form of the research grant from the U.S. Army Research Office, Engineering Science Division to the Arizona State University which made this work possible.

REFERENCES

[1] R.J. Asaro, Crystal Plasticity, J. Appl. Mechanics, Vol. 50 (1983), pp. 921-934.
[2] S. Nemat-Nasser and M. Hori, Micromechanics: Overall Properties of Heterogeneous Materials, North-Holland, Amsterdam (1993).
[3] D. Krajcinovic, Damage Mechanics, ASME Press, New York, NY (to appear).
[4] D. Krajcinovic, Damage Mechanics, Mech. of Mater., Vol. 8 (1989), pp. 117-198.
[5] V.A. Lubarda and D. Krajcinovic, Tensorial Representation of the Effective Elastic Properties of the Damaged Material, Int. J. Damage Mech., Vol. 3 (1994), pp. 38-56.
[6] B. Budiansky and R.J. O'Connell, Elastic Moduli of a Cracked Solid, Int. J. Solids Structures, Vol. 12 (1976), pp. 81-97.
[7] V.A. Lubarda and D. Krajcinovic, Damage Tensors and the Crack Density Distribution, Int. J. Solids Structures, Vol. 30 (1993), pp. 2859-2877.
[8] D. Krajcinovic and S. Mastilovic, Some Fundamental Issues of Damage Mechanics, submitted for publication.
[9] Z.P. Bazant and L. Cedolin, Stability of Structures, Elastic, Inelastic, Fracture and Damage Theories, Oxford Univ. Press, new York, NY.
[10] V.K.S. Shante and S. Kirkpatrick, An Introduction to Percolation Theory, Adv. Physics, Vol. 20 (1971), pp. 325-357.
[11] J.R. Rice, The Localization of Plastic Deformation, in: Proc. of 14th Int. Congress of Theor. and Appl. Mechanics, W.T. Koiter Ed., pp. 207-220, North-Holland, Amsterdam.

Submitted to
Probabilistic Engineering
Mechanics

RANDOM INELASTIC BEHAVIOR OF COMPOSITE MATERIALS WITH LOCAL LOAD SHARING

Marc P. Mignolet

Associate Professor
Department of Mechanical and Aerospace Engineering,
Arizona State University, Tempe, AZ 85287-6106.

Kaushik Mallick

All Plastic and Fiberglass, Inc.
Mobile, AL 36608.

ABSTRACT

The response of a very long composite layer being stretched beyond the elastic limit in a displacement controlled experiment is investigated. It is assumed that the load carried by a fiber is transferred, at failure, to its two neighbors. This local load sharing rule is shown to lead to the propagation of the fiber breaking process and to be the source of random spatial variations in the loads carried by the fibers. Then, a set of evolution equations is derived that governs the spatial distribution of the random loads in three types of unbroken fibers. The complexity associated with the determination of the solution to these equations has led to a Monte Carlo study that suggested an approximate solution technique. It is shown that this simpler, approximate formulation represents very well the initial set of equations. Finally, it is shown that the local load sharing rule leads to a much higher probability of broken fibers and to higher loads carried by the fibers than a global load sharing predicts. It is shown however that the mean value of these loads is well approximated by the global load sharing rule except for the location of the peak which is largely overpredicted by the global load sharing model.

Introduction

The accurate prediction of the behavior of composite materials is rendered difficult by the presence of dissimilar phases, i.e. the matrix and the fibers, by the complex behavior of their interfaces, as well as by the natural variability of the mechanical properties of the fibers. In particular, the mechanical behavior of the composite material beyond the elastic regime is dictated by the complex interplay of the failure characteristics of the fibers and the load transfer from the broken fibers to the remaining ones through the matrix. A number of studies have in the past been devoted to the modeling of this load transfer mechanism to predict the failure process of composite materials. Many of these investigations have relied on the parallel bar model in which the load imposed on an array of fibers is carried equally by all of them.[1] Although this

"democratic model" remains widely used, several alternative descriptions of the load transfer mechanism have been proposed, e.g. Ref. 2-10, some of which emphasize the local effects of the failure of a fiber.[2–7] In these studies, the force carried by a broken fiber is transmitted only to its neighbors, not to the entire array, through the assistance of the matrix.

An interesting feature of these local load sharing mechanisms is their capability to exhibit the propagation of a crack, i.e. the breaking of a fiber may, after load transfer, lead to the failure of one of its neighbors which in turn could break and so on. It should however be recognized that the local aspects of this failure mechanism render the mean-field analysis of the composite material beyond its initial elastic regime more challenging than if a global load sharing mechanism had been adopted since the state of a given fiber (broken or intact) and the force it carries not only depends on its strength and the externally applied load but also on the strength of the neighboring fibers.

The role of the present investigation is to provide a theoretical assessment of the effects of random variations in the strengths of the fibers in a composite material under a local load sharing rule. It is assumed that the fibers remain elastic until failure at which point the load they were carrying is transmitted, through the matrix, to the two adjacent fibers, if they still exist. The source of randomness in the system originates in the strengths of the fibers which are modeled as independent random variables uniformly distributed in a given interval. Particularizing further the problem, a single composite layer will be considered that is subjected to a displacement controlled experiment, the displacement, or stretch, being incremented in infinitesimal steps. Under these conditions, the present investigation will focus on the determination of the random properties of the composite from the first failure of a fiber until the complete failure of the layer. Emphasis is placed on the quantitative effects of the local load sharing mechanism on the global behavior of the composite rather than on the physical specificities of the load transfer mechanism. Thus, of particular interest in this investigation will be the probability of existence of various types of fibers and the probability density functions of the forces they carry. The results of both numerical simulations and theoretical predictions are analyzed in comparison with the global load sharing (democratic) model.

The Displacement Controlled Experiment

Consider a single, infinitely long, layer of a fiber reinforced composite material which is subjected, as shown in Fig. 1, to the action of discrete forces F_k. These loads which act directly on the fibers are selected to produce a displacement controlled experiment in which the fibers are all stretched by amounts dx, $2\,dx$, $3\,dx$,... It is desired to obtain the statistical distribution, mean value in particular, of the forces F_k that must be applied to produce a given stretch x of the fibers.

For simplicity, it is assumed that the fibers are all characterized by the same Young's modulus E, cross section area A, and underformed length L_0. Further, the strengths of the fibers, S_k, are modeled as independent random variables uniformly distributed in the interval $[\,S_{\min}\,,S_{\max}\,]$. When a given fiber, the m^{th} one say, breaks, the load it carries is set to zero, see Fig. 2, and the fiber-to-fiber interaction through the adjacent matrix leads to a transfer of a fraction ρ of the load carried by the failing fiber to each of its two neighbors.

Under these conditions, it is seen that the forces F_k are deterministic quantities for values of the stretch x that create forces $F_k < S_{\min}$. Specifically, it is found that

$$F_k = EA\left(\frac{x}{L_0}\right) \quad \text{for } x < \frac{L_0\,S_{\min}}{E\,A} \text{ and } k = 0, \pm 1, \pm 2, \cdots \tag{1}$$

When x exceeds the value $\dfrac{L_0\,S_{\min}}{E\,A}$, failure occurs in some fibers and the corresponding loads are transmitted to their neighbors. The randomness of the fiber strengths implies that the fiber breaking process, and consequently the loads F_k, are also random. The assumptions on the fiber strengths, independence and identical distribution, and on the unboundedness of the domain imply that F_k is in fact a spatially homogeneous stochastic process for $x \geq \dfrac{L_0\,S_{\min}}{E\,A}$.

It is desired to evaluate the distribution of the loads F_k carried by the fibers. To this end, introduce first the dimensionless forces and displacement, $\bar{F}_k$ and $\bar{x}$, according to

$$F_k = S_{\min} + (S_{\max} - S_{\min})\,\bar{F}_k \tag{2}$$

and

$$x = \frac{L_0}{E\,A}\left[\, S_{\min} + (S_{\max} - S_{\min})\,\bar{x}\,\right]. \tag{3a}$$

Similarly, the random strength S_k can be expressed as

$$S_k = S_{\min} + (S_{\max} - S_{\min})\,\bar{S}_k \tag{3b}$$

where $\bar{S}_k$ are independent random variables uniformly distributed in $[0, 1]$.

Clearly then, the layer behaves both elastically and deterministically for $\bar{x} < 0$, while the fiber breaking process creates, for $\bar{x} > 0$, both an inelastic response and a random distribution of forces $\bar{F}_k$. Note finally that all fibers are broken for $\bar{x} = 1$.

In evaluating the distribution of the loads $\bar{F}_k$, it should first be recognized that there exist broken fibers and three types of unbroken ones, as shown in Fig. 3. The terms regular, stopping, and singular will be used to denote fibers which are, respectively, surrounded by 2, 1, and 0 unbroken fibers. Since regular fibers have not been involved in the failure process of any of their unbroken neighbors, the load they carry is still governed by Eq. (1), even for $\bar{x} > 0$. Relying on Eq. (2) and (3), it is found that the normalized force $\bar{F}_k$ corresponding to a regular fiber is simply governed by $\bar{F}_k = \bar{x}$. Such a simple relationship does not exist for stopping and singular fibers because the load(s) that was (were) transferred from their broken neighbor(s) is (are) a function of the neighbors' random strength.

The various types of fibers and their properties can thus be summarized as follows:

Regular fibers: 2 unbroken neighbors

probability of existence: $p = p(\bar{x})$

force carried: deterministic, $\bar{F}_k = \bar{x}$

Stopping fibers: 1 unbroken neighbor

probability of existence: $q = q(\bar{x})$

force carried: random with distribution $Q(f, \bar{x})$, nonzero for $f \in [\bar{x}, 1]$

Singular fibers: 0 unbroken neighbor

probability of existence: $r = r(\bar{x})$

force carried: random with distribution $R(f, \bar{x})$, nonzero for $f \in [\bar{x}, 1]$

Broken fibers: probability of existence: $1 - p - q - r$

force carried: deterministic, $F_k = 0$, $\bar{F}_k = -\left[\frac{S_{min}}{S_{max} - S_{min}}\right]$

With these notations, it is found that the mean of the forces F_k and $\bar{F}_k$ are, respectively,

$$E[F_k] = S_{min} + (S_{max} - S_{min})\, E[\bar{F}_k] \tag{4}$$

and

$$E[\overline{F}_k] = p(\bar{x})\,\bar{x} + q(\bar{x}) \int_{\bar{x}}^{1} f\, Q(f, \bar{x})\, df + r(\bar{x}) \int_{\bar{x}}^{1} f\, R(f, \bar{x})\, df - \left[1 - p(\bar{x}) - q(\bar{x}) - r(\bar{x})\right]\left[\frac{S_{min}}{S_{max} - S_{min}}\right]. \tag{5}$$

The determination of the probabilities $p(\bar{x})$, $q(\bar{x})$, $r(\bar{x})$ and probability density functions $Q(f, \bar{x})$ and $R(f, \bar{x})$ will be approached as follows. First, the breaking of a fiber and its propagation in the layer will be analyzed. These results will then be used to derive a set of ordinary and partial differential equations that govern the evolution of the functions $p(\bar{x})$, $q(\bar{x})$, $r(\bar{x})$, $Q(f, \bar{x})$, and $R(f, \bar{x})$ as the variable $\bar{x}$ is increased from 0 to 1. A Monte Carlo analysis will then be performed to provide insight into the behavior of these functions. These numerical results will in turn be used to produce a reduced set of ordinary differential equations that describe approximately the evolution of $p(\bar{x})$, $q(\bar{x})$, and $r(\bar{x})$ as $\bar{x}$ is increased from 0 to 1. The accuracy of this approximation will be evaluated by comparison with the results of the Monte Carlo simulation data. Finally, the differences between the present local load sharing rule and a global one will be discussed.

Failure Mechanism and Propagation

Consider, as in Fig. 2 and 3, a composite layer which has already undergone inelastic deformation and assume that the corresponding functions $p(\bar{x})$, $q(\bar{x})$, $r(\bar{x})$, $Q(f,\bar{x})$, and $R(f,\bar{x})$ are known. Then, as a stretch increment $d\bar{x}$ is applied to the system, an instantaneous increase of the loads $\bar{F}_k$ is also produced. The initial force increment $d\bar{F}_k = d\bar{x}$ provokes the failure of fibers that were carrying forces equal to their respective strengths at the end of the previous stretch increase. These failures lead to a redistribution (increase) of the forces in the surrounding fibers which in turn can lead to new failures. The failure process continues until each fiber is subjected to a force that is less than its strength.

In this section, it is desired to determine the probability associated with the failure of a total $N = n$ of fibers, not counting the initial one, some of which may be regular, stopping and/or singular, that is initiated by an increase in stretch, from $\bar{x}$ to $\bar{x} + d\bar{x}$. To this end, it is first noted that the initiation of the fiber breaking process is associated with either a regular, a stopping, or a singular fiber.

Initiation at a Regular Fiber

Note first that the failure of a regular fiber leads to a breaking process that can extend both left and right of the initiating fiber the index of which will be denoted by m. The homogeneous character of the fiber strengths S_k implies that the left and right propagating failure processes are characterized by identical probabilities so that it is sufficient to consider only one of these mechanisms, the right propagating one say. For this process and with $n \geq 2$,

$$Pr\,[(N=n) \cap (\textit{fiber } m \textit{ is regular})] = Pr\,[(\textit{fiber } m \textit{ is regular}) \cap (\bar{F}_m + d\bar{F}_m \geq \bar{S}_m) \mid \bar{S}_m \geq \bar{x}]$$

$$\times \left\{ \prod_{i=1}^{n-1} Pr\,[(\textit{fiber } m+i \textit{ is regular}) \cap (\bar{F}'_{m+i} \geq \bar{S}_{m+i}) \mid \bar{S}_{m+i} \geq \bar{x}] \right\} Pr\,[\textit{failure stops}] \qquad (6)$$

where $\bar{F}'_{m+i}$ denotes the dimensionless force in the fiber $m+i$ <u>after</u> the failure of the fiber $m+i-1$. Thus,

$$F'_{m+i} = F_{m+i} + \rho\, F'_{m+i-1} \qquad (7a)$$

or

$$\bar{F}'_{m+i} = \bar{F}_{m+i} + \rho\,\bar{F}'_{m+i-1} + \rho\left(\frac{S_{\min}}{S_{\max} - S_{\min}}\right), i \geq 1 \tag{7b}$$

where

$$\bar{F}'_{m} = \bar{x} \tag{8}$$

and

$$\bar{F}_{m+i} = \bar{x} \quad i = 1, 2, \ldots, n-2 \tag{9}$$

since the fibers $m+1$, $m+2$,..., $m+n-1$ are all regular. The solution of the above recurrence relation, Eq. (7b) and (9), with the initial condition given by Eq. (8) is readily determined to be

$$\bar{F}'_{m+i} = \left[\frac{1-\rho^i}{1-\rho} + \rho^i\right]\bar{x} + \rho\,\frac{1-\rho^i}{1-\rho}\,\frac{S_{\min}}{S_{\max} - S_{\min}}. \tag{10}$$

Relying again on the regular character of the fibers $m+1$, $m+2$, ..., $m+n-1$, it is found that

$$Pr\left[(\textit{fiber } m+i \textit{ is regular}) \cap (\bar{F}'_{m+i} \geq \bar{S}_{m+i}) \mid \bar{S}_{m+i} \geq \bar{x}\right] = Pr\left[\textit{fiber } m+i \textit{ is regular}\right] \frac{Pr\left[\bar{x} \leq \bar{S}_{m+i} \leq \bar{F}'_{m+i}\right]}{Pr\left[\bar{S}_{m+i} \geq \bar{x}\right]}$$

$$= \frac{p}{p+q'}\,\frac{\bar{F}'_{m+i} - \bar{x}}{1-\bar{x}} = \frac{p}{p+q'}\,a_i\,\frac{\bar{x} + \bar{x}_0}{1-\bar{x}} \quad \text{for } \bar{F}'_{m+i} \leq 1 \tag{11a}$$

where

$$q' = \frac{q}{2} = Pr\left[\textit{fiber } m+i \textit{ is stopping} \mid \textit{fiber } m+i-1 \textit{ is regular}\right] \tag{11b}$$

$$a_i = \rho\,\frac{1-\rho^i}{1-\rho} \tag{11c}$$

and

$$\bar{x}_0 = \frac{S_{\min}}{S_{\max} - S_{\min}}. \tag{11d}$$

When $\bar{F}'_{m+i} \geq 1$, it is found that

$$Pr\left[(\textit{fiber } m+i \textit{ is regular}) \cap (\bar{F}'_{m+i} \geq \bar{S}_{m+i}) \mid \bar{S}_{m+i} \geq \bar{x}\right] = \frac{p}{p+q'} \quad \text{for } \bar{F}'_{m+i} \geq 1. \tag{11e}$$

Note that $Pr\left[\textit{fiber } m+i \textit{ is regular}\right] = \frac{p}{p+q'}$ since the regular character of the fiber $m+i-1$ restricts the

fiber $m+i$ to be either regular or stopping.

The probability $Pr\,[(\textit{fiber } m \textit{ is regular}) \cap (\bar{F}_m + d\bar{F}_m \geq \bar{S}_m) \mid \bar{S}_m \geq \bar{x}]$ is similarly computed as

$$Pr\,[(\textit{fiber } m \textit{ is regular}) \cap (\bar{F}_m + d\bar{F}_m \geq \bar{S}_m) \mid \bar{S}_m \geq \bar{x}] = p\,\frac{Pr\,[\bar{x} \leq \bar{S}_m \leq \bar{F}_m + d\bar{F}_m]}{Pr\,[\bar{S}_m \geq \bar{x}]} = p\,\frac{d\bar{x}}{1-\bar{x}}. \tag{12}$$

Consider now the last term in Eq. (6), $Pr\,[\textit{failure stops}]$, and note in particular that the fiber breaking process stops with n fibers breaking in addition to the initial one, if and only if

(1) the fibers $m+n$ and $m+n+1$ are both regular but the former one breaks while the latter successfully carries its load

(2) the fiber $m+n$ is regular and breaks while the following one is a stopping fiber which sustains the transmitted force

(3) the fiber $m+n$ is a stopping one and breaks

Accordingly,

$$\begin{aligned} Pr\,[\textit{failure stops}] &= Pr\,[(\textit{fiber } m+n \textit{ is regular}) \cap (\bar{F}'_{m+n} \geq \bar{S}_{m+n}) \mid \bar{S}_{m+n} \geq \bar{x}] \\ &\times Pr\,[(\textit{fiber } m+n+1 \textit{ is regular}) \cap (\bar{F}'_{m+n+1} \leq \bar{S}_{m+n+1}) \mid \bar{S}_{m+n+1} \geq \bar{x}] \\ &+ Pr\,[(\textit{fiber } m+n \textit{ is regular}) \cap (\bar{F}'_{m+n} \geq \bar{S}_{m+n}) \mid \bar{S}_{m+n} \geq \bar{x}] \\ &\times Pr\,[(\textit{fiber } m+n+1 \textit{ is stopping}) \cap (\bar{F}''_{m+n+1} \leq \bar{S}_{m+n+1}) \mid \bar{S}_{m+n+1} \geq \bar{F}_{m+n+1}] \\ &+ Pr\,[(\textit{fiber } m+n \textit{ is stopping}) \cap (\bar{F}''_{m+n} \geq \bar{S}_{m+n}) \mid \bar{S}_{m+n} \geq \bar{F}_{m+n}] = P_1 + P_2 + P_3 \end{aligned} \tag{13}$$

where $\bar{F}_{m+i}$ and $\bar{F}''_{m+i}$ designate, respectively, the dimensionless forces in the stopping fiber $m+i$ before and after the failure of the regular fiber $m+i-1$. Proceeding as in Eq. (7)-(10), it is found that

$$\bar{F}''_{m+i} = \bar{F}_{m+i} + \rho\,\bar{F}'_{m+i-1} + \rho\,\bar{x}_0 = \bar{F}_{m+i} + a_i\,(\bar{x} + \bar{x}_0). \tag{14}$$

The probabilities P_1, P_2, and P_3, Eq. (13), can readily be written as

$$P_1 = Pr\,[(\textit{fiber } m+n \textit{ is regular}) \cap (\bar{F}'_{m+n} \geq \bar{S}_{m+n}) \mid \bar{S}_{m+n} \geq \bar{x}]$$

$$\times\left\{\frac{p}{p+q'} - Pr\left[(\textit{fiber } m+n+1 \textit{ is regular}) \cap (\bar{F}'_{m+n+1} \geq \bar{S}_{m+n+1}) \mid \bar{S}_{m+n+1} \geq \bar{x}\right]\right\} \qquad (15a)$$

$$P_2 = Pr\left[(\textit{fiber } m+n \textit{ is regular}) \cap (\bar{F}'_{m+n} \geq \bar{S}_{m+n}) \mid \bar{S}_{m+n} \geq \bar{x}\right]$$

$$\times Pr\left[(\textit{fiber } m+n+1 \textit{ is stopping}) \cap (\bar{F}''_{m+n+1} \leq \bar{S}_{m+n+1}) \mid \bar{S}_{m+n+1} \geq \bar{F}_{m+n+1}\right] \qquad (15b)$$

and

$$P_3 = \frac{q}{p+q'} - Pr\left[(\textit{fiber } m+n \textit{ is stopping}) \cap (\bar{F}''_{m+n} \leq \bar{S}_{m+n}) \mid \bar{S}_{m+n} \geq \bar{F}_{m+n}\right] \qquad (15c)$$

where $Pr\left[(\textit{fiber } m+i \textit{ is regular}) \cap (\bar{F}'_{m+i} \geq \bar{S}_{m+i}) \mid \bar{S}_{m+i} \geq \bar{x}\right]$, $i = n-1, n$, can be evaluated by using Eq. (11) while, in view of Eq. (14),

$$\Theta_i = Pr\left[(\textit{fiber } m+i \textit{ is stopping}) \cap (\bar{F}''_{m+i} \leq \bar{S}_{m+i}) \mid \bar{S}_{m+i} \geq \bar{F}_{m+i}\right]$$

$$= \frac{q'}{p+q'} \frac{Pr\left[\bar{F}_{m+i} + a_i(\bar{x} + \bar{x}_0) \leq \bar{S}_{m+i}\right]}{Pr\left[\bar{S}_{m+i} \geq \bar{F}_{m+i}\right]}. \qquad (16)$$

The independence of the fiber strengths $\bar{S}_k$ implies that the random force $\bar{F}_{m+i}$ and strength $\bar{S}_{m+i}$ are also independent so that

$$Pr\left[\bar{F}_{m+i} + a_i(\bar{x} + \bar{x}_0) \leq \bar{S}_{m+i}\right] = \int_{\bar{x}}^{1-a_i(\bar{x}+\bar{x}_0)} \int_{f+a_i(\bar{x}+\bar{x}_0)}^{1} \frac{Q(f,\bar{x})}{1-\bar{x}}\, ds\, df$$

$$= \frac{1}{1-\bar{x}} \int_{\bar{x}}^{1-a_i(\bar{x}+\bar{x}_0)} \left[1 - a_i(\bar{x} + \bar{x}_0) - f\right] Q(f,\bar{x})\, df. \qquad (17)$$

One finds similarly

$$Pr\left[\bar{S}_{m+i} \geq \bar{F}_{m+i}\right] = \frac{1}{1-\bar{x}} \int_{\bar{x}}^{1} \left[1 - f\right] Q(f,\bar{x})\, df \qquad (18)$$

so that

$$\Theta_i = \frac{\int_{\bar{x}}^{1-a_i(\bar{x}+\bar{x}_0)} \left[1 - a_i\,(\bar{x}+\bar{x}_0) - f\right] Q(f,\bar{x})\,df}{\int_{\bar{x}}^{1} \left[1-f\right] Q(f,\bar{x})\,df}. \tag{19}$$

Note that this expression is valid only for $1-a_i\,(\bar{x}+\bar{x}_0) \geq \bar{x}$ or $(1+a_i)\,\bar{x} \leq 1-a_i\,\bar{x}_0$. In the contrary, $\Theta_i = 0$.

Combining Eq. (6), (11)-(13), and (15)-(16), and introducing the sequence of functions $\alpha_n(\bar{x}) = \alpha_n$ defined by the recurrence relation

$$\alpha_i = \left[\rho\,\frac{1-\rho^i}{1-\rho}\right]\alpha_{i-1} \quad \text{for } (1+a_i)\,\bar{x} \leq 1 - a_i\,\bar{x}_0 \tag{20a}$$

or

$$\alpha_i = \left[\frac{1-\bar{x}}{\bar{x}+\bar{x}_0}\right]\alpha_{i-1} \quad \text{for } (1+a_i)\,\bar{x} \geq 1 - a_i\,\bar{x}_0 \tag{20b}$$

for $i \geq 1$, and

$$\alpha_0 = 1, \quad \alpha_i = 0 \quad \text{for } i < 0 \tag{20c}$$

it is found that

$$Pr\,[N=n] = \frac{d\bar{x}}{(\bar{x}+\bar{x}_0)}\,\frac{1}{(p+q')^{n+1}}\left[\alpha_n\left[\frac{p\,(\bar{x}+\bar{x}_0)}{1-\bar{x}}\right]^{n+1}(p+q'\,\Theta_{n+1}) - \alpha_{n+1}\left[\frac{p\,(\bar{x}+\bar{x}_0)}{1-\bar{x}}\right]^{n+2}\right.$$

$$\left. + \alpha_{n-1}\left[\frac{p\,(\bar{x}+\bar{x}_0)}{1-\bar{x}}\right]^{n} q'\,(p+q')\,(1-\Theta_n)\right] \tag{21}$$

and

$$\Theta_i = \frac{\int_{\bar{x}}^{1-\gamma_i} (1-\gamma_i - f)\,Q(f,\bar{x})\,df}{\int_{\bar{x}}^{1} \left[1-f\right] Q(f,\bar{x})\,df} \tag{22}$$

with

$$\gamma_i = \frac{\alpha_i}{\alpha_{i-1}} (\bar{x} + \bar{x}_0). \tag{23}$$

The above relations, Eq. (21) in particular, would appear to be, as Eq. (6), only valid for $n \geq 2$. It can however be shown that they are also valid for $n = 0$ and $n = 1$ because of the definition of $\alpha_0(\bar{x})$ and $\alpha_1(\bar{x})$, Eq. (20c).

Initiation at a Stopping Fiber

The determination of the probability that a total of $N = n$ fibers, not counting the initial one, are broken when the fiber initiating the failure process is a stopping one, is computed in a totally analogous manner as in the previous section. Note however that Eq. (7) and (9) are still valid but the correct initial condition is

$$\bar{F}'_m = \bar{F}_m \tag{24}$$

where $\bar{F}_m$ is a random variable distributed in the interval $[\bar{x}, 1]$ according to the probability density function $Q(f, \bar{x})$. The force in the regular fiber $m+i$ immediately after the failure of the fiber $m+i-1$ is then

$$\bar{F}'_{m+i} = \rho^i \bar{F}_m + \frac{a_i}{\rho} (\bar{x} + \rho \bar{x}_0). \tag{25}$$

Proceeding as in the last section, it can be shown that

$$Pr[N = n] = \frac{d\bar{x}}{1-\bar{x}} \frac{q}{(p+q')^{n+1}} \left[p^n (p + q' \Phi_{n+1}) \left[\prod_{i=1}^{n} \Psi_i \right] - p^{n+1} \left[\prod_{i=1}^{n+1} \Psi_i \right] \right.$$

$$\left. + q' p^{n-1} (p+q') (1 - \Phi_n) \left[\prod_{i=1}^{n-1} \Psi_i \right] \right], n \geq 0, \tag{26}$$

where the following convention is applicable

$$\prod_{i=1}^{0} \Psi_i = 1 \quad \text{and} \quad \prod_{i=1}^{k} \Psi_i = 0 \quad \text{for } k < 0. \tag{27}$$

Further, the terms Ψ_i and Φ_i, $i \geq 1$, are defined as

$$\Psi_i = 1 - \int_{\bar{x}}^{\min(1,\delta_i)} \frac{1 - \frac{a_i}{\rho}(\bar{x} + \rho\,\bar{x}_0) - \rho^i f}{1 - \bar{x}}\, Q(f, \bar{x})\, df \tag{28}$$

where

$$\delta_i = \frac{\left[\rho - (\bar{x} + \rho\,\bar{x}_0)\frac{\alpha_i}{\alpha_{i-1}}\right]}{\left[\rho - (1-\rho)\frac{\alpha_i}{\alpha_{i-1}}\right]} \tag{29}$$

and

$$\Phi_0 = 1 \tag{30a}$$

$$\Phi_i = \frac{\int_{\bar{x}}^{\min(1,\delta_i)} \int_{\bar{x}}^{\varepsilon_i} \left[1 - f_i - \rho^i f_0 - a_{i-1}\,\bar{x} - a_i\,\bar{x}_0\right] Q(f_0, \bar{x})\, Q(f_i, \bar{x})\, df_i\, df_O}{\int_{\bar{x}}^{1} (1-f)\, Q(f, \bar{x})\, df} \tag{30b}$$

with

$$\varepsilon_i = 1 - \rho^i f_0 - a_{i-1}\,\bar{x} - a_i\,\bar{x}_0. \tag{31}$$

Initiation at a Singular Fiber

It remains to analyze the effect of the breaking of a singular fiber. Clearly, the failure process is limited to the initiating singular fiber. Thus,

$$Pr\,[N = 0] = \frac{r\,d\bar{x}}{\int_{\bar{x}}^{1} (1-f)\, R(f, \bar{x})\, df} \tag{32a}$$

and

$$Pr\,[N = n] = 0 \quad \text{for } n \geq 1. \tag{32b}$$

The Evolution Equations and their Numerical Solutions

Derivation

The results derived in the previous section permit the derivation of a set of ordinary and partial differential equations for the variables $p(\bar{x})$, $q(\bar{x})$, $r(\bar{x})$, $Q(f,\bar{x})$, and $R(f,\bar{x})$. Consider first the probability $p(\bar{x})$ and note that

$$p(\bar{x}+d\bar{x}) = p(\bar{x}) - Pr\,[\,\textit{initiation of failure at a regular fiber}\,]$$

$$\times\Big[\,1+2\ \textit{corresponding expected number of broken regular fibers}\,\Big]$$

$$-\,Pr\,[\,\textit{initiation of failure at a stopping fiber}\,]$$

$$\times\Big[\,\textit{corresponding expected number of broken regular fibers}\,\Big]. \tag{33}$$

Note that the expected number of broken regular fibers, which does not include the possible initial one, can be written as $\sum_{n=0}^{\infty} n\ Pr\,[N_{reg}=n]$, where the probability that n regular fibers break, $Pr\,[N_{reg}=n]$, can be determined from Eq. (21) and (26). Then, it can be shown that Eq. (33) reduces to the first order ordinary differential equation

$$\frac{dp}{d\bar{x}} = -\frac{p}{1-\bar{x}}\left[1+\frac{2p}{p+q'}\sum_{n=0}^{\infty}\left(\frac{p(\bar{x}+\bar{x}_0)}{(p+q')(1-\bar{x})}\right)^n \alpha_n\right]$$

$$-\frac{2\,p\,q'}{(p+q')\displaystyle\int_{\bar{x}}^{1}(1-f)\,Q(f,\bar{x})\,df}\sum_{n=0}^{\infty}\left(\frac{p}{p+q'}\right)^n\left(\prod_{i=1}^{n}\Psi_i\right) \tag{34}$$

Balance equations similar to Eq. (33) can be derived for the probabilities q and r and for the probability density functions $Q(f,\bar{x})$ and $R(f,\bar{x})$ which, after some lengthy but straightforward algebraic manipulations, can be shown to reduce to the following differential equations

$$\frac{dq}{d\bar{x}} = \frac{2p}{1-\bar{x}}\left[1 - \frac{2q'}{p+q'}\sum_{n=0}^{\infty}\left(\frac{p(\bar{x}+\bar{x}_0)}{(p+q')(1-\bar{x})}\right)^n \alpha_n\right]$$

$$- \frac{4q'^2}{(p+q')\int_{\bar{x}}^{1}(1-f)\,Q(f,\bar{x})\,df}\sum_{n=0}^{\infty}\left(\frac{p}{p+q'}\right)^n\left(\prod_{i=1}^{n}\Psi_i\right) \tag{35}$$

$$\frac{dr}{d\bar{x}} = \frac{2pq'}{(p+q')(1-\bar{x})}\sum_{n=0}^{\infty}\left(\frac{p(\bar{x}+\bar{x}_0)}{(p+q')(1-\bar{x})}\right)^n \alpha_n\,\Theta_{n+1}$$

$$+ \frac{2q'^2}{(p+q')\int_{\bar{x}}^{1}(1-f)\,Q(f,\bar{x})\,df}\sum_{n=0}^{\infty}\left(\frac{p}{p+q'}\right)^n\left(\prod_{i=1}^{n}\Psi_i\right)\Phi_{n+1} - \frac{r}{\int_{\bar{x}}^{1}(1-f)\,R(f,\bar{x})\,df} \tag{36}$$

$$\frac{\partial}{\partial\bar{x}}(qQ) = -q\frac{\partial Q}{\partial f} + F_1 \tag{37}$$

and

$$\frac{\partial}{\partial\bar{x}}(rR) = -r\frac{\partial R}{\partial f} + F_2. \tag{38}$$

The terms F_1 and F_2 can be expressed in the form

$$F_1 = \frac{2p}{\bar{x}+\bar{x}_0}\sum_{n=0}^{\infty}\left[\frac{p(\bar{x}+\bar{x}_0)}{(p+q')(1-\bar{x})}\right]^{n+1}\left(\alpha_n - \frac{\bar{x}+\bar{x}_0}{1-\bar{x}}\alpha_{n+1}\right)\delta\left(f - \bar{x}(1+\frac{\alpha_{n+1}}{\alpha_n}) - \frac{\alpha_{n+1}}{\alpha_n}\bar{x}_0\right)$$

$$-\frac{2q'Q(f,\bar{x})}{\bar{x}+\bar{x}_0}\sum_{n=0}^{\infty}\left(\frac{p(\bar{x}+\bar{x}_0)}{(p+q')(1-\bar{x})}\right)^{n+1}\alpha_n + 2q'\sum_{n=0}^{\infty}\left(\frac{p}{p+q'}\right)^{n+1}\frac{\left(\prod_{i=0}^{n}\Psi_i\right)(1-\Psi_{n+1})}{\int_{\bar{x}}^{1}(1-f)\,Q(f,\bar{x})\,df}\frac{1}{\rho^{n+1}}Q\left(\frac{f}{\rho^{n+1}} - \frac{a_{n+1}}{\rho^{n+2}}(\bar{x}+\rho\bar{x}_0),\bar{x}\right)$$

$$-\frac{2q'Q(f,\bar{x})}{\int_{\bar{x}}^{1}(1-f)\,Q(f,\bar{x})\,df} - \frac{2q'^2}{p+q'}\frac{Q(f,\bar{x})}{\int_{\bar{x}}^{1}(1-f)\,Q(f,\bar{x})\,df}\sum_{n=0}^{\infty}\left(\frac{p}{p+q'}\right)^n\left(\prod_{i=1}^{n}\Psi_i\right) \tag{39}$$

where $\delta(f)$ denotes the Dirac delta function and

$$F_2 = \frac{2\,q'}{\bar{x}+\bar{x}_0}\,\frac{1-f}{\int_{\bar{x}}^{1}(1-f)\,Q(f,\bar{x})\,df}\sum_{n=0}^{\infty}\alpha_n\left[\frac{p\,(\bar{x}+\bar{x}_0)}{(p+q')\,(1-\bar{x})}\right]^{n+1} Q\left(f-\frac{\alpha_{n+1}}{\alpha_n}\,(\bar{x}+\bar{x}_0),\bar{x}\right)$$

$$+\frac{2\,q'^2}{p+q'}\,\frac{1-f}{\left[\int_{\bar{x}}^{1}(1-f)\,Q(f,\bar{x})\,df\right]^2}\sum_{n=0}^{\infty}\left(\frac{p}{p+q'}\right)^n\left(\prod_{i=1}^{n}\Psi_i\right)F_3-\frac{r\,R(f,\bar{x})}{\int_{\bar{x}}^{1}(1-f)\,R(f,\bar{x})\,df} \tag{40}$$

where

$$F_3=\int_{v_1}^{v_2} Q(v,\bar{x})\,Q\left(f-\rho^{n+1}\,v-a_n\,\bar{x}-a_{n+1}\,\bar{x}_0\right)dv \tag{41}$$

and

$$v_1=\max\left[\bar{x},\frac{1}{\rho^{n+1}}\,(f-1-a_n\,\bar{x}-a_{n+1}\,\bar{x}_0)\right] \tag{42a}$$

$$v_2=\min\left[1,\frac{1}{\rho^{n+1}}\,(f-\bar{x}-a_n\,\bar{x}-a_{n+1}\,\bar{x}_0)\right]. \tag{42b}$$

The differential equations (34)-(38) require a set of initial and boundary conditions for the functions $p(\bar{x})$, $q(\bar{x})$, $r(\bar{x})$, $Q(f,\bar{x})$ and $R(f,\bar{x})$. Clearly, at $\bar{x}=0$, no bar has yet failed and

$$p(0)=1 \quad q(0)=0 \quad r(0)=0. \tag{43}$$

For very small values of $\bar{x}$, a few fibers are broken but the load they carry is in fact very close to the elastic value $\bar{F}_k=\bar{x}$. It is then concluded that

$$\lim_{\bar{x}\to 0} Q(f,\bar{x})=\lim_{\bar{x}\to 0} R(f,\bar{x})=\delta(f-\bar{x}). \tag{44}$$

Finally, the probability density functions must satisfy the normalization conditions

$$\int_{\bar{x}}^{1} Q(f,\bar{x})\,df=\int_{\bar{x}}^{1} R(f,\bar{x})\,df=1. \tag{45}$$

Numerical Solutions

Of particular interest in the present investigation is the study of the distribution of the forces in the fibers when $S_{min} \ll S_{max}$. In this case, the parameter $\bar{x}_0$ is approximately zero. Although this assumption provides a minor simplification of Eq. (34)-(36), the numerical evaluation of the functions $p(\bar{x})$, $q(\bar{x})$, $r(\bar{x})$, $Q(f,\bar{x})$, and $R(f,\bar{x})$ that satisfy these equations represents a serious computational challenge in view of the strong nonlinear character of Eq. (37) and (38). This numerical approach can be circumvented by proceeding with a Monte Carlo simulation of the fiber breaking process. To this end, a composite layer containing 100,000 fibers was subjected to a displacement controlled experiment. Shown in Fig. 4-10 are the probabilities p, q, and r for $\bar{x} \in [0,1]$ (Fig. 4), and the probability density functions $Q(f,\bar{x})$ and $R(f,\bar{x})$ for $\bar{x}=0.1$, 0.2, and 0.4.

It can be observed from these figures that the probability density function $R(f,\bar{x})$ has essentially a triangular shape, so that

$$R(f,\bar{x}) \approx \begin{cases} \frac{4}{\bar{x}^2}(f-\bar{x}) & \text{for } f \in [\bar{x}, 1.5\,\bar{x}] \\ \frac{4}{\bar{x}^2}(2\,\bar{x}-f) & \text{for } f \in [1.5\,\bar{x}, 2\,\bar{x}] \end{cases} . \tag{46}$$

A reliable approximation of the probability density function $Q(f,\bar{x})$ can also be obtained. To this end, note first that for $\bar{x} \approx 0$, $Q(f,\bar{x})$ is very close to a step function extending from $\bar{x}$ to $1.5\,\bar{x}$. As $\bar{x}$ increases, the sharp transition at $f=1.5\,\bar{x}$ appears to remain while the function $Q(f,\bar{x})$ decreases almost linearly both left and right of this value. Noting that the two slopes are very similar, it is proposed to approximate $Q(f,\bar{x})$ in the following way

$$Q(f,\bar{x}) \approx \begin{cases} \frac{2}{\bar{x}} - a\,(f-\bar{x}) & \text{for } f \in [\bar{x}, 1.5\,\bar{x}] \\ a\,(2\,\bar{x}-f) & \text{for } f \in [1.5\,\bar{x}, 2\,\bar{x}] \end{cases} \tag{47}$$

where a denotes the common unknown slope of $Q(f,\bar{x})$ in $f \in [\bar{x}, 1.5\,\bar{x}]$ and $f \in [1.5\,\bar{x}, 2\,\bar{x}]$. This variable must be such that the above approximate representation of $Q(f,\bar{x})$, Eq. (47), satisfies Eq. (37) in some way. Specifically, it will required that the error in Eq. (37) have a zero mean. That is,

$$\int_{\bar{x}}^{1} f\left[\frac{\partial}{\partial \bar{x}}(q\,Q)+q\,\frac{\partial Q}{\partial f}-F_1\right]df=0. \tag{48}$$

This Galerkin-type approach leads to the following ordinary differential equation for the slope a

$$\frac{q\,\bar{x}}{24}\,\frac{d(a\,\bar{x}^2)}{d\bar{x}}=-\left[\frac{5}{4}\,\bar{x}+\frac{(a\,\bar{x}^2)\,\bar{x}}{24}\right]\frac{dq}{d\bar{x}}-q\left[\frac{1}{4}+\frac{a\,\bar{x}^2}{24}\right]-q\,Q(1,\bar{x})+\int_{\bar{x}}^{1} f\,F_1\,df. \tag{49}$$

The expression for the term $\int_{\bar{x}}^{1} f\,F_1\,df$ is omitted here for brevity, it is readily computed by relying on Eq. (40). Equation (47) indicates that the slope a affects the probability density function $Q(f,\bar{x})$ through the product $a\,\bar{x}^2$. Thus, it is suggested to associate to Eq. (49) the initial condition

$$\lim_{\bar{x}\to 0} a(\bar{x})\,\bar{x}^2 = \textit{finite}. \tag{50a}$$

A limiting analysis of the various terms in Eq. (49) demonstrates that the above condition can indeed be enforced. In fact, it is found that

$$\lim_{\bar{x}\to 0} a(\bar{x})\,\bar{x}^2 = 0 \tag{50b}$$

which is consistent with Fig. 5.

The knowledge, even approximate, of the probability density functions $Q(f,\bar{x})$ and $R(f,\bar{x})$ permits the evaluation of the terms Θ_i, Eq. (22), Ψ_i, Eq. (28), and Φ_i, Eq. (30). Equations (34)-(36), complemented by Eq. (49), represent then a well defined set of first order differential equations that can be solved by standard techniques. To test the validity of this approximate formulation, it was decided to investigate first the behavior of the probabilities p, q, and r, for $\bar{x} \approx 0$. In this case, it is sufficient to impose $a = 0$ for all values of $\bar{x}$. Shown in Fig. 4 are the probabilities $p(\bar{x})$, $q(\bar{x})$, and $r(\bar{x})$ computed by Monte Carlo simulation and from Eq. (34)-(36), (46), and (47). It is readily seen that this simple approximation already provides a very reliable model for the probabilities of existence of regular, stopping, and singular fibers for $\bar{x} \in [0, 0.45]$. A similar accuracy is also obtained in connection with the average load carried by the fibers, Eq. (5), see Fig. 12. Note that the numerical solution of Eq. (34)-(36) was halted at $\bar{x}=0.45$ because the system had already entered the less interesting softening range. If needed, a reliable approximation of this behavior can also be obtained by allowing the slope to vary according to Eq. (49).

Local and Global Load Sharing: A Comparison

When all of the fibers share the external load, there is no spatial variation of the force in the fibers and $\bar{F}_k = \bar{x}$ if the fiber is not broken. The probability that a given fiber is broken is thus readily evaluated as

$$Pr\,[\,broken\ fiber\,] = \bar{x}. \tag{51}$$

Relying on the independence of the fiber strengths $\bar{S}_k$ it is then found that

$$p_G(\bar{x}) = (1 - \bar{x})^3 \tag{52}$$

$$q_G(\bar{x}) = 2\,\bar{x}\,(1 - \bar{x})^2 \tag{53}$$

$$r_G(\bar{x}) = \bar{x}^2\,(1 - \bar{x}) \tag{54}$$

and

$$Q_G(f, \bar{x}) = R_G(f, \bar{x}) = \delta(f - \bar{x}). \tag{55}$$

A comparison of the probabilities $p(\bar{x})$, $q(\bar{x})$, and $r(\bar{x})$ corresponding to the local and global load sharing models is presented in Fig. 11. It is seen that the global load sharing model overpredicts the probability of finding regular, stopping, and singular fibers. This observation is expected since the local transfer mechanism leads to a propagation of the fiber breaking process that is not consistent with a global load sharing rule. The existence of a smaller number of unbroken fibers is also consistent with the increase loads they carry, compare Eq. (55) and Fig. 5-10. Surprisingly, these two effects seem to cancel each other when considering the mean value of the force, Fig. 12, which is very close, for $\bar{x} \in [0, 0.5]$, to the parabolic shape $\bar{x}\,(1 - \bar{x})$ predicted by the global load sharing rule except for the location of the peak which is largely overestimated by the global load sharing model.

Summary

In this paper, a single composite layer has been considered and its random inelastic response in a displacement controlled experiment has been investigated when a local load sharing mechanism is present. It was first recognized that the randomness in the fiber strengths and the force transfer that is associated with a local load sharing rule permit the propagation of the breaking of fibers. This process results in the

existence of three different types of unbroken fibers which were termed regular, stopping, and singular, they are surrounded by 2, 1, and 0 unbroken fibers, respectively. It was then recognized that the load carried by regular fibers is the same as if failure had not occurred. The forces in the stopping and singular fibers were however found to be random and to be in general larger than the values obtained in the absence of failure.

For a given applied displacement $\bar{x}$, the determination of the probabilities of existence of regular, stopping, and singular fibers, denoted by $p(\bar{x})$, $q(\bar{x})$ and $r(\bar{x})$, and the probability density functions of the force carried by the stopping and singular fibers, $Q(f,\bar{x})$ and $R(f,\bar{x})$, was approached as follows. First, the breaking of a fiber and its propagation in the layer was analyzed from a stochastic point of view. In particular, the probability associated with the breaking of n fibers was determined when the process is initiated at a regular, a stopping, or at a singular fiber.

A set of "continuity-like" equations was then derived by analyzing the changes in fiber types and in load carried that result from the fiber breaking process. In turn, these relations were seen to reduce to a set of ordinary and partial differential equations that govern the evolution of the functions $p(\bar{x})$, $q(\bar{x})$, $r(\bar{x})$, $Q(f,\bar{x})$, and $R(f,\bar{x})$ as the variable $\bar{x}$ is increased from 0 to 1. The complexity of these equations motivated the search for an approximate solution technique.

To this end, a Monte Carlo simulation study was undertaken to provide insight into the behavior of these functions. It was in particular recognized that the probability density functions $Q(f,\bar{x})$ and $R(f,\bar{x})$ can be accurately represented by the expressions given in Eq. (46)-(47) for the particular case of interest. Introducing these approximations in Eq. (34)-(36) led to a much simpler numerical problem that can be solved by using traditional ordinary differential equation solvers. The accuracy of these approximate results was demonstrated; a reliable approximation of the probabilities p, q, r, but also of the probability density functions $Q(f,\bar{x})$ and $R(f,\bar{x})$ was obtained.

Finally, a comparative analysis of the behavior of the composite layer under both local and global load sharing was performed. It was shown in particular that the global mechanism can seriously overestimate the number of unbroken fibers and underestimate the distribution of the forces in the fibers. However, it was found that the mean value of the loads carried by the fibers is reasonably well predicted by the global load sharing model except for the location of the peak which is largely overestimated by the global load

sharing model.

References

1. Daniels, H.E., The Statistical Theory of the Strength of Bundles of Threads I, *Proceedings of the Royal Society*, **183A** (1945) 405-435.

2. Harlow, D.G.& Phoenix, S.L., Probability Distributions for the Strength of Composite Materials I: Two-Level Bounds, *International Journal of Fracture*, **17** (1981) 347-372.

3. Harlow, D.G.& Phoenix, S.L., Probability Distributions for the Strength of Composite Materials II: A Convergent Sequence of Tight Bounds, *International Journal of Fracture*, **17** (1981) 601-630.

4. Harlow, D.G. & Phoenix, S.L., Probability Distributions for the Strength of Fibrous Materials Under Local Load Sharing I: Two-Level Failure and Edge Effects, *Advances in Applied Probability*, **14** (1982) 68-94.

5. Kuo, C.-C. & Phoenix, S.L., Recursions and Limit Theorems for the Strength and Lifetime Distributions of a Fibrous Composite, *Journal of Applied Probability*, **24** (1987) 137-159.

6. Grigoriu, M., Reliability Analysis of Dynamic Daniels Systems with Local Load-Sharing Rule, *Journal of Engineering Mechanics*, **116** (1990) 2625-2642.

7. Curtin, W.A., The "Tough" to Brittle Transition in Brittle Matrix Composites, *Journal of the Mechanics and Physics of Solids*, **41** (1993) 217-245.

8. Smalley, R.F., Turcotte, D.L. & Solla, S.A., A Renormalization Group Approach to the Stick-Slip Behavior of Faults, *Journal of Geophysical Research*, **90** (1985) B2 1894-1900.

9. Sornette, D., Elasticity and Failure of a Set of Elements Loaded in Parallel, *Journal of Physics A*, **22** (1989) L243-L250.

10. Sornette, D., Rupture in the Bubble Model, *Journal of Physics A*, **22** (1989) L619-L625.

Acknowledgements

The support of this work by the grant DAAL03-91-G0030 of the US Army Research Office, Engineering and Science Division, Structural Mechanics Branch, is gratefully acknowledged.

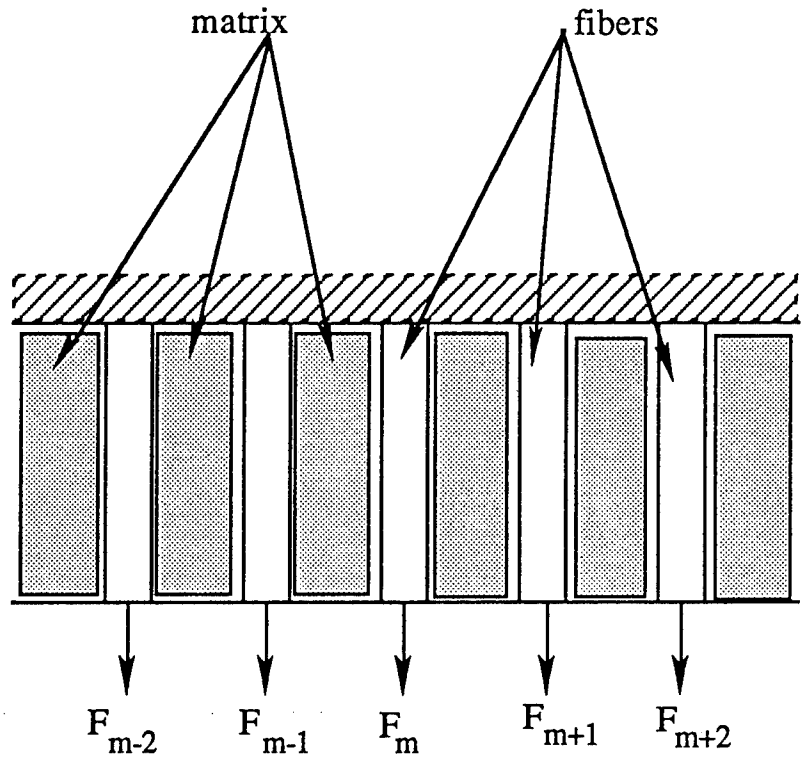

Fig. 1. The composite layer under tension

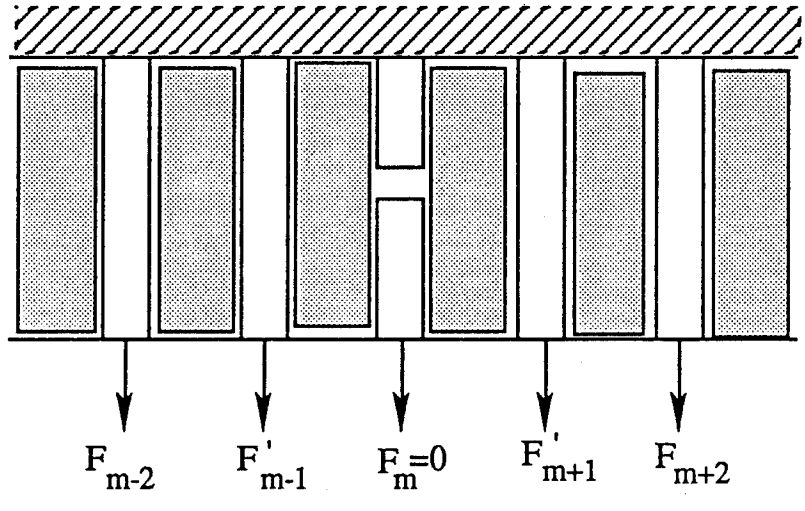

Fig. 2. The load transfer mechanism

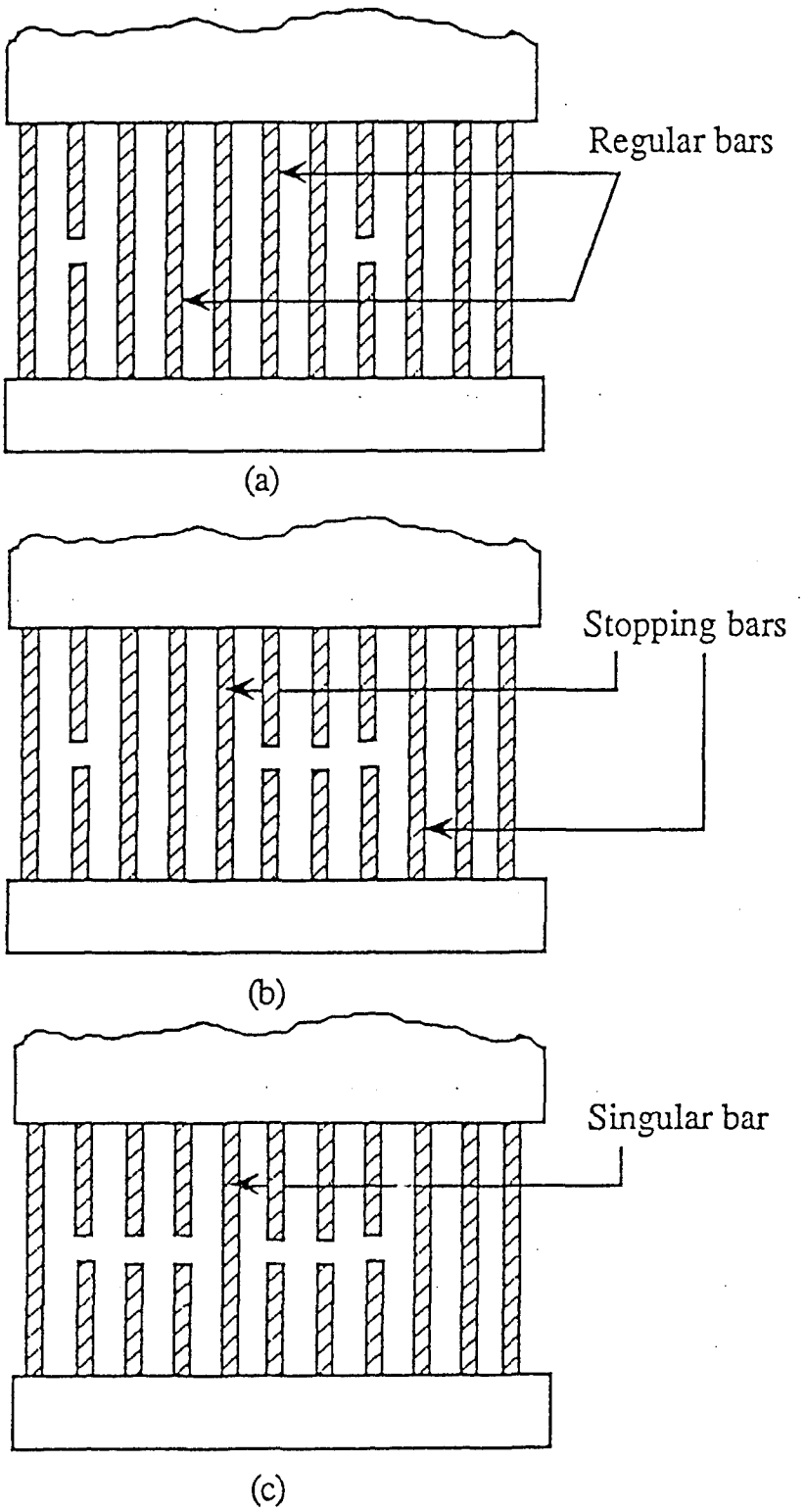

Figure 3. Definition of regular, stopping, and singular fibers

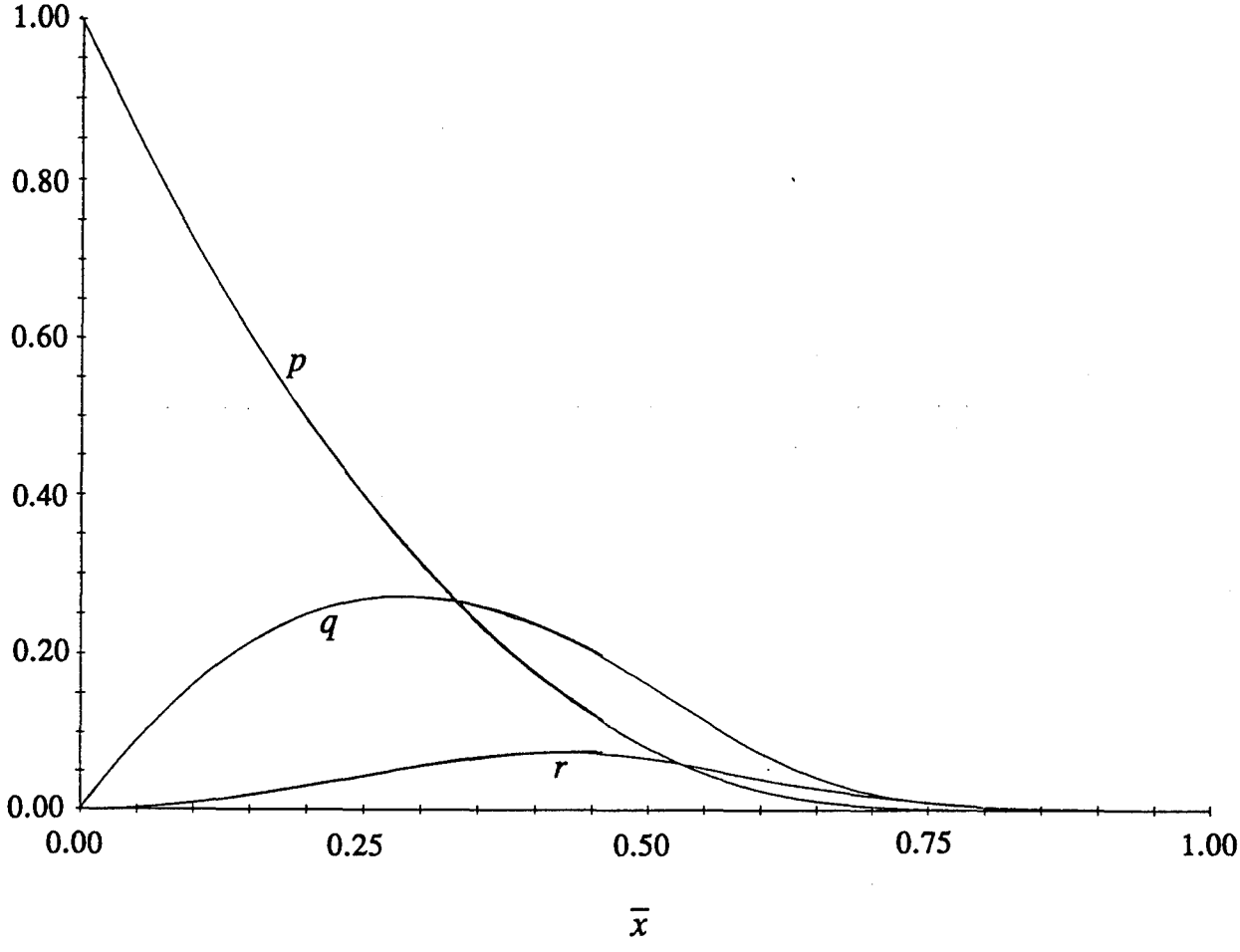

Fig. 4 Evolution of the probabilities p, q, and r obtained by Monte Carlo simulation and by solving the evolution equations, Eq. (34)-(36)

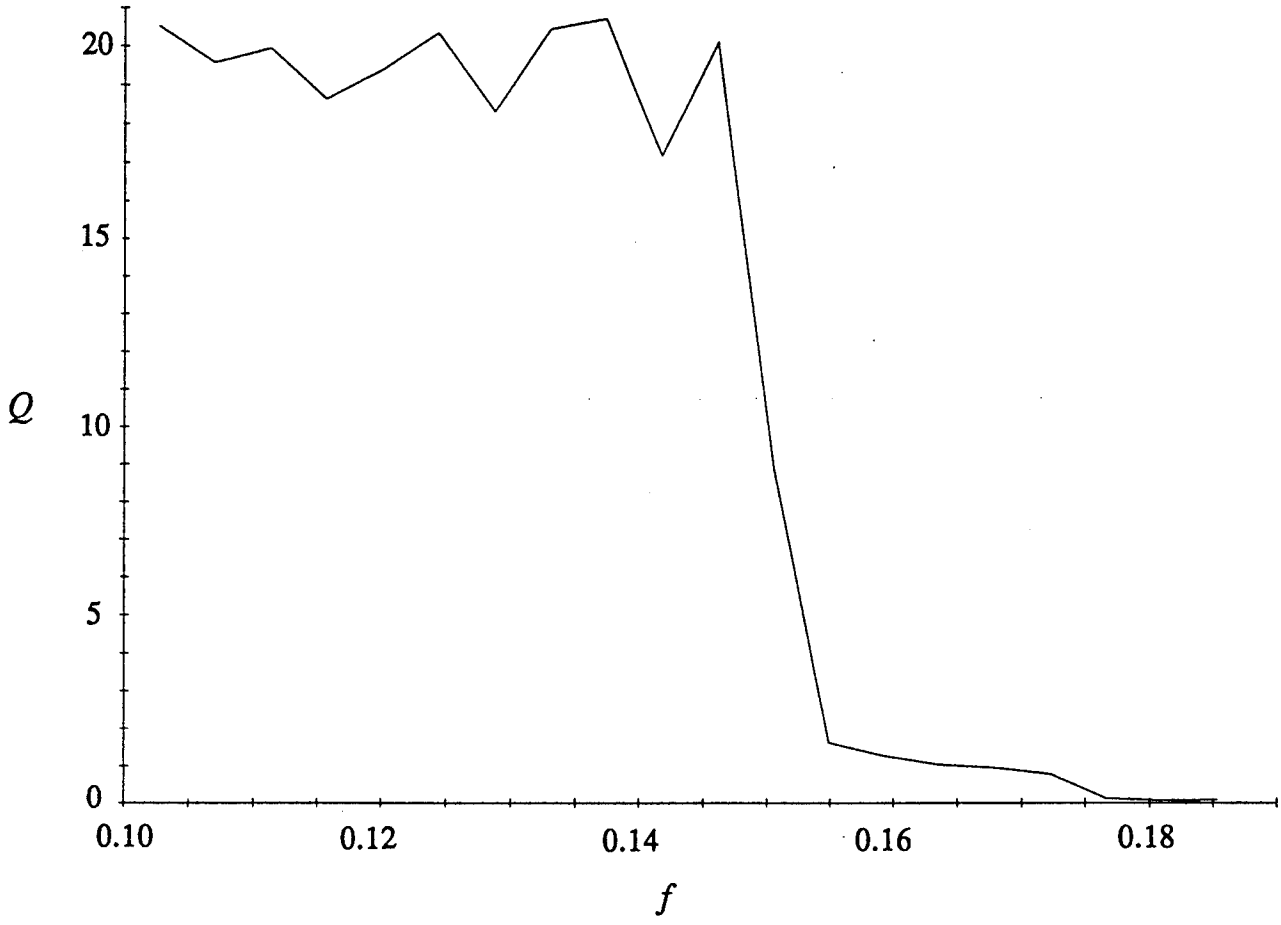

Fig. 5 Probability density function $Q(f,\bar{x})$ for $\bar{x}$=0.1

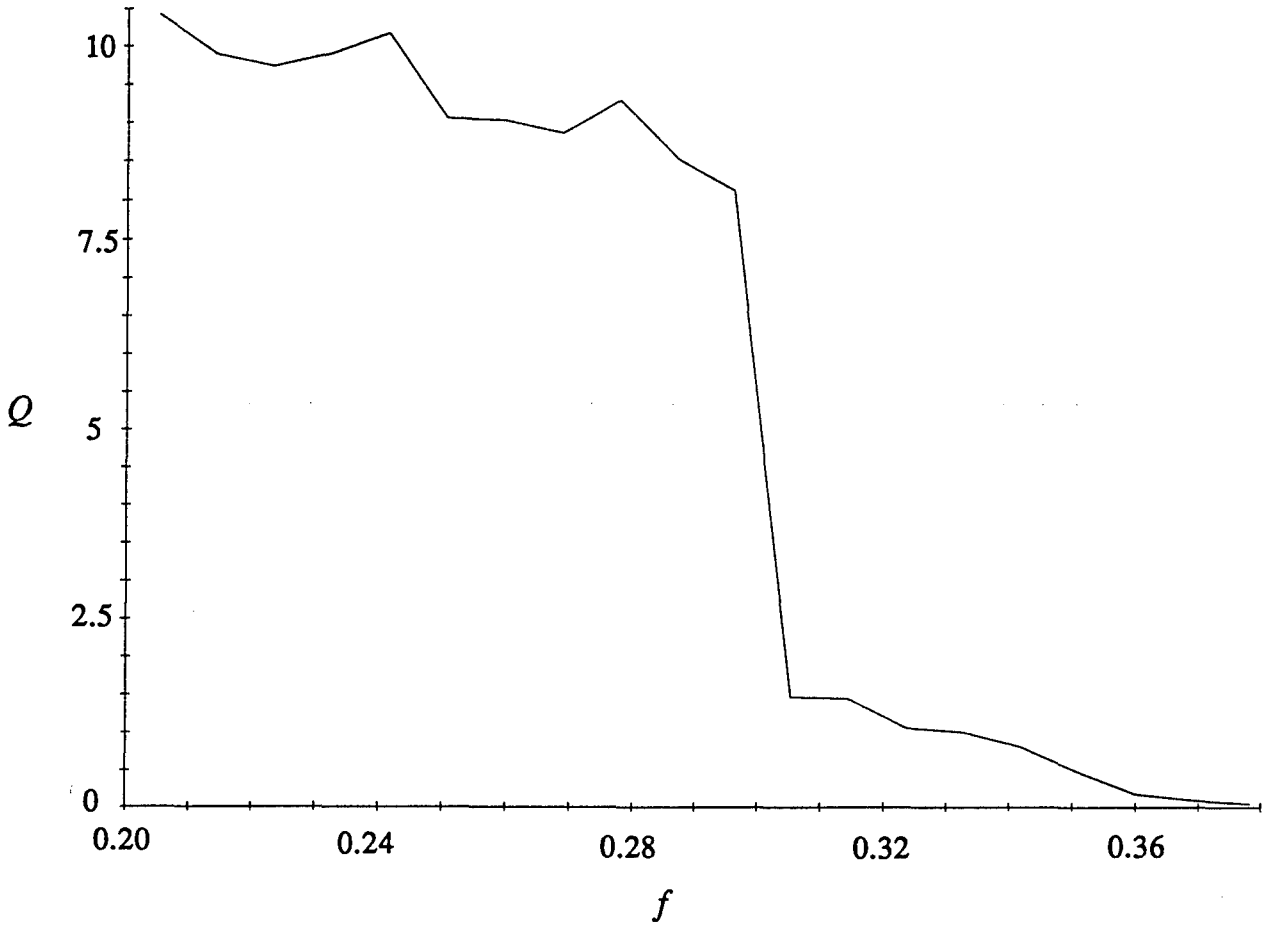

Fig. 6 Probability density function $Q(f,\bar{x})$ for $\bar{x}$=0.2

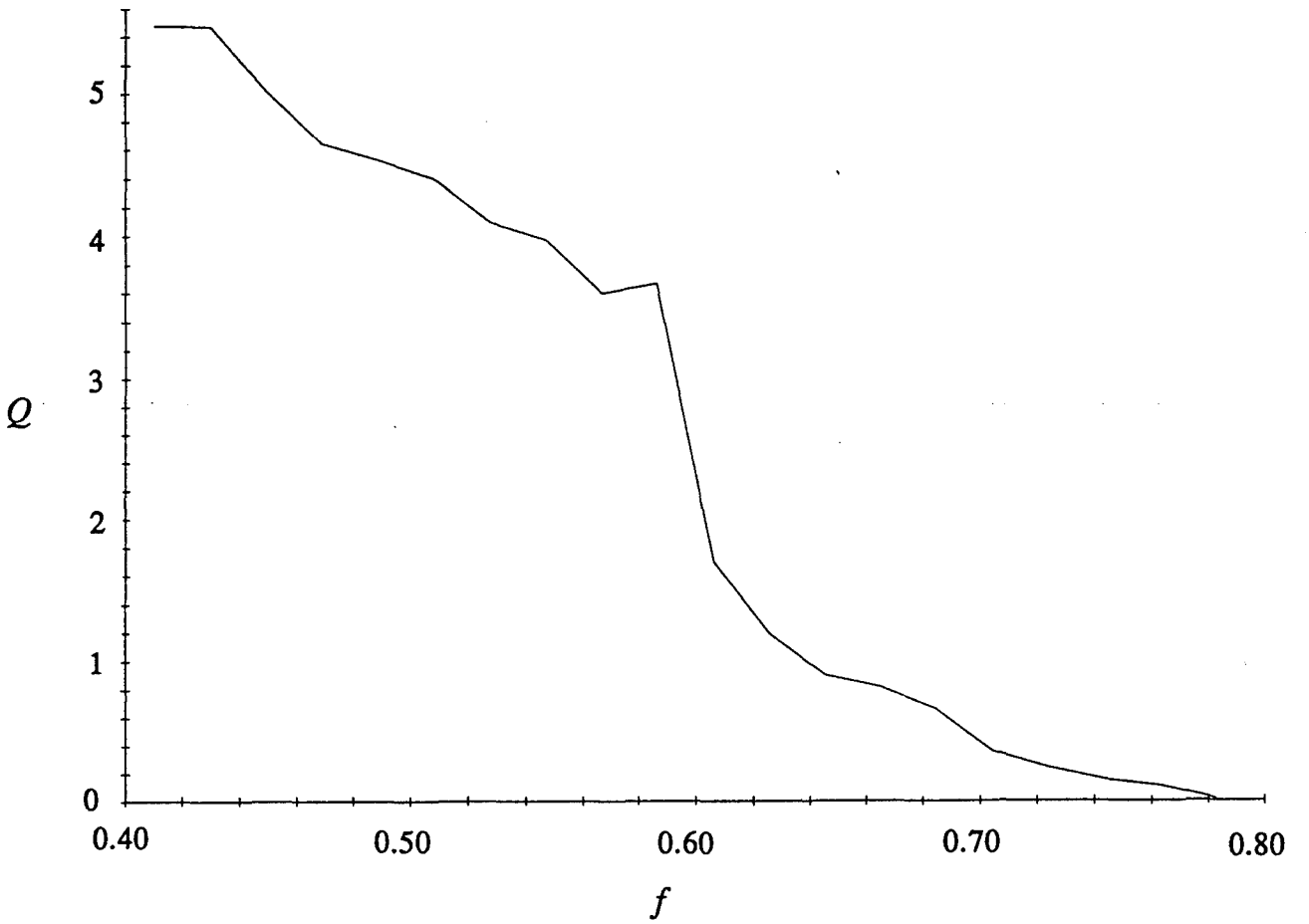

Fig. 7 Probability density function $Q(f,\bar{x})$ for $\bar{x}$=0.4

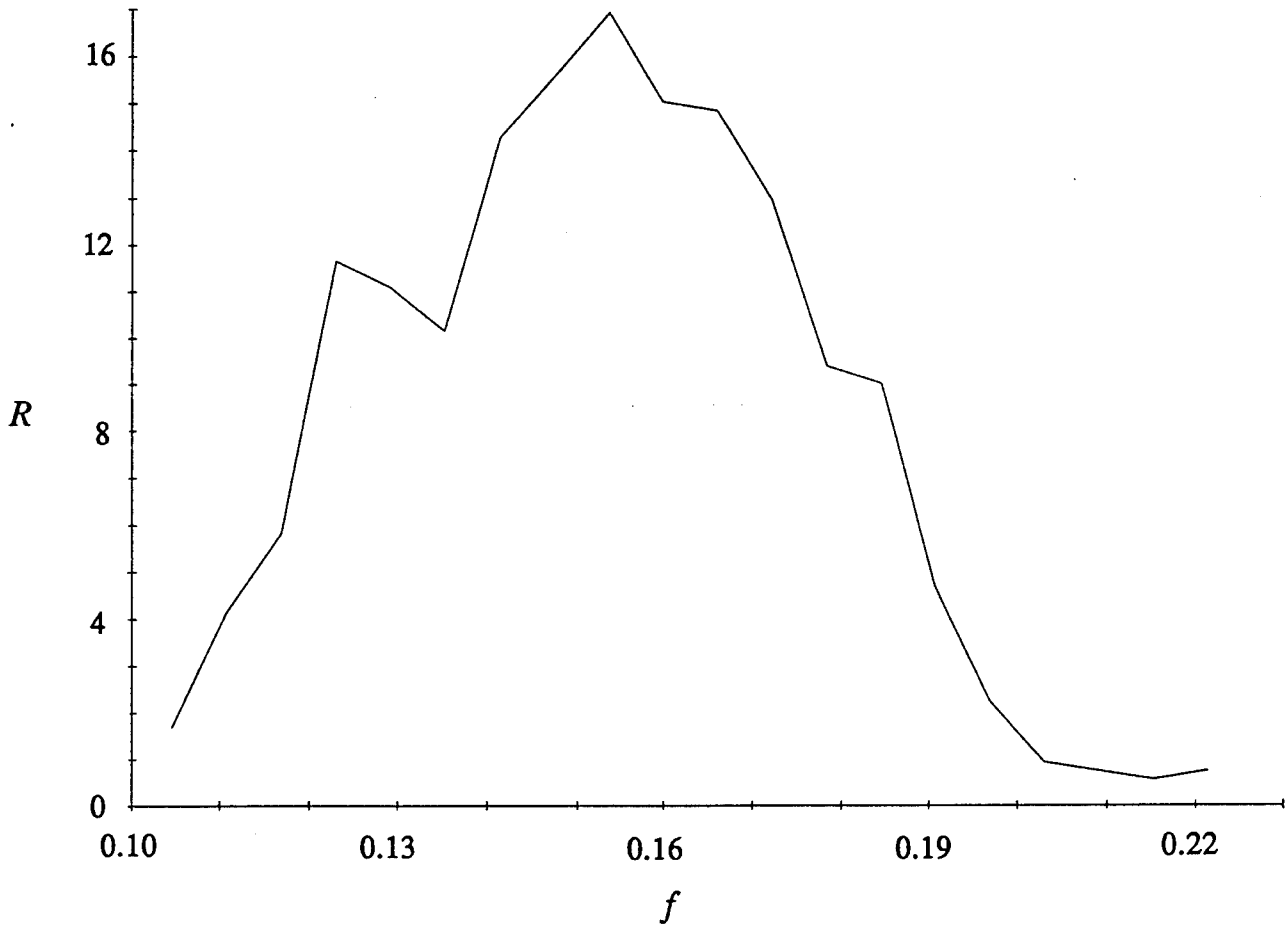

Fig. 8 Probability density function $R(f,\bar{x})$ for $\bar{x}$=0.1

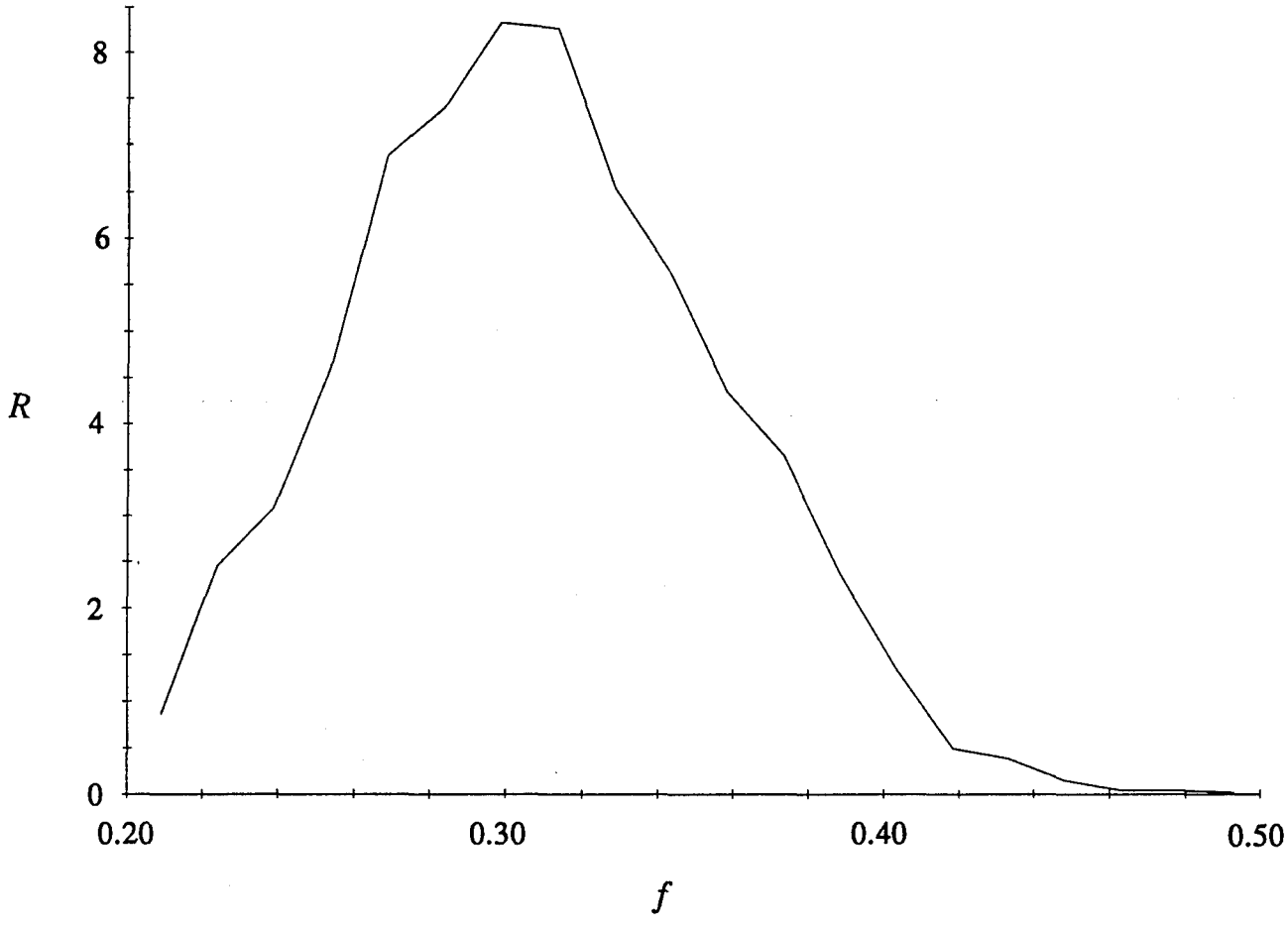

Fig. 9 Probability density function $R(f,\bar{x})$ for $\bar{x}$=0.2

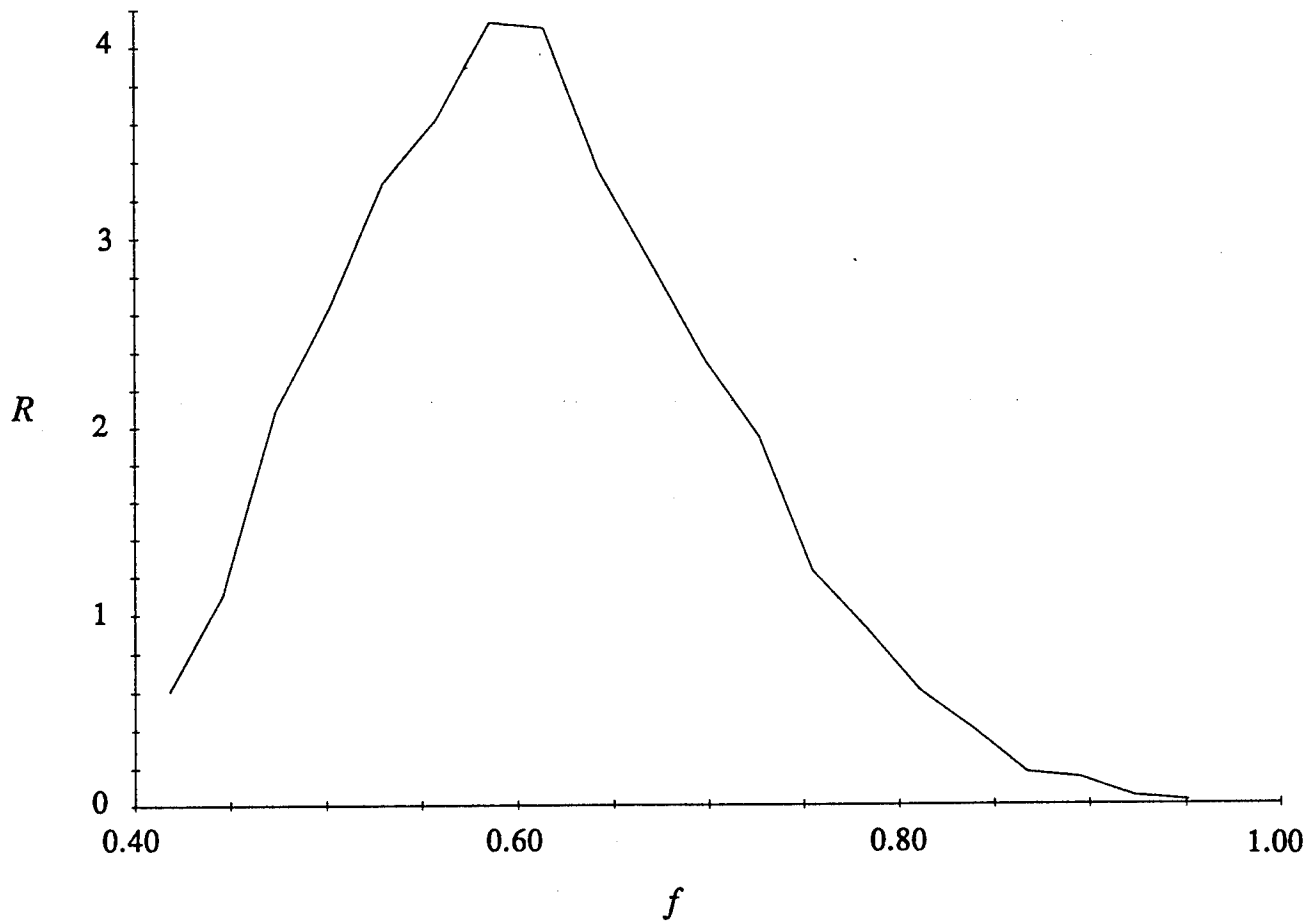

Fig. 10 Probability density function $R(f,\bar{x})$ for $\bar{x}$=0.4

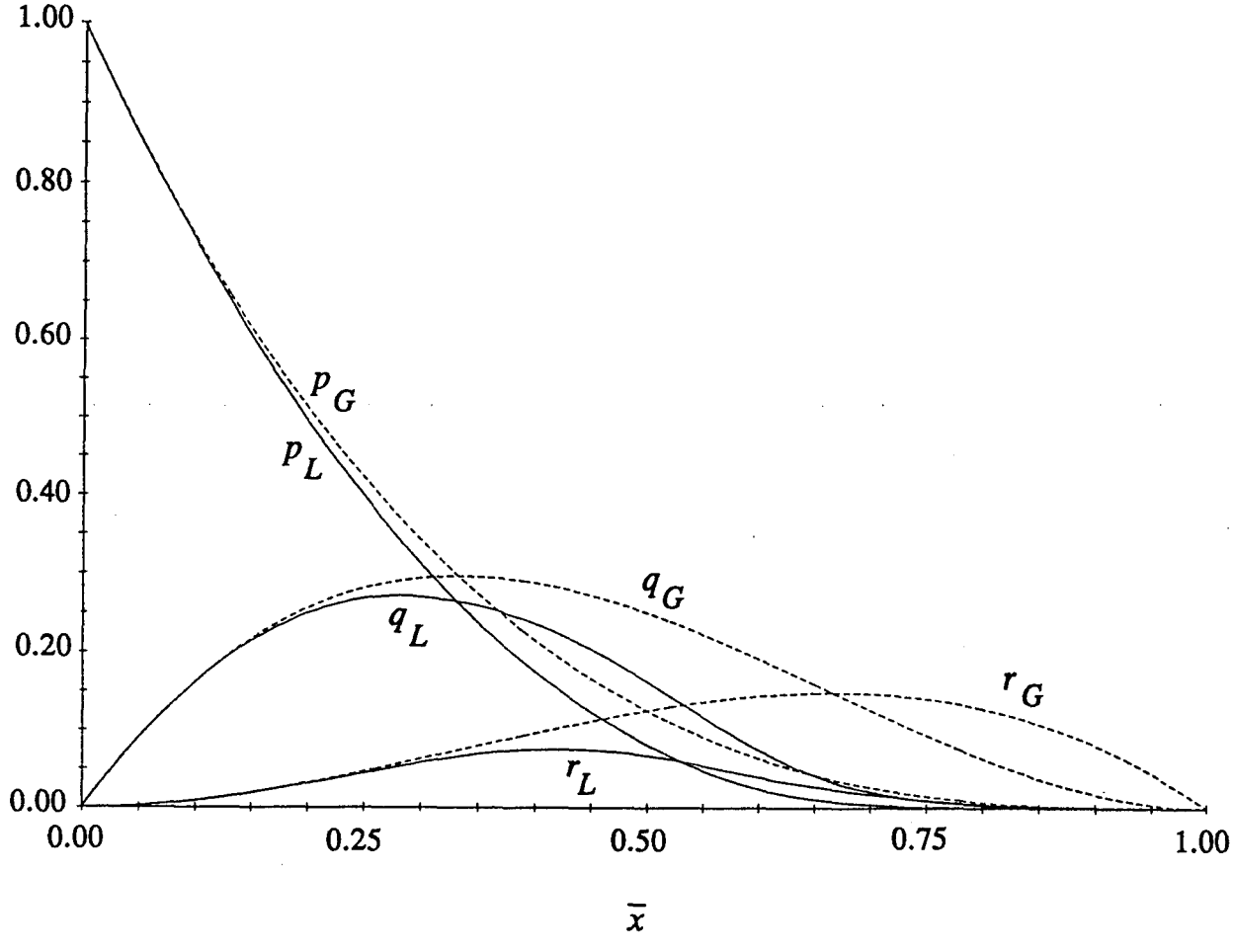

Fig. 11 Evolution of the probabilities p, q, and r for the local (—) and global (---) load sharing models

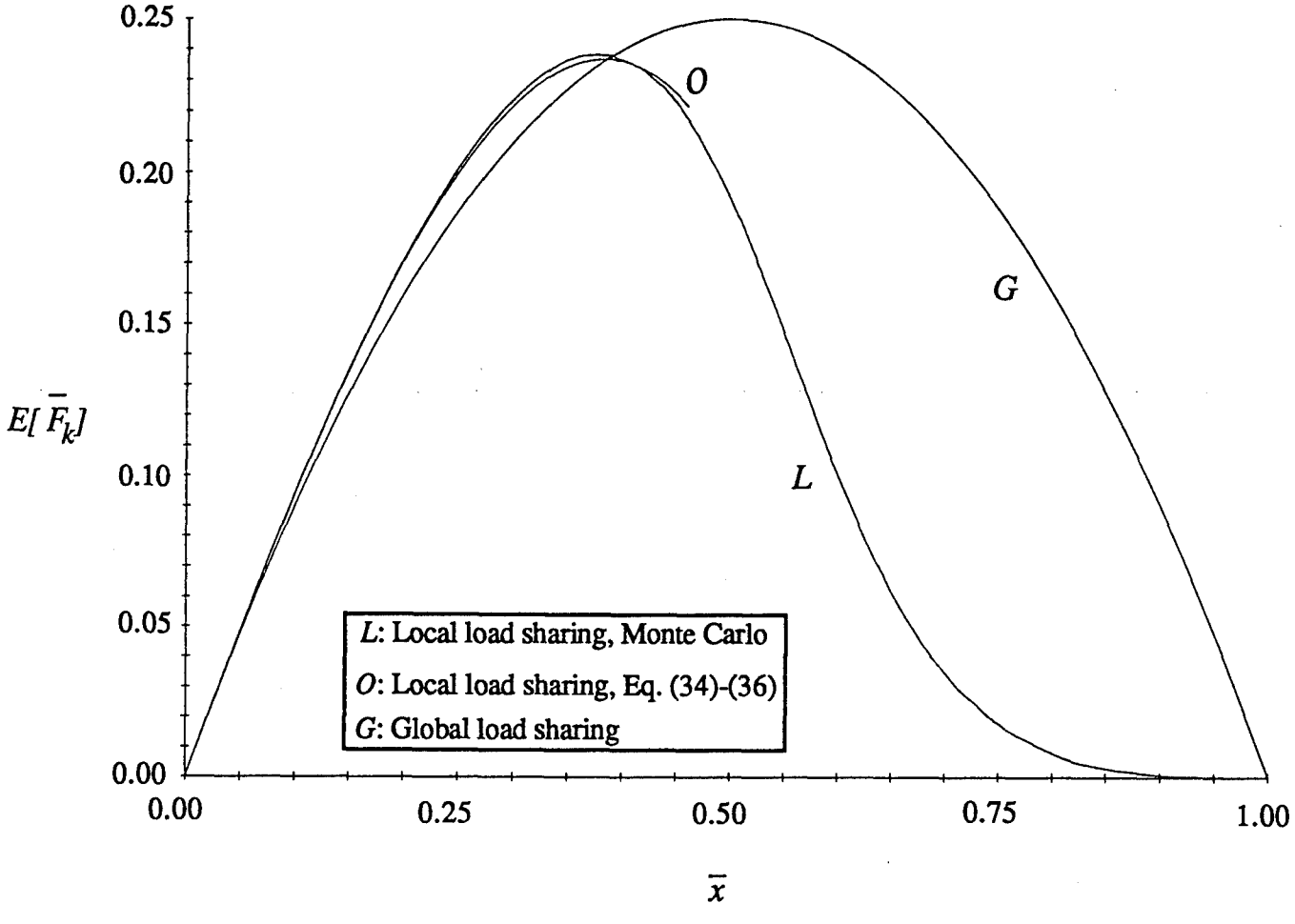

Fig. 12 Mean value of the force carried by the fibers for the local and global load sharing models

Submitted to Journal of Fluids and Structures

FIBER CLUSTERING IN COMPOSITE MATERIALS: A FLOW INDUCED INSTABILITY

Marc P. Mignolet

Associate Professor, Department of Mechanical and Aerospace Engineering, Arizona State University, Tempe, Arizona, 85287-6106.

ABSTRACT

In an attempt to explain the phenomenon of fiber clustering, the low Reynolds number flow through an array of rigid cylinders is investigated. Both cases of a regular and a slightly perturbed array of cylinders are studied. In particular, the forces exerted on the cylinders by the fluid are derived for both cases and a stability analysis is conducted to predict the motion of the array.

Introduction

The design of a manufacturing process that leads to composite materials possessing optimal properties represents an important technological challenge. One of the difficulties that are often encountered is the lack of uniformity of the distribution of fibers in the matrix. This generic problem which affects both short and continuous fibers composites originates in particular in the flow of the resin through the arrangement of fibers. Consider for example the process of impregnation of thermoplastic composites which starts with the introduction of a polymeric matrix into a fiber tow. As a result of heating, the matrix softens and starts flowing into the spaces separating the adjacent fiber tows. While flowing through the "channels" formed by the adjacent tows, the viscous mass exerts significant pressures and shears on the tows which may cause both their flexure and rigid body displacement. This process may lead to concentration of fibers into small areas, or clusters, and to the formation of matrix-rich domains which are almost devoid of fibers. One of the possible explanation of this phenomenon associates the fiber clustering with an initial irregularity of the array of fibers. The goal of the present investigation is to test the validity of this mechanism. To this end, the motion of a fluid (the resin) through an array of cylinders (the fibers) will be investigated. In

particular, the present study will focus on the determination of the change in the forces exerted by the fluid on the cylinders as they move away from their initially regular arrangement. Finally, these results will be used to test the stability of the entire array of fibers.

The Flow Equations

The fluid flow past an array of cylinders has been the subject of a large number of both theoretical and experimental investigations. The two limiting cases of a fully turbulent flow, corresponding to a very large Reynolds number (see Chen et al., 1990, Conca. et al., 1990, and references therein), and of a creeping motion, modeling very low Reynolds number situations (see in particular Tamada and Fujikawa, 1957, Miyagi, 1958, Hasimoto, 1959, Kirsch and Fuchs, 1967, Happel and Brenner, 1973, White, 1974, Drummond and Tahir, 1984 and references therein), have been especially emphasized. In the context of the manufacturing of thermoplastics it is found that a low mean velocity, U, a high kinematic viscosity, ν, and a small diameter of the fibers, D, lead to a very small Reynolds number

$$\mathrm{Re} = \frac{U\,D}{\rho\,\nu} \ll 1 \tag{1}$$

where ρ is the mass density of the resin. The theory of linear creeping flows thus represents an appropriate framework for the present analysis.

The derivation of the flow equations corresponding to the limiting case of a very small Reynolds number is a classical topic of fluid mechanics. Neglecting all inertia terms, Stokes first showed that the continuity and momentum equations reduced to

$$div\,\underline{V} = 0 \tag{2}$$

and

$$\mu\,\nabla^2\,\underline{V} = \nabla P \tag{3}$$

where $\underline{V}$ and P are the velocity and the pressure fields, respectively. Further, the symbol μ denotes the dynamic viscosity which is defined as

$$\mu = \rho \nu. \tag{4}$$

Introducing the vorticity vector $\underline{\omega}$ as

$$\underline{\omega} = curl\, \underline{V} \tag{5}$$

it is readily shown that Eq. (2) and (3) can be rewritten in the form

$$\nabla^2 P = 0 \tag{6}$$

and

$$\nabla^2 \underline{\omega} = \underline{0}. \tag{7}$$

A series of investigations (see White, 1974, and Happel and Brenner, 1973, for details) have shown that Eq. (6) and (7) lead, in the case of three-dimensional flows around immersed bodies, to accurate estimates of the flow characteristics in a large domain surrounding the body, and consequently of the drag and lift forces. In the far field, however, Stokes' equation, Eq. (3), predicts inertia terms that are not negligible, as was initially assumed in its derivation. Further, the solution of plane flow problems by relying on Eq. (7) is affected by Stokes' paradox: it is not always possible to find a steady solution of Eq. (6) and (7) that also satisfies the boundary conditions on the surface of the immersed body (no-slip condition) and in the far-field. These weaknesses of Stokes' equation have led Oseen to conserve the inertia term $\rho U \frac{\partial \underline{V}}{\partial x}$ in the formulation, leading to the following steady momentum equation

$$\rho U \frac{\partial \underline{V}}{\partial x} = -\nabla P + \mu \nabla^2 \underline{V}. \tag{8}$$

The above relation, at the contrary of Stokes' equation, leads to a uniformly valid approximation of the three-dimensional fluid flow around an immersed body. Further, it admits steady two dimensional solutions that satisfy the required boundary conditions on the immersed body and in the far-field. Notwithstanding these advantages, it should be noted that Stokes' and Oseen's equations, Eq. (7) and (8), both represent zeroth order approximations of the Navier-Stokes equations corresponding to a low Reynolds number.

Thus, it cannot in general be inferred that the use of Eq. (8) will lead to estimates of the forces acting on the body that are more accurate than the corresponding approximations derived from Eq. (7). (Happel

and Brenner, 1973). In the context of the flow through a perturbed array of fibers, this observation indicates that the simplest of the two momentum equations, that is Eq. (7), be used provided that it yields an acceptable flow field. The lack of a fluid only "far field" and the existence of a Stokes' creeping flow through a regular arrangement of cylinders (see Hasimoto, 1959, Sangani and Acrivos, 1982, Drummond and Tahir, 1984) suggest that Stokes' paradox will not be present. Consequently, Eq. (7) will indeed yield the required low Reynolds number approximation.

Assumed Solution

In the case of a two-dimensional flow, the vorticity vector can be written in the form

$$\underline{\omega}^T = \left[0, 0, \omega_z \right] \tag{9}$$

with

$$\omega_z = \frac{\partial v}{\partial x} - \frac{\partial u}{\partial y} \tag{10}$$

where u and v denote the components of the velocity in the plane of motion,

$$\underline{V} = [u, v, 0]. \tag{11}$$

Introducing the polar coordinates (r, θ), it can be shown that the solutions of Eq. (7) and (9) admit the representations

$$\omega_z = F_1\, \theta \ln r + F_2 \ln r + F_3\, \theta + F_4 + \sum_{m=1}^{\infty} \left(B_m\, r^{-m}\, e^{-im\theta} + C_m\, r^{-m}\, e^{im\theta} + D_m\, r^{m}\, e^{-im\theta} + E_m\, r^{m}\, e^{im\theta} \right) \tag{12}$$

where $B_m, C_m, D_m, E_m, m = 1, ..$ and F_1, F_2, F_3, F_4 are arbitrary constants. The single-valuedness of the vorticity component ω_z under a rotation by an angle 2π around the z-axis requires that the coefficients F_1 and F_3 be identically zero. Further, imposing that ω_z vanish at infinity, $r = \infty$, leads to the condition

$$F_2 = F_4 = 0 \tag{13}$$

and

$$D_m = E_m = 0\,,\ m = 1,..\tag{14}$$

Finally, the real character of the vorticity vector for all values of r and θ requires that the constants B_m and C_m be complex conjugates of each other, or

$$C_m = \bar{B}_m\,,\ m = 1,\ldots\tag{15}$$

Under these conditions, it is found that ω_z can be expressed in the form

$$\omega_z = \sum_{m=1}^{\infty}\left(B_m\, r^{-m}\, e^{-im\theta} + \bar{B}_m\, r^{-m}\, e^{im\theta}\right) = \sum_{m=1}^{\infty}\left(\frac{B_m}{z^m} + \frac{\bar{B}_m}{\bar{z}^m}\right)\tag{16}$$

where

$$z = x + i\,y = r\,e^{i\theta}.\tag{17}$$

The next step of the analysis consists in the determination of the velocity field $\underline{V}$ that corresponds to the vorticity component ω_z, Eq. (16). This computation is greatly simplified by introducing first the complex velocity W as

$$W = u - i\,v\tag{18}$$

and noting that

$$\frac{\partial W}{\partial \bar{z}} = \frac{1}{2}\left(\frac{\partial}{\partial x} + i\,\frac{\partial}{\partial y}\right)(u - i\,v) = \frac{1}{2}\left[\left(\frac{\partial u}{\partial x} + \frac{\partial v}{\partial y}\right) - i\left(\frac{\partial v}{\partial x} - \frac{\partial u}{\partial y}\right)\right] = -\frac{i}{2}\,\omega_z\tag{19}$$

where the last equality results from Eq. (2) and (10). Then integrating Eq. (16) with respect to $\bar{z}$ yields

$$W = \frac{1}{2i}\left[\sum_{m=2}^{\infty}\left(\frac{B_m\,\bar{z}}{z^m} - \frac{\bar{B}_m}{(m-1)\,\bar{z}^{m-1}}\right) + B_1\,\frac{\bar{z}}{z} + \bar{B}_1\ln\bar{z}\right] + \sum_{m=0}^{\infty}\frac{A_m}{z^m} + \frac{1}{2i}\,\bar{B}_1\ln z\tag{20}$$

where A_m, $m = 1,..$ are arbitrary complex constants. Note that the term $\frac{1}{2i}\,\bar{B}_1\ln z$ is required to produce single-valued velocity components u and v.

The singularity displayed by the flow field, Eq. (20), at $z=0$ is clearly inadmissible unless that point does not belong to the fluid domain. More precisely, it can be argued that this point must coincide with the center of one of the fibers. Symmetry considerations dictate, however, that no one cylinder has a privileged role in the analysis. Thus, there must be a singularity of the flow field, Eq. (20), at the center of each fiber and (see also Tamada and Fujikawa, 1957, Drummond and Tahir, 1984)

$$W = \sum_p \sum_q W_{pq} \tag{21a}$$

where

$$W_{pq} = \frac{1}{2i}\left[\sum_{m=2}^{\infty} \left(\frac{B_m^{pq}\,(\bar{z}-\bar{s}_{pq})}{(z-s_{pq})^m} - \frac{\bar{B}_m^{pq}}{(m-1)\,(\bar{z}-\bar{s}_{pq})^{m-1}} \right) + B_1^{pq}\,\frac{(\bar{z}-\bar{s}_{pq})}{(z-s_{pq})} \right.$$

$$\left. + \bar{B}_1^{pq} \ln \left| \frac{z-s_{pq}}{s_{pq}} \right|^2 + \sum_{m=0}^{\infty} \frac{A_m^{pq}}{(z-s_{pq})^m} \right]. \tag{21b}$$

In the above relation, the double summation over the cylinder indices p and q extends over the entire array and s_{pq} denotes, as in Fig. 1, the complex number associated with the position vector of the fiber in the p^{th} column and the q^{th} row.

The boundary conditions, to be described next, will provide the necessary equations to compute the values of the complex coefficients A_m^{pq} and B_m^{pq} corresponding to each of the fibers, thus completing the determination of the velocity field in the array. Once this information is available, it is quite simple to determine the pressure field and the forces exerted on the cylinders. Specifically, note first from Eq. (3) that

$$\mu\,\nabla^2 W = \mu\left(\nabla^2 u - i\,\nabla^2 v\right) = \mu\left(\frac{\partial P}{\partial x} - i\,\frac{\partial P}{\partial y}\right) = 2\,\frac{\partial P}{\partial z}. \tag{22}$$

Then, using the identity

$$\nabla^2 W = 4\,\frac{\partial^2 W}{\partial z\,\partial \bar{z}} \tag{23}$$

and integrating Eq. (22) over z, it is found that

$$P = 2\,\mu\,\frac{\partial W}{\partial \bar{z}} + g(\bar{z}) = -\,i\,\mu\,\omega_z + g(\bar{z}) \tag{24}$$

where $g(\bar{z})$ denotes a function of $\bar{z}$ such that the corresponding pressure field P is real. Finally, the complex force acting on the fiber pq can be evaluated as (Miyagi, 1958)

$$F^{pq} = F_x^{pq} + i\, F_y^{pq} = \int_{pq} (i\, P + \mu\, \omega_z)\, dz \tag{25}$$

where the notation $\int_{pq}$ denotes the integral over the contour of the circle pq. Combining Eq. (24) and (25), it is found that

$$F^{pq} = i \int_{pq} g(\bar{z})\, dz + 2\, \mu \int_{pq} \omega_z\, dz = 4\, i\, \pi\, \mu\, B_1^{pq}. \tag{26}$$

No-Slip Boundary Conditions

To give rise to a bonafide velocity distribution, the constants A_m^{pq} and B_m^{pq} must yield vanishing components u and v on the exterior surface of each fiber. Denoting by a the common radius of the fibers, it is then required that

$$W = 0 \quad \text{for } z = s_{rs} + a\, e^{i\theta} \tag{27}$$

at every angle θ and for all cylinder indices p and q. Combining Eq. (21) and (27) and expanding the terms $(s_{rs} - s_{pq} + a\, e^{i\theta})^{-m}$ and $\ln \left| s_{rs} - s_{pq} + a\, e^{i\theta} \right|^2$ in the form

$$(s_{rs} - s_{pq} + a\, e^{i\theta})^{-m} = (s_{rs} - s_{pq})^{-m} \sum_{t=0}^{\infty} \binom{-m}{t} \left[\frac{a}{s_{rs} - s_{pq}} \right]^t e^{it\theta} \quad \text{for } (r,s) \neq (p,q) \tag{28}$$

and

$$\ln \left| s_{rs} - s_{pq} + a\, e^{i\theta} \right|^2 = \ln \left| s_{rs} - s_{pq} \right|^2 + \sum_{t=1}^{\infty} \frac{(-1)^{t-1}}{t} \left[\frac{a}{s_{rs} - s_{pq}} \right]^t e^{it\theta}$$

$$+ \sum_{t=1}^{\infty} \frac{(-1)^{t-1}}{t} \left[\frac{a}{\bar{s}_{rs} - \bar{s}_{pq}} \right]^t e^{-it\theta} \quad \text{for } (r,s) \neq (p,q) \tag{29}$$

yields a Fourier-like expansion of W involving the powers of $e^{i\theta}$. Since the functions $e^{it\theta}$ form a basis over

the domain $\theta \in [0, 2\pi]$, it is necessary, to satisfy Eq. (27), that the coefficient of each power $e^{it\theta}$ in the expansion of W be set to zero. That is,

$$\sum_{\substack{p,q \\ (p,q)\neq(r,s)}} \left[\sum_{m=0}^{\infty} \frac{A_m^{pq}}{(s_{rs}-s_{pq})^m} + \frac{1}{2i} B_1^{pq} \left[\frac{\bar{s}_{rs}-\bar{s}_{pq}}{s_{rs}-s_{pq}} \right] - \frac{1}{2i} B_1^{pq} \left[\frac{a}{s_{rs}-s_{pq}} \right]^2 + \frac{1}{2i} \bar{B}_1^{pq} \ln \left| \frac{s_{rs}-s_{pq}}{s_{pq}} \right|^2 \right.$$

$$\left. + \sum_{m=2}^{\infty} \frac{B_m^{pq}}{2i} \left[\frac{(\bar{s}_{rs}-\bar{s}_{pq})}{(s_{rs}-s_{pq})^m} - \frac{m\,a^2}{(s_{rs}-s_{pq})^{m+1}} \right] - \sum_{m=2}^{\infty} \frac{\bar{B}_m^{pq}}{2i\,(m-1)\,(\bar{s}_{rs}-\bar{s}_{pq})^{m-1}} + A_0^{rs} + \frac{\bar{B}_1^{rs}}{i} \ln a = 0 \right.$$

(30)

$$\sum_{\substack{p,q \\ (p,q)\neq(r,s)}} \left[\sum_{m=0}^{\infty} \frac{A_m^{pq}}{(s_{rs}-s_{pq})^{m+t}} a^t \binom{-m}{t} + \frac{1}{2i} B_1^{pq} \left[\frac{(\bar{s}_{rs}-\bar{s}_{pq})\,(-a)^t}{(s_{rs}-s_{pq})^{t+1}} \right.\right.$$

$$\left. + (-1)^{t+1} \left[\frac{a}{s_{rs}-s_{pq}} \right]^{t+2} + \frac{1}{2i} \bar{B}_1^{pq} \frac{(-1)^{t-1}}{t} \left[\frac{a}{(s_{rs}-s_{pq})} \right]^t \right.$$

$$\left. + \sum_{m=2}^{\infty} \frac{B_m^{pq}}{2i} \left[\frac{(\bar{s}_{rs}-\bar{s}_{pq})\,a^t}{(s_{rs}-s_{pq})^{m+t}} \binom{-m}{t} + \frac{a^{t+2}}{(s_{rs}-s_{pq})^{m+t+1}} \binom{-m}{t+1} \right] - \frac{1}{2i} \frac{\bar{B}_{t+1}^{rs}}{t\,a^t} = 0 \quad t = 1, 2, \ldots \right. \quad (31)$$

$$\sum_{\substack{p,q \\ (p,q)\neq(r,s)}} \left[\frac{B_1^{pq}}{2i} \frac{a}{(s_{rs}-s_{pq})} + \frac{\bar{B}_1^{pq}}{2i} \frac{a}{(\bar{s}_{rs}-\bar{s}_{pq})} + \sum_{m=2}^{\infty} \frac{B_m^{pq}\,a}{2i\,(s_{rs}-s_{pq})^m} + \sum_{m=2}^{\infty} \frac{\bar{B}_m^{pq}}{2i} \frac{a}{(\bar{s}_{rs}-\bar{s}_{pq})^m} \right] + \frac{A_1^{rs}}{a} = 0$$

(32)

$$\sum_{\substack{p,q \\ (p,q)\neq(r,s)}} \left[-\frac{\bar{B}_1^{pq}}{4i} \left[\frac{a}{(\bar{s}_{rs}-\bar{s}_{pq})} \right]^2 - \sum_{m=2}^{\infty} \frac{\bar{B}_m^{pq}}{4i} \frac{m\,a^2}{(\bar{s}_{rs}-\bar{s}_{pq})^{m+1}} \right] + \frac{A_2^{rs}}{a^2} + \frac{1}{2i} B_1^{rs} = 0 \quad (33)$$

$$\sum_{\substack{p,q \\ (p,q)\neq(r,s)}} \left[-\frac{\bar{B}_1^{pq}}{2i} \frac{(-1)^t}{t} \left[\frac{a}{(\bar{s}_{rs}-\bar{s}_{pq})} \right]^t - \sum_{m=2}^{\infty} \frac{\bar{B}_m^{pq}}{2i} \binom{-m+1}{t} \frac{a^t}{(m-1)\,(\bar{s}_{rs}-\bar{s}_{pq})^{m+t-1}} \right]$$

$$+\frac{A_t^{rs}}{a^t}+\frac{B_{t-1}^{rs}}{2i}\frac{1}{a^{t-2}}=0 \quad t=3,4,\ldots \tag{34}$$

Flow Past a Regular Array

It will be seen in the next section that the determination of the flow past a perturbed array of cylinders requires the knowledge of the corresponding solution for a regular arrangement. The latter flow field can be determined either by relying on the power series expressions derived by Drummond and Tahir (1984) or by a direct application of Eq. (31)-(34). In the case of a regular array, it is expected that the cylinders all have an identical effect on the flow, or equivalently, that

$$B_m^{pq}=B_m^0 \quad \text{for } \textit{all } p \text{ and } q \text{ and } m=1,.. \tag{35}$$

and

$$A_m^{pq}=A_m^0 \quad \text{for } \textit{all } p \text{ and } q \text{ and } m=1,.. \tag{36}$$

for some complex numbers A_m^0 and B_m^0. Then, introducing Eq. (35) and (36) in Eq. (31)-(34) yields the following linear system of equations

$$\sum_{m=1}^{\infty} A_m^0\, a^t \binom{-m}{t} F_{m+t}(0,0)+\frac{B_1^0}{2i}\left[(-a)^t\, G_{t+1}(0,0)+(-1)^{t+1}\, a^{t+2}\, F_{t+2}(0,0)\right]+\frac{\bar{B}_1^0}{2i}\left[\frac{(-1)^{t-1}}{t}\, a^t\, F_t(0,0)\right]$$

$$+\sum_{m=2}^{\infty}\frac{B_m^0}{2i}\left[\binom{-m}{t} a^t\, G_{m+t}(0,0)+\binom{-m}{t+1} a^{t+2}\, F_{m+t+1}(0,0)\right]-\frac{1}{t\,a^t}\frac{\bar{B}_{t+1}^0}{2i}=0 \tag{37}$$

$$\frac{A_1^0}{a}+a\frac{B_1^0}{2i}F_1(0,0)+a\frac{\bar{B}_1^0}{2i}\overline{F_1(0,0)}+\sum_{m=2}^{\infty}\frac{B_m^0}{2i}\,a\,F_m(0,0)+\sum_{m=2}^{\infty}\frac{\bar{B}_m^0}{2i}\,a\,\overline{F_m(0,0)}=0 \tag{38}$$

$$\frac{A_2^0}{a^2}+\frac{B_1^0}{2i}-\frac{\bar{B}_1^0}{2i}\frac{a^2}{2}\overline{F_2(0,0)}-\sum_{m=2}^{\infty}\frac{\bar{B}_m^0}{2i}\frac{m\,a^2}{2}\overline{F_{m+1}(0,0)}=0 \tag{39}$$

and

$$\frac{A_t^0}{a^t}+\frac{1}{a^{t-2}}\frac{B_{t-1}^0}{2i}-\frac{\bar{B}_1^0}{2i}\left[\frac{(-a)^t}{t}\overline{F_t(0,0)}\right]-\sum_{m=2}^{\infty}\frac{\bar{B}_m^0}{2i}\left[\binom{-m+1}{t}\frac{a^t}{(m-1)}\overline{F_{m+t-1}(0,0)}\right]=0. \tag{40}$$

In the above equations, the symbols $F_m(0,0)$ and $G_m(0,0)$ have been used for brevity to designate the following series

$$F_m(0,0)=\sum_{\substack{p,q\\(p,q)\neq(0,0)}}\frac{1}{s_{pq}^m}\quad m=1,\ldots \tag{41}$$

and

$$G_m(0,0)=\sum_{\substack{p,q\\(p,q)\neq(0,0)}}\frac{\bar{s}_{pq}}{s_{pq}^m}\quad m=2,\ldots \tag{42}$$

where the summation over the indices p and q extends over the entire array with the exception of the cylinder $(0,0)$. It should be noted that the coefficients $F_m(0,0)$ and $G_m(0,0)$ are affected by convergence problems. In particular, $F_2(0,0)$ and $G_3(0,0)$ are indeterminate; their values depend on the order of summation. Drummond and Tahir (1984) have resolved this issue by using symmetries. For the geometries that they considered, (unstaggered array, triangular and square staggered arrays) they have proved that the appropriate values of the coefficients $F_m(0,0)$ and $G_m(0,0)$ are obtained by performing first the summation perpendicular to the mean flow.

The determination of the coefficients A_m^0 and B_m^0 requires a final scaling condition specifying, for example, the mean fluid velocity across the array (see Drummond and Tahir, 1984, for details).

Flow Past a Perturbed Array

The determination of the fluid flow past an arbitrary irregular array of cylinders can be obtained, as in the case of a regular arrangement, by relying on Eq. (30)-(34). Because of the lack of symmetry in the positioning of the fibers, the simplifying assumptions given by Eq. (35) and (36) will however cease to be valid and a severe increase in the level of complexity of the analysis will result. In this respect, note that an

investigation of the stability of the array requires only the knowledge of the fluid flow past a slightly perturbed array the cylinders of which are located at the points

$$s'_{pq} = s_{pq} + \delta s_{pq}. \tag{43}$$

In this relation, the symbol s_{pq} denotes the position of the cylinder (p, q) in the regular array while δs_{pq} represents its small mispositioning. Introducing Eq. (43) in Eq. (30)-(34) and linearizing the resulting relations provides a first order approximation of the forces being exerted on the cylinders as a result of their motions. Retaining only the linear term in δs_{pq}, it is found that the principle of superposition holds; the forces resulting from the mispositioning of two or more cylinders equal the sum of the contributions corresponding to each of the displacements δs_{pq} as if they were acting alone.

This observation implies that the analysis can be conducted by considering that only one cylinder, with indices $p = q = 0$, is not in place, that is

$$\delta s_{pq} = 0 \quad \text{for } (p, q) \neq (0, 0) \tag{44}$$

Then, the coefficients A_m^{pq} and B_m^{pq} can be expressed in the form

$$A_m^{pq} = A_m^0 + \delta A_m^{pq} \tag{45}$$

and

$$B_m^{pq} = B_m^0 + \delta B_m^{pq} \tag{46}$$

where δA_m^{pq} and δB_m^{pq} are the small perturbation terms corresponding to the mispositioning δs_{00}. Further, to account for the finite memory of the fluid, it will be required that

$$\delta A_m^{pq} \to 0 \quad \textit{as } p \textit{ and/or } q \to \pm\infty \tag{47}$$

and

$$\delta B_m^{pq} \to 0 \quad \textit{as } p \textit{ and/or } q \to \pm\infty. \tag{48}$$

Letting r and/or s tend toward infinity in Eq. (30), it is readily found from Eq. (47) and (48) that

$$\sum_{p,q} \delta A_0^{pq} = 0 \tag{49}$$

and

$$\sum_{p,q} \delta B_1^{pq} = 0. \tag{50}$$

Even with the above simplifying assumption, the determination of the solution of Eq. (30)-(34) appears to be quite cumbersome since there exists in general a different set of coefficients δA_m^{pq} and δB_m^{pq} for each cylinder. To this end, note that every double summation term appearing in Eq. (30)-(34) is in fact expressible as a discrete two-dimensional Fourier convolution. Thus, it can be expected that the determination of the coefficients δA_m^{pq} and δB_m^{pq} can be greatly simplified by introducing the Fourier transforms

$$\delta B_m(\theta,\phi) = \sum_{p,q} \delta B_m^{pq}\, e^{ip\theta}\, e^{iq\phi} \tag{51}$$

and

$$\delta A_m(\theta,\phi) = \sum_{p,q} \delta A_m^{pq}\, e^{ip\theta}\, e^{iq\phi}. \tag{52}$$

In fact, combining Eq. (30)-(34) and (43)-(52), it can be shown that

$$\sum_{m=1}^{\infty} F_m(\theta,\phi)\,\delta A_m(\theta,\phi) - \left[a^2 F_2(\theta,\phi) - \frac{H(\theta,\phi)}{(1-e^{i\theta})(1-e^{i\phi})} \right] \frac{\delta B_1(\theta,\phi)}{2i} - \sum_{m=2}^{\infty} \left[\frac{\overline{F_{m-1}(-\theta,-\phi)}}{(m-1)} \right] \frac{\overline{\delta B_m(-\theta,-\phi)}}{2i}$$

$$+ \left[\ln a^2 + \frac{L(\theta,\phi)}{(1-e^{i\theta})(1-e^{i\phi})} \right] \frac{\overline{\delta B_1(-\theta,-\phi)}}{2i} - \sum_{m=2}^{\infty} \left[m\, a^2\, F_{m+1}(\theta,\phi) - G_m(\theta,\phi) \right] \delta B_m(\theta,\phi) =$$

$$- \delta s_{00} \frac{B_1^0}{2i} \left[-2\, a^2\, F_3(\theta,\phi) - 2\, a^2\, F_3(0,0) + G_2(\theta,\phi) + G_2(0,0) \right]$$

$$- \sum_{m=1}^{\infty} m\, \delta s_{00}\, A_m^0 \left[F_{m+1}(\theta,\phi) + (-1)^m F_{m+1}(0,0) \right] + \overline{\delta s_{00}} \frac{B_1^0}{2i} \left[F_1(\theta,\phi) + F_1(0,0) \right]$$

$$- \sum_{m=2}^{\infty} \frac{B_m^0}{2i} \left\{ m\, \delta s_{00} \left[G_{m+1}(\theta,\phi) + (-1)^{m-1} G_{m+1}(0,0) - a^2 (m+1) \left(F_{m+2}(\theta,\phi) + (-1)^{m+1} F_{m+2}(0,0) \right) \right] \right.$$

$$\left. - \overline{\delta s_{00}} \left[F_m(\theta,\phi) + (-1)^{m-1} F_m(0,0) \right] - \delta s_{00} \frac{\bar{B}_1^0}{2i} \left[F_1(\theta,\phi) + F_1(0,0) \right] \right.$$

$$\left. - \sum_{m=2}^{\infty} \frac{\bar{B}_m^0}{2i} \overline{\delta s_{00}} \left[\overline{F_m(-\theta,-\phi)} + (-1)^{m-1} \overline{F_m(0,0)} \right] - \overline{\delta s_{00}} \frac{\bar{B}_1^0}{2i} \left[\overline{F_1(-\theta,-\phi)} + \overline{F_1(0,0)} \right] \right. \tag{53}$$

$$\sum_{m=1}^{\infty}\left[a^t\binom{-m}{t}F_{m+t}(\theta,\phi)\right]\delta A_m(\theta,\phi)+\sum_{m=2}^{\infty}a^t\left[\binom{-m}{t}G_{m+t}(\theta,\phi)+a^2\binom{-m}{t+1}F_{m+t+1}(\theta,\phi)\right]\frac{\delta B_m(\theta,\phi)}{2i}$$

$$-\frac{1}{t\,a^t}\frac{\overline{\delta B_{t+1}(-\theta,-\phi)}}{2i}+\left[(-1)^t\,a^t\,G_{t+1}(\theta,\phi)+(-1)^{t+1}\,a^{t+2}\,F_{t+2}(\theta,\phi)\right]\frac{\delta B_1(\theta,\phi)}{2i}-\frac{(-a)^t}{t}\,F_t(\theta,\phi)\,\frac{\overline{\delta B_1(\theta,\phi)}}{2i}=$$

$$-\delta s_{00}\sum_{m=1}^{\infty}\binom{-m}{t}a^t\,A_m^0\left[F_{m+t+1}(\theta,\phi)+(-1)^{m+t}\,F_{m+t+1}(0,0)\right]-(-a)^t\,\frac{B_1^0}{2i}\left[(t+1)\,\delta s_{00}\left(G_{t+2}(\theta,\phi)+(-1)^t\,G_{t+2}(0,0)\right)\right.$$

$$\left.-a^2\,(t+2)\,\delta s_{00}\left(F_{t+3}(\theta,\phi)+(-1)^t\,F_{t+3}(0,0)\right)-\overline{\delta s_{00}}\left(F_{t+1}(\theta,\phi)+(-1)^t\,F_{t+1}(0,0)\right)\right.$$

$$-\sum_{m=2}^{\infty}\binom{-m}{t}a^t\,\frac{B_m^0}{2i}\left[(m+t)\,\delta s_{00}\left(G_{m+t+1}(\theta,\phi)+(-1)^{m+t-1}\,G_{m+t+1}(0,0)\right)-\overline{\delta s_{00}}\left(F_{m+t}(\theta,\phi)+(-1)^{m+t-1}\,F_{m+t}(0,0)\right)\right.$$

$$\left.+a^2\binom{-m}{t+1}\delta s_{00}\,(m+t+1)\left(F_{m+t+2}(\theta,\phi)+(-1)^{m+t+1}\,F_{m+t+2}(0,0)\right)-(-a)^t\,\frac{\bar{B}_1^0}{2i}\,\delta s_{00}\left[F_{t+1}(\theta,\phi)+(-1)^t\,F_{t+1}(0,0)\right]\right.$$

(54)

$$\frac{\delta A_1(\theta,\phi)}{a}+\sum_{m=1}^{\infty}a\,F_m(\theta,\phi)\,\frac{\delta B_m(\theta,\phi)}{2i}+\sum_{m=1}^{\infty}a\,\overline{F_m(-\theta,-\phi)}\,\frac{\overline{\delta B_m(-\theta,-\phi)}}{2i}$$

$$=-a\,\delta s_{00}\left[\sum_{m=1}^{\infty}\frac{B_m^0}{2i}\,m\,(F_{m+1}(\theta,\phi)+(-1)^m\,F_{m+1}(0,0))\right]$$

$$-a\,\overline{\delta s_{00}}\left[\sum_{m=1}^{\infty}\frac{\bar{B}_m^0}{2i}\,m\left(\overline{F_{m+1}(-\theta,-\phi)}+(-1)^m\,\overline{F_{m+1}(0,0)}\right)\right]\qquad(55)$$

$$\frac{1}{a^2}\,\delta A_2(\theta,\phi)-\sum_{m=2}^{\infty}\left[\frac{m\,a^2}{2}\,\overline{F_{m+1}(-\theta,-\phi)}\right]\frac{\overline{\delta B_m(-\theta,-\phi)}}{2i}+\frac{\delta B_1(\theta,\phi)}{2i}-\left[\frac{a^2}{2}\,\overline{F_2(-\theta,-\phi)}\right]\frac{\overline{\delta B_1(-\theta,-\phi)}}{2i}$$

$$=\overline{\delta s_{00}}\sum_{m=1}^{\infty}\frac{\bar{B}_m^0}{2i}\,\frac{m\,(m+1)\,a^2}{2}\left[\overline{F_{m+2}(-\theta,-\phi)}+(-1)^{m+1}\,\overline{F_{m+2}(0,0)}\right]\qquad(56)$$

and

$$\frac{1}{a^t}\,\delta A_t(\theta,\phi)+\frac{1}{a^{t-2}}\,\frac{\delta B_{t-1}(\theta,\phi)}{2i}-\sum_{m=2}^{\infty}\left[\binom{-m+1}{t}\frac{a^t}{(m-1)}\,\overline{F_{m+t-1}(-\theta,-\phi)}\right]\frac{\overline{\delta B_m(-\theta,-\phi)}}{2i}$$

$$-\frac{(-a)^t}{t}\,\overline{F_t(-\theta,-\phi)}\,\frac{\overline{\delta B_1(-\theta,-\phi)}}{2i}=\overline{\delta s_{00}}\left[(-a)^t\,\frac{\bar{B}_1^0}{2i}\left(\overline{F_{t+1}(-\theta,-\phi)}+(-1)^t\,\overline{F_{t+1}(0,0)}\right)\right.$$

$$\left.+\sum_{m=2}^{\infty}\binom{-m+1}{t}a^t\,\frac{(m+t-1)}{(m-1)}\,\frac{\bar{B}_m^0}{2i}\left(\overline{F_{m+t}(-\theta,-\phi)}+(-1)^{m+t-1}\,\overline{F_{m+t}(0,0)}\right)\right. \tag{57}$$

where

$$F_m(\theta,\phi)=\sum_{\substack{p,q\\(p,q)\neq(0,0)}}\frac{1}{s_{pq}^m}\,e^{ip\theta}\,e^{iq\phi}\qquad m=1,\ldots \tag{58}$$

and

$$G_m(\theta,\phi)=\sum_{\substack{p,q\\(p,q)\neq(0,0)}}\frac{\bar{s}_{pq}}{s_{pq}^m}\,e^{ip\theta}\,e^{iq\phi}\qquad m=2,\ldots \tag{59}$$

$$H(\theta,\phi)=\sum_{p,q}\left[\frac{\bar{s}_{pq}}{s_{pq}}-\frac{\bar{s}_{(p-1)q}}{s_{(p-1)q}}-\frac{\bar{s}_{p(q-1)}}{s_{p(q-1)}}+\frac{\bar{s}_{(p-1)(q-1)}}{s_{(p-1)(q-1)}}\right]e^{ip\theta}\,e^{iq\phi} \tag{60}$$

$$L(\theta,\phi)=\sum_{p,q}\ln\left|\frac{s_{pq}\,s_{(p-1)(q-1)}}{s_{(p-1)q}\,s_{p(q-1)}}\right|^2 e^{ip\theta}\,e^{iq\phi}. \tag{61}$$

Note in Eq. (60) and (61) that the terms $\frac{\bar{s}_{rs}}{s_{rs}}$ and $\ln|s_{rs}|^2$ are ignored if $(r,s)=(0,0)$. Further, the convention on the order of summation, already discussed in connection with the flow past a regular array, is also selected here. Finally, note from Eq. (50) and (51), that

$$\delta B_1(0,0)=0. \tag{62}$$

Stability Analysis

The solution of Eq. (53)-(57) provides a representation of the coefficients δB_1^{pq} and of the associated function $\delta B_1(\theta,\phi)$ in the form

$$\delta B_1^{pq} = \alpha^{pq}\,\delta s_{00} + \beta^{pq}\,\overline{\delta s_{00}} \tag{63}$$

and

$$\delta B_1(\theta,\phi) = \alpha(\theta,\phi)\,\delta s_{00} + \beta(\theta,\phi)\,\overline{\delta s_{00}}. \tag{64}$$

The perturbation of the force exerted by the fluid on the fiber (r,s) due to the motion of the cylinder $(0,0)$ can thus be expressed as

$$\delta F^{rs} = 4\,i\,\pi\,\mu\,\delta B_1^{rs} = (4\,i\,\pi\,\mu\,\alpha^{rs})\,\delta s_{00} + (4\,i\,\pi\,\mu\,\beta^{rs})\,\overline{\delta s_{00}} \tag{65}$$

Relying on the superposition principle discussed in the previous section, it is found that the change in the force exerted on the fiber (r,s) due to the motion of <u>all</u> cylinders is

$$\delta F_{rs} = \sum_{p,q}\left[(4\,i\,\pi\,\mu\,\alpha^{(r-p)(s-q)})\,\delta s_{pq} + (4\,i\,\pi\,\mu\,\beta^{(r-p)(s-q)})\,\overline{\delta s_{pq}}\right]. \tag{66}$$

Separating the real and imaginary components, it can be shown that the above relation can be rewritten in the form

$$\begin{bmatrix}\delta F_x^{rs}\\ \delta F_y^{rs}\end{bmatrix} = \sum_{p,q}\begin{bmatrix} f_{11}^{(r-p)(s-q)} & f_{12}^{(r-p)(s-q)}\\ f_{21}^{(r-p)(s-q)} & f_{22}^{(r-p)(s-q)}\end{bmatrix}\begin{bmatrix}\delta x^{pq}\\ \delta y^{pq}\end{bmatrix} \tag{67}$$

where

$$\delta s_{pq} = \delta x_{pq} + i\,\delta y_{pq} \tag{68}$$

$$f_{11}^{pq} = -4\,\pi\,\mu\left[Img(\alpha^{pq}) + Img(\beta^{pq})\right] \tag{69}$$

$$f_{12}^{pq} = 4\,\pi\,\mu\left[Re(\beta^{pq}) - Re(\alpha^{pq})\right] \tag{70}$$

$$f_{21}^{pq} = 4\,\pi\,\mu\left[Re(\alpha^{pq}) + Re(\beta^{pq})\right] \tag{71}$$

$$f_{22}^{pq} = 4\,\pi\,\mu\Big[\,Img(\beta^{pq}) - Img(\alpha^{pq})\,\Big]. \tag{72}$$

In the above relations, the notations $Img(z)$ and $Re(z)$ designate the real and imaginary parts of a complex number z.

It is seen from Eq. (67) that the fluid act as a "series of springs" since the forces are proportional to the displacements. For stability, the stiffness matrix must only possess eigenvalues with positive real parts. These eigenvalues, denoted in the sequel by λ, and their corresponding eigenvectors $\Big[\,....\delta x_{pq}\,\delta y_{pq}\,\delta x_{p(q+1)}\,\delta y_{p(q+1)}....\,\Big]$ satisfy the following equations

$$\sum_{p,q}\begin{bmatrix} f_{11}^{(r-p)(s-q)} & f_{12}^{(r-p)(s-q)} \\ f_{21}^{(r-p)(s-q)} & f_{22}^{(r-p)(s-q)} \end{bmatrix}\begin{bmatrix} \delta x^{pq} \\ \delta y^{pq} \end{bmatrix} = -\,\lambda\begin{bmatrix} \delta x^{rs} \\ \delta y^{rs} \end{bmatrix} \tag{73}$$

for all r and s. Note that the left-hand-side of the above condition represents a discrete two-dimensional Fourier convolution. Thus, introducing the Fourier transforms

$$\delta x(\theta,\phi) = \sum_{p,q} \delta x_{pq}\; e^{ip\theta}\; e^{iq\phi} \tag{74}$$

$$\delta y(\theta,\phi) = \sum_{p,q} \delta y_{pq}\; e^{ip\theta}\; e^{iq\phi} \tag{75}$$

$$f_{11}(\theta,\phi) = \sum_{p,q} f_{11}^{pq}\; e^{ip\theta}\; e^{iq\phi} = 2\,\pi\,\mu\,i\Big[\,\alpha(\theta,\phi) + \beta(\theta,\phi) - \overline{\alpha(-\theta,-\phi)} - \overline{\beta(-\theta,-\phi)}\,\Big] \tag{76}$$

and similarly

$$f_{12}(\theta,\phi) = 2\,\pi\,\mu\Big[\,\beta(\theta,\phi) - \alpha(\theta,\phi) - \overline{\alpha(-\theta,-\phi)} + \overline{\beta(-\theta,-\phi)}\,\Big] \tag{77}$$

$$f_{21}(\theta,\phi) = 2\,\pi\,\mu\Big[\,\alpha(\theta,\phi) + \beta(\theta,\phi) + \overline{\alpha(-\theta,-\phi)} + \overline{\beta(-\theta,-\phi)}\,\Big] \tag{78}$$

$$f_{22}(\theta,\phi) = 2\,i\,\pi\,\mu\Big[\,\alpha(\theta,\phi) - \beta(\theta,\phi) - \overline{\alpha(-\theta,-\phi)} + \overline{\beta(-\theta,-\phi)}\,\Big] \tag{79}$$

it is found that Eq. (73) reduces to the 2x2 eigenvalue problem

$$\begin{bmatrix} f_{11}(\theta,\phi) & f_{12}(\theta,\phi) \\ f_{21}(\theta,\phi) & f_{22}(\theta,\phi) \end{bmatrix}\begin{bmatrix} \delta x(\theta,\phi) \\ \delta y(\theta,\phi) \end{bmatrix} = -\,\lambda\begin{bmatrix} \delta x(\theta,\phi) \\ \delta y(\theta,\phi) \end{bmatrix}. \tag{80}$$

The eigenvalues $\lambda = \lambda(\theta, \phi)$ must be such that a nontrivial solution of Eq. (80) exists. This is achieved when

$$\lambda(\theta,\phi) = -\frac{1}{2}\Big[\, f_{11}(\theta,\phi) + f_{22}(\theta,\phi)\,\Big] \pm \frac{1}{2}\Big[\,(f_{11}(\theta,\phi) - f_{22}(\theta,\phi))^2 + 4\, f_{12}(\theta,\phi)\, f_{21}(\theta,\phi)\,\Big]^{\frac{1}{2}} \qquad (81)$$

Numerical Results

In order to illustrate the above theoretical development, two square arrays have been considered; the first one is unstaggered with a distance between fibers of $\sqrt{2}$ while the second one is staggered at 45^o with a unit distance between fibers. In order to numerically simulate the specific order of summation associated with Eq. (41), (42) and (58)-(61), the domain of the indices p and q was selected to be $(p,q) \in [-10,10] \times [-5000,5000]$. The adequacy of these limits was established by comparing the values of the coefficients A_m^0 and B_m^0, corresponding to a regular array, with the theoretical results of Drummond and Tahir (1984).

Shown in Fig. 2-6 are contour plots of the eigenvalues corresponding to fiber radii, 0.1, 0.2 and 0.4. The presence of negative values of $\lambda(\theta, \phi)$ reveals that the array is unstable for all cases considered. Further, note that the magnitude of the most negative eigenvalue increases as the fiber diameter increases, or equivalently as the fiber concentration increases. It is then concluded that the instability of an array is most pronounced at high fiber concentrations. Finally, note that the values of the parameters θ and ϕ that are associated with the most negative eigenvalue do not seem to vary substantially with either staggering or fiber concentration for $a \geq 0.2$. Figures 3-6 suggest that $\phi \approx 0$ (or 2π) and $\theta \approx 1.1$.

Conclusions

In an attempt to explain the phenomenon of fiber clustering in composite materials, the low Reynolds number flow through an array of rigid cylinders (modeling the fibers) has been investigated. Specifically, the present study emphasized the determination of the forces exerted by the viscous fluid (the resin) on the cylinders for an arbitrary array. These results were then used to study the stability of a slightly imperfect

square array of fibers. The stability analysis reveals that

(1) within the assumption of low Reynolds number, the stability of the array of fibers is independent of both the flow velocity and the fluid viscosity.

(2) the array of fibers is unstable, that is, small deviations of the fiber locations from a perfectly regular square, staggered or unstaggered, array will lead in time to a disordered arrangement of fibers.

(3) the magnitude of the most negative eigenvalue, which quantifies the rate at which the disorder grows, increases with the concentration of fibers.

(4) the value of the most negative eigenvalue and the corresponding mode of instability do not appear to vary substantially with the staggering.

(5) the dominant mode of instability, corresponding to the most negative eigenvalue, appears to be independent of both fiber concentration and staggering for moderate to high fiber concentrations.

Acknowledgements

The support of this work by the grant DAAL03-91-G0030 of the US Army Research Office, Engineering and Science Division, Structural Mechanics Branch is gratefully acknowledged.

References

Chen, S.S., Fujita, K., and Au-Yang, M.K., 1990, *Flow Induced Vibration - 1990* -, Proceedings of the 1990 Pressure Vessels and Piping Conference, Nashville, TN, June 17-21, ASME, Publication PVP-189.

Conca, C., Planchard, J., and Vanninathan, M., 1990, "Limits of the Resonance Spectrum of Tube Arrays Immersed in a Fluid," *Journal of Fluids and Structures*, Vol. 4, pp. 541-558.

Drummond, J.E., and Tahir, M.I., 1984, "Laminar Viscous Flow Through Regular Arrays of Parallel Solid Cylinders," *International Journal of Multiphase Flow*, Vol. 10, No. 5, pp. 515-540.

Gordon, D., 1978, "Numerical Calculations of Viscous Flow Fields Through Cylinder Arrays," *Computers and Fluids*, Vol. 6, pp. 1-13.

Happel, J., and Brenner, H., 1973, *Low Reynolds Number Hydrodynamics*, Noordhoff, Leyden.

Hasimoto, H., 1959, "On the Periodic Fundamental Solutions of the Stokes Equations and their Application to Viscous Flow Past a Cubic Array of Spheres," *Journal of Fluid Mechanics*, Vol. 5, pp. 317-328.

Hjellming, L.N., and Walker, J.S., 1990, "Motion of Continuous Fibers through a Newtonian Resin for High Fiber Volume Fraction," *Journal of Composite Materials*, Vol. 24, pp. 853-878.

Kirsch, A.A., and Fuchs, N.A., 1967, "The Fluid Flow in a System of Parallel Cylinders Perpendicular to the Flow Direction at Small Reynolds Numbers," *Journal of the Physical Society of Japan*, Vol. 22, No. 5, pp. 1251-1255.

Kuwabara, S., 1959, "The Forces Experienced by Randomly Distributed Parallel Circular Cylinders or Spheres in a Viscous Flow at Small Reynolds Numbers," *Journal of the Physical Society of Japan*, Vol. 14, No. 4, pp. 527-532.

Miyagi, T., 1958, "Viscous Flow at Low Reynolds Numbers Past an Infinite Row of Equal Circular Cylinders," *Journal of the Physical Society of Japan*, Vol. 13, No. 5, pp. 493-496.

Sangani, A.S., and Acrivos, A., 1982, "Slow Flow Past Periodic Arrays of Cylinders with Application to Heat Transfer," *International Journal of Multiphase Flow*, Vol. 8, No. 3, pp. 193-206.

Tamada, K., and Fujikawa, H., 1957, "The Steady Two Dimensional Flow of Viscous Fluid at Low Reynolds Numbers Passing Through an Infinite Row of Equal Parallel Circular Cylinders," *Quarterly Journal of Mechanics and Applied Mathematics*, Vol. 10, Part 4, pp. 425-432.

Tamada, K., and Fujikawa, H, 1959, "The Steady Flow of Viscous Fluid at Low Reynolds Numbers Passing Obliquely Through a Plane Grid Made by Equal Parallel Circular Cylinders," *Journal of the Physical Society of Japan*, Vol. 14, No. 2, pp. 202-216.

White, F.M., 1974, *Viscous Fluid Flow*, McGraw-Hill.

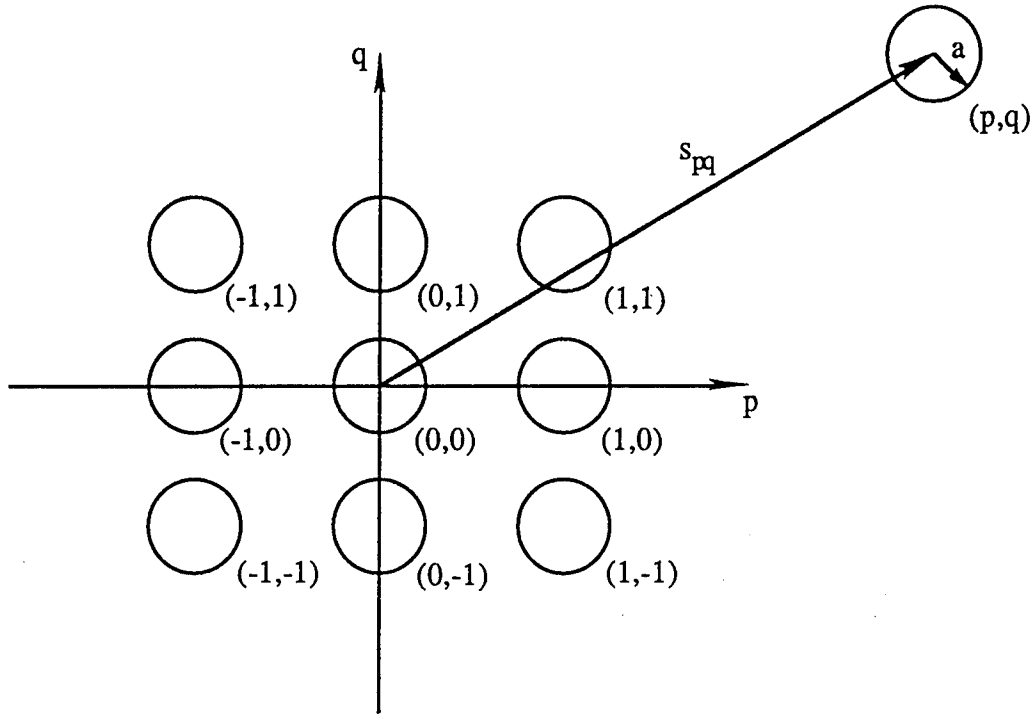

(a) Unstaggered Array

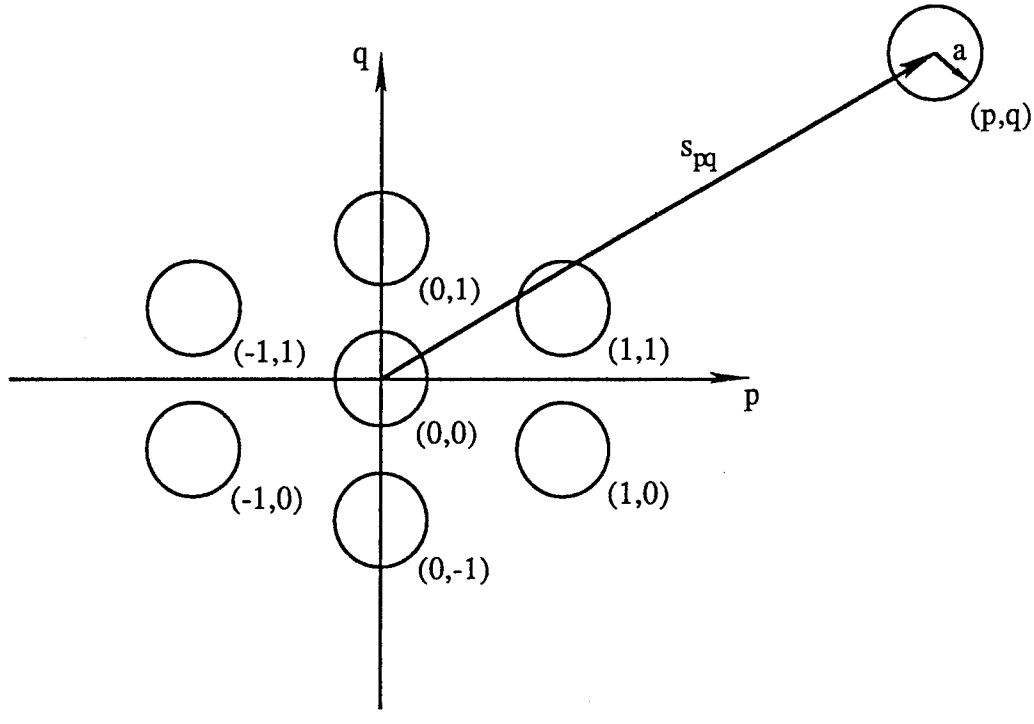

(b) Staggered Array

Fig. 1 Array Geometry

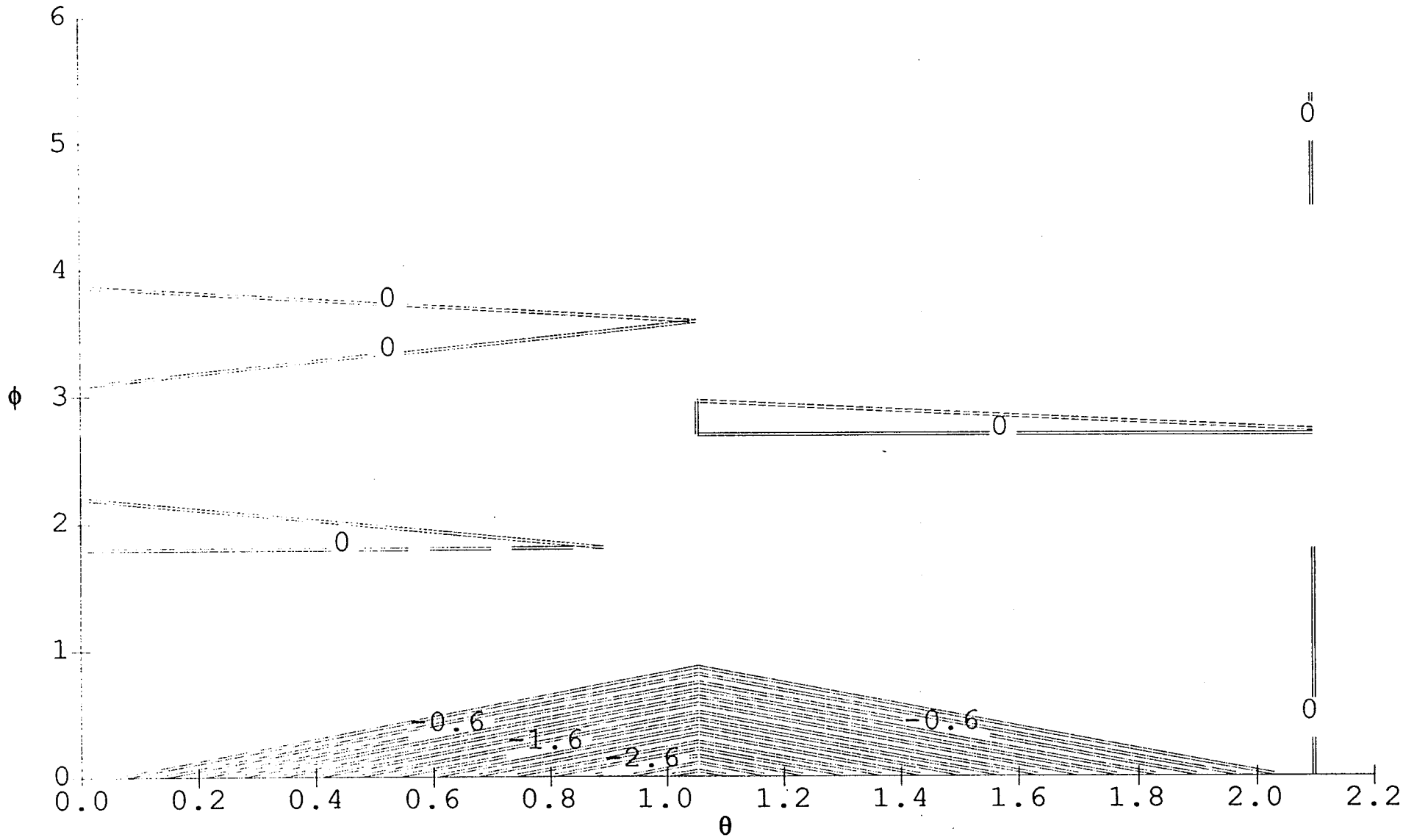

Fig. 2 Contour plot of the lowest eigenvalue, unstaggered array, a=0.2

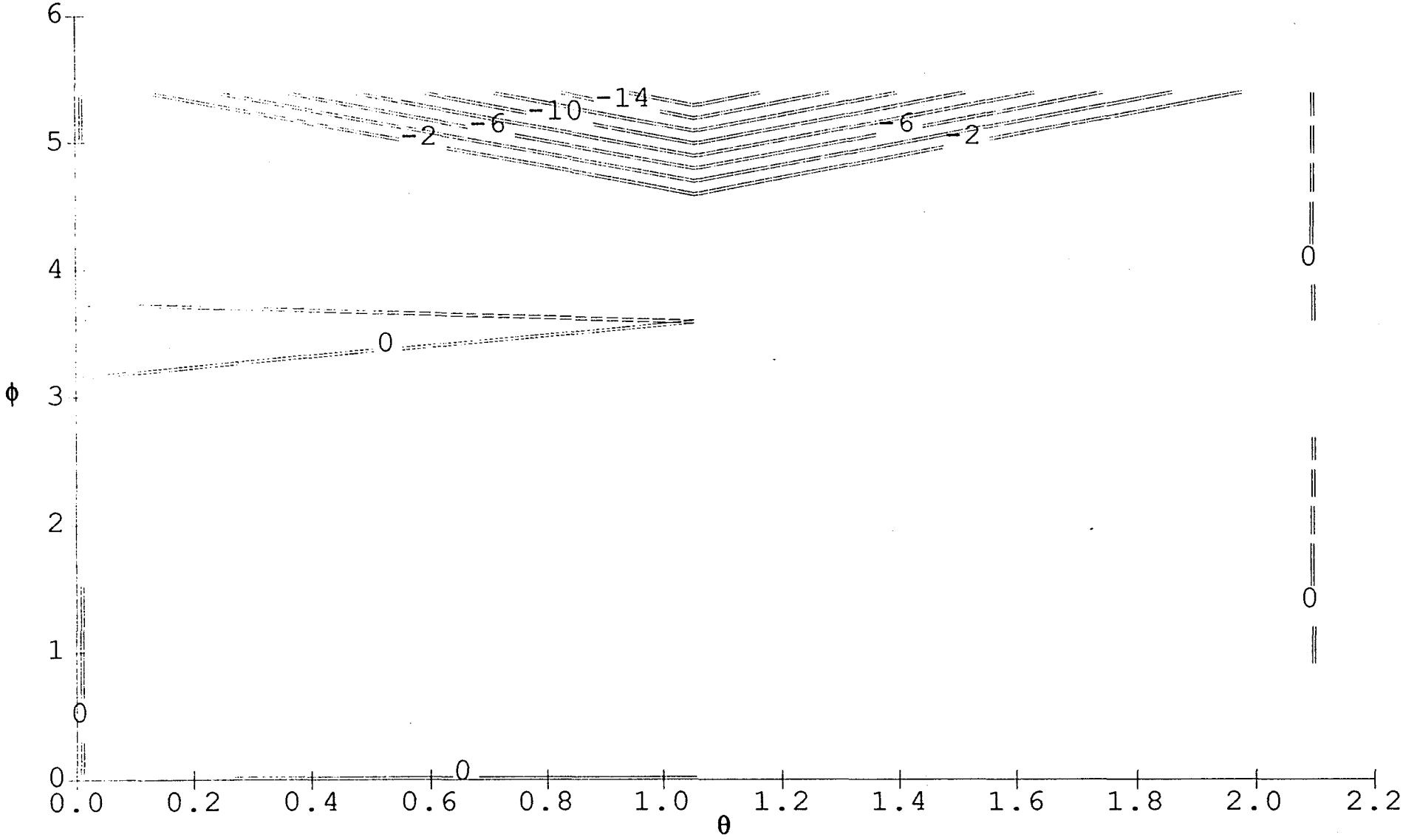

Fig. 3 Contour plot of the lowest eigenvalue, unstaggered array, a=0.4

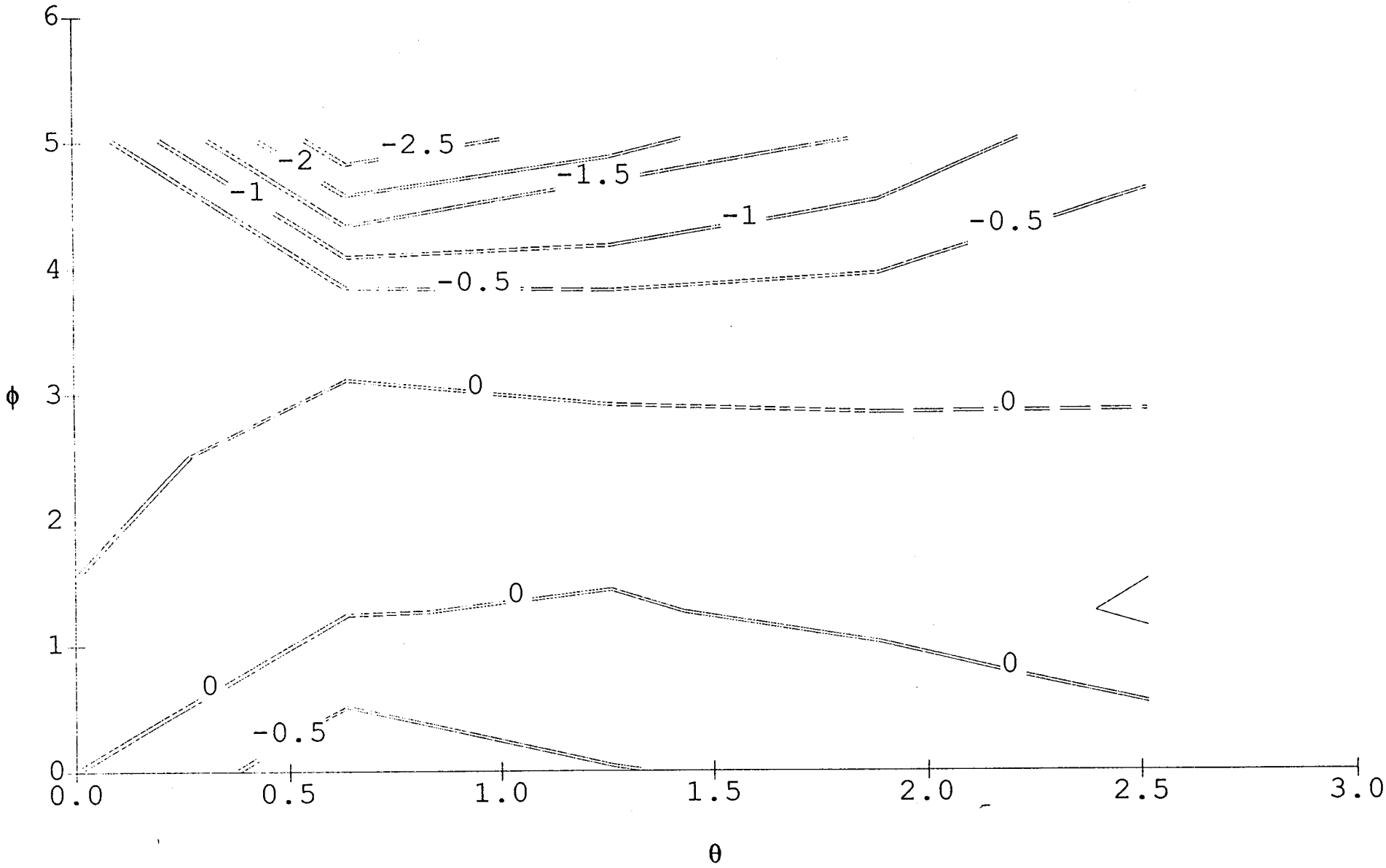

Fig. 4 Contour plot of the lowest eigenvalue, staggered array, a=0.1

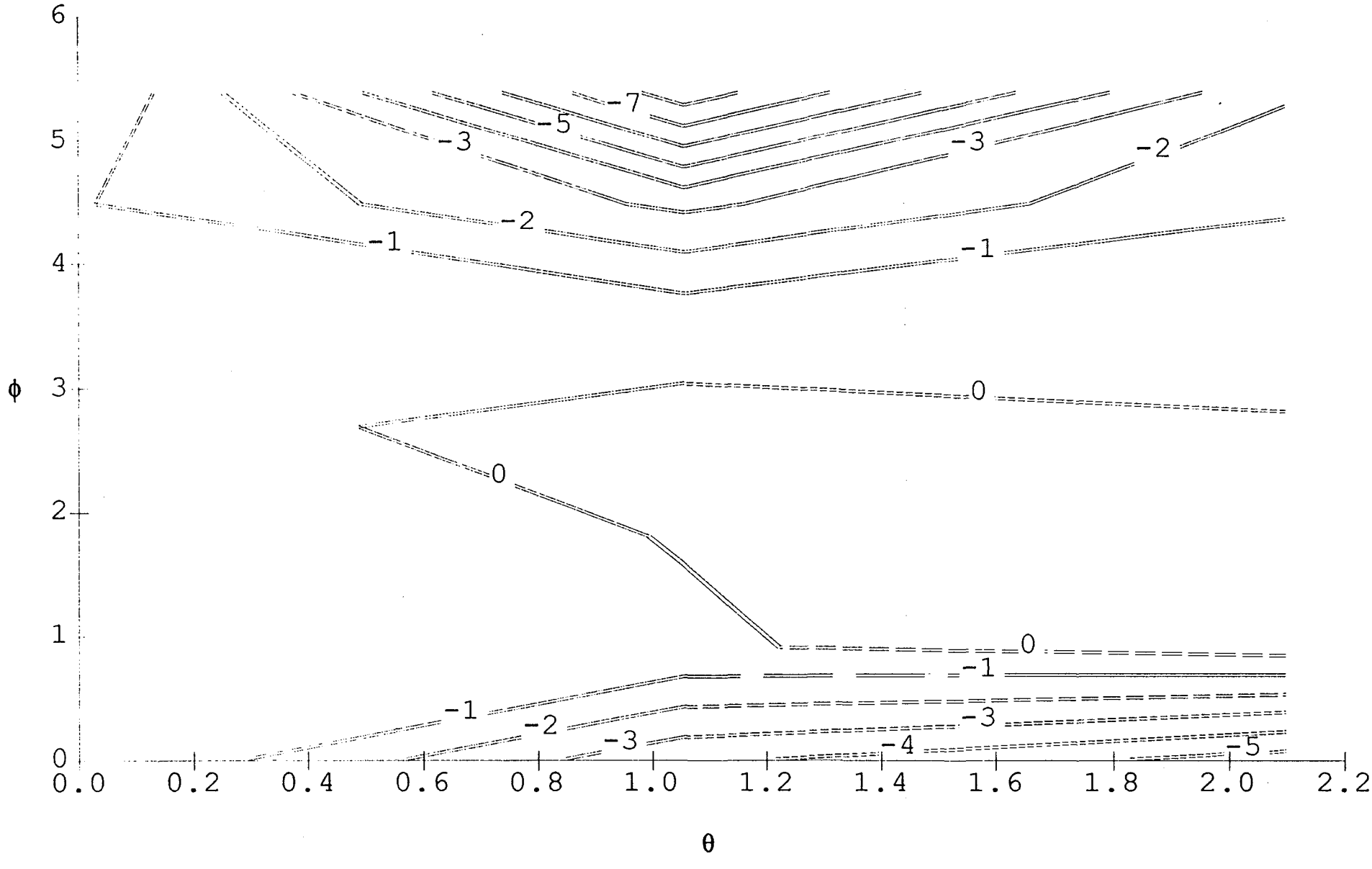

Fig. 5 Contour plot of the lowest eigenvalue, staggered array, a=0.2

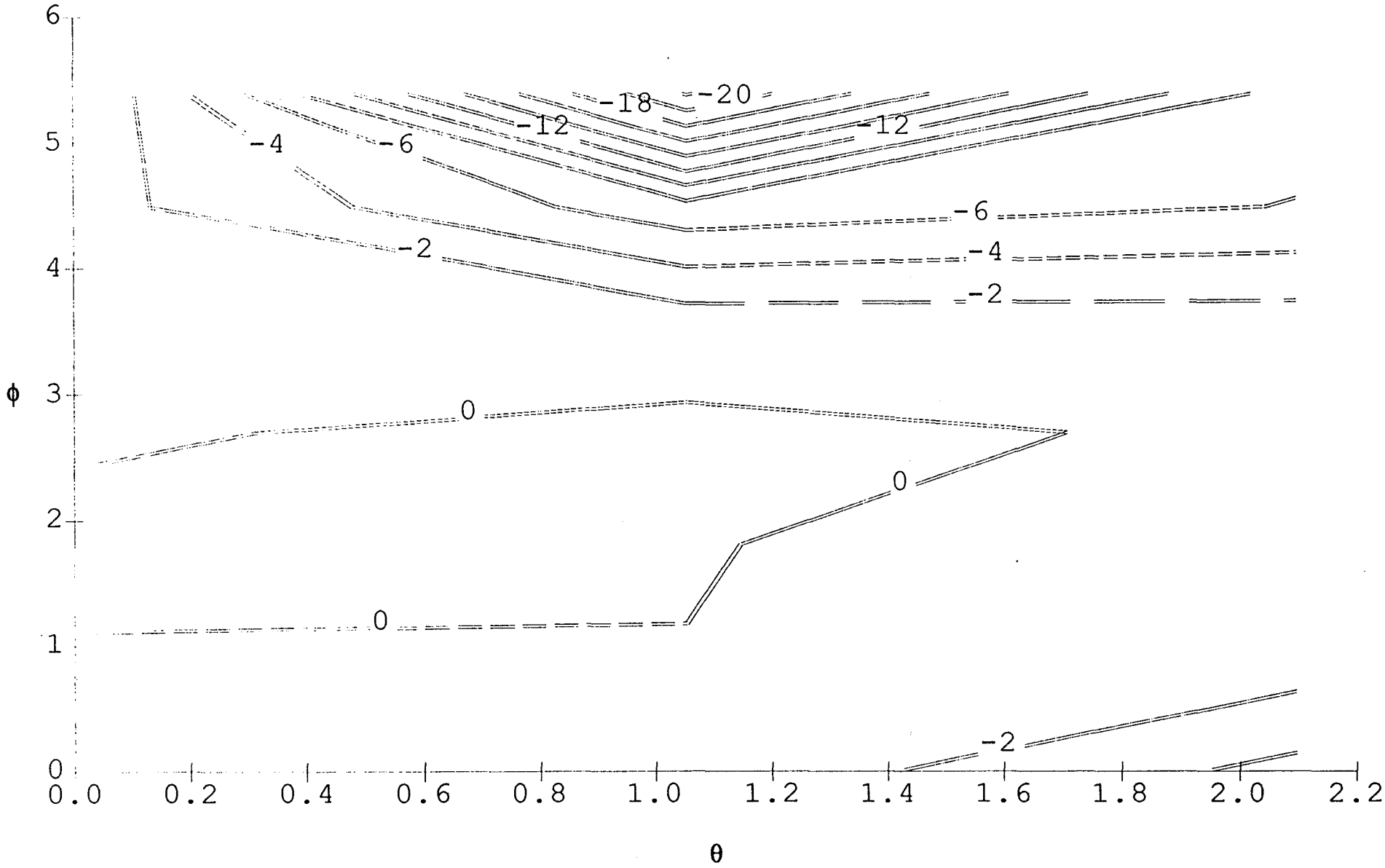

Fig. 6 Contour plot of the lowest eigenvalue, staggered array, a=0.4